

---

Assembly and composition of the cECM is  
critical for heart physiology

---

**Dissertation**

von

**Kay Lammers**

22nd March 2022

zur Erlangung des akademischen Grades

Doktor der Naturwissenschaften (Dr. rer. nat.)

vorgelegt am Fachbereich Biologie/Chemie

der Universität Osnabrück



---

Hauptberichterstatter: Prof. Dr. Achim Paululat  
(Zoologie-Entwicklungsbiologie, Universität Osnabrück)

Berichterstatter: Prof. Dr. Jürgen Heinisch  
(Genetik, Universität Osnabrück)

---

# Contents

|          |   |           |
|----------|---|-----------|
| <b>1</b> | <b>Summary</b>  | <b>1</b>  |
| <b>2</b> | <b>Introduction</b>   | <b>3</b>  |
| 2.1      | The <i>Drosophila</i> heart . . . . .   | 3         |
| 2.1.1    | The <i>Drosophila</i> cardiac ECM . . . . .   | 6         |
| 2.2      | Methods to assess heart parameters . . . . .  | 8         |
| 2.2.1    | Optical coherence tomography (OCT) . . . . .  | 10        |
| 2.2.2    | Semi-automatic optical heartbeat analysis (SOHA) . . . . .  | 10        |
| 2.3      | Aim of this thesis . . . . .  | 13        |
| <b>3</b> | <b>Publication 1</b>  | <b>14</b> |
| <b>4</b> | <b>Publication 2</b>  | <b>27</b> |
| <b>5</b> | <b>Publication 3</b>  | <b>44</b> |
| <b>6</b> | <b>Unpublished Data</b>   | <b>60</b> |
| 6.1      | Introduction . . . . .  | 60        |
| 6.2      | Materials and methods . . . . .   | 61        |
| 6.2.1    | Recording the <i>Drosophila</i> heart rate . . . . .  | 61        |
| 6.2.2    | Preparation of Sylgard®184 silicone elastomer plates . . . . .  | 61        |
| 6.2.3    | Dissection method . . . . .   | 62        |
| 6.2.4    | Tissue glue fixation method . . . . .   | 62        |
| 6.2.5    | Diethylether anaesthesia method . . . . .   | 62        |
| 6.2.6    | HIRO software . . . . .   | 63        |
| 6.2.7    | Fly lines . . . . .   | 68        |
| 6.2.8    | Software . . . . .  | 68        |
| 6.3      | Results . . . . .   | 69        |
| 6.3.1    | Identifying the optimal preparation stage . . . . .   | 69        |
| 6.3.2    | Determination of the optimal preparation method . . . . .   | 70        |
| 6.3.3    | Confirming the heart rhythm of control lines . . . . .  | 70        |
| 6.3.4    | Analysing the influence of RNAi-mediated downregulation of critical cardiac ECM proteins . . . . .      | 70        |
| 6.4      | Discussion . . . . .  | 79        |
| 6.4.1    | Intact anaesthetised <i>Drosophila</i> larvae are the most reliable for heart-beat recordings . . . . . | 79        |
| 6.4.2    | Reduced expression of different heart ECM proteins significantly affects heart performance . . . . .    | 80        |

|           |   |            |
|-----------|---|------------|
| 6.5       | Summary . . . . .   | 84         |
| 6.6       | Outlook . . . . .   | 86         |
| <b>7</b>  | <b>Appendix</b>   | <b>98</b>  |
| 7.1       | Abbreviations . . . . .   | 98         |
| 7.2       | Java Code . . . . .   | 99         |
| 7.2.1     | Java UML diagrams . . . . .   | 99         |
| 7.2.2     | Important Java methods . . . . .  | 103        |
| 7.3       | Index of figures, tables, UML Diagrams and crucial code listings . . . . .                | 110        |
| <b>8</b>  | <b>Curriculum vitae</b>   | <b>114</b> |
| <b>9</b>  | <b>Erklärung über die Eigenständigkeit der<br/>wissenschaftlich erbrachten Leistungen</b> | <b>115</b> |
| <b>10</b> | <b>Erklärung über etwaige frühere Promotionsversuche</b>                                  | <b>116</b> |
| <b>11</b> | <b>Danksagung</b>   | <b>117</b> |

# 1 Summary

The present study focuses on the cardiac function of *Drosophila melanogaster*. *Drosophila* heart parameters are evolutionarily conserved, making *Drosophila* a useful human heart disease model. This model enables the *in vivo* investigation of physiological and genetic methods. This thesis is subdivided into four parts: parts 1-3 comprise the introductions of three publications, and part 4 presents unpublished data.

The first publication is about the heart physiology of *Drosophila*. It explains how intracardiac valve cells work and proves their participation in blood flow directionality. A data-based model shows the orientation of myofibrils within the valve cell. The myofibrils allow the valve cells to oscillate between a roundish and elongated cell shape. A toll-GFP enhancer line was shown to mediate strong reporter gene activity in the intracardiac valve of third instar larvae, pupae and adults. Transmission electron microscopy (TEM) analyses and immunohistochemical studies showed the differentiation of larval valve cells for the first time.

The second publication focuses on the cardiac extracellular matrix (ECM), which contains two unique proteins - Lonely heart (Loh) and Pericardin (Prc). The study demonstrated that Loh is crucial for Prc recruitment to the developing matrix. Loh is anchored to the ECM by its thrombospondin type 1 repeat (TSR1-1) with its embedded putative glycosaminoglycan (GAG)-binding side. The N-terminus of Loh is proposed to face the plasma membrane. Prc is presumably recruited by two Loh TSR1 domains (TSR1-2 and TSR1-4). Nearly all *Drosophila* tissues, except salivary glands, create Prc networks through ectopic Loh expression. The study also found that the amount of Prc and Loh in the cardiac ECM influences heart function.

The third publication investigated a set of neuropeptides and their ability to modulate cardiac function in third instar larvae. The results showed that 11 of the 19 tested peptides significantly affected the heart function in semi-intact larvae. Furthermore, the peptides' *in vivo* relevance was tested through the knockdown of chronotropic peptide precursors. The study found that a RNAi mediated knockdown of all respective peptide precursors affected the heart rate. By combining semi-intact heart preparations and *in vivo* analyses, we identified several heartbeat-modulatory peptides in *Drosophila*.

The unpublished data introduces a new software program called HIRO. It is written in Java, platform-independent and can easily detect the heart rhythm. Only mild anaesthesia and basic equipment are needed to record the *Drosophila* heartbeat. HIRO was used to show the influence of the RNAi-mediated downregulation of critical ECM proteins in *Drosophila* third instar larvae. The screen revealed Myospheroid and Laminin A as promising candidates that can significantly affect the heart parameters. HIRO is optimised for future applications and can be used as a high-throughput screening software with a simple setup. Taken together, this thesis provides new insights into the physiology and function of the *Drosophila* heart. The developed software HIRO comes with a user-friendly interface and a

step-by-step introduction to easily conduct heart parameter measurements. HIRO will help to expand our knowledge of the fundamental processes in the model organism *Drosophila melanogaster*.

## 2 Introduction

Cardiovascular diseases are the international most common non-communicable diseases (Kaptoge et al., 2019). Their detection and evaluation are fundamental for improving patient prognoses. Heart failure is a complex disease, that is influenced by genetic and environmental factors. *Drosophila melanogaster* has become an essential model for human diseases, including cancer, cardiovascular diseases and neurological and metabolic disorders (Millburn et al., 2016). Model organisms enable the *in vivo* investigation of genetic and physiological approaches. The *Drosophila* heart is an excellent model for investigating cardiac development, cardiac performance and cardiac physiology. There are morphological differences between adult vertebrate hearts and the larval dorsal vessel of *Drosophila*; however, heart parameters are evolutionarily conserved from flies to humans (Sláma, 2012). *Drosophila* has three major body compartments (head, thorax and abdomen) that are mutually interconnected and form an open body cavity (Miller, 1997). A simple tubular heart ensures the circulation of body fluid (haemolymph) throughout the body.

### 2.1 The *Drosophila* heart

The tubular heart of *Drosophila melanogaster* has emerged as an excellent model system for investigating the genetic, cellular and molecular mechanisms of heart functionality. Its primary function is to ensure the correct flow direction and distribution of haemolymph (Lammers et al., 2017). The haemolymph transports hemocytes, signalling molecules, bioactive peptides, lipids and hormones.

The heart develops from the mesoderm during embryogenesis. At developmental stage 11, signalling pathways driven by the proteins Decapentaplegic (Dpp), Wingless (Wg) and Notch (N) determine the fate of heart cell precursors, called cardioblasts (Lockwood and Bodmer, 2002; Zaffran and Frasch, 2002; Tao and Schulz, 2007). Two bilateral rows of 52 cardioblasts and 20–25 pericardial cells appear (Fig. 1). Matrix proteins, including Collagens and Laminins, link both cell types to the ectoderm at stage 13 (Chartier et al., 2002). Cardioblasts and pericardial cells migrate towards the dorsal side and finally meet at the dorsal midline at stage 16, forming the embryonic heart tube. The embryonic and larval heart is located within segments T2 and A7 (Fig. 2).

During embryogenesis and metamorphosis, subpopulations of cardioblasts undergo additional transformations. Four of the now called cardiomyocytes within each segment express *seven up* (*svp*), and eight cells express the transcription factor *tinman* (*tin*) (Bodmer, 1993; Lo and Frasch, 2001). The expression of *svp* induces differentiation into ostia cells. Ostial cells are specialised cardiomyocytes that provide haemolymph inflow openings in the heart. One ostia is built from two flap-like cells. The embryonic and larval heart harbour more pairs of Svp-positive cells that have differentiated into ostia. During metamorphosis, the vessel is reconfigured into a four-chambered heart, and four Svp-positive cell pairs differentiate into



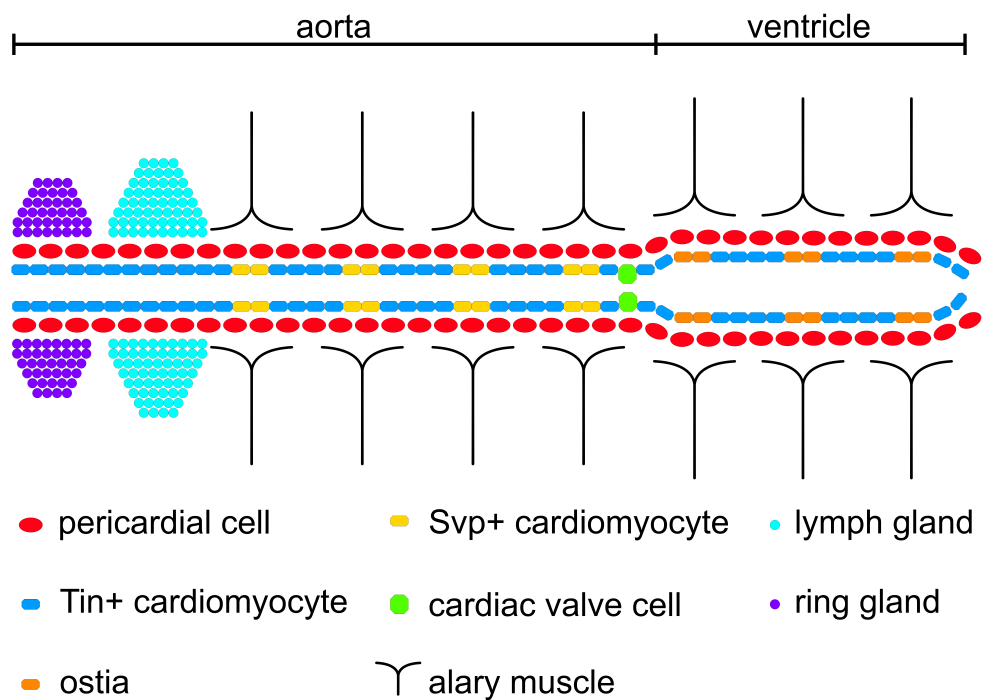


**Figure 1: The larval heart of *Drosophila*.** The heart consists of Tinman (Tin)- and Seven up (Svp)-positive cells. The cardiomyocytes are flanked by pericardial cells. The valve cells are the 19th cell pair (counted from posterior) and separate the heart chamber from the aorta. The Svp-positive cells in the heart chamber form the ostia, and in the larval aorta they are progenitors of the adult ostia cells.

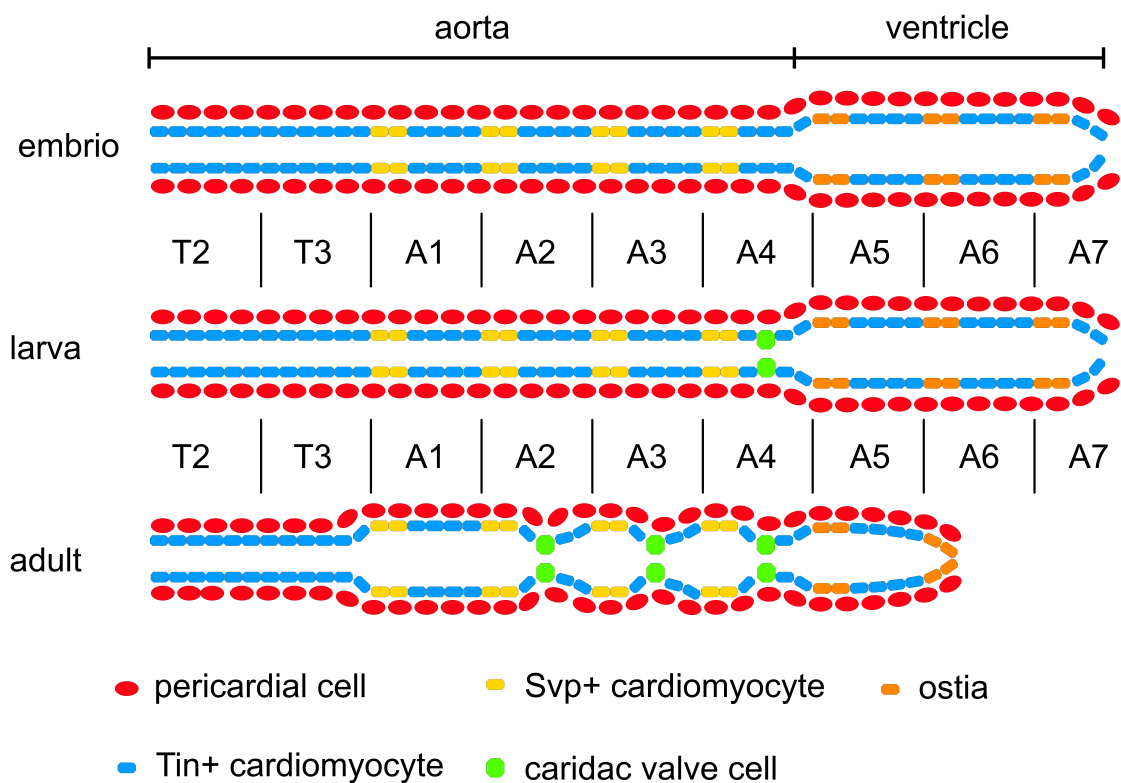


**Figure 2: The *Drosophila* heart in all developmental stages.** Embryonic Tinman (Tin)-positive cardioblasts differentiate during development into larval cardiomyocytes. The ostia are Seven up (Svp)-positive cells and are distinguishable from other cardiomyocytes by their openings to the lumen. The heart chamber and aorta are separated by valve cells in the larval heart. In contrast, the adult heart is divided into a four-chambered tube due to the existence of two additional valve pairs. For simplicity, lymph and ring gland are not depicted.

additional ostia (Fig. 2). The *tin*-expressing cells differentiate into cardiomyocytes, which form the contractile part of the heart and produce the pumping motion. The pericardial cells lack the myogenic function but act as a haemolymph filter and have a crucial role in homeostasis (Rugendorff et al., 1994; Ivy et al., 2015). They are arranged in two rows next to the cardiomyocytes (Sellin et al., 2006).

The *Drosophila* heart is divided into two regions: the anterior aorta and the posterior heart chamber. These two regions are separated by a pair of intracardiac valve cells (Lehmacher et al., 2012). The larval heart has one pair of valves, while the adult heart contains three pairs. Valve cells have a sponge-like appearance, which is caused by large cavities. This structure allows them to change their shape synchronously to the heartbeat and to open or close the intersection between the aorta and heart chamber (Lammers et al., 2017). This function regulates the unidirectional flow of haemolymph in a posterior–anterior direction. The larval dorsal vessel is connected to the body cavity and is held in place by seven pairs of alary muscles. These muscles enable a flexible heart suspension system and are involved in maintaining the position of the heart (Rotstein and Paululat, 2016; Bataillé et al., 2020). During metamorphosis, the heart becomes dramatically remodelled, and the sixth and seventh abdominal segments are histolysed (Fig. 2). The Svp-positive larval ostia precursors differentiate and become ostia (Molina and Cripps, 2001). The adult heart of *Drosophila* is divided into four chambers that are separated by two additional differentiated valve cells. These cells appear in segments A2 and A3 (Fig. 2). The cardiac ECM connects the dorsal vessel with the alary muscles and contributes to a flexible heart positioning.

### 2.1.1 The *Drosophila* cardiac ECM

The extracellular space is covered by a dense meshwork of proteoglycans, glycoproteins and fibrous proteins, constituting the extracellular matrix (ECM). A specialised ECM surrounds the *Drosophila* heart. It forms a cage-like network that covers the entire heart tube and is associated with the pericardial cells. The matrix must withstand the continuous forces caused by the heartbeat. Accordingly, the ECM needs to be rigid but still flexible, and it must guarantee tissue integrity, functionality and organ performance (Rotstein and Paululat, 2016). There are three groups of ECM components: structural components, transmembrane receptors and secreted adaptor proteins.

#### Structural proteins

The extracellular matrix requires stabilising components; these are Laminins and Collagen IV. Glycoproteins and proteoglycans are connected to a dense meshwork of proteins (Pozzi et al., 2017). Laminins can bind to cells, to themselves and to other ECM components (Li et al., 2002; Pozzi et al., 2017). They are large heterotrimeric glycoproteins composed of three non-identical  $\alpha$ ,  $\beta$  and  $\gamma$  chains (Timpl and Rohde, 1979). The *Drosophila* genome encodes two Laminin  $\alpha$  chains (Laminin A (LanA) and Wing blister (Wb)), one  $\beta$  chain (Laminin B1

(LanB1)) and one  $\gamma$  chain (Laminin B2 (LanB2)). It has been shown that LanA likely binds to PS1 Integrin (Gotwals et al., 1994). Laminins are needed for the accumulation of major ECM components, such as Collagen IV and Perlecan (Urbano et al., 2009). Collagen IV can be found in all animals, which indicates its central role in development and evolution. *Drosophila* harbours two genes encoding  $\alpha$  chains of Collagen IV, Viking (Vkg) and Collagen at locus 25C (Cg25C) (Natzle et al., 1982; Le Parco et al., 1986; Rodriguez et al., 1996). The most common variant, found in nearly all basement membranes, consists of two  $\alpha 1$  subunits and one  $\alpha 2$  subunit (Yurchenco, 2011). Collagen and Laminin networks are stabilised by Nidogen and Perlecan (Haag et al., 1999; Kular et al., 2014).

### **Adaptor proteins**

Nidogen and Perlecan form complexes with Laminin and Collagen IV. Nidogen consists of three globular domains (G1 to G3). The protein forms a stable complex with Laminin through binding of its G3 domain to the Laminin  $\gamma$ -subunit, and the G2 domain interacts with Collagen IV and Perlecan (Mann et al., 1989; Hopf et al., 2001). The *Drosophila* *Nidogen/entactin* (*Ndg*) gene can be found in all basement membranes, but a loss of *Ndg* does not affect viability, fertility or ECM assembly in general (Dai et al., 2018; Wolfstetter et al., 2019; Töpfer and Holz, 2020). *Terribly reduced optic lobes* (*trol*) encodes the *Drosophila* homolog of vertebrate Perlecan and is subdivided into five distinct domains. For example, domain V can bind to the Laminin–Nidogen complex and  $\beta$  Integrins (Talts et al., 1999; Friedrich et al., 1999).

### **Transmembrane cell adhesion receptors**

The ECM is connected to the actin cytoskeleton by adhesive transmembrane receptors (Hynes, 1987; Manso et al., 2006). These receptors are Integrins or Dystroglycans (Dg). Integrins are heterodimers and are composed of  $\alpha$  and  $\beta$  subunits; the *Drosophila* genome encodes two  $\beta$  and five  $\alpha$  subunits (Bloor and Brown, 1998; Brown et al., 2000). Integrins harbour three conserved amino acids – arginine (R), glycine (G) and aspartic acid (D) – termed the RGD-motif, which mediates the interaction with the Laminin–Nidogen complex (Ruoslahti, 1987). The transmembrane receptors  $\beta$ PS-Integrin and Dg are present along the luminal and abluminal domain of the heart tube. Previous studies have shown that the absence of the  $\beta$ PS-Integrin subunit is lethal (Gotwals et al., 1994; Roote and Zusman, 1996).

### **Cardiac-specific ECM proteins**

The cardiac ECM of *Drosophila* is highly specialised and contains the unique Collagen IV-like protein Pericardin (Prc) (Chartier et al., 2002). The *pericardin* gene encodes a protein of 1713 amino acids. Prc has a short N-terminal domain and a long C-terminal domain; it also contains two conserved motifs that are present in several proteins of the collagen family. A signal peptide at the N-terminal side and a single potential Integrin-binding site (RGD) is located at the C-terminus side (Chartier et al., 2002; Drechsler et al., 2013). Pericardin is

released into the haemolymph and is recruited to the outer surface of the heart tube, where it forms large extracellular fibres. It is subsequently integrated into the existing network formed by Collagen IV, Perlecan, and Nidogen. The A Disintegrin and Metalloprotease with Thrombospondin Type 1 Motifs (ADAMTS)-like protein Lonely heart (Loh) is crucial for recruiting Prc to the cardiac matrix and is essential for dorsal vessel integrity (Drechsler et al., 2013; Rotstein et al., 2018). Without one of these proteins, the alary muscles and pericardial cells retract from the heart tube. As a result, the heart tube collapses and shows a dissociation phenotype.

Loh belongs to the class of secreted ADAMTS-like proteins. The 7547 base pairs long *lonely heart* gene harbours 13 exons. Until now, three Loh isoforms have been identified: loh-RD, loh-RA and loh-RC. Isoform A includes a signal peptide, five TSR1 domains, an ADAM spacer region and a C-terminal protease and lacunin (PLAC) domain. Loh is expressed from embryonic stage 13 onwards until the end of embryogenesis in cardioblasts and pericardial cell precursors (Drechsler et al., 2013). Its main function is to recruit Pericardin to the dorsal vessel. Loh and Prc are both crucial for organ stability and integrity. The absence of either protein leads to heart failure and heart collapse (Drechsler et al., 2013; Rotstein and Paululat, 2016).

## 2.2 Methods to assess heart parameters

*Drosophila* is not only a powerful model organism to identify the genes that are critical for heart development, but it can be used to identify genes that are crucial for proper heart function. A heartbeat is a two-step pumping action. The pacemaker sends out an electrical signal that causes the cardiomyocytes to contract. The valve cells open the heart lumen, and the contraction wave pushes haemolymph through the aorta. This step of the two-step pumping phase is called systole. Next, the cardiomyocytes relax, the ostia cells open the heart lumen, and fresh haemolymph enters the heart lumen. This step, the longer of the two, is called diastole. An electrocardiogram was applied as the first attempt to determine the *Drosophila* adult heartbeat (Burch, 1971). The cardiac mechanism was found to be different from fly to fly, but the authors identified the *Drosophila* heart as a useful cardiac research model. Two different units are used to specify the *Drosophila* heart rate: hertz (Hz – cycles per second) and beats per minute (BPM). This thesis uses the Hz unit; all BPM values have been converted to Hz. Optical attempts to record the *Drosophila* heartbeat were made in prepupae (White et al., 1989). The authors found a heartbeat of 2.9 Hz. The first larval heart rhythm was determined as between 2.33 Hz to 2.77 Hz (Gu and Singh, 1995). Many approaches have been developed to measure cardiac function, namely, a multielectrode array system, sensor cardiography, atomic force microscopy and optical coherence tomography. Two primary methods have been used in recent publications to measure the *Drosophila* heartbeat. The first method is optical coherence tomography (OCT). The second method uses dense array setups such as semi-automatic optical heartbeat analysis (SOHA).

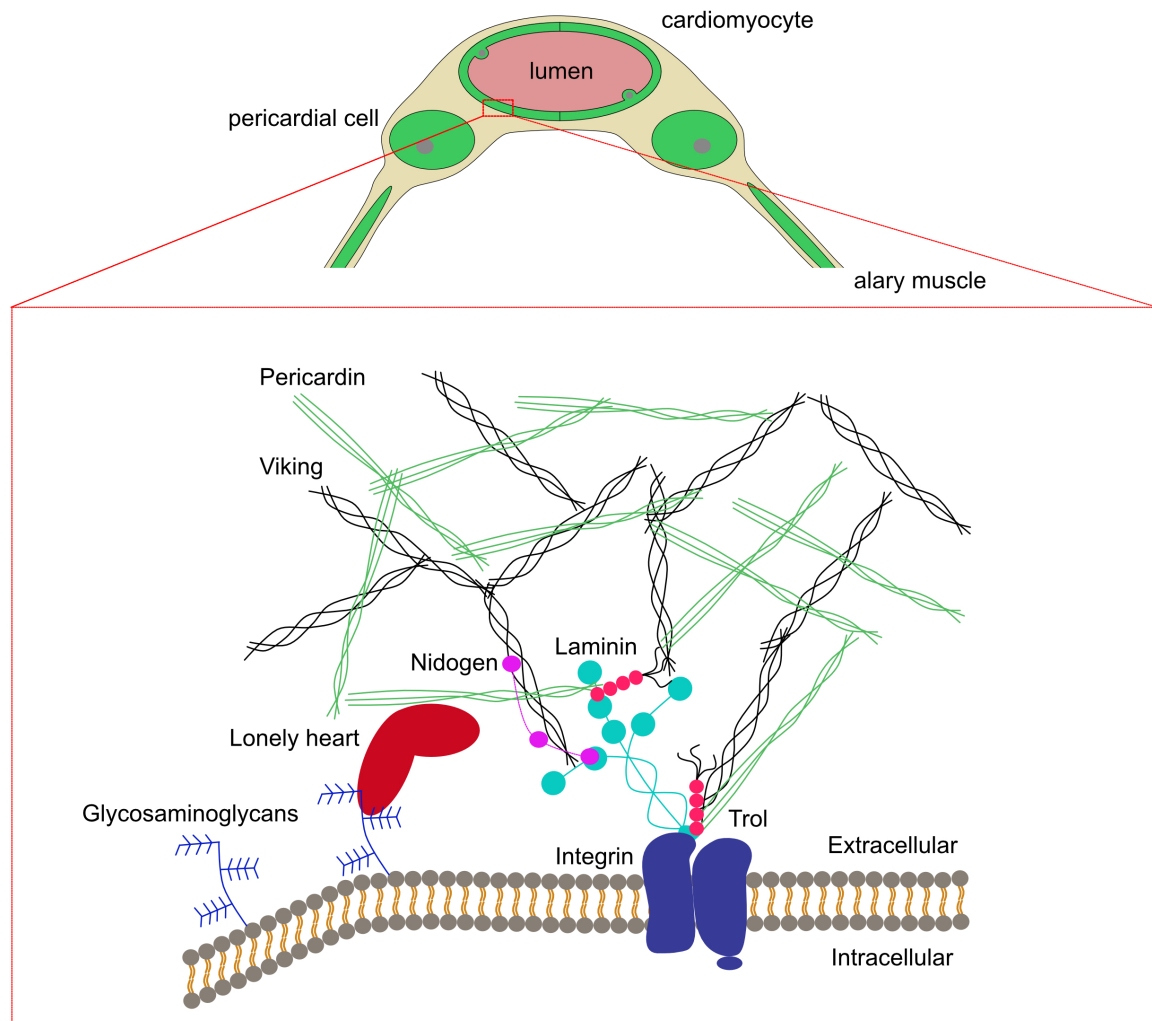


**Figure 3: The cardiac ECM of *Drosophila*.** The figure shows an overview of the *Drosophila* heart and its ECM. The larval heart of *Drosophila* is embedded in a cage of extracellular proteins. Transmembrane proteins like Integrins and Glycosaminoglycans connect the cytoskeleton to the extracellular matrix. Several structural components like Laminin, Collagen IV and Pericardin enhance a dense meshwork. The adaptor proteins Nidogen and Perlecan stabilise, attach and interconnect these networks (modified after Rotstein et al. 2018).

### 2.2.1 Optical coherence tomography (OCT)

OCT is a non-contact imaging technique that generates high-resolution cross-sectional tissue images (Aumann et al., 2019). In the first implementation of OCT, the source emits light, which is split by a beam splitter into the sample and the reference arm (Fig. 4 A). The interference of the back-reflected light from the sample and the reference mirror is then captured by a detector. This allows OCT to create two- and three-dimensional images. OCT systems can be classified into time domain and fourier domain (FD) systems. FD-OCT provides a more efficient implementation. It uses spectral information to generate scans without the need for mechanical scanning of the optical path length. The first use of OCT to observe the heartbeat of *Drosophila* was published in 2006 (Choma et al., 2006; Wolf et al., 2006). Additionally, one study has analysed the body fluid velocity by using nanoparticles as an image contrast enhancer (Choma et al., 2010).

### 2.2.2 Semi-automatic optical heartbeat analysis (SOHA)

Semi-automatic optical heartbeat analysis (SOHA) is a movement detection algorithm that detects cardiac movements associated with individual contractile and relaxation events (Ocorr et al., 2009). The first version of SOHA is based on a MatLab script and provides two movement algorithms (Fig. 4 D). The "Average Frame Darkness" algorithm uses a frame-by-frame approach and measures the darkness intensity for every movie frame. The "Pixel-by-Pixel" algorithm compares the change in darkness of all pixels from one frame to the next. The most recent version of SOHA consists of a stand-alone software that allows the user to select a region of interest, correct individual intervals, and modify additional settings (Cammarato et al., 2015).

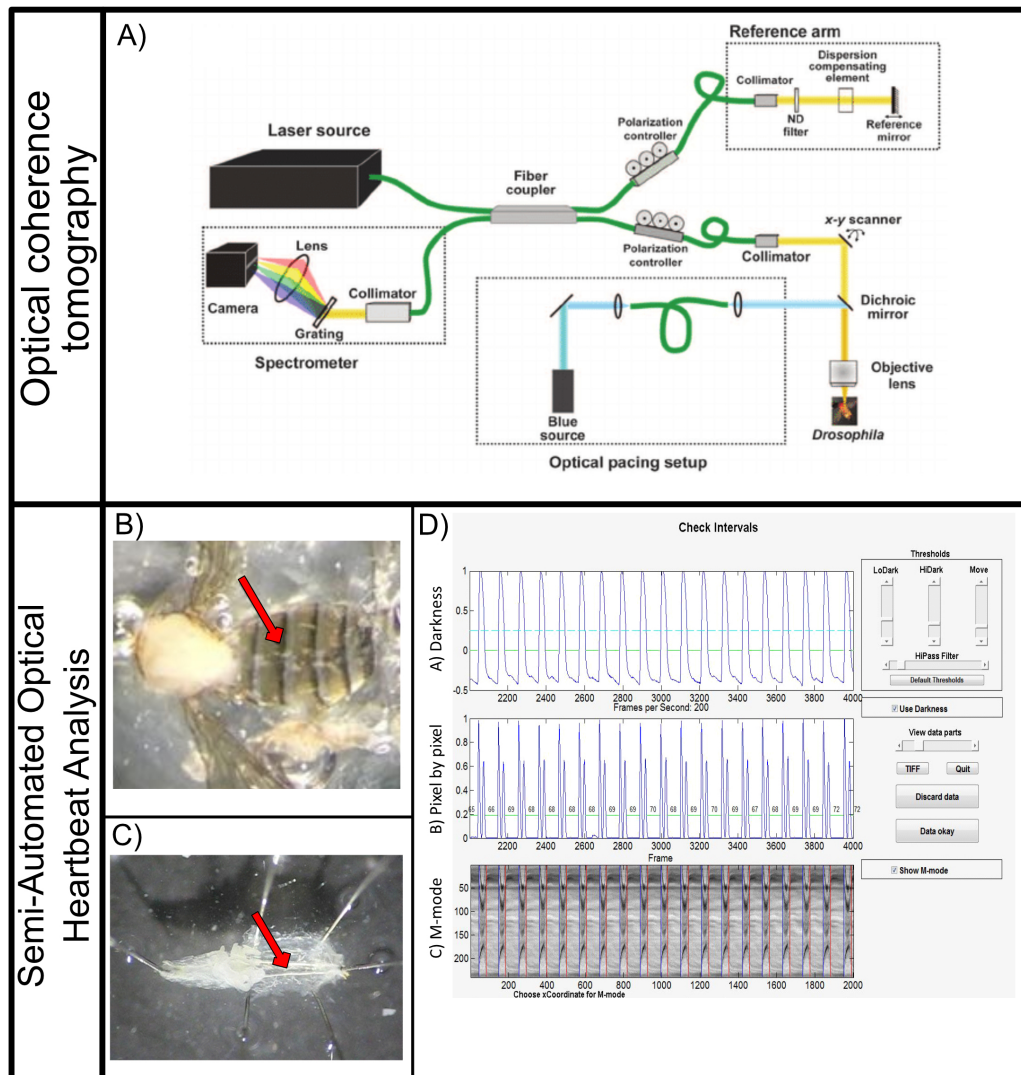


**Figure 4: Optical coherence tomography and semi-automated optical heartbeat analysis.** A) Scheme of the OCT imaging and pacing system (modified after Artero et al. (2018)). B, C) Dissected adult fly and third instar larva. Arrows point at the heart location D) The Graphical user interface of semi-automated optical heartbeat analysis.



**Table 1: Recent publications with OCT measurements.**

| Publication                | Developmental stage | Genotype               | Heart rate |
|----------------------------|---------------------|------------------------|------------|
| Choma et al. (2006)        | Adult               | <i>OreR</i>            | 6 Hz       |
| Wolf et al. (2006)         | Adult               | <i>w<sup>118</sup></i> | 4,52 Hz    |
|                            | Adult               | <i>w<sup>118</sup></i> | 8,52 Hz    |
| Yu et al. (2010)           | Adult               | <i>w<sup>118</sup></i> | 6,5 Hz*    |
| Choma et al. (2011)        | Pre-pupa            | <i>OreR</i>            | 2,25 Hz    |
| Dorn et al. (2011)         | Adult               | <i>tincΔ4-Gal4</i>     | 5,5 Hz*    |
| Piazza and Wessells (2011) | Adult               | <i>yw×Canton-S</i>     | 2.6 Hz*    |
|                            | Adult               | <i>yw×Canton-S</i>     | 2.4 Hz*    |
| Tsai et al. (2011)         | Adult               | n.d.                   | 4,97 Hz    |
|                            | Adult               | n.d.                   | 5,28 Hz    |
|                            | Adult               | n.d.                   | 6,12 Hz    |
| Abraham and Wolf (2013)    | Adult               | <i>w<sup>118</sup></i> | 6,33 Hz*   |
| Guo et al. (2013)          | Adult               | <i>w<sup>118</sup></i> | 5 Hz*      |
| Liao et al. (2013)         | Adult               | <i>twi-24B-Gal4/+</i>  | 4,36 Hz    |
| Zhou et al. (2013)         | Larva               | n.d.                   | 6,2 Hz     |
| Alex et al. (2015)         | Adult               | <i>24B-Gal4</i>        | 6,43Hz     |
| Hardy et al. (2015)        | Adult               | Wild collected         | 10 Hz      |
| Li et al. (2015)           | Adult               | <i>24B-Gal4/+</i>      | 4,37 Hz    |
| Men et al. (2016)          | Larva               | n.d.                   | 4,62 Hz    |
|                            | Pre-pupa            | n.d.                   | 1,43 Hz    |
|                            | Adult               | n.d.                   | 6,53 Hz    |
| Zhu et al. (2016)          | Intact larva        | n.d.                   | 3,17 Hz*   |
|                            | In situ larva       | n.d.                   | 2,08 Hz*   |
| Bunney et al. (2017)       | Larva               | <i>Canton-S</i>        | 3,1 Hz*    |
| Lam et al. (2018)          | Adult               | <i>Canton-S</i>        | 6,08 Hz*   |
| Lee et al. (2019)          | Adult               | n.d.                   | 4.77 Hz*   |

The asterisks represent values obtained from figures; n.d., not described

**Table 2: Recent publications with SOHA measurements.**

| Publication                     | Developmental stage | Genotype                      | Heart rate           |
|---------------------------------|---------------------|-------------------------------|----------------------|
| Lim et al. (2014)               | Adult               | $w^{1118}$                    | 1,54 Hz              |
|                                 | Adult               | <i>Dot</i> -Gal4              | 1,64 Hz              |
| Hardy et al. (2015)             | Adult               | Wild collected                | 1,64 Hz <sup>*</sup> |
| Martínez-Morentin et al. (2015) | Adult               | <i>tincΔ4::Gal4</i>           | 2 Hz                 |
|                                 | Adult               | UAS- <i>scoxi</i>             | 1,67 Hz              |
| Lammers et al. (2017)           | Larva               | $w^{1118}$                    | 2.88 Hz              |
| Monck et al. (2017)             | Adult               | $w^{1118}$                    | 1,79 Hz              |
| Calpena et al. (2018)           | Adult               | <i>GMH5</i> -Gal4/+           | 2,22 Hz <sup>*</sup> |
| Chakraborty et al. (2018)       | Adult               | <i>GMH5-Gal4</i> ;<br>UAS-GFP | 2,4 Hz <sup>*</sup>  |
| Kronert et al. (2018)           | Adult               | <i>PwMhc2</i> /+              | 2,22 Hz <sup>*</sup> |
|                                 | Adult               | <i>R146N-15</i> /+            | 2,5 Hz <sup>*</sup>  |
| Vaughan et al. (2018)           | Adult               | $w^{1118}$                    | 1,8 Hz <sup>*</sup>  |
| Chang et al. (2020)             | Adult               | $yw^R$                        | 1,1 Hz <sup>*</sup>  |

The asterisks represent values obtained from figures

### 2.3 Aim of this thesis

*Drosophila* is an excellent model system for examining heart development and studying cardiovascular diseases. The heart parameters are evolutionarily conserved from *Drosophila* to humans (Sláma, 2012). This thesis focused on measuring the heart parameters of *Drosophila* and is divided into four chapters. The first chapter is focused on the physiology of the intracardiac valve cells and their contribution to the directionality of haemolymph flow within the heart. The second chapter examines the Loh-mediated recruitment of the tissue-specific ECM component Pericardin to the cardiac ECM and the influence of different Loh levels on the heart parameters. The third chapter analysed a set of neuropeptides and their ability to modulate cardiac function.

Measurement of the *Drosophila* heartbeat depends on many different factors including genotype, sex, developmental stage, temperature, anaesthesia and preparation method (Table 1, Table 2). The main goal is to minimise the factors that might influence the heart rhythm. The measurement method must ensure the integrity and reproducibility of the data. These considerations were the inspiration to produce a software that could easily detect the heart rhythm with basic equipment and gentle anaesthesia. Thus, the fourth chapter is focused on the HIRO software, which is optimised for future applications, particularly with regard to convenience and scientific reproducibility.

### 3 Publication 1

**Formation and function of intracardiac valve cells in the *Drosophila* heart** (2017).

Kay Lammers<sup>1\*</sup>, Bettina Abeln<sup>1\*</sup>, Mirko Hüsken<sup>1\*</sup>, Christine Lehmacher<sup>1</sup>, Olympia Eka-  
terini Psathaki<sup>2</sup>, Esther Alcorta<sup>3</sup>, Heiko Meyer<sup>1</sup> and Achim Paululat<sup>1</sup>

1 University of Osnabrück, Department of Zoology and Developmental Biology, Barbar-  
astraße 11, Osnabrück 49076, Germany.

2 University of Osnabrück, Biology, EM unit, Barbarastrasse 11, Osnabrück 49076, Germany.

3 Departamento de Biología Funcional, Facultad de Medicina, Universidad de Oviedo, C/Ju-  
lián Clavería s/n, Oviedo 33.006, Spain.

\*These authors contributed equally to this work

The vertebrate heart is complex compared to the *Drosophila* tube-shaped heart. Both tis-  
sues contain cardiac valves that presumably have the same function, as well as similarit-  
ies at the molecular level (e.g., the VEGF/PDGF pathway). The *Drosophila* heart serves as  
a good model for studying basic development processes and understanding fundamental  
functionalities. This publication describes how intracardiac valve cells work and how they  
contribute to regulating the blood flow directionality in *Drosophila melanogaster*. The valve  
cells change their shape synchronously to the heart rate. Consequently, they can open and  
close the intersection between the heart chamber and the aorta region. We developed a  
data-based model that shows that the orientation of myofibrils within valve cells is crucial  
to the periodic switch between a roundish and elongated cell shape. In this context, we  
characterised the protein expression in a toll-GFP-enhanced *Drosophila* line. toll-GFP me-  
diates strong reporter gene activity in the intracardiac valves of third-instar larvae, pupae  
and adults. We additionally showed the differentiation of larval valve cells for the first time.  
Moreover, we discovered that larval membranous vesicles of endocytic origin account for  
the characteristic shape of the cells and likely represent the structural basis for their func-  
tionality. The preparation of the insects and the recording of highspeed videos of the in-  
tracardiac valve cell was one part of my contribution to this first publication. Furthermore,  
I injected microparticles into the body cavity to investigate the haemolymph flow in semi-  
intact third instar larvae. I also stained third-instar larvae to investigate RNAi-mediated  
phenotypes in valve cells. This publication was fundamental for future valve cell develop-  
ment studies.

## RESEARCH ARTICLE

# Formation and function of intracardiac valve cells in the *Drosophila* heart

Kay Lammers<sup>1,\*</sup>, Bettina Abeln<sup>1,\*</sup>, Mirko Hüsken<sup>1,\*</sup>, Christine Lehmacher<sup>1</sup>, Olympia Ekaterini Psathaki<sup>2</sup>, Esther Alcorta<sup>3</sup>, Heiko Meyer<sup>1</sup> and Achim Paululat<sup>1,‡</sup>

## ABSTRACT

*Drosophila* harbours a simple tubular heart that ensures haemolymph circulation within the body. The heart is built by a few different cell types, including cardiomyocytes that define the luminal heart channel and ostia cells that constitute openings in the heart wall allowing haemolymph to enter the heart chamber. Regulation of flow directionality within a tube, such as blood flow in arteries or insect haemolymph within the heart lumen, requires a dedicated gate, valve or flap-like structure that prevents backflow of fluids. In the *Drosophila* heart, intracardiac valves provide this directionality of haemolymph streaming, with one valve being present in larvae and three valves in the adult fly. Each valve is built by two specialised cardiomyocytes that exhibit a unique histology. We found that the capacity to open and close the heart lumen relies on a unique myofibrillar setting as well as on the presence of large membranous vesicles. These vesicles are of endocytic origin and probably represent unique organelles of valve cells. Moreover, we characterised the working mode of the cells in real time. Valve cells exhibit a highly flexible shape and, during each heartbeat, oscillating shape changes result in closing and opening of the heart channel. Finally, we identified a set of novel valve cell markers useful for future in-depth analyses of cell differentiation in wild-type and mutant animals.

**KEY WORDS:** Cardiac valves, Cardiogenesis, *Drosophila melanogaster*, Endocytosis

## INTRODUCTION

Directionality of blood and lymph flow in vertebrates is regulated by cardiac valves, veins and the vessels of the lymphatic system. The histology of valves differs in adaptation to various pressures and flow rates present in tubular systems. In mammals, the valves that separate the heart chambers consist of a core of connective tissue with collagen and elastin as major constituents whereas venous valves are largely cellular flaps, which are lined with a thin matrix (Armstrong and Bischoff, 2004). Valves passively regulate unidirectional flow when the leaflets of the valve flip to the centre of the vessel and thereby close the luminal space. Several classes of diseases are connected to the dysfunction of valves. Stenosis of cardiac tissue caused by rigidification of the connective tissue

prevents valves from closing the lumen completely. Lymphoedema patients suffer from a lymphatic dysfunction resulting in an accumulation of interstitial fluid, which can be caused by abnormal lymphatic valve morphology, e.g. in distichiasis patients in which mutations in the *Foxc2* gene may be causative of the disease (Fang et al., 2000). Besides *Foxc2*, several factors crucial to valve morphogenesis have been identified in human or mouse models in recent years. These include ephrin-B2, Integrin  $\alpha 9$  and VEGFR3 signalling components (Bazigou et al., 2011).

The complexity of the circulatory system in vertebrates together with the identification of conserved genes and a functional analogy prompted us to ask whether *Drosophila* can serve as a model to understand basic mechanisms of valve morphogenesis, as well as molecular pathways involved in valve differentiation. Directionality of haemolymph flow within the *Drosophila* larval heart tube is regulated by two means: (i) a directional contraction wave running along the heart tube, and (ii) an intracardiac valve cell that separates the posterior heart chamber from the aorta portion (Lehmacher et al., 2012; Miller, 1950; Molina and Cripps, 2001; Rizki, 1978; Sellin et al., 2006; Wu and Sato, 2008; Zeitouni et al., 2007; present study). Experimental data on how the valves act and on the extent to which they contribute to the control of flow properties within the heart are not yet available. Moreover, specification and differentiation of valve cells have also not been analysed in detail – except for work by Zeitouni and colleagues, who showed that differentiation of the three intracardiac valves present in the adult heart depends on platelet-derived growth factor (PDGF) signalling (Zeitouni et al., 2007). Recent data showed that the transcriptional adapter protein Pygopus, a component of the Wnt signalling pathway, plays a role in differentiation and orientation of the myofibrils in valve cells (Tang et al., 2014). Beside that, little is known about the respective developmental processes.

In the present study, we investigated how intracardiac valve cells work and how they may contribute to the regulation of blood flow directionality in *Drosophila melanogaster*. We found that the valve cells, as a consequence of the contractile forces of the cardiac tube, change their shape synchronously to the heartbeat to effectively close and open the intersection between the heart chamber and the aorta region. Furthermore, we established a data-based model in which the orientation of myofibrils within valve cells is crucial to the periodic switch between a roundish and an elongated shape of the cells. The respective switch is probably essential to proper valve cell performance. In addition, we characterised expression of a *toll*-GFP enhancer line. We show that the enhancer mediates strong reporter gene activity in the intracardiac valves of third-instar larvae, pupae and adults. Finally, utilising a combination of transmission electron microscopy (TEM) analyses and immunohistochemical studies, we characterised the differentiation of the larval valve cells for the first time. We found that large membranous vesicles of endocytic origin, probably unique organelles of valve cells, account for the

<sup>1</sup>University of Osnabrück, Department of Zoology and Developmental Biology, Barbarastraße 11, Osnabrueck 49076, Germany. <sup>2</sup>University of Osnabrück, Biology, EM unit, Barbarastraße 11, Osnabrueck 49076, Germany. <sup>3</sup>Departamento de Biología Funcional, Facultad de Medicina, Universidad de Oviedo, C/Julián Clavería s/n, Oviedo 33.006, Spain.

\*These authors contributed equally to this work

‡Author for correspondence (paululat@biologie.uni-osnabrueck)

 A.P., 0000-0002-8845-6859

Received 13 January 2017; Accepted 26 February 2017

characteristic shape of the cells and likely represent the structural basis of their functionality.

## MATERIALS AND METHODS

### *Drosophila* strains

Strain *w*<sup>1118</sup> was used as a wild type (WT). The *toll*-GFP line (*tl*-GFP) was provided by Robert Schulz (Wang et al., 2005). Gal4 drivers were *handC*-Gal4 (Hallier et al., 2015; Paululat and Heinisch, 2012; Sellin et al., 2006) and *tin*<sup>ΔC</sup>-Gal4, provided by Manfred Frasch (Zaffran et al., 2006). All RNAi lines were obtained from the Vienna *Drosophila* Resource Center (VDRC) (Vienna, Austria) (Dietzl et al., 2007). Viking::GFP and UAS-mCD8GFP were obtained from the Bloomington *Drosophila* Stock Center (Bloomington, IN, USA). GFP trap lines (Morin et al., 2001) were provided by the *Drosophila* Genomics and Genetic Resources centre (Kyoto, Japan). The collection of *rab*-Gal4 reporter lines was provided by Robin Hiesinger (Chan et al., 2011).

### Immunohistochemistry and TEM

Primary antibodies used were anti-βPS-Integrin [1:3, CF.6G11, supernatant, Developmental Studies Hybridoma Bank (DSHB), Iowa City, IA, USA] and anti-α-Spectrin (1:25, 3A9, supernatant, DSHB). Rabbit anti-GFP (1:1000) was obtained from Abcam (ab6556; Cambridge, UK). Secondary antibodies (Dianova, Hamburg, Germany) were used 1:100 for Cy2-conjugated and 1:200 for Cy3-conjugated antibodies. TRITC-conjugated Phalloidin (Fluka, Sigma-Aldrich, Hamburg, Germany) was used 1:100.

Preparation of semi-thin sections and TEM was performed as described (Albrecht et al., 2011, 2006; Lehmacher et al., 2012, 2009; Tögel et al., 2008).

### Animal preparation and image analysis

For bright-field live recordings of valve cells, wandering third-instar larvae were pinned onto Sylgard 184 silicone elastomer plates filled with temperate artificial haemolymph and dissected from the ventral side. After removing viscera and allowing specimens to recover for 10 min, the Sylgard plate was placed on the focusing stage of an upright microscope (Leica DMLB). Heartbeat was recorded with a high-speed video camera with up to 200 frames s<sup>-1</sup>. Animals that failed to reestablish a regular heartbeat were excluded from analyses. All recordings were made at 22°C to ensure constant conditions for all specimens. Intact non-dissected larvae were glued onto a Sylgard plate with Tissue-Tek® (Sakura) with dorsal side upwards. Artificial haemolymph contains 108 mmol l<sup>-1</sup> NaCl, 5 mmol l<sup>-1</sup> KCl, 2 mmol l<sup>-1</sup> CaCl<sub>2</sub>, 8 mmol l<sup>-1</sup> MgCl, 1 mmol l<sup>-1</sup> NaH<sub>2</sub>PO<sub>4</sub>, 4 mmol l<sup>-1</sup> NaHCO<sub>3</sub> and 5 mmol l<sup>-1</sup> Hepes, pH 7.1; prior to use, the buffer was supplemented with sucrose (final concentration 10 mmol l<sup>-1</sup>) and trehalose (final concentration 10 mmol l<sup>-1</sup>) (Vogler and Ocorr, 2009). Recordings were captured with a Leica Fluotar (×5, ×10 or ×20) and a Basler piA-640 camera controlled by FireCapture® software (Torsten Edelmann). Recordings were further processed with VirtualDub® (Avery Lee) or with ImageJ (Rasband, 1997–2016). Heart parameters were analysed using SOHA (Semi-Automated Optical Heartbeat Analysis) software (Fink et al., 2009; Ocorr et al., 2014).

### Particle injection

Red-coloured monodisperse spheric polystyrene particles with a diameter of 5.2 μm (microParticles GmbH, Berlin, Germany) were dissolved in artificial haemolymph (approximately 1.2×10<sup>3</sup> particles μl<sup>-1</sup>). A small amount (20 μl) of particle stock

solution was pipetted into the posterior half of a semi-intact larva or injected into the posterior body region of an immobilised intact larva or pupa using an Eppendorf microinjector (Femtojet®), a Narishige micro-manipulator and hand-made glass capillaries.

## RESULTS

The lumen of the *Drosophila* heart is established by two rows of contralateral-situated cardiomyocytes connected by a dorsal and a ventral adhesion zone (Medioni et al., 2008). In the larva, one pair of cardiomyocytes, which is the 34th pair of cells counted from the anterior, builds the intracardiac valve that partitions the heart tube into an anterior aorta and a posterior heart chamber (Lehmacher et al., 2012; Medioni et al., 2009; Rotstein and Paululat, 2016). During metamorphosis, two additional valves differentiate, resulting in three intracardiac valves in total that subdivide the adult heart into four chambers. The valves in the adult fly are formed by the 22nd, the 28th and the 34th pair of cardiomyocytes (Lehmacher et al., 2012; Rotstein and Paululat, 2016; Tang et al., 2014; Zeitouni et al., 2007).

### Intracardiac valve cells – mode of operation

Imaging of valve cells in dissected larvae is technically feasible with bright-field or differential interference contrast (DIC) illumination without the need for additional contrast enhancement. In this study, valve cells were identified based on their position within the heart tube and their unique shape and histology (Fig. 1; Movie 1; and paragraphs below). For each animal we captured several individual recordings, and all recordings were further processed to deduce relevant heartbeat parameters, such as valve cell motility, diastolic and systolic luminal diameters, diastolic and systolic period, or haemolymph streaming velocity.

A typical complete contraction cycle of the heart takes 2.88±0.08 Hz (corresponds to a heart cycle of ~347 ms) on average under the conditions used (Fig. 1). This is in line with previous measurements that range between 2.4 Hz and 4.5 Hz (Alex et al., 2015; Gu and Singh, 1995; Sanyal et al., 2006; Sénatore et al., 2010; Sláma and Farkaš, 2005). Several parameters influence heartbeat rate, i.e. temperature (Andersen et al., 2015; Ray and Dowse, 2005), composition of the artificial haemolymph (Zhu et al., 2016) and age (Sláma and Farkaš, 2005; Wessells and Bodmer, 2007).

In the present analysis, we focused on the dynamic activity of the valve cells. First, we aimed to elucidate how the valve cells contribute to closing the heart lumen during each heart contraction cycle. Our analyses of slow-motion recordings revealed that the two valve cells periodically occupy the entire luminal space by changing their shape, thereby closing the heart lumen (Fig. 1A4 and A5). The maximal luminal distance between the opposing valve cells is 77 μm during diastole whereas the heart lumen is completely closed during systole [Fig. 1A1 and B (blue lines)]. The luminal heart diameter posterior to the position of the valve cells varies between approximately 145 μm (diastole) and 72 μm (systole) during a single beating cycle of the heart of a selected individual [Fig. 1A1 and B (red lines)]. A frame-by-frame analysis of the recordings revealed that the closed state persists for approximately 173 ms on average (contact time) in the specimen used to illustrate valve cell behaviour in Fig. 1. This is about one-third of the time of a complete heartbeat cycle. To demonstrate that this value reflects the normal behaviour of valve cells we analysed heart rate and valve cell contact time in several individuals. Although we found minor variations, the mean valve cell contact time always spans one-third of the total time required to complete one heartbeat cycle (Fig. 1C).

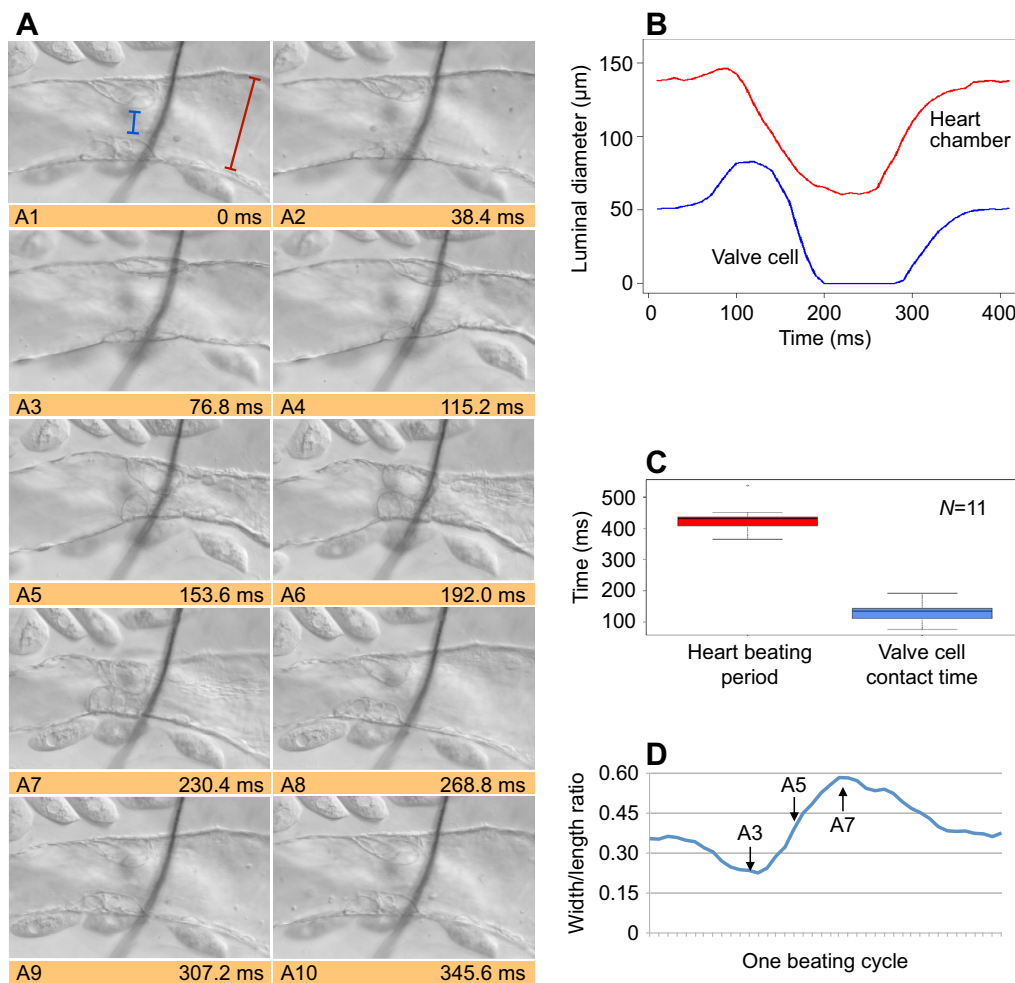


**Fig. 1. Video-microscopy analysis of *Drosophila* intracardiac valve motility in semi-intact third-instar larvae.** (A) Movement and cell shape change of the intracardiac valve cells was monitored in dissected semi-intact third-instar larvae. Shown are selected single frames from a recording captured at 200 frames  $s^{-1}$  (Movie 1). A1–A10 represent, in total, one heartbeat period subdivided into 10 intervals. For example, A3 shows the two valve cells at the maximum luminal distance whereas A6 shows the two valve cells when closing the heart lumen. The black line running across the valve cells is a tracheal branch that runs above the heart and connects the two major dorsal trunks. (B) Several recordings, including the one from which pictures A1–A10 were taken, were used to measure the luminal distance between valve cells (illustrated by a blue line in A1) and between cardiomyocytes constituting the heart chamber (illustrated by a red line in A1). One contraction cycle is shown. Posterior to the valve cells, the luminal diameter oscillates between  $\sim 70 \mu m$  (systole) and  $\sim 150 \mu m$  (diastole). Luminal distance between the valve cells oscillates between zero (contact phase, diastole) and  $\sim 80 \mu m$  (systole). (C) The heartbeat period and valve cell contact time measured in 11 individual animals to illustrate individual variability. On average, the valve cell contact time is one-third of a heartbeat period. The box-and-whisker diagram shows the upper and lower quartiles (first and third quartiles) of the data set, and the median (second quartile) is indicated as a horizontal line inside the box. Vertical lines (whiskers) represent the interquartile range (maximum 1.5 interquartile range), and the outliers are plotted as individual points. (D) As shown in A, the shape of the valve cells oscillates between a roundish shape (e.g. A7) and an elongated spindle-like shape (e.g. A3) during the heartbeat. This is exemplarily illustrated by plotting the width/length ratio of a single selected valve cell against time.

### Haemolymph flow in semi-intact third-instar larvae

To assess the relevance of the valve cells to fluid streaming inside the heart, we tracked the movement of particles that were added into the open body cavity of a dissected semi-intact larva (Fig. 2; Movies 2A, 2B, 2C and 4). The particles we used display a high contrast, which allows precise and fast video-based tracking approaches at high frame rates. Thus, we utilised particle injection to study the haemolymph flow inside the heart tube in detail. In this context, the streaming properties alongside the valves of semi-intact specimens were of particular interest.

Evaluation of several recordings substantiated that haemolymph (particles) enters the heart tube via the three pairs of ostia located in the posterior heart chamber. Video analysis further confirmed that during the diastolic filling phase the heart

chamber acts as a suction pump. Particles in the outer vicinity of the ostia accelerate during entry into the heart chamber (Fig. 2; Movie 2A). During late diastolic phase, particles move inside the heart chamber but do not pass the valve. Indeed, valve cells are in close contact and thus seal the luminal diameter during this phase. At the beginning of the systolic phase, the valve opens and haemolymph (particles) streams towards anterior (Movie 2B). Streaming velocity is highest within the aorta during the systolic phase. At the end of the systolic phase, haemolymph streaming slows down and the characteristic movement of particles close to the valve indicates turbulent flow in this part of the heart tube (Movie 2B).

Measuring the velocity of the particles within the aorta region revealed that during systole, particles stream inside the heart tube at

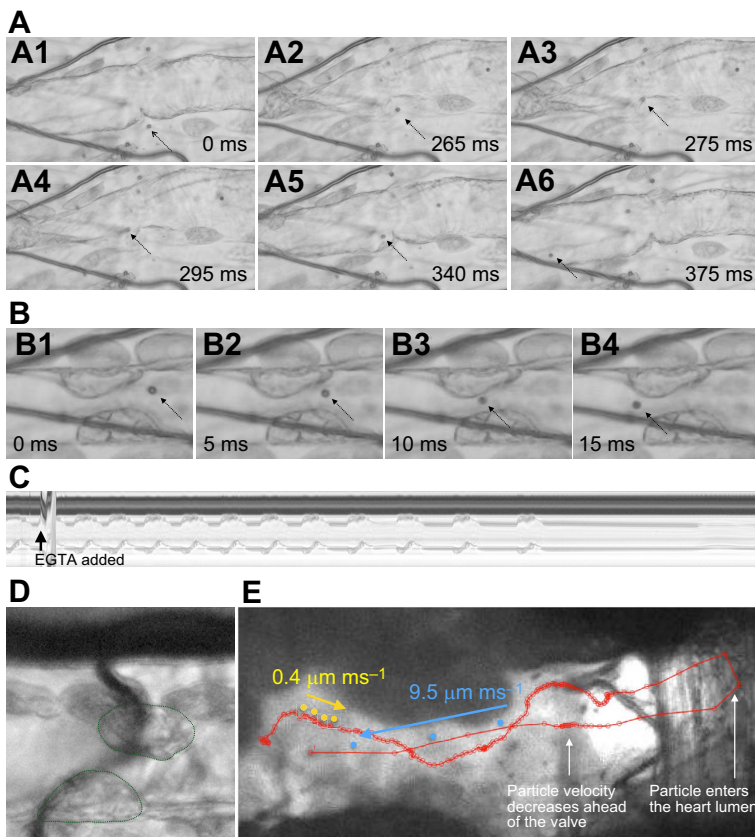


**Fig. 2. Injection of coloured polystyrene particles to visualise flow directionality and streaming behaviour in the heart tube.**

(A) Entry of particles into the heart via ostia was monitored in dissected semi-intact third-instar larvae. A1–A6 represent selected single frames from a recording captured at 200 frames  $s^{-1}$  (Movie 2A). This shows that the  $5.2 \mu\text{m}$  polystyrene particles easily enter the heart via the ostial opening present in the heart proper. (B) Illustrates how fast particles pass the valve cells. B1–B4 represent selected single frames from a recording captured at 200 frames  $s^{-1}$  (Movie 2B). (C) M-mode trace from a 15 s recording shows heart wall movements in a semi-intact dissected third-instar larva treated with EGTA. Note that the heartbeat slows down and finally stops when treated with EGTA. (D) The valve cells (labelled with a dotted green line) from an animal in which the heartbeat was stopped by EGTA application. The valve cells display a semi-roundish shape. (E) Tracking of an injected particle during a 4 s period taken from a longer recording. An intact white prepupa, glued to a microscopic glass, was injected without dissection. Direction of particle movement is indicated by arrows (yellow, outside of the heart; blue, inside the heart tube). Time interval between each reading point is 20 ms. Note that particles move slower outside the heart lumen (yellow dots,  $0.4 \mu\text{m ms}^{-1}$ , measured for nine particles) and they accelerate in the vicinity of the ostia. Inside the heart proper, particles move towards the anterior and become slower near the valve cells. When the valve opens during the contraction cycle, particles move rapidly into the aorta (blue dots,  $9.5 \mu\text{m ms}^{-1}$ , measured for 14 particles). In addition, the recording illustrates that haemolymph flow is unidirectional and valve cells prevent, in the context of an intact animal, backflow.

approximately  $10 \mu\text{m ms}^{-1}$  (Fig. 2), associated with a Reynolds number ( $Re$ ) of approximately 0.5, indicating that laminar flow conditions are prevalent within the heart tube (velocity  $\sim 0.01 \text{ m s}^{-1}$ ; density of artificial haemolymph  $\sim 1000 \text{ kg m}^{-3}$ ; luminal diameter  $\sim 0.15 \text{ mm}$ ; dynamic viscosity  $\sim 0.001 \text{ Pa s}^{-1}$ ). It is important to note that we measured only systolic movements in dissected semi-intact third-instar larvae. The reason for this restriction is the fact that during diastole we observed backflow of particles from the aorta into the posterior heart chamber, which we consider artificial and caused by the preparation procedure (see Movie 2C). Visualising haemolymph streaming in intact specimens showed that in larvae and prepupae haemolymph streaming is unidirectional (Choma et al., 2011; Drechsler et al., 2013). This indicates that unidirectional haemolymph flow inside the heart tube is affected by the dissection procedure, presumably due to an impaired connection of the heart tube to the alary muscles.

#### Haemolymph flow in intact pupae

Particle injection into intact living insects has recently been successfully used to analyse parameters of haemolymph circulation in *Anopheles* (Chintapalli and Hillyer, 2016; League et al., 2015). We now performed such experiments in intact *Drosophila*. It should be noted that image quality dramatically decreased due to limitations caused by the continual darkening of the cuticle (pupa) and the massive line-of-sight obstruction caused by tissues located next to and around the heart tube. Nevertheless, we were able to capture a number of recordings with sufficient quality for further data processing. As a result, we found that the particles behave similarly and exhibit comparable velocities after both injection into intact specimens and application onto dissected animals (Fig. 2E; Movie 4), with one important exception. In

contrast to the situation in dissected semi-intact specimens, haemolymph flow in the heart tube of intact animals is clearly unidirectional. This result demonstrates, as expected, that proper heart function requires a closed system, providing high-pressure/low-pressure time windows for efficient heart chamber refilling and pumping phases. Again, we estimated the Reynolds numbers for particles outside of the heart tube and particles that move inside the heart. Due to the limited image quality, we were not able to distinguish clearly between heart chamber, aorta and valve position. Nevertheless, the  $Re$  is between 0.5 and 10, indicating laminar flow properties within the intact insect body cavity and the heart tube. For a more detailed analysis, it will be necessary to increase image quality, to determine viscosity, and to measure the density of the haemolymph more precisely – issues that will be addressed in future investigations.

#### Shape dynamics of intracardiac valve cells

During a regular heartbeat, the intracardiac valve cells oscillate between two morphologically distinct states (Fig. 1A1–A10; Movie 1) that determine whether the passage between the heart chamber and the aorta is closed or open. In the open state, each valve cell displays an elongated, flattened shape (Fig. 1A3). With ongoing heart cycle, the valve cells change their shape and become roundish or pear-shaped (Fig. 1A4–A6) and the luminal distance between the valve cells decreases, finally causing a complete closure of the luminal diameter (Fig. 1B) and preventing backflow of haemolymph from the aorta into the heart chamber. We monitored the shape change of valve cells as a function of the relationship between width and length of the cells during heartbeat (Fig. 1D). As a result, we found that valve cells undergo an oscillating deformation process in which the width/length ratio

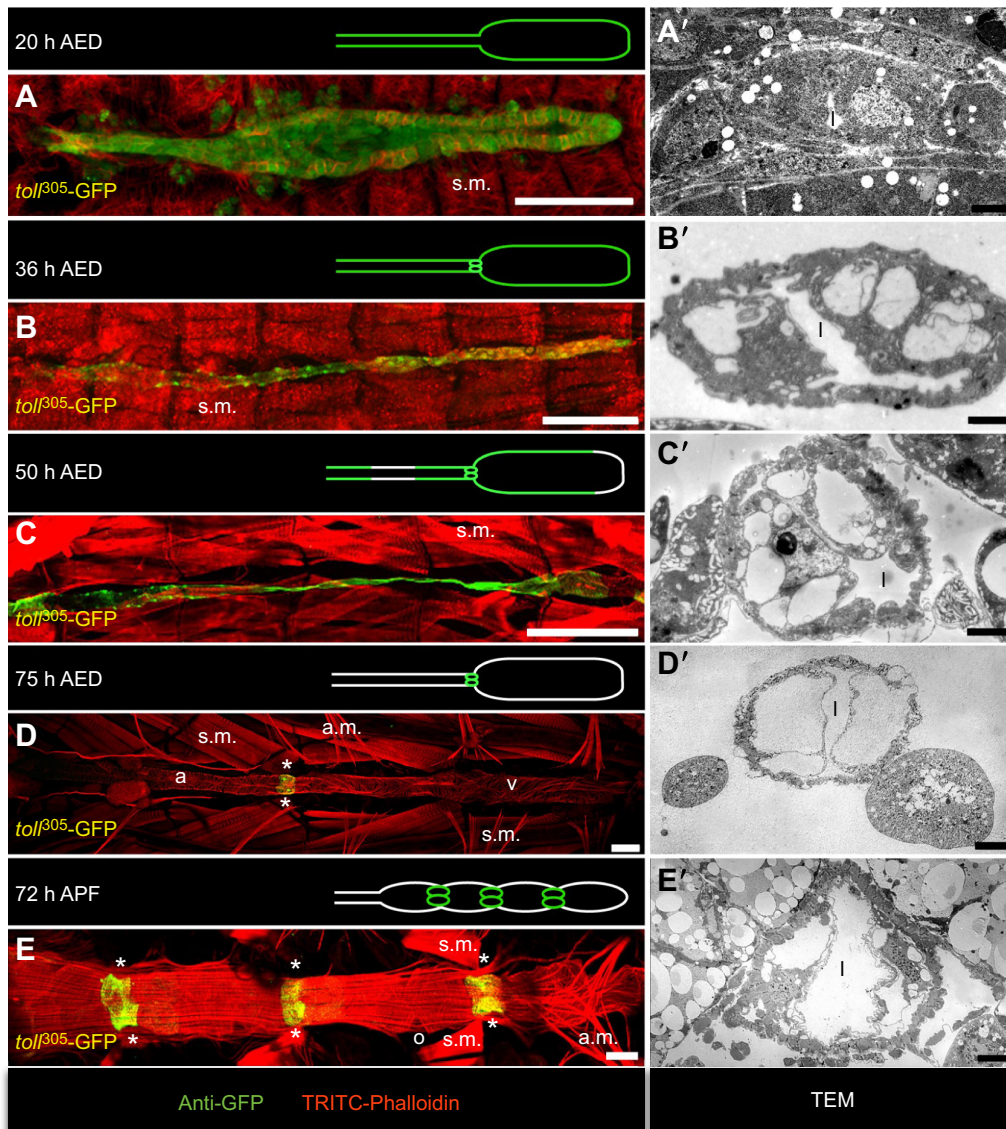


**Fig. 3.** *tol*-GFP expression in the heart and differentiation of intracardiac valve cells. (A–E) Pictures show the dorsal vessel of a stage 16 embryo (A), larvae (B–D) and an imago (E) stained for GFP (*tol*-GFP, green channel) and Phalloidin (red channel). The broad expression of the *tol*-GFP reporter in all cardiomyocytes of the embryo (A) and the first-instar larvae (B) vanishes in the second-instar larvae (C) and concentrates in the intracardiac valve cells in the third-instar larvae (D, asterisks) and the adult (E, asterisks). A'–E' show electron micrographs of cross-sectioned valve cells of specimens with the same age. At the ultrastructural level, the embryonic valve cells (A') are indistinguishable from adjacent cardiomyocytes, compared with Lehmacher et al. (2012). In the first-instar larvae (B'), intracellular vesicles arise and occupy most of the cell volume at the end of the third-instar larval stage (D'). Valve cells in the adult (E') display the same histology with respect to the valvosomes. In E', a cross section through the posterior valve cells is shown. a, aorta; AED, after egg laying; a.m., alary muscle; APF, after puparium formation; l, heart lumen; o, ostia; s.m., somatic muscle; v, ventricle. Scale bars: 50  $\mu$ m (A–E), 2.5  $\mu$ m (A'–C') and 10  $\mu$ m (D', E').

changes by a factor of two during one cardiac cycle. The nucleus, which is a less deformable compartment of the cell, dictates to some extent the shape of the cell in the closed state (e.g. Fig. 6). Because of the unique histology of the valve cells (see below), we consider two mechanisms that may allow the extensive shape changes: (i) the cell changes its shape upon contraction but keeps its volume constant, or (ii) the cells oscillate between a compressed and a relaxed state with variable volumes. To address these possibilities, we conducted immunostainings on third-instar larval hearts. We argue that the concomitant fixation arrests the valve cells either in the elongated, in the roundish or in an intermediate state. Subsequent stainings with anti-Spectrin antibodies and evaluation of randomly picked images were then used to reconstruct the valve

cells in 3D and to measure, by approximation, the volume of the cells. The corresponding results indicate that valve cell volume remains constant during contraction, suggesting that cell compression plays only a minor role, if any.

#### Identification of molecular markers to study differentiation of valve cells

The availability of molecular markers, antibodies or valve cell-specific reporter constructs represents a prerequisite for future studies on the differentiation and function of the intracardiac valves. To identify such markers, we screened a GFP protein trap-in collection available at the Kyoto DGGR Stock Center for larval heart and intracardiac valve cell expression. Furthermore, we



included publicly available transgenic GFP-reporter lines with expression in embryonic cardiomyocytes in our screening, arguing that GFP expression is presumably maintained in all or in a subset of heart cells throughout development. Finally, we analysed the expression of *rab* genes. We did this because our ultrastructural analysis of valve cells (see paragraphs below) revealed that the unique morphology of this cell type is established predominantly by huge vesicular structures within the cells. Since Rab proteins are key regulators of vesicle trafficking and turnover, participation of Rab family members in the formation of these vesicles appears likely.

Interestingly, our screening of publicly available GFP-reporter lines identified only one transgenic *Drosophila* line that exhibited very high GFP expression in larval and adult intracardiac valve cells and virtually no expression in other heart cells (Fig. 3). This particular line has been generated and described earlier by the

Schulz laboratory (Wang et al., 2005). It expresses GFP under the control of a 305 bp *toll* enhancer element in all cardiomyocytes of the embryonic dorsal vessel. We found that the broad embryonic *toll*-GFP expression diminishes during transition from the first- to second-instar larval stage (Fig. 3B,C) and is later upregulated in the valve cells of third-instar larval hearts (Fig. 3D). At this developmental stage, the two cells constituting the larval valve are the only cardiomyocytes with remarkable GFP expression. Valve cell-specific GFP expression in this line persists during metamorphosis, and in the adult fly all three pairs of valve cells are strongly labelled (Fig. 3E). Thus, *toll*<sup>305</sup>-GFP (*toll*-GFP herein) is an excellent marker to visualise the differentiation of valve cells in the larval and adult heart of living or fixed animals. Furthermore, this reporter line is highly beneficial in order to identify the position of the valve cells in histological studies, such as TEM analyses.

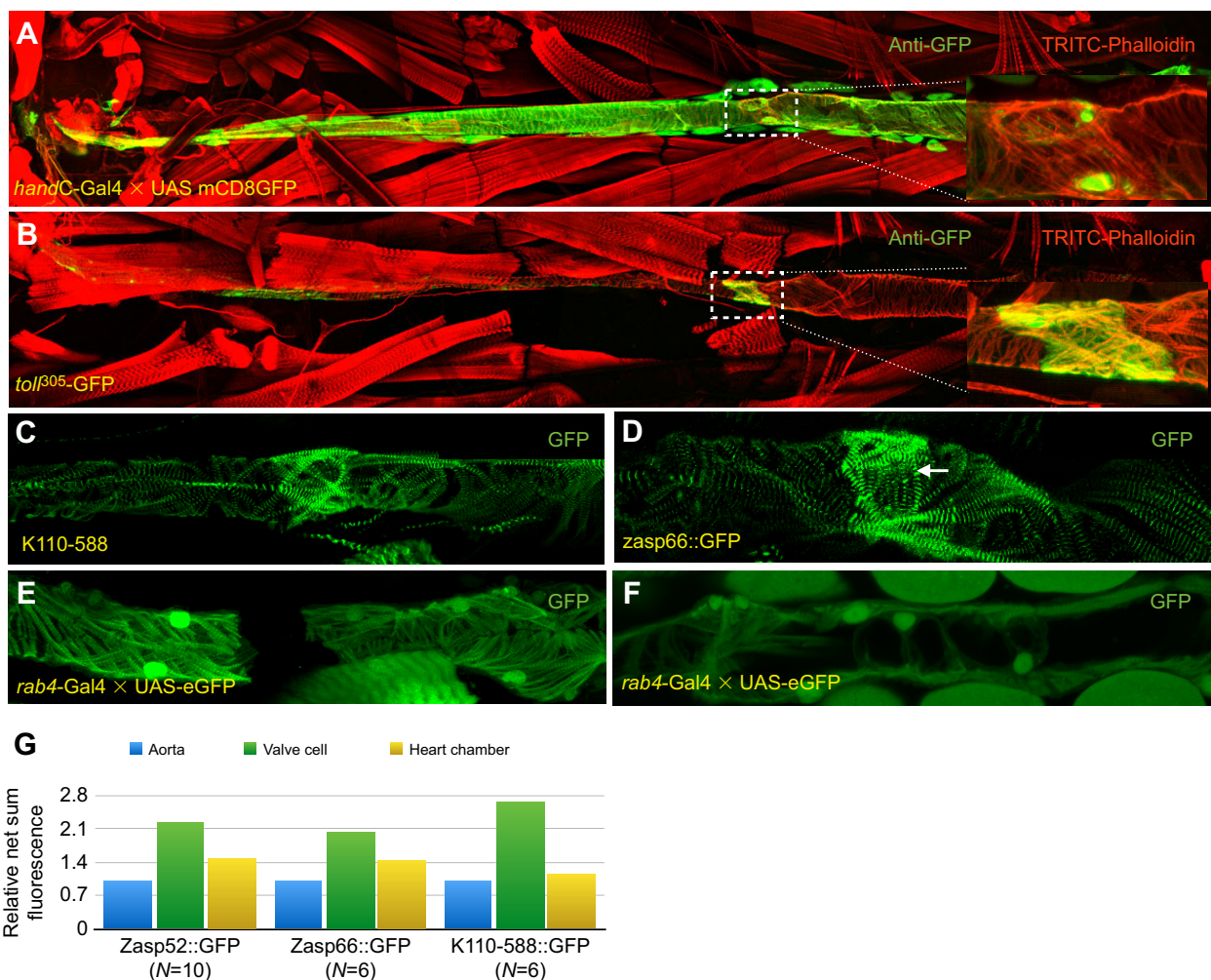


**Fig. 4. Markers for intracardiac valve cells in third-instar larvae.** (A) The cardiac valve cells of a third-instar larval heart show a higher density of actin-myosin filament network than the adjacent cardiomyocytes. To label all heart cells, *hand*-driven mCD8-GFP (green channel) was used. TRITC-coupled Phalloidin (red channel) was used to label actin filaments. (B) A 305 bp genomic fragment from the *toll* gene drives expression of the GFP reporter in the heart cells with very high peak expression in the valve cells (green channel). TRITC-Phalloidin was used to stain actin filaments (red channel). (C) The GFP protein trap line K110-588 (Morin et al., 2001) enables visualisation of the sarcomeres in cardiomyocytes and the somatic muscles. The valve cells display a higher number of sarcomeres than the adjacent cardiomyocytes. (D) The same result was obtained when analysing the GFP protein trap line K110-740 (Morin et al., 2001) in which the GFP is inserted into the *zasp66* gene. (E,F) GFP expression driven by *rab*-Gal4 enhancer lines. The *rab4* enhancer drives GFP strongly in all cardiomyocytes with the exception of the valve cells (E) whereas the *rab5* enhancer is active in all cardiomyocytes (F). (G) In total, 22 stacks with valve cells labelled for Zasp52::GFP ( $N=10$ ), Zasp66::GFP ( $N=6$ ) and K110-588 ( $N=6$ ) were processed with ImageJ using the 'sum slices' plug-in to calculate the net sum fluorescence intensity of all myofibres present in a valve cell (green), in a cardiomyocyte of the aorta (blue) and the heart chamber region (yellow). Density of myofibres is highest in valve cells.

Among the GFP protein trap lines (Morin et al., 2001), we identified several lines displaying GFP expression in sarcomeres of third-instar larval cardiomyocytes (Fig. 4C,D). Strongest expression in intracardiac valve cells was apparent in lines in which GFP is trapped to *Zasp52* (K110-621, not shown), CG14669 (K110-588, Fig. 4C) and *Zasp66* (K110-740, Fig. 4D). These lines were subsequently applied to characterise density and orientation of myofibres in valve cells.

We also analysed 27 lines in which the *gal4* gene was trapped to the open reading frame of one of the *Drosophila rab* encoding genes (Chan et al., 2011). Each line was crossed to a UAS-eGFP effector line and analysed for GFP expression within the hearts of third-instar larvae. We found several lines lacking any detectable cardiac-specific GFP fluorescence (*rab 3, 9, 10, 14, 19, 26, 27, 30, 32, 40, X4, X5, X6*) whereas another set of lines displayed GFP expression in all cardiomyocytes, including valve cells [*rab 1, 2, 5* (Fig. 4F), *6, 7, 8, 11, 23, 35, X1*]. Of note, certain *rab*-Gal4 lines exhibited a strongly reduced, presumably absent, level of GFP expression in valve cells, compared with the adjacent cardiomyocytes [*rab 4* (Fig. 4E), *18* (only some individuals), *21, 39* (only some individuals)]. The latter group of lines might be useful to express reporter genes or other transgenes in all cardiomyocytes, except for the valve cells.

#### Valve cells exhibit a unique myofibrillar architecture

It was described earlier that the intracardiac valves display an intense criss-cross meshwork of sarcomeres (Fig. 4A–D) that distinguishes them from all other cardiomyocytes (Lehmacher et al., 2012; Monier et al., 2005). To substantiate this initial observation, we investigated the orientation and density of myofibres in valve cells systematically using the GFP protein trap lines mentioned above. We used unfixed, dissected third-instar larval hearts from animals expressing *Zasp66::GFP*, *Zasp52::GFP* or *K110-588::GFP* to measure the volume fluorescence intensity of anterior- and posterior-located cardiomyocytes in comparison with valve cells by using the ‘sum slices’ plug-in of ImageJ. In contrast to the sum fluorescence intensity of cardiomyocytes of the aorta, which was arbitrarily set to 1, the sum fluorescence intensity of valve cells was increased 2.3-fold and the sum fluorescence intensity of cardiomyocytes of the posterior heart chamber was increased 1.4-fold (Fig. 4G). We conclude from these results that the valve cells, compared with other cardiomyocytes, are highly contractile, indicating that myogenic activity represents an important factor enabling the cells to perform the characteristic oscillating shape changes described above (Fig. 1D).

Next, we asked whether myofibres in valve cells display a similar orientation and meshwork structure compared with adjacent cardiomyocytes. Orientation of myofibres in dipteran heart cells is described as circular, which allows contraction of the heart tube and thereby haemolymph transport through the heart lumen (Angioy et al., 1999; Lehmacher et al., 2012; Wasserthal, 1999). However, in valve cells the orientation of myofibres often appeared reticulated. In addition, we found numerous myofibrils that extended from the cell membrane towards the luminal membrane of the valve cell [Fig. 4D (arrow)]. Myofibrils with such an orientation were not found in the adjacent cardiomyocytes. We postulate that the specific architecture of the myofibrillar network accounts for the characteristic contraction dynamics and shape changes valve cells perform during the diastolic and systolic phases of heart contraction.

Based on the observations described above, we speculated that contraction of myofibres, especially those that orientate perpendicular to the *a–p*-axis, converts the valve into the open

state, which is characterised by an elongated shape of the individual cells (Fig. 1A1–A4). This elongation and the concomitant withdrawal from the luminal space presumably results in a maximum flow rate of haemolymph through the valve. By contrast, relaxation of the valve’s myofibres might result in a roundish shape, promoted by the vesicular compartments of the valve cells, and thus closure of the heart lumen. To test this hypothesis, we added the  $\text{Ca}^{2+}$  chelator EGTA to semi-intact third-instar larvae in order to induce muscle relaxation (Fig. 2C,D). As expected, shortly after EGTA application (arrow in Fig. 2C) the heartbeat stopped. Significantly, adding EGTA also caused the valve cells to adopt a semi-roundish shape (Fig. 2D); thus, muscle tension indeed represents a key factor determining valve cell shape. The result that the heart lumen was not completely closed (Fig. 2D) is presumably due to the fact that the dissection procedure caused an impairment of the functional anatomy, e.g. disconnection of alary muscles and heart tube, which might be relevant to the correct histology and function of valve cells.

#### Valve cell differentiation starts post-embryonically with the formation of large vesicular compartments

The characteristic histology of the intracardiac valve cells in adult flies was already noticed by Miller (1950), Rizki (1978) and Zeitouni et al. (2007) and led to the description of valve cells as ‘spongy’ cells. The ‘spongy’ appearance is caused by large cavities or vesicles that can be visualised with bright-field illumination, immunohistochemistry or TEM (Figs 1, 3 and 5). In this study, we established the timepoint during development at which valve cells start to differentiate and to form their typical histology. Because the total number of cells that build the heart tube is the same in embryos and larvae, and neither cell death nor cell division takes place during this developmental period, valve cell progenitors must already be present in the embryonic heart. The larval valve is built by the 34th pair of cardiomyoblasts and we argue that, in the embryo, this pair of cardiomyoblasts represents the progenitor of the functional valve cells. TEM analyses of stage 16–17 embryos revealed that these prospective valve cells are histologically indistinguishable from adjacent cardiomyocytes at this stage of development (Fig. 3A’). Reference images for cardiomyocytes can be found elsewhere (Lehmacher et al., 2012). The first differences at the ultrastructural level between valve cells and adjacent cardiomyocytes became obvious in late first-instar larvae (about 36 h after egg laying). Some larger and several smaller membranous vesicles, occupying a large portion of the cell’s total volume, were abundant in the cytoplasm of the two prospective valve cells (Fig. 3B’). Interestingly, such vesicles were only present in valve cells and not in any adjacent cardiomyocytes of this or of later developmental stages. Incipient in second-instar larval stage and lasting until the end of the third-instar larval stage, the valve cells increase in size due to cell growth, and the characteristic vesicles mature into a small number of large vesicles, the valvosomes, which now occupy most of the cell’s volume (Fig. 3C’,D’). During metamorphosis, a second and a third pair of valve cells differentiate at defined positions within the heart, resulting in a total of three valves in the adult fly (Fig. 3E) (Lehmacher et al., 2012; Sellin et al., 2006; Tang et al., 2014; Zeitouni et al., 2007). These adult valve cells also harbour the characteristic large vesicles, indicating that the functional anatomy of larval and adult valve cells is, in principle, the same.

Observations from live imaging (Fig. 1; Movies 1, 2A, 2B, 2C and 3), TEM, as well as previous work (Miller, 1950) clearly indicate that the large vesicles, which occupy most of the valve cell volume, represent an important structural element that defines the

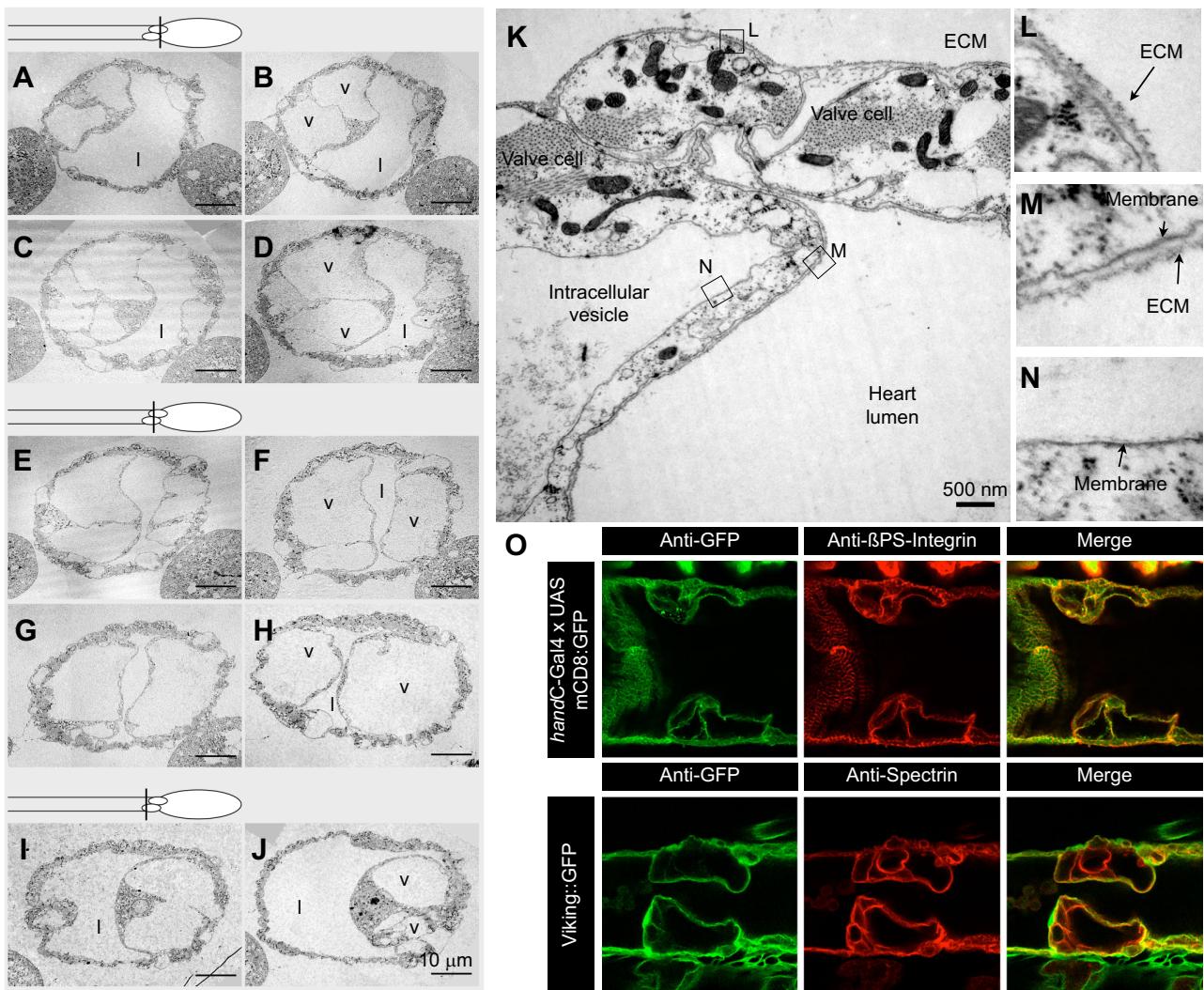


**Fig. 5. Ultrastructure of valve cell.** (A–J) Selected ultra-thin cross sections taken from a series of 70-nm sections through the valve cells of third-instar larvae of wild type (WT). The three schemes illustrate the corresponding position in the heart, respectively. A is from the posterior and J from the anterior. (K) A cross section through an intracardiac valve cell at high magnification. Shown is the dorsal adhesive zone where the two opposite valve cells meet. ECM is detectable on the cell membrane facing the body cavity (L) and on the cell membrane facing the cardiac lumen (M) but is nearly absent on the inner side of the vesicle membrane (N). (O) Illustrates the membranous nature of the valve's vesicles. The upper row shows anti-GFP (green) and anti- $\beta$ PS-Integrin (red) staining of valve cells. Note that mCD8::GFP and Integrin label the vesicles. The bottom row shows anti-GFP (green) and anti-Spectrin (red) staining of valve cells. GFP is expressed as a Collagen::GFP fusion protein (Viking::GFP) and is not detectable at the vesicles whereas Spectrin clearly outlines these organelles. l, lumen; v, vesicle.

shape (and probably also the function) of the valve cell. To verify this hypothesis, we analysed the larval valve cells at lower (Fig. 5A–J) and higher (Fig. 5K–N) magnification using ultra-thin serial sections for TEM analysis. Three-dimensional reconstruction of the cells revealed that 50–80% of their volume is occupied by the cavities (Lehmacher et al., 2012, and this study) – a result supporting the assumption that the cavities represent important structural elements. Their membranous nature is verified by two independent approaches. First, we analysed cross sections at higher magnification with TEM (Fig. 5K–N) and found that the intracellular cavities are essentially extracellular matrix (ECM)-free membranous structures (Fig. 5N). By contrast, the cell membranes, which face the body cavity of the animal or the cardiac lumen, are decorated with electron-dense ECM (Fig. 5L,M). In addition, we stained the valve cells of larvae with antibodies that recognise either Spectrin, a cytoskeletal protein that lines the intracellular side of plasma membranes, or  $\beta$ PS-Integrin, a protein

that assembles into membrane-spanning heterodimers (Fig. 5O). For co-staining, we used either mCD8 to label membranes or Viking::GFP, which labels CollagenIV, an ECM protein (Fig. 5O). Anti- $\beta$ PS-Integrin and anti-Spectrin antibodies both recognised epitopes lining the large cavities inside the valve cells, indicating the membranous nature of these structures (Fig. 5O). This finding is further supported by co-localisation with membrane-associated mCD8-GFP expressed under the control of the cardiac-specific *handC-Gal4* driver [Fig. 5O (upper row)] (Paululat and Heinisch, 2012; Sellin et al., 2006). Our results are in agreement with a previous analysis (Lehmacher et al., 2012) that also described the membranous nature of the cavities (Fig. 5K–N). To visualise the presence or absence of ECM proteins at the membranes of the cavities, we used protein traps for Trol/Perlecan (Trol::GFP) or CollagenIV (Viking::GFP, shown herein). We found that the respective matrix proteins are not detectable at the inner surface of the cavities [Fig. 5O (bottom row)], indicating the absence of

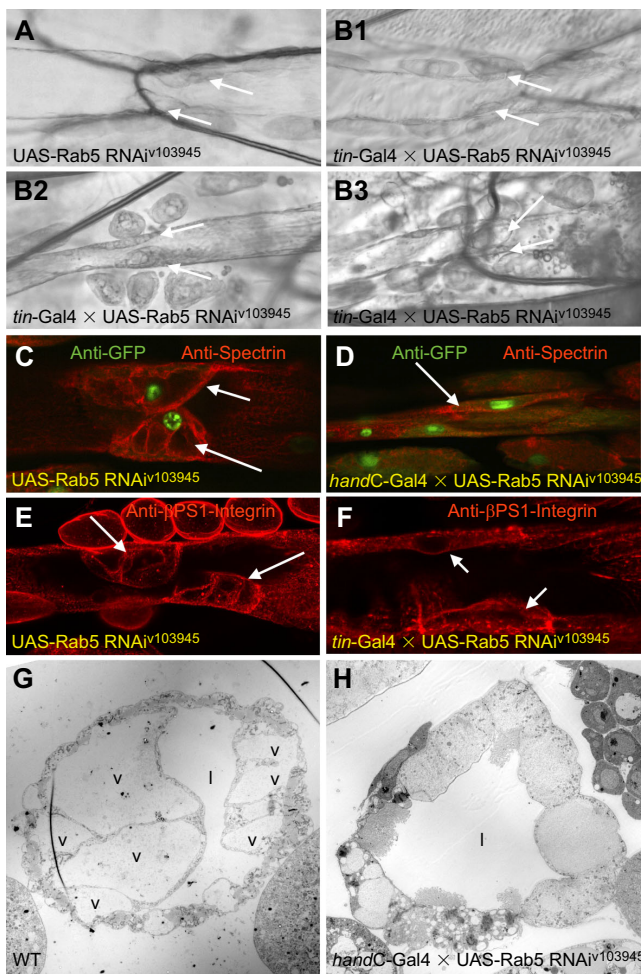


**Fig. 6. RNAi-mediated phenotypes in valve cells.** (A and B) Selected single frames from recordings captured at 200 frames  $s^{-1}$ . (A) Illustrates the valve cells from an animal with the genotype *yw*; *UAS-Rab5 RNAi<sup>103945</sup>* (control). (B1–B3) Show the valve cells in three different animals with the genotype *yw*; *tin-Gal4*; *UAS-Rab5 RNAi<sup>103945</sup>*. The valve cells lack their typical histology and overall appearance. (C) The heart of a third-instar larva with the genotype *yw*; *handC-Gal4*; *handC-GFP*, stained for anti-GFP (nuclei of all cardiomyocytes) and anti-Spectrin (outlines the cell membrane) (maximum projection). The typical histology of the valve cells is seen. (D) The heart of a third-instar larva with the genotype *yw*; *handC-Gal4*; *handC-GFP*, *UAS-Rab5 RNAi<sup>103945</sup>*, stained for anti-GFP (nuclei of all cardiomyocytes) and anti-Spectrin (outlines the cell membrane) (maximum projection). Downregulation of Rab5 inhibits valve cell differentiation. The typical histology is not visible. (E) The heart of a third-instar larva with the genotype *yw*; *UAS-Rab5 RNAi<sup>103945</sup>* (control), stained for anti- $\beta$ PS1-Integrin (maximum projection). Both valve cells with their characteristic appearance are recognisable. (F) The heart of a third-instar larva with the genotype *yw*; *tin-Gal4*; *UAS-Rab5 RNAi<sup>103945</sup>*, stained for anti- $\beta$ PS1-Integrin (maximum projection). Downregulation of Rab5 results in inhibition of valve cell differentiation. Ultra-thin cross sections of valve cells from wild type (WT) (G) and from animals in which Rab5 was downregulated (H) were analysed using transmission electron microscopy (TEM). Mutant valve cells lack the characteristic large membranous vesicle free of material and display several additional abnormalities. Knockdown specificity was tested using two independent RNAi lines, with the following results: *tin-Gal4*×*UAS-RNAi<sup>34096</sup>* gives rise to 20% of animals with valve cell abnormalities, *tin-Gal4*×*UAS-RNAi<sup>103945</sup>* results in 64% of animals with valve cell abnormalities. (A–F) White arrows point to valve cells. l, lumen; v, vesicle.

ECM material inside the valve cavities. By definition, membranous vesicles within a cell are assigned to certain types of organelles that exert diverse functions in metabolism, trafficking or storage. The

large vesicles described herein represent yet unassigned, unique cellular microcompartments. Because of their exclusive appearance in valve cells, we named these vesicles ‘valvosomes’ and suggest the designation for future use.

### Downregulation of *rab5* results in valve cells with aberrant vesicle content

The giant vesicles present in valve cells may arise *de novo* as derivatives of the Golgi apparatus (like lysosomes), upon endocytosis (like endosomes), upon membrane invagination (like pinosomes) or as a result of a combination of these processes, including vesicle fusion, which may predominantly account for the increase in size of the valvosomes upon larval development. As a proof-of-principle approach, we inhibited vesicle turnover and endosome maturation in particular by inducing RNAi-mediated downregulation of *rab5* expression. The *rab5* gene is expressed in all cardiomyocytes, including the intracardiac valve cells (Fig. 4). We chose Rab5 as a target because it was shown that inactivation of the protein inhibits a broad range of early endocytic events (Somsel Rodman and Wandinger-Ness, 2000). To ensure knockdown specificity, we analysed two independent *rab5*-RNAi constructs (IR34096, IR103945). Both lines display WT intracardiac valve cells. However, when crossed to a heart-specific Gal4 driver line – here we used *tin-Gal4* – the third-instar larval offspring displayed severely mis-differentiated valve cells (Fig. 6). Typically, downregulation of *rab5* resulted in smaller valve cells. Yet, the extent of the phenotype was variable and ranged between cells that were only slightly reduced in size to valve cells that were nearly indistinguishable from the adjacent cardiomyocytes (Fig. 6B1–B3, D and F). In addition, while in most cases both valve cells were affected, we also found animals where only one cell was reduced in size. Of note, the reduced size of the valve cells was caused primarily by absence or malformation of the valvosomes (Fig. 6). We are aware of the fact that downregulation of *rab5* may induce a broad range of effects on cell differentiation and cell physiology. Nevertheless, reduction or absence of valvosomes in valve cells as a result of *rab5* knockdown indicates that endocytotic processes are crucial to valve cell differentiation. Characterising these processes in detail will be a major task of future investigations.

### DISCUSSION

Fluid flow in biological tubes is a fundamental phenomenon for which a variety of solutions has evolved in animals. In many cases, flow directionality is ensured by the presence of valves or gate-like barriers that prevent backflow. Biological tubes with such barriers include, e.g. renal tubes, lymphatic vessels, the digestive tract and the circulatory system. Valves enhance the efficiency of directional flow and thereby the organ’s overall performance. Despite the simple tube-like architecture of the *Drosophila* heart, numerous studies have demonstrated the suitability of the fly heart to investigate physiology and genetics of cardiogenesis, and cardiac function in general. In contrast to the vertebrate heart, the *Drosophila* cardiac system is not coupled to oxygen transport, and heart failure does not result in immediate death. Nevertheless, flies with certain genetic defects in cardiac development and function suffer from reduced fitness and longevity (e.g. Drechsler et al., 2013; Ocorr et al., 2007). However, specific manipulations of the cardiac ECM may increase longevity (Sessions et al., 2016). Since severe malformations of the heart, or even a complete non-functional heart, do not necessarily result in lethality, consequences of severe heart malformations or heart failure can be examined in living animals. This established *Drosophila* as an ideal model for

studying heart development and physiology. Herein, we focused on the analysis of the intracardiac valve in *Drosophila*. Although known for a long time, the respective cells have not been studied in detail. We now characterised the histology, presented molecular markers for future in-depth studies, included functional data, and used RNAi-mediated gene knockdown to investigate formation and differentiation of the intracardiac valve cells.

### Intracardiac valve cells regulate the directionality of haemolymph flow inside the heart tube

The pumping activity of the tubular heart in insects ensures haemolymph circulation within the open body cavity. The directionality of haemolymph flow is thought to be regulated by distinct anatomical features of the heart tube. One is represented by flap-like cells – the ostia – that constitute the inflow tract, through which the haemolymph enters the heart lumen. A single ostia is built by two flap-like cells. In total, the *Drosophila* heart harbours six (larvae) or 10 (adult) functional ostia that regulate the inflow of haemolymph into the heart proper (Hetz et al., 1999; Iklé et al., 2008; Lehmacher et al., 2012; Molina and Cripps, 2001; Ryan et al., 2005). In larvae, the ostia allow haemolymph to enter the heart during diastole and prevent, due to their flap-like histology, backflow from the heart proper into the body cavity during systole. When haemolymph enters the heart, only the heart proper is filled, indicating that a barrier situated between the heart proper and the anterior aorta ensures efficient refilling. This barrier is constituted by the intracardiac valve, which represents a second anatomical structure preventing backflow and which has been analysed in detail in the present study. The intracardiac valve consists of two histologically unique cells. During each cardiac cycle, the shape of these two intracardiac valve cells oscillates between an elongated and a roundish appearance (Fig. 1A and D). While elongated, the heart lumen stays largely open and allows haemolymph streaming from the heart chamber towards the aorta (Figs 1 and 2). By the end of the systolic phase, the valve cells become roundish and touch each other (Fig. 1A,B). At that time, the transition between the heart chamber and the aorta is closed. The contact time of the two valve cells spans about 1/4–1/3 of a complete cardiac cycle (Fig. 1C). Treatment of hearts of dissected third-instar larvae with EGTA, which induces relaxation of myofibres, causes the valve cells to adopt a semi-roundish shape (Fig. 2C,D). This indicates that valve cells, which exhibit a higher density as well as a special arrangement of myofibres compared with the adjacent cardiomyocytes (Fig. 4), elongate upon contraction and become roundish upon relaxation. This direct interconnection between muscle tension and cell shape is remarkable, because it represents a highly robust and effective means to couple heart contraction with valve opening. While the valve cells are likely to be affected by the same contraction wave as the adjacent cardiomyocytes, the individual arrangements of myofibres result in distinct, yet concerted, responses of the two cell types. The unique histology of the valve cells, which we consider the basis for the highly flexible shape of the cells, is discussed below.

Unidirectionality of haemolymph streaming requires an intact body anatomy. We injected microparticles into the bodies of dissected and intact animals to demonstrate flow properties and valve cell functionality. The speed at which the injected particles move inside the heart lumen is about the same in intact and dissected animals (Fig. 2A,B and E). Calculation of the *Re* indicates that free streaming inside the heart tube follows the rules of laminar flow. Slow streaming velocities are seen in close proximity to the valve

cells upon heart lumen closure. Of note, in dissected animals the net flow of haemolymph is quite low due to the fact that haemolymph streams forwards and backwards. This effect is most likely caused by an inefficient filling phase of the heart proper (Figs 1 and 2; Movie 1). However, injection of microparticles into intact animals clearly demonstrated that haemolymph flow is unidirectional (anterograde) (Fig. 2E; Movies 2A, 2B and 2C). Thus, our results demonstrate that an intact anatomy is crucial to an efficient anterograde haemolymph flow inside the heart and therefore to efficient circulation within the insect.

### Differentiation of the intracardiac valve

Intracardiac valve cells have been identified due to their unique histology in the larval as well as the adult *Drosophila* heart (Figs 1–3) (Lehmacher et al., 2012; Miller, 1950; Rizki, 1978; Tang et al., 2014; Zeitouni et al., 2007). In third-instar larvae, one intracardiac valve separates the heart into the anterior aorta and the posterior heart chamber (Fig. 3D). This pair of valve cells persists during pupal development and constitutes the third valve of the adult heart. Two additional valves differentiate from the 22nd and the 28th pair of cardiomyocytes, giving rise to a total of three valves subdividing the adult heart into four separate sections (Fig. 3E). In a candidate screening, we identified several molecular markers that allow identification of valve cells in living or fixed specimens. However, only one reporter line, *toll*-GFP, shows a very strong reporter gene expression in the valve cells of third-instar larvae, pupae and adult flies (Fig. 3). This line, which was generated and described previously (Wang et al., 2005), was subsequently used to label valve cells in animals, e.g. for TEM analysis. Several GFP protein trap lines, predominantly obtained from the collection at Kyoto (Morin et al., 2001), helped to elucidate the unique structure of valve cells. For example, *Zasp52::GFP* and *Zasp66::GFP* lines mark the sarcomeres in living cells (Fig. 4C,D). Density and orientation of myofibres differ in valve cells compared with adjacent cardiomyocytes. As stated above, we consider especially the orientation of the myofibres essential to the oscillating shape changes of valve cells. Orientation of myofibres perpendicular to the *a-p*-axis of the heart tube most likely results in *a-p* elongation of the valve cells upon contraction. Indeed, applying EGTA to hearts caused relaxation and a semi-roundish (more relaxed) shape of the valve cells (Fig. 2D). We propose a model in which the density and orientation of the myofibres present in the valve cells are crucial to valve cell functionality. Upon contraction, the valve cells convert from a roundish into a flattened shape, which converts the heart lumen from a closed to an open state.

Our TEM analysis (Figs 3 and 5) revealed that valve cell differentiation initiates post-embryonically. Valve cells become histologically distinguishable from the adjacent cardiomyocytes no earlier than in the late 1st-instar larval stage, when the differentiating valve cells start to adopt a unique shape with an expansion towards the heart luminal space (Fig. 3). During second- and third-instar larval development, the valve cells display some characteristic features that turned out to be unique to this cell type: (i) a periodical heartbeat-dependent change between an elongated and a roundish shape, (ii) a more intense myofibre network and a distinct myofibre orientation compared with adjacent cardiomyocytes, and (iii) the appearance of large membranous vesicles that occupy most of the cell volume.

We assume that in fully functional valve cells the large vesicles provide a unique structural element, which allows the cells to easily flatten upon contraction and to effectively expand upon relaxation, thereby opening and closing the luminal space of the heart tube. RNAi-mediated downregulation of *rab5* in valve cells resulted in

cells that failed to adopt the typical roundish shape (Fig. 6B,D,F,H). Besides general cellular defects, *rab5* downregulation affects the formation of the described large vesicles (Fig. 6D,F,H). This result indicates that endosomal maturation plays a major role in valve cell differentiation, which needs to be studied further in the future. Preliminary analyses showed that animals lacking fully differentiated valve cells display problems with sealing the heart lumen during a cardiac cycle. However, there are still no clear data on how this impairment affects streaming properties within the heart. To address this issue, we are currently working on optimising particle injection into living mutant animals, with the aim of reliably visualising haemolymph streaming inside the heart. Several methods have been applied to analyse pumping activity of the heart in adult *Drosophila* (Choma et al., 2010), prepupal *Drosophila* (Drechsler et al., 2013) and adult *Anopheles* (Glenn et al., 2010), but these methods lack the possibility of tracking individual particle movements inside the heart lumen. It will thus be interesting to analyse how mutant valve cells modulate hydrodynamic parameters, such as velocity and directionality of haemolymph flow, *in vivo*.

### ***Drosophila* intracardiac valve cells and mammalian endocardial cushion cells**

Cardiac valves in *Drosophila* and in the mammalian heart have the same function that is the regulation of flow directionality. This function however is achieved by a different histology: single cells harbouring large intracellular vesicles (valvosomes) that support cell shape changes in the *Drosophila* system, and multicellular valves that originate from valve endothelial cells (VECs) and valve interstitial cells (VICs) that produce matrix-rich cushions in the vertebrate embryo (Wu et al., 2017). Interestingly, VEGF/PDGF signalling plays a role in the formation of the adult intracardiac valves in *Drosophila* and also in endocardial cushion formation and valve remodeling in mammals (Zeitouni et al., 2007). For none of the mammalian valve models the existence of huge intracellular membranous vesicles (valvosomes) was described. Thus, this feature is presumably unique to the simple single cell valve model. Nevertheless, striking similarities between *Drosophila* and mammalian valves are obvious on the molecular level (VEGF/PDGF pathway) and on the functional level (regulating unidirectional flow).

In conclusion, our work describes the function and significance of intracardiac valve cells and provides first insights into the differentiation and histology of these important cells. Thus, it represents a valuable basis for future studies aiming to understand the development and the mode of operation in more detail.

### **Acknowledgements**

We thank Robert A. Schulz for providing fly stocks. We acknowledge K. Etzold and W. Mangerich for their invaluable assistance with TEM analyses and Mechthild Krabusch and Martina Biedermann for technical assistance. Furthermore we thank Sara Timm, Bianca Esch, Franz Kahlich, Kristina Rauf and Martin Schwärzel for additional help.

### **Competing interests**

The authors declare no competing or financial interests.

### **Author contributions**

Conceptualization, A.P., E.A. and H.M.; Methodology, K.L.; Investigation, K.L., B.A., M.H., C.L., O.E.P.; Writing - Original Draft, A.P.; Writing - Review & Editing, A.P. and H.M.; Supervision, E.A., H.M. and A.P. Project Administration, A.P.; Funding Acquisition, E.A. and A.P.

### **Funding**

This work was supported by grants from the Deutsche Forschungsgemeinschaft to A.P. (SFB 944), the Deutscher Akademischer Austauschdienst (IPID program) and

from the State of Lower-Saxony (ZN2832). B.A. received a fellowship from the State of Lower-Saxony (Lichtenberg-Stipendium). E.A. was supported by grants from the Ministerio de Economía y Competitividad [SAF2013-48759-P] and the Principado de Asturias [GRUPIN14-012].

### **Supplementary information**

Supplementary information available online at <http://jeb.biologists.org/lookup/doi/10.1242/jeb.156265.supplemental>

### **References**

- Albrecht, S., Wang, S., Holz, A., Bergter, A. and Paululat, A. (2006). The ADAM metalloprotease Kuzbanian is crucial for proper heart formation in *Drosophila melanogaster*. *Mech. Dev.* **123**, 372–387.
- Albrecht, S., Altenhein, B. and Paululat, A. (2011). The transmembrane receptor Uncoordinated5 (*Unc5*) is essential for heart lumen formation in *Drosophila melanogaster*. *Dev. Biol.* **350**, 89–100.
- Alex, A., Li, A., Tanzi, R. E. and Zhou, C. (2015). Optogenetic pacing in *Drosophila melanogaster*. *Sci. Adv.* **1**, e1500639.
- Andersen, J. L., MacMillan, H. A. and Overgaard, J. (2015). Temperate *Drosophila* preserve cardiac function at low temperature. *J. Insect Physiol.* **77**, 26–32.
- Angjoo, A. M., Boassa, D. and Dulcis, D. (1999). Functional morphology of the dorsal vessel in the adult fly *Protophormia terraenovae* (Diptera, Calliphoridae). *J. Morphol.* **240**, 15–31.
- Armstrong, E. J. and Bischoff, J. (2004). Heart valve development: endothelial cell signaling and differentiation. *Circ. Res.* **95**, 459–470.
- Bazigou, E., Lyons, O. T. A., Smith, A., Venn, G. E., Cope, C., Brown, N. A. and Makinen, T. (2011). Genes regulating lymphangiogenesis control venous valve formation and maintenance in mice. *J. Clin. Invest.* **121**, 2984–2992.
- Chan, C.-C., Scoggin, S., Wang, D., Cherry, S., Dembo, T., Greenberg, B., Jin, E. J., Kuey, C., Lopez, A., Mehta, S. Q. et al. (2011). Systematic discovery of Rab GTPases with synaptic functions in *Drosophila*. *Curr. Biol.* **21**, 1704–1715.
- Chintapalli, R. T. V. and Hillyer, J. F. (2016). Hemolymph circulation in insect flight appendages: physiology of the wing heart and circulatory flow in the wings of the mosquito *Anopheles gambiae*. *J. Exp. Biol.* **219**, 3945–3951.
- Choma, M. A., Suter, M. J., Vakoc, B. J., Bouma, B. E. and Tearney, G. J. (2010). Heart wall velocimetry and exogenous contrast-based cardiac flow imaging in *Drosophila melanogaster* using Doppler optical coherence tomography. *J. Biomed. Opt.* **15**, 056020.
- Choma, M. A., Suter, M. J., Vakoc, B. J., Bouma, B. E. and Tearney, G. J. (2011). Physiological homology between *Drosophila melanogaster* and vertebrate cardiovascular systems. *Dis. Model. Mech.* **4**, 411–420.
- Dietzl, G., Chen, D., Schnorrer, F., Su, K.-C., Barinova, Y., Fellner, M., Gasser, B., Kinsey, K., Oettel, S., Scheiblaue, S. et al. (2007). A genome-wide transgenic RNAi library for conditional gene inactivation in *Drosophila*. *Nature* **448**, 151–156.
- Drechsler, M., Schmidt, A. C., Meyer, H. and Paululat, A. (2013). The conserved ADAMTS-like protein lonely heart mediates matrix formation and cardiac tissue integrity. *PLoS Genet.* **9**, e1003616.
- Fang, J., Dagenais, S. L., Erickson, R. P., Arlt, M. F., Glynn, M. W., Gorski, J. L., Seaver, L. H. and Glover, T. W. (2000). Mutations in *FOXO2* (*MFH-1*), a forkhead family transcription factor, are responsible for the hereditary lymphedema-distichiasis syndrome. *Am. J. Hum. Genet.* **67**, 1382–1388.
- Fink, M., Callol-Massot, C., Chu, A., Ruiz-Lozano, P., Izpisua Belmonte, J. C., Giles, W., Bodmer, R. and Ocorr, K. (2009). A new method for detection and quantification of heartbeat parameters in *Drosophila*, zebrafish, and embryonic mouse hearts. *BioTechniques* **46**, 101–113.
- Glenn, J. D., King, J. G. and Hillyer, J. F. (2010). Structural mechanics of the mosquito heart and its function in bidirectional hemolymph transport. *J. Exp. Biol.* **213**, 541–550.
- Gu, G.-G. and Singh, S. (1995). Pharmacological analysis of heartbeat in *Drosophila*. *J. Neurobiol.* **28**, 269–280.
- Hallier, B., Hoffmann, J., Roeder, T., Tögel, M., Meyer, H. and Paululat, A. (2015). The bHLH transcription factor Hand regulates the expression of genes critical to heart and muscle function in *Drosophila melanogaster*. *PLoS ONE* **10**, e0134204.
- Hetz, S. K., Psota, E. and Wasserthal, L. T. (1999). Roles of aorta, ostia and tracheae in heartbeat and respiratory gas exchange in pupae of *Troides rhadamantus* Staudinger 1888 and *Ornithoptera priamus* L. 1758 (Lepidoptera, Papilionidae). *Int. J. Insect Morphol. Embryol.* **28**, 131–144.
- Iklé, J., Elwell, J. A., Bryantsev, A. L. and Cripps, R. M. (2008). Cardiac expression of the *Drosophila* Transglutaminase (*CG7356*) gene is directly controlled by myocyte enhancer factor-2. *Dev. Dyn.* **237**, 2090–2099.
- League, G. P., Onuh, O. C. and Hillyer, J. F. (2015). Comparative structural and functional analysis of the larval and adult dorsal vessel and its role in hemolymph circulation in the mosquito *Anopheles gambiae*. *J. Exp. Biol.* **218**, 370–380.
- Lehmacher, C., Tögel, M., Pass, G. and Paululat, A. (2009). The *Drosophila* wing hearts consist of syncytial muscle cells that resemble adult somatic muscles. *Arthropod. Struct. Dev.* **38**, 111–123.

- Lehmacher, C., Abeln, B. and Paululat, A.** (2012). The ultrastructure of *Drosophila* heart cells. *Arthropod. Struct. Dev.* **41**, 459-474.
- Medioni, C., Astier, M., Zmojdian, M., Jagla, K. and Sémériva, M.** (2008). Genetic control of cell morphogenesis during *Drosophila melanogaster* cardiac tube formation. *J. Cell Biol.* **182**, 249-261.
- Medioni, C., Sénatore, S., Salmand, P.-A., Lalevéé, N., Perrin, L. and Sémériva, M.** (2009). The fabulous destiny of the *Drosophila* heart. *Curr. Opin. Genet. Dev.* **19**, 518-525.
- Miller, A.** (1950). The internal anatomy and histology of the imago. In *Biology of Drosophila* (ed. M. Demerec), pp. 420-534. New York: John Wiley & Sons, Inc.
- Molina, M. R. and Cripps, R. M.** (2001). Ostia, the inflow tracts of the *Drosophila* heart, develop from a genetically distinct subset of cardial cells. *Mech. Dev.* **109**, 51-59.
- Monier, B., Astier, M., Sémériva, M. and Perrin, L.** (2005). Steroid-dependent modification of Hox function drives myocyte reprogramming in the *Drosophila* heart. *Development* **132**, 5283-5293.
- Morin, X., Daneman, R., Zavortink, M. and Chia, W.** (2001). A protein trap strategy to detect GFP-tagged proteins expressed from their endogenous loci in *Drosophila*. *Proc. Natl. Acad. Sci. USA* **98**, 15050-15055.
- Ocorr, K., Akasaka, T. and Bodmer, R.** (2007). Age-related cardiac disease model of *Drosophila*. *Mech. Ageing Dev.* **128**, 112-116.
- Ocorr, K., Vogler, G. and Bodmer, R.** (2014). Methods to assess *Drosophila* heart development, function and aging. *Methods* **68**, 265-272.
- Paululat, A. and Heinisch, J. J.** (2012). New yeast/*E. coli*/*Drosophila* triple shuttle vectors for efficient generation of *Drosophila* P element transformation constructs. *Gene* **511**, 300-305.
- Rasband, W. S.** (1997-2016). *ImageJ*. Bethesda, Maryland, USA: U. S. National Institutes of Health. <http://imagej.nih.gov/ij/>.
- Ray, V. M. and Dowse, H. B.** (2005). Mutations in and deletions of the Ca<sup>2+</sup> channel-encoding gene *cacophony*, which affect courtship song in *Drosophila*, have novel effects on heartbeating. *J. Neurogenet.* **19**, 39-56.
- Rizki, T. M.** (1978). The circulatory system and associated cells and tissues. In *The Genetics and Biology of Drosophila*, Vol. 2b (ed. M. Ashburner and T. R. F. Wright), pp. 397-452. New York, NY: Academic Press.
- Rotstein, B. and Paululat, A.** (2016). On the morphology of the *Drosophila* heart. *J. Cardiovas. Dev. Dis.* **3**, 15.
- Ryan, K. M., Hoshizaki, D. K. and Cripps, R. M.** (2005). Homeotic selector genes control the patterning of seven-up expressing cells in the *Drosophila* dorsal vessel. *Mech. Dev.* **122**, 1023-1033.
- Sanyal, S., Jennings, T., Dowse, H. and Ramaswami, M.** (2006). Conditional mutations in SERCA, the Sarco-endoplasmic reticulum Ca(2+)-ATPase, alter heart rate and rhythmicity in *Drosophila*. *J. Comp. Physiol. B* **176**, 253-263.
- Sellin, J., Albrecht, S., Kölsch, V. and Paululat, A.** (2006). Dynamics of heart differentiation, visualized utilizing heart enhancer elements of the *Drosophila melanogaster* bHLH transcription factor Hand. *Gene Expr. Patterns* **6**, 360-375.
- Sénatore, S., Rami Reddy, V., Sémériva, M., Perrin, L. and Lalevéé, N.** (2010). Response to mechanical stress is mediated by the TRPA channel painless in the *Drosophila* heart. *PLoS Genet.* **6**, e1001088.
- Sessions, A. O., Kaushik, G., Parker, S., Raedschelders, K., Bodmer, R., Van Eyk, J. E. and Engler, A. J.** (2016). Extracellular matrix downregulation in the *Drosophila* heart preserves contractile function and improves lifespan. *Matrix Biol.* **1**, 1-13.
- Sláma, K. and Farkaš, R.** (2005). Heartbeat patterns during the postembryonic development of *Drosophila melanogaster*. *J. Insect Physiol.* **51**, 489-503.
- Somsel Rodman, J. and Wandinger-Ness, A.** (2000). Rab GTPases coordinate endocytosis. *J. Cell Sci.* **113**, 183-192.
- Tang, M., Yuan, W., Bodmer, R., Wu, X. and Ocorr, K.** (2014). The role of Pygopus in the differentiation of intracardiac valves in *Drosophila*. *Genesis* **52**, 19-28.
- Tögel, M., Pass, G. and Paululat, A.** (2008). The *Drosophila* wing hearts originate from pericardial cells and are essential for wing maturation. *Dev. Biol.* **318**, 29-37.
- Vogler, G. and Ocorr, K.** (2009). Visualizing the beating heart in *Drosophila*. *J. Vis. Exp.* **28**, 1425.
- Wang, J., Tao, Y., Reim, I., Gajewski, K., Frasch, M. and Schulz, R. A.** (2005). Expression, regulation, and requirement of the Toll transmembrane protein during dorsal vessel formation in *Drosophila melanogaster*. *Mol. Cell. Biol.* **25**, 4200-4210.
- Wasserthal, L. T.** (1999). Functional morphology of the heart and of a new cephalic pulsatile organ in the blowfly *Calliphora vicina* (Diptera: Calliphoridae) and their roles in hemolymph transport and tracheal ventilation. *Int. J. Insect Morphol. Embryol.* **28**, 111-129.
- Wessells, R. J. and Bodmer, R.** (2007). Age-related cardiac deterioration: insights from *Drosophila*. *Front. Biosci.* **12**, 39-48.
- Wu, M. and Sato, T. N.** (2008). On the mechanics of cardiac function of *Drosophila* embryo. *PLoS ONE* **3**, e4045.
- Wu, B., Wang, Y., Xiao, F., Butcher, J. T., Yutzey, K. E. and Zhou, B.** (2017). Developmental mechanisms of aortic valve malformation and disease. *Annu. Rev. Physiol.* **79**, 21-41.
- Zaffran, S., Reim, I., Qian, L., Lo, P. C., Bodmer, R. and Frasch, M.** (2006). Cardioblast-intrinsic Tinman activity controls proper diversification and differentiation of myocardial cells in *Drosophila*. *Development* **133**, 4073-4083.
- Zeitouni, B., Sénatore, S., Séverac, D., Aknin, C., Sémériva, M. and Perrin, L.** (2007). Signalling pathways involved in adult heart formation revealed by gene expression profiling in *Drosophila*. *PLoS Genet.* **3**, e174.
- Zhu, Y. C., Uradu, H., Majeed, Z. R. and Cooper, R. L.** (2016). Optogenetic stimulation of *Drosophila* heart rate at different temperatures and Ca<sup>2+</sup> concentrations. *Physiol. Rep.* **4**, e12695.

## 4 Publication 2

### **Distinct domains in the matricellular protein Lonely heart are crucial for cardiac extracellular matrix formation and heart function in *Drosophila* (2018)**

Barbara Rotstein<sup>\*</sup>, Yanina Post<sup>1\*</sup>, Marcel Reinhardt<sup>1</sup>, Kay Lammers<sup>1</sup>, Annika Buhr<sup>1</sup>, Jürgen J. Heinisch<sup>2</sup>, Heiko Meyer<sup>1</sup>, and Achim Paululat<sup>1</sup>

1 University of Osnabrück, Department of Zoology and Developmental Biology, Barbarastrasse 11, Osnabrück 49076, Germany.

2 University of Osnabrück, Department of Genetics, Barbarastrasse 11, Osnabrück 49076, Germany.

\*These authors contributed equally to this work

Extracellular matrices (ECMs) have a broad range of biological and structural functions, including forming the cell shape and maintaining organ integrity. The cardiac ECM is exposed to continual mechanical stress generated by the heart contraction. This publication examined the Lonely heart (Loh)-mediated recruitment of the tissue-specific ECM component Pericardin to the ECM in *Drosophila melanogaster*. We found that the presence of the first thrombospondin type 1 repeat (TSR1-1), with its embedded putative glycosaminoglycan (GAG)-binding site, is crucial for anchoring Loh to the ECM. Additionally, the two other thrombospondin repeats, TSR1-2 and TSR1-4, were found to be crucial for the proper interaction and recruitment of Pericardin but were not essential for Loh localisation. Furthermore, our data suggest that the N-terminal part of Loh faces the plasma membrane and anchors the protein to the cell surface. Pericardin interacts with the Loh C-terminal domain. Ectopic Loh expression induces ectopic Prc networks on nearly every *Drosophila* tissue except for the salivary glands. A more detailed analysis using the compartment-specific expression in wing discs was also carried out. My contribution to this publication was the heart function examination, which showed that increased Loh levels at the surface of cardiac cells lead to enhanced matrix deposition and impaired heart function.





# Distinct domains in the matricellular protein Lonely heart are crucial for cardiac extracellular matrix formation and heart function in *Drosophila*

Received for publication, September 14, 2017, and in revised form, March 29, 2018. Published, Papers in Press, March 29, 2018, DOI 10.1074/jbc.M117.817940

Barbara Rotstein<sup>†1</sup>, Yanina Post<sup>†1</sup>, Marcel Reinhardt<sup>†</sup>, Kay Lammers<sup>†</sup>, Annika Buhr<sup>†</sup>, Jürgen J. Heinisch<sup>§</sup>, Heiko Meyer<sup>†</sup>, and Achim Paululat<sup>†2</sup>

From the Departments of <sup>†</sup>Zoology and Developmental Biology and <sup>§</sup>Genetics, Faculty of Biology & Chemistry, University of Osnabrück Barbarastrasse 11, 49076 Osnabrück, Germany

Edited by Amanda J. Fosang

The biomechanical properties of extracellular matrices (ECMs) are critical to many biological processes, including cell–cell communication and cell migration and function. The correct balance between stiffness and elasticity is essential to the function of numerous tissues, including blood vessels and the lymphatic system, and depends on ECM constituents (the “matrisome”) and on their level of interconnection. However, despite its physiological relevance, the matrisome composition and organization remain poorly understood. Previously, we reported that the ADAMTS-like protein Lonely heart (Loh) is critical for recruiting the type IV collagen–like protein Pericardin to the cardiac ECM. Here, we utilized *Drosophila* as a simple and genetically amenable invertebrate model for studying Loh-mediated recruitment of tissue-specific ECM components such as Pericardin to the ECM. We focused on the functional relevance of distinct Loh domains to protein localization and Pericardin recruitment. Analysis of Loh deletion constructs revealed that one thrombospondin type 1 repeat (TSR1-1), which has an embedded WXXW motif, is critical for anchoring Loh to the ECM. Two other thrombospondin repeats, TSR1-2 and TSR1-4, the latter containing a CXXCXXG motif, appeared to be dispensable for tethering Loh to the ECM but were crucial for proper interaction with and recruitment of Pericardin. Moreover, our results also suggested that Pericardin in the cardiac ECM primarily ensures the structural integrity of the heart, rather than increasing tissue flexibility. In conclusion, our work provides new insights into the roles of thrombospondin type 1 repeats and advances our understanding of cardiac ECM assembly and function.

Extracellular matrices (ECMs),<sup>3</sup> which support and protect cells and provide mechanical linkage between tissues like mus-

This work was supported by funding from the German Research Foundation (SFB 944: Physiology and Dynamics of Cellular Microcompartments) (to A. P.) and by State of Lower-Saxony, Hannover, Germany, Grant 11-76251-99-15/12 (ZN2832). The authors declare that they have no conflicts of interest with the contents of this article.

This article contains Table S1, Fig. S1, and Movies S1–S4.

<sup>1</sup> Both authors contributed equally to this work.

<sup>2</sup> To whom correspondence should be addressed. Tel.: 49541-9692861; E-mail: paululat@biologie.uni-osnabrueck.de.

<sup>3</sup> The abbreviations used are: ECM, extracellular matrix; PLAC, protease and lacunin; TSP, thrombospondin; FL, full-length; eGFP, enhanced GFP; ROI, region of interest; UAS, upstream activation sequence; BM,

cles and epidermis, are generally assembled in a similar manner. After incorporation of transmembrane receptors, such as integrins and dystroglycans (1, 2), meshwork-forming components like laminin and collagen IV are able to anchor. By interacting with each other, they form a complex network with distinct biomechanical properties, which is furthermore stabilized by nidogen (3, 4) and allows other proteins (e.g. perlecan) to bind to the matrix as well (5).

Whereas these steps can be found ubiquitously, the *Drosophila* cardiac ECM is different from the matrices of other tissues or organs in several ways. It forms a 3D meshwork that connects the contractile heart tube to the alary muscles and, thereby, to the epidermis (6, 7). Within this meshwork, embedded pericardial cells differentiate into a distinct population of cell types, such as nephrocytes (8–10) or wing hearts (11, 12).

In flies, the cardiac ECM combines two important biomechanical features: elasticity that accounts for a flexible connection between heart and alary muscle cells and a high tensile strength that withstands forces produced by lifelong heart contractions. One major difference between cardiac ECMs and matrices of other tissues is the presence of the ADAMTS-like adapter protein Lonely heart (Loh), which can be found exclusively at the surface of the heart and chordotonal organs. Here, Lonely heart is essential to proper recruitment of the type IV collagen–like protein Pericardin (13). Pericardin (Prc) is secreted into the hemolymph by pericardial nephrocytes and adipocytes, and, as soon as it becomes recruited to the cardiac matrix by Lonely heart, it starts to form a stable network (14). By this mechanism the heart is provided with an exceptional ECM that allows it to withstand the strong mechanical forces of a heartbeat. Lack of Pericardin or its anchor Lonely heart leads to a total collapse of the dorsal vessel and dissociation of the pericardial cells and alary muscles from the heart tube. Concomitants are severely impaired heartbeat and absence of heart-mediated hemolymph transport. Accordingly, corresponding mutant animals exhibit decreased fitness and shortened lifespan (13).

The ADAMTS (a disintegrin and metalloproteinase with thrombospondin motifs) superfamily consists of two classes of proteins: ADAMTS and ADAMTS-like proteins. Their main

basement membrane; TRITC, tetramethylrhodamine isothiocyanate; GAG, glycosaminoglycan.

difference is that ADAMTS-like proteins, such as Loh, lack the proteolytically active motif within the ADAM spacer. Both classes share several domains, with most of them being poorly defined. In addition to a spacer region, a changing number of thrombospondin type 1 repeats (TSR1) can be found next to a protease and lacunin (PLAC) domain and a signal peptide (15). These ancillary domains apparently ensure proper substrate specificity as well as cell-surface or ECM tethering (16, 17).

TSR1 motifs were initially discovered in thrombospondins (TSPs), which belong to the family of calcium-binding glycoproteins that are secreted into the extracellular matrix of all complex organisms. TSPs have been shown to bind to fibronectin, laminin, collagen, and other matricellular proteins to form complex networks on the cell surface. TSP superfamily members are involved in regulation of spinal cord outgrowth (e.g. F-spondin) or act as specific anti-angiogenic factors in brain development (e.g. BAI-1). In addition, they can be critical to directed ECM proteolysis (16). TSPs are modular proteins containing several types of repetitive sequence motifs (Fig. 1). One of the most characteristic motifs is the evolutionarily conserved thrombospondin type 1 repeat (TSR1), which is ~60 amino acids in length and supposed to form an antiparallel three-stranded structure that interacts with glycoproteins of the extracellular matrix. The human genome harbors ~90 genes encoding TSR1-containing proteins (18), whereas ~14 corresponding proteins are present in *D. melanogaster* (19). Among these, some have been shown to contribute to heart development during embryogenesis. These proteins are the transmembrane receptor Uncoordinated 5 (Unc5) (20) and the ADAMTS-like protein Lonely heart (Loh) (13).

To understand the molecular mechanism by which Lonely heart ensures proper cardiac ECM formation in more detail, we analyzed a large set of individually mutated Loh proteins for their capability to incorporate into the ECM and recruit Pericardin. To allow quantitative measurements of Pericardin recruitment efficiency, we applied an *in vivo* recruitment assay established previously in our laboratory (13). In addition to the ECM of somatic muscles, we also investigated other types of matrices present in *Drosophila* for their capability to recruit Pericardin in a Loh-dependent manner. Furthermore, we analyzed whether Pericardin, once recruited to a target matrix, has an intrinsic capacity to self-assemble into a meshwork independent of Loh. To perform the analysis, we used imaginal discs to express full-length Loh in distinct compartments of the disc and evaluated potential spreading of the Pericardin meshwork over neighboring zones that lacked Loh.

Finally, to achieve an initial understanding of the biomechanical relevance of Pericardin, we searched for physiological consequences of ectopic Pericardin deposition. In this respect, body wall muscles represent an effective readout system to investigate, for example, altered animal locomotion or lifespan. We found that incorporation of Pericardin into the matrix of somatic muscles has no influence on lifespan but impairs contraction, thereby affecting the general locomotion performance.

## Results

We have shown previously that Loh is essential and sufficient to recruit Pericardin from the hemolymph toward a given

matrix (13). Here, we did a follow-up study aiming to understand the molecular mechanisms by which Lonely heart itself adheres to the cardiac matrix and, furthermore, how the protein recruits and assembles Pericardin, two processes that were not addressed until now. As depicted in Fig. 1, the Loh sequence contains an N-terminal signal peptide as well as five TSR1-like repeats. Of note, the number, size, and position of predicted TSR1 repeats differ, depending on the search and prediction algorithm used (Fig. 1A). Additionally, Loh contains two predicted glycosaminoglycan (GAG)-binding sites located within two of the TSR1 domains. Up to now, the functionality of these sites has not been confirmed experimentally.

It has been shown for ADAMTS-1 and other proteins that anchoring to the extracellular matrix requires the C-terminal presence of TSR motifs, suggesting an interaction with glycosaminoglycans, such as heparan sulfate, which are predeposited at the matrix (15). This work provides initial evidence that Lonely heart anchors to *Drosophila* matrices in a similar manner.

## Functional analysis of distinct Lonely heart domains

In this study, a series of *lonely heart* mutations were generated to establish corresponding transgenic *Drosophila* lines as well as transiently transfected insect cell lines. Subsequently, a combined analysis of both systems was performed to investigate the molecular functions of individual domains present in the Loh protein in detail. Each of the established transgenic *Drosophila* lines carries a UAS-*loh* construct, consisting either of the full-length (FL) WT sequence (positive control) or of specifically mutated forms of *loh* lacking certain domains (Fig. 1B). Additionally, a construct lacking the ADAM spacer region, but retaining the antigenic region recognized by our anti-Loh antibody, was generated. However, after inducing expression by crossing to *mef2*-Gal4 or *prc*-Gal4 driver lines, this construct could not be detected by Western blot analysis (data not shown), indicating that the resulting protein is highly unstable and thus degraded. Consequently, this construct was excluded from further analysis. All other constructs were analyzed for their capability to recruit Pericardin by applying a previously established ectopic expression *in vivo* recruitment assay (13). Before performing these experiments, we verified that the individual Loh constructs were expressed properly and located to the cell surface, which was a prerequisite for the follow-up experiments. Corresponding analyses were done using a cell culture system (Sf21 cells; Fig. 2) as well as transgenic *Drosophila* (Fig. 3).

## Secretion and anchoring capability of Loh mutant constructs in transgenic animals and Sf21 cells

Pericardin recruitment to the ECM of a certain tissue depends on the presence of Loh at the target cell surface. This presence in turn requires successful processing, secretion, and anchoring of Loh. Therefore, we tested full-length WT Loh, as well as the individually mutated forms of the protein, for proper secretion and localization. In this context, Sf21 cells (expression driven by a constitutively active polyhedrin promoter) and somatic muscle cells (expression driven by *mef2*-Gal4) were analyzed. For visualizing Loh, we used a polyclonal anti-Loh

## Functional domains of Lonely heart

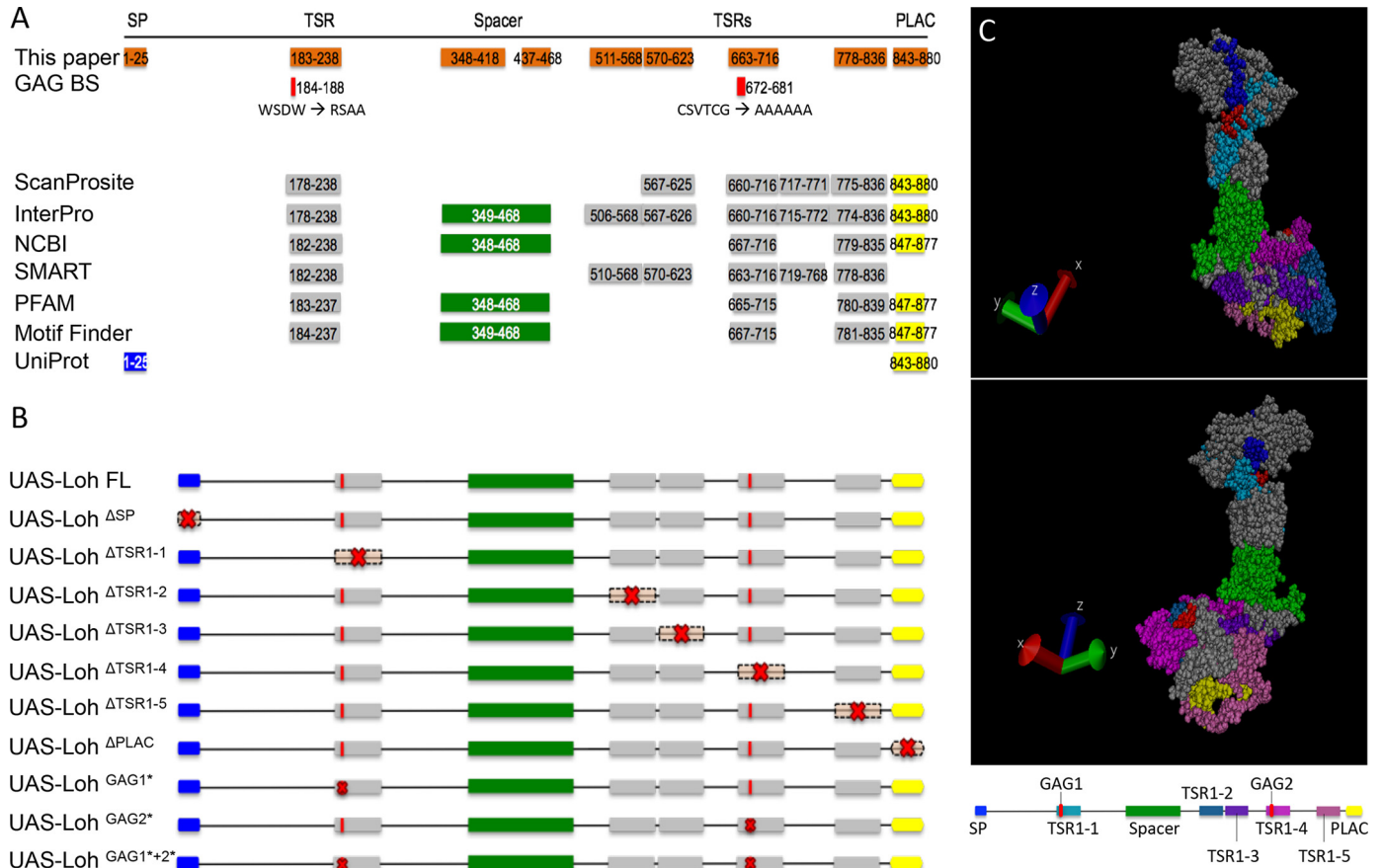


**Figure 1. Lonely heart domain structure and constructs used in this study.** *A*, the Lonely heart isoform A sequence (GenBank<sup>TM</sup> entry AAF52956.3) was used to identify functional motifs. An N-terminal signal peptide, a variable number of thrombospondin repeats type I, an ADAM spacer region, and a single C-terminal PLAC domain were recognized by ScanProsite, Interpro, NCBI, SMART, PFAM, Motif Finder, and UniProt. Additionally, two putative glycosaminoglycan (GAG) binding sites were identified that locate within two thrombospondin repeat type I motifs (44, 45). Numbers depict the respective amino acid positions. *B*, Lonely heart constructs used in this study. *Red crosses* indicate mutated protein motifs. Nomenclature indicates deletions ( $\Delta$ ) or point mutations (\*). Due to algorithm-dependent, inconsistent predictions of the TSR1 domains, constructs were generated based on the protein structure proposed previously (13). *SP*, signal peptide. *C*, 3D model of Lonely heart with *color-coded* protein domains. All thrombospondin domains locate to the surface of the protein. Modeling was performed using YASARA (42) and VMD version 1.9.3 (University of Illinois).

antibody recognizing a peptide sequence within the ADAM spacer region of the protein. This antibody was described previously (13).

To ensure comparable transfection efficiencies of the Sf21 cells, eGFP was inserted into a second multiple cloning site present in the used expression vector; the resulting GFP signal was then used as a loading control for Western blot analysis (Fig. 2M) as well as a cytoplasmic counterstain for immunocytochemistry (Fig. 2, A–L). Captured images were processed for fluorescence intensity profiling to analyze Loh secretion and surface localization. As expected, full-length Loh was successfully secreted and anchored to the cell surface (Fig. 2A). As a negative control, UAS-Loh<sup>ΔSP</sup> that lacks the N-terminal signal sequence was used. The respective construct failed to become secreted and distributed uniformly within the cytoplasm (Fig. 2C). A similar localization was observed for Loh<sup>GAG1\*+2\*</sup>, in which both speculative GAG-binding sites are mutated (Fig. 2K). The constructs Loh<sup>ΔTSR1-1</sup> and Loh<sup>GAG1\*</sup> also showed impaired surface location and apparently accumulated in secretory vesicles close to the plasma membrane (Fig. 2, D and I). The respective localization patterns of these constructs may indicate that secretion still occurred, but anchoring to the ECM was

compromised. Mutations in the remaining thrombospondin type I repeat domains (Loh<sup>ΔTSR1-2</sup>, Loh<sup>ΔTSR1-3</sup>, Loh<sup>ΔTSR1-4</sup>, Loh<sup>ΔTSR1-5</sup>), as well as lack of the PLAC domain (Loh<sup>ΔPLAC</sup>) or a mutation in the second speculative GAG binding site (Loh<sup>GAG2\*</sup>), did not affect secretion or anchoring (Fig. 2, E, F, G, H, J, and L). To address the question of whether the mislocalized constructs are expressed and secreted properly, but fail to incorporate into the ECM, Western blotting analyses of transfected Sf21 cells as well as of the respective construct-specific cell culture media were performed. If ECM incorporation fails, whereas expression and secretion are still proper, the respective Loh constructs should be detectable in the culture medium. As depicted in Fig. 2M, all constructs were expressed and exhibited molecular masses in line with expectations. To ensure comparable transfection rates, GFP was co-transfected and used as a loading control. Interestingly, in addition to the cell lysate (Fig. 2M), Loh<sup>ΔTSR1-1</sup>, Loh<sup>GAG1\*</sup>, and Loh<sup>GAG1\*+2\*</sup> were also present in the cell culture medium (Fig. 2N), which strongly indicates that the respective constructs are not able to bind efficiently to the ECM. Thus, these data are in line with the results of the immunofluorescence stains (Fig. 2, D, I, and K). Of note, the Loh<sup>ΔTSR1-5</sup> construct was also present in the culture

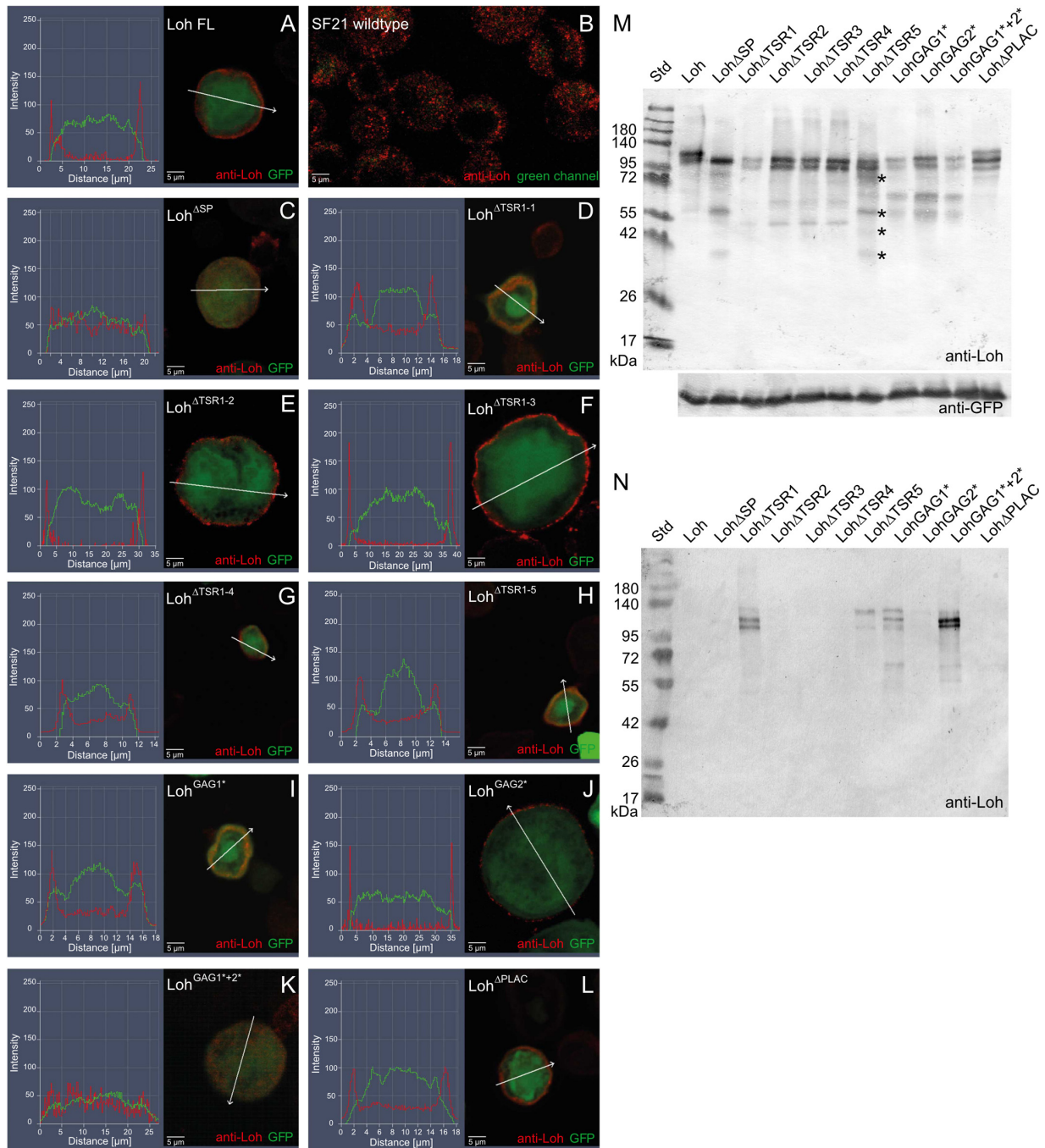


**Figure 2. Expression and localization of mutated Loh constructs in Sf21 cells.** Sf21 cells were transfected with WT and individually mutated Loh constructs. Successful transfection was monitored by simultaneous expression of cytoplasmic GFP (*green channel*). WT as well as mutated Loh were visualized by anti-Loh antibody staining (*red channel*). Intensity profiling of stained cells was used to determine the subcellular localization of individual Loh constructs. The respective regions of evaluation are marked (*arrows in A–L*). Full-length Loh (*A*) is secreted and accumulates at the surface of the cell. Anti-Loh staining of untransfected cells results in a spotted distribution of low-intensity signals (overexposed to visualize the shape of the cells) (*B*). Loh lacking the signal peptide is not secreted and retained in the cytoplasm (*C*). The constructs Loh<sup>ΔTSR1-1</sup> and Loh<sup>GAG1\*+2\*</sup> show no distinct surface location but accumulate in a patchy manner close to the plasma membrane (*D* and *I*). A similar behavior is observed for Loh<sup>GAG1\*</sup>, yet with a broader distribution in the cytoplasm (*K*). Individual mutations in the remaining thrombospondin type I repeat domains (Loh<sup>ΔTSR1-2</sup>, Loh<sup>ΔTSR1-3</sup>, Loh<sup>ΔTSR1-4</sup>, and Loh<sup>ΔTSR1-5</sup>), as well as lack of the PLAC domain (Loh<sup>ΔPLAC</sup>) or a mutation in the second speculative GAG binding site (Loh<sup>GAG2\*</sup>), do not affect secretion or anchoring (*E–H*, *J*, and *L*). *M*, Western blotting of construct-specific cell lysates confirms expression and adequate molecular mass of all Loh constructs. Asterisks indicate putative degradation products that are unique to Loh<sup>ΔTSR1-5</sup> and do not appear in the case of any other TSR1 deletion construct. Co-transfected GFP was used as a loading control. *N*, Western blotting of construct-specific cell culture media confirms the presence of Loh<sup>ΔTSR1-1</sup>, Loh<sup>ΔTSR1-5</sup>, Loh<sup>GAG1\*</sup>, and Loh<sup>GAG1\*+2\*</sup>, indicating proper secretion but impaired binding of the respective constructs to the ECM. The depicted blots are representative of three individual biological replicates.

## Functional domains of Lonely heart

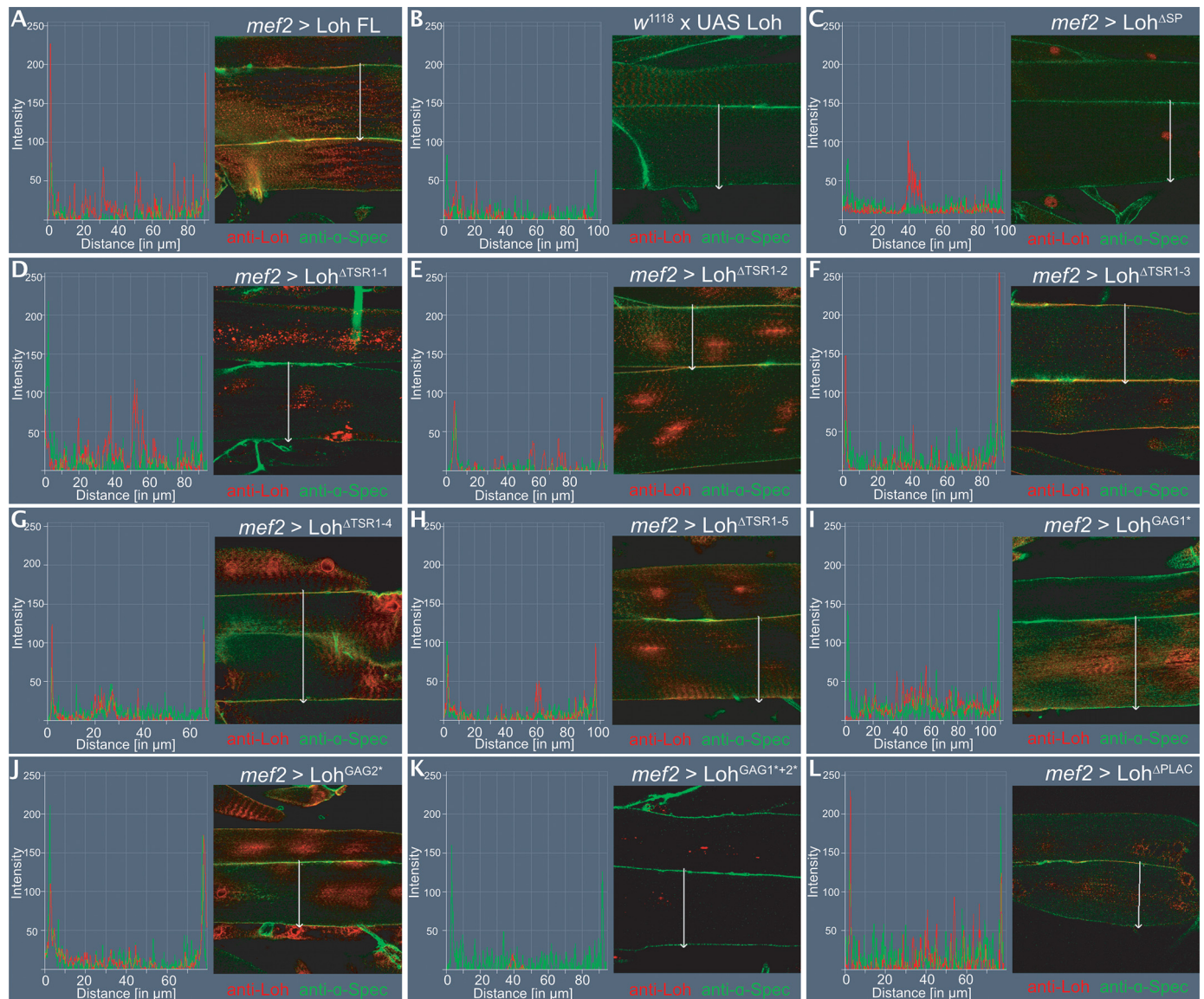


**Figure 3. Expression and localization of mutated Loh constructs in somatic muscles.** All UAS constructs were inserted at the 86F8 landing site on the 3R chromosome. Expression was driven by crossing in *mef2*-Gal4, which induces expression of the target construct in the muscle lineage. Loh localization was visualized by anti-Loh antibody staining (red channel). Muscles were counterstained with anti- $\alpha$ -spectrin antibodies (green channel). Intensity profiling of stained cells was used to determine the subcellular localization of individual Loh constructs. The respective regions of evaluation are marked (arrows in A–L). Full-length Loh, driven by *mef2*-Gal4, is secreted and accumulates at the surface of the muscle (A). The UAS-Loh FL construct alone (negative control) shows no expression (B). Loh lacking the signal peptide is not secreted but appears to be directed to the nucleus (C). Loh lacking TSR1-2, TSR1-3, TSR1-4, or TSR1-5 is properly secreted and locates to the surface of the cells (E–H). A similar pattern is observed for the construct harboring a mutation in the second speculative GAG binding site (J). Loh that lacks TSR1-1 is not present at the muscle surface (D), which is also the case for the construct carrying a mutation in the first putative GAG-binding site (I). Mutating both predicted GAG-binding sites simultaneously results in complete loss of Loh incorporation into the muscle ECM (K). Deleting the PLAC domain (L) has no effect on secretion or localization of Loh.

medium, although immunocytochemistry detected it at the cell surface (Fig. 2H). One explanation for this discrepancy is a reduced stability of the construct, which is indicated by presence of additional bands on Western blots, probably degradation products that are unique to Loh<sup>ΔTSR1-5</sup> and do not appear in the case of any other TSR1 deletion construct (Fig. 2M, asterisks). This reduced stability may be caused by impaired protein folding, which in turn could result in less efficient ECM incorporation. In this context, the essentially identical band composition that we observed for constructs holding similar mutations (e.g. TSR1 deletion constructs 1–4 and GAG substitutions 1, 2, and 1 + 2; Fig. 2M) indicates proper folding and stability of

the respective proteins. Of note, the tryptophan residues present in the speculative GAG1 motif as well as the cysteine residues present in putative GAG2 (Fig. 1A) are probably of significance to the structure of the TSR domain in which they are embedded (19). However, as depicted above, substitution of the respective motifs apparently does not severely affect stability of the corresponding entire proteins (Fig. 2M).

To assess secretion and ECM incorporation in *Drosophila*, we expressed Loh and its mutated forms in somatic muscle cells using *mef2*-Gal4 as a driver (Fig. 3). Flat preparations of third instar larvae were fixed and immunostained for Loh. To visualize cell borders, anti-spectrin antibodies were used for counter-

staining. This allowed us to perform intensity profiling to check for Loh secretion and surface localization in somatic muscles. In line with our results using cultured Sf21 cells, we found that most of the tested constructs were secreted and localized to the ECM. However, Loh<sup>ΔTSR1-1</sup>, Loh<sup>GAG1\*</sup>, and Loh<sup>GAG1\*+2\*</sup> were again absent from the cell surface (Fig. 3, D, I, and K), which confirms the cell culture data and emphasizes the high relevance of these domains to proper ECM incorporation. The data of the localization and anchoring analyses as well as Pericardin recruitment efficiencies are summarized in Table S1.

#### Quantitative analysis of Pericardin recruitment efficiency

Utilizing the transgenic lines introduced above, we tested whether mutated forms of Loh still harbor the capability to recruit Pericardin to the ECM of muscle cells and whether Pericardin, if recruited, assembles into a network of ECM fibers. It has been shown previously that the full-length form of Loh, when expressed in muscles or adipocytes, is sufficient to recruit Pericardin from the circulating hemolymph and incorporate it into the surface meshwork of ECM fibers (13). We quantified the capacity of mutated forms of Loh to recruit Pericardin using a “sum pixel intensity” region of interest (ROI)-based approach. For normalization of the Pericardin signal in stained specimens of different genotypes, we utilized F-actin staining with phalloidin, a method that has recently been described and successfully used (21). As controls, we used animals that harbored the full-length UAS-Loh (UAS-Loh FL) construct but lacked Gal4 (negative control; Fig. 4A), UAS-Loh FL expressed by *mef2*-Gal4 (positive control; Fig. 4B), and UAS-Loh<sup>ΔSP</sup> driven by *mef2*-Gal4 (Fig. 4C). Our previous tests have shown that deleting the signal peptide completely inhibits secretion and Pericardin recruitment (Fig. 4C). We confirmed that full-length WT Loh is able to recruit Pericardin to the ECM of muscle cells. In addition, *mef2*-Gal4–driven expression of UAS-Loh<sup>ΔTSR1-3</sup>, UAS-Loh<sup>ΔTSR1-5</sup>, and UAS-Loh<sup>ΔPLAC</sup> results in considerable Pericardin recruitment (Fig. 4, F, H, and L), indicating that these protein domains play no major role in Pericardin assembly. By contrast, *mef2*-Gal4–driven expression of UAS-Loh<sup>ΔTSR1-1</sup>, UAS-Loh<sup>ΔTSR1-2</sup>, UAS-Loh<sup>ΔTSR1-4</sup>, UAS-Loh<sup>GAG1\*</sup>, UAS-Loh<sup>GAG2\*</sup>, and UAS-Loh<sup>GAG1\*+2\*</sup> does not result in significant Pericardin accumulation (Fig. 4, D, E, G, I, J, and K), which suggests that these distinct domains of Lonely heart are responsible for efficient Pericardin recruitment. Thrombospondin repeat 1 (TSR1-1), with its embedded speculative GAG-binding site, appears to be most critical to Loh anchoring (Fig. 3D), whereas TSR1-2 and TSR1-4 are dispensable for anchoring but important for recruiting Pericardin toward a certain matrix (Figs. 3 (E and G) and 4 (E and G)). Furthermore, our results show that lack of the PLAC domain has no impact on Loh secretion, ECM adhesion, or Pericardin recruitment (Figs. 3L and 4L). We are aware of the fact that a slight reduction in Pericardin recruitment efficiency may not be measurable by our *in vivo* approach.

We completed this set of experiments by testing all generated Loh constructs for their ability to recruit Pericardin to a tissue other than somatic muscles (Fig. S1). Pericardin-Gal4, as well as *Cg*-Gal4, mediates strong expression of the Gal4 transgene in adipocytes, and it has been shown that Loh is able to recruit

Pericardin under these experimental conditions (13). Although not quantitatively proven in detail, our results using adipocytes as a second test tissue confirmed our observations from analyzing recruitment of Pericardin to somatic muscles. The analysis of adipocytes turned out to be more difficult because fat cells are a natural source of Pericardin production. Thus, there is always a certain amount of Pericardin at the cell surface, which is normally released into the hemolymph. Exposing Loh at the adipocyte surface apparently results in retention of the produced Pericardin rather than recruitment of it from the hemolymph. Nevertheless, in-line with our data from the muscle recruitment assay, mutations in the first or second thrombospondin type 1 repeat or in the first or second putative GAG-binding site result in loss of Pericardin recruitment to the adipocytes (Fig. S1, C, D, G, and H). This is also observed for the construct holding simultaneous mutations in both speculative GAG binding sites (Fig. S1E). Additionally, deleting the fourth TSR domain leads to considerably reduced Prc recruitment (Fig. S1J).

#### Tissue-specific analysis of Pericardin recruitment

Once recruited, Pericardin readily assembles into the preexisting or continuously forming meshwork of ECM fibers, indicating that not only the cardiac ECM, but also the ECM of muscles and adipocytes, harbor all the constituents needed for Pericardin incorporation. However, it is still unknown whether matrices in general harbor an intrinsic capacity to assemble and to incorporate Pericardin and whether Loh alone is necessary and sufficient or if other, yet unknown recruitment factors are also required. To answer this question, we expressed Loh in a variety of additional cells and tissues, including salivary glands, wing imaginal discs, and glial cells of the central nervous system, by crossing the UAS-Loh full-length transgenic line to the different tissue-specific Gal4 driver lines. Again, we used the anti-Loh antibody to confirm proper secretion and the presence of Loh at the respective cell surface. Subsequently, we monitored redistribution of Pericardin to the Loh-exposing tissues using the anti-Pericardin antibody (Fig. 5). We found that in addition to adipocytes and muscle cells (Fig. 5, A and B), also wing imaginal disc cells (Fig. 5E) and glial cells (Fig. 5C) are capable of recruiting Pericardin as long as Loh is exposed at the surface of the respective cells. This finding supports the hypothesis that the ability to recruit and incorporate Pericardin is a general property of a wide range of matrices. Interestingly, salivary glands are the only type of tissue that appears to be incapable of recruiting Pericardin. A careful microscopic analysis confirmed that Loh is produced and that it locates to the outer surface of the salivary gland cells (Fig. 5D). Thus, we can exclude the possibility that Loh itself is not stably present at the matrix and therefore fails to recruit Pericardin. It rather appears likely that a certain property of the salivary gland ECM or lack of a critical ECM constituent impedes Pericardin recruitment to this tissue.

#### Recruitment of Pericardin to distinct wing disc compartments

Previous work showed that Pericardin requires Loh for recruitment and proper incorporation into the ECM; however, proper Loh localization does not require Pericardin (13). To

## Functional domains of Lonely heart

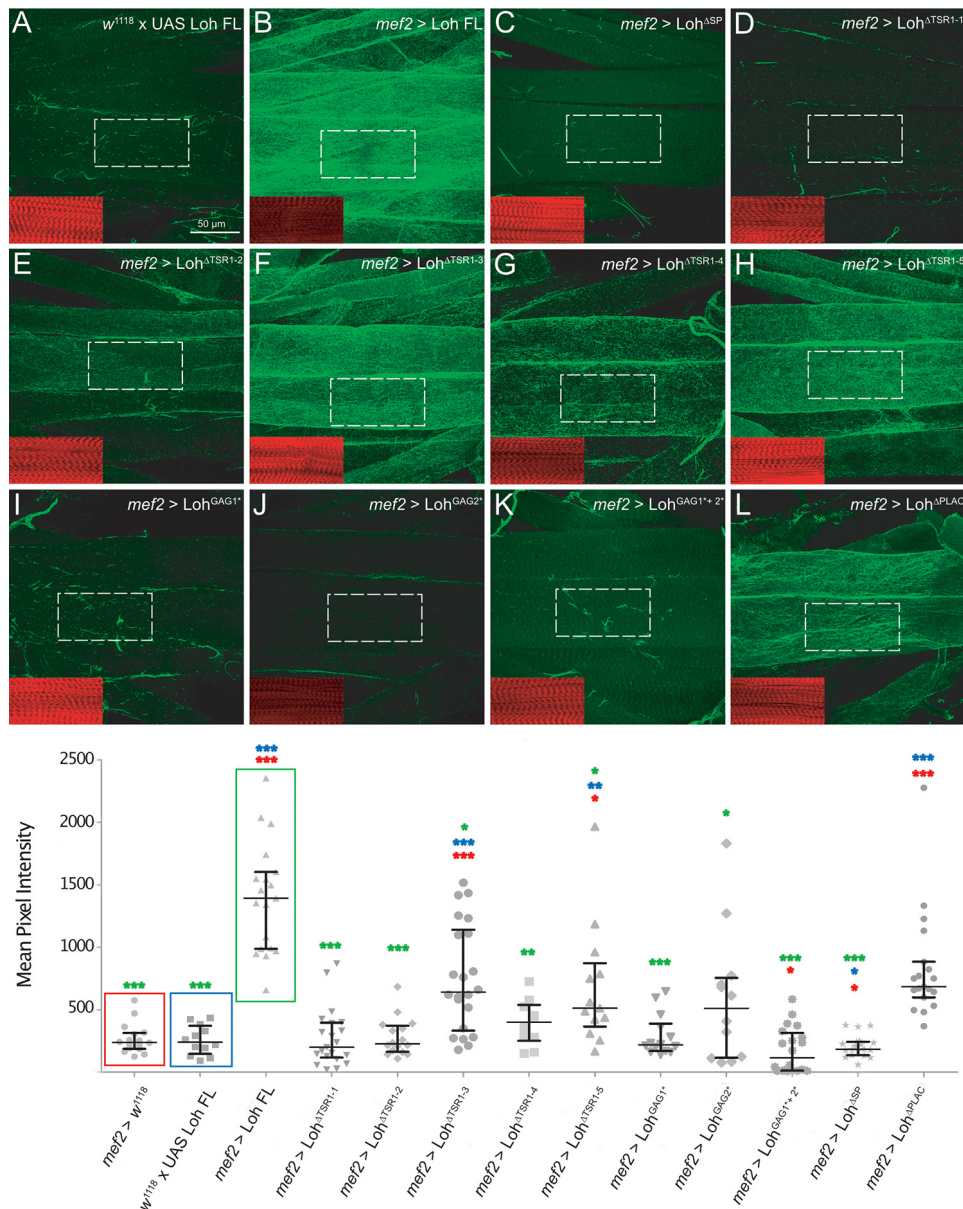


**Figure 4. Pericardin recruitment efficiency.** To quantify Pericardin recruitment efficiency of individual Loh constructs, expression was driven by crossing in *mef2*-Gal4. Third instar larval offspring were prepared and stained for Pericardin (anti-Prc, green channel) and counterstained for F-actin (phalloidin, red channel, inset). Images were recorded with identical settings, and ROIs were measured using the “sum slices” method implemented into ImageJ. As a negative control, animals with the genotype *w<sup>1118</sup>*, +/UAS-Loh FL were used (A). Pixel intensity obtained for Pericardin staining (green channel) was normalized against F-actin staining (red channel). Quantification is presented as a scatter plot. Full-length Loh recruits Pericardin to the muscle matrix (B). Significant recruitment is also obvious for Loh constructs lacking the third TSR domain (UAS-Loh<sup>ΔTSR1-3</sup>) (F), the fifth TSR domain (UAS-Loh<sup>ΔTSR1-5</sup>) (H), or the PLAC domain (UAS-Loh<sup>ΔPLAC</sup>) (L). In Loh constructs lacking the signal peptide, no Pericardin signal above background is observed (C). Loh harboring a deleted first thrombospondin type 1 repeat (UAS-Loh<sup>ΔTSR1-1</sup>) (D) or a mutation of the embedded speculative GAG-binding site (UAS-Loh<sup>GAG1\*</sup>) (J) exhibits a considerably reduced capacity to recruit Pericardin. A strong reduction of Pericardin recruitment is also seen in Loh<sup>ΔTSR1-2</sup>, in Loh<sup>ΔTSR1-4</sup>, and in Loh<sup>GAG2\*</sup> mutants (E, G, and J). Loh proteins carrying mutations in both predicted GAG binding sites (Loh<sup>GAG1\*+2\*</sup>) do also exhibit severely impaired Pericardin recruitment (K). Deleting the PLAC domain has no effect on Loh secretion on Pericardin recruitment (L). The box plot/scatter plot (bottom) depicts quantification of the construct-specific recruitment efficiencies. Colored asterisks indicate the respective significance levels (Student’s *t* test; \*, *p* < 0.05; \*\*, *p* < 0.01; \*\*\*, *p* < 0.001) as calculated for the individual controls (colored boxes).

understand the molecular mechanisms by which Loh recruits and assembles Pericardin, we aimed to distinguish between two possible models. 1) Loh may act as a crystallization seed that recruits Pericardin from the hemolymph, either directly or via additional linker proteins. In a second step, the matrix-bound Pericardin molecules promote additional recruitment, assembly, and ECM incorporation of Pericardin from the hemolymph. Consequently, Pericardin matrices should spread over a tissue even if Loh is not present underneath. 2) Pericardin only

adheres and incorporates if Loh localizes underneath; thus, coordinated self-assembly and spreading of Pericardin over a tissue that lacks Loh is not possible. To discriminate between these two possibilities, we expressed full-length Loh (UAS-Loh FL) in different compartments of the wing discs by utilizing *dpp*-Gal4, *ci*-Gal4, *hh*-Gal4, and *sd*-Gal4 as drivers (see Fig. 6). In each case, we found that Pericardin recruitment is restricted to those areas that express and display Loh. For example, *hh*-Gal4 drives Loh expression exclusively in cells

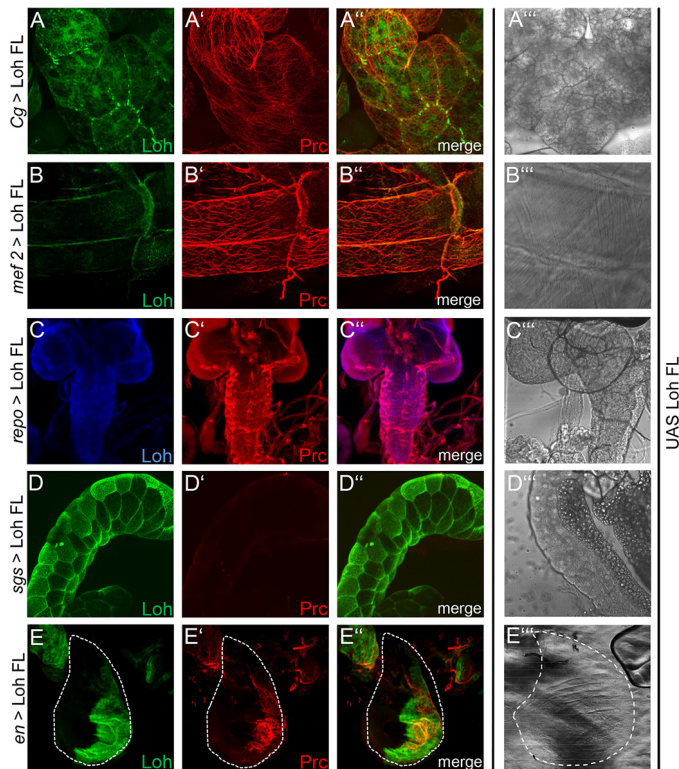


**Figure 5. Tissue-specific recruitment of Pericardin.** Lonely heart was ectopically expressed in different tissues to analyze the ability of the corresponding extracellular matrices to incorporate Pericardin. Drivers used are *Cg*-Gal4 for adipocytes (A), *mef2*-Gal4 for myocytes (B), *repo*-Gal4 for glial cells of the central nervous system (C), *sgs*-Gal4 for salivary glands (D), and *en*-Gal4 for imaginal discs (E). Anti-Loh staining (green (A, B, D, and E) or blue (C) channel) and anti-Pericardin staining (red channel (panels labeled with a prime symbol)) are shown individually and as merged images (panels labeled with a double prime symbol). A''', B''', C''', D''', and E''' depict bright-field images of the individual tissues. Dashed lines (E) highlight the border of the wing imaginal disc. All panels show maximum intensity projections of confocal sections. With the exception of salivary glands (D), Pericardin is recruited to all tissues tested (A, B, C, and E).

of the posterior wing compartment (Fig. 6C, green channel). Consequently, Pericardin, synthesized and secreted by adipocytes of the fat body, adheres exclusively to this domain without spreading out into the anterior wing compartment (Fig. 6C, red channel). These results strongly support the second model proposed above, which postulates a necessity of underlying Loh for proper Pericardin recruitment and incorporation. Thus, the distinct localization of Loh allows for a temporally and spatially highly specific Pericardin incorporation into specialized extracellular matrices, such as the cardiac ECM.

#### Analysis of the biochemical interactions in Pericardin-containing extracellular matrices

To understand the molecular mechanisms that facilitate Loh-dependent Pericardin incorporation into extracellular matrices in more detail, we analyzed the biochemical interactions characteristic to these matrices. In this effort, we utilized a series of GFP-tagged ECM proteins (LanA::GFP, LanB1::GFP, Vkg::GFP,  $\beta$ PS-integrin::GFP, and Pericardin::GFP) (22) and analyzed them for co-immunoprecipitation with Pericardin, nidogen, and laminin. Of note, co-immunoprecipitation of Loh and Pericardin has already been confirmed (13). As depicted in

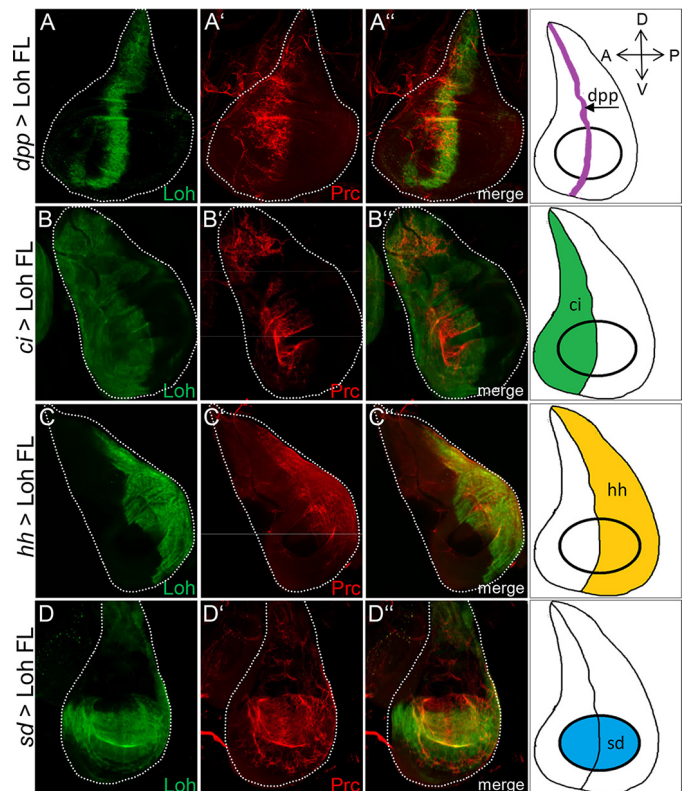


**Figure 6. Pericardin recruitment to distinct compartments of the wing disc surface.** Ectopic expression of UAS-Loh FL in different compartments of third instar larval wing imaginal discs using *dpp*-Gal4 (expressed along the anterior-posterior boundary; A–A''), *ci*-Gal4 (anterior compartment; B–B''), *hh*-Gal4 (posterior compartment; C–C''), and *sd*-Gal4 (expressed in the wing pouch; D–D'') as drivers. Loh is visualized using an anti-Loh antibody (green channel), and Pericardin is visualized using an anti-Pericardin antibody (red channel). The right column depicts a schematic illustration of the compartment-specific Gal4 expression for all driver lines used. Pericardin recruitment is restricted to areas that express and display Loh. Orientation of imaginal discs is indicated in the top right corner.

Fig. 7A, the GFP-tagged proteins exhibited a molecular mass consistent with expected values (including posttranslational modifications), thus indicating the presence of stable fusions. Furthermore, the respective proteins could be extracted from corresponding larval homogenates in rather convenient amounts. The only construct that could not be detected with anti-GFP antibodies was Pericardin::GFP. However, the fact that endogenous Pericardin as well as laminin was present in Pericardin::GFP pulldown fractions but absent in corresponding control preparations ( $w^{1118}$ ; Fig. 7 (B and D)) indicates that Pericardin::GFP can be isolated from corresponding transgenes, but in rather limited amounts. Further analyses revealed that Pericardin co-immunoprecipitates with LanA::GFP, LanB1::GFP, Vkg::GFP, and Pericardin::GFP, but not with  $\beta$ PS-integrin::GFP (Fig. 7B). The fact that the bands detected in the Pericardin::GFP sample correspond to the size of WT Pericardin (Fig. 7B, asterisks) confirms that endogenous Pericardin is labeled and not the GFP fusion protein. Nidogen co-immunoprecipitates with LanA::GFP, LanB1::GFP, and Vkg::GFP, but not with  $\beta$ PS-integrin::GFP and Pericardin::GFP (Fig. 7C), whereas laminin co-immunoprecipitates with Vkg::GFP and with Pericardin::GFP, but not with  $\beta$ PS-integrin::GFP (Fig. 7D). Despite a rather ineffective Pericardin::GFP isolation (Fig. 7A),



## Functional domains of Lonely heart

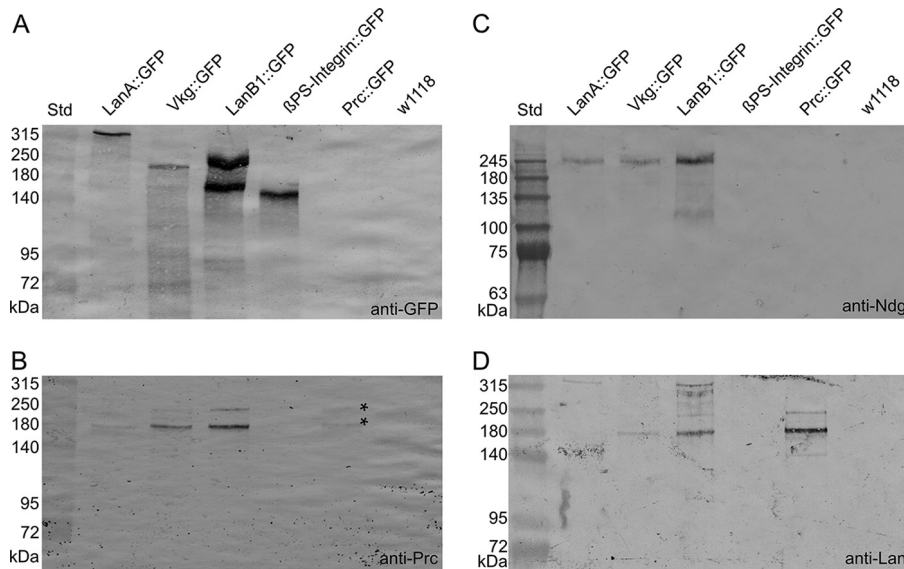


**Figure 7. Pericardin co-immunoprecipitates with distinct ECM components.** GFP-tagged ECM proteins (laminin A, LanA::GFP; laminin B1, LanB1::GFP; Viking, Vkg::GFP;  $\beta$ PS-integrin,  $\beta$ PS-integrin::GFP; Pericardin, Pericardin::GFP) were purified from third instar larvae and subjected to Western blot analysis. Anti-GFP antibodies were applied to estimate the protein-specific purification efficiency (A). Anti-Pericardin (Prc; B), anti-nidogen (Ndg; C), and anti-laminin (Lan; D) antibodies were used to assess co-immunoprecipitation of the individual ECM components with the purified GFP fusion proteins. The rather weak detection of endogenous Pericardin in the Pericardin::GFP sample is indicated (B; asterisks). The observation that nidogen migrates significantly higher than expected (predicted molecular mass, 149.1 kDa) presumably reflects extensive posttranslational modification of the protein. Similar mass shifts, predominantly caused by N- and O-glycosylation, have been reported for nidogens from other species (4). The depicted blots are representative of two individual biological replicates.

a distinct laminin signal is present in the respective fraction (Fig. 7D), which indicates a strong interaction between Pericardin and laminin. Of note, we did not observe co-immunoprecipitation of  $\beta$ PS-integrin with laminin, although an interaction has been reported before (23). This discrepancy may be due to misfolding of the  $\beta$ PS-integrin::GFP fusion construct that we used in our study. Thus, our finding that Pericardin does not co-precipitate with integrin must be considered preliminary. The data of the immunoprecipitation assay are summarized in the assembly model depicted in Fig. 10.

### Incorporation of Pericardin into the matrix of somatic muscles affects contraction performance

To achieve an initial understanding of the physiological relevance of Pericardin, we analyzed whether recruitment and assembly of the protein into ectopic matrices affected the biomechanical properties of the corresponding matrix. We considered recruitment of Pericardin to muscles to be a useful readout model because biomechanical modulations of the muscle matrix probably have a direct influence on contraction efficiency and, thereby, on locomotion in general. To measure muscle performance, we analyzed the distance a larva covers within a straight run of 10 s (Fig. 8A'), as well as the number of contractions that occur during this time frame (Fig. 8A''). Based on these data, we also calculated the distance covered by a single contraction (Fig. 8A). As depicted, specimens with Pericardin ectopically incorporated into the muscle matrix exhibit reduced movement speed. Interestingly, the effect is not caused by a reduced contraction rate in corresponding animals, which is comparable with that of controls (Fig. 8A''), but by a reduced distance covered per contraction (Fig. 8A). This result may indicate that artificial incorporation of Pericardin into the ECM of muscle cells increases stiffness of the matrix, which even-

tually impairs proper contraction of the tissue. We also assessed possible effects on lifespan and found no significant influence of ectopic Pericardin deposition under laboratory conditions (Fig. 8B).

### Overexpression of Lonely heart in cardiomyocytes leads to matrix phenotypes and affects heart performance

The primary function of Loh is the recruitment of Pericardin toward the cardiac matrix. Pericardin requires the presence of Loh to become properly incorporated into the ECM meshwork and for full functionality (13, 14). Therefore, we tested whether the amount of Loh present at the surface of cardiac cells directly affects ECM architecture (e.g. by recruiting increased or reduced quantities of Pericardin or other, yet unknown Loh interactors). An ultrastructural analysis of the cardiac matrix of homozygous *loh*<sup>MB05750</sup> mutant wandering third instar larvae, compared with WT, revealed no visible difference with respect to, for example, thickness of the matrix (Fig. 9A). By contrast, overexpression of full-length Loh (UAS-Loh FL) in cardiac cells results in irregular matrix deposition characterized by a dramatic increase in the width of the matrix (Fig. 9A, arrowheads). Heart performance, measured by high-speed video microscopy in semi-intact third instar larvae, is also affected when full-length Loh is overexpressed in cardiac cells. Corresponding animals display a considerably reduced heart rate, concomitant with severe arrhythmia (Fig. 9, B and C). Of note, arrhythmia includes long periods of heartbeat arrest, which emphasizes the severity of the phenotype. Representative examples are shown in Fig. 9B and in Movies S1–S4.

## Discussion

In contrast to matrices present at the surface of most other tissues, the cardiac ECM is exposed to permanent mechanical

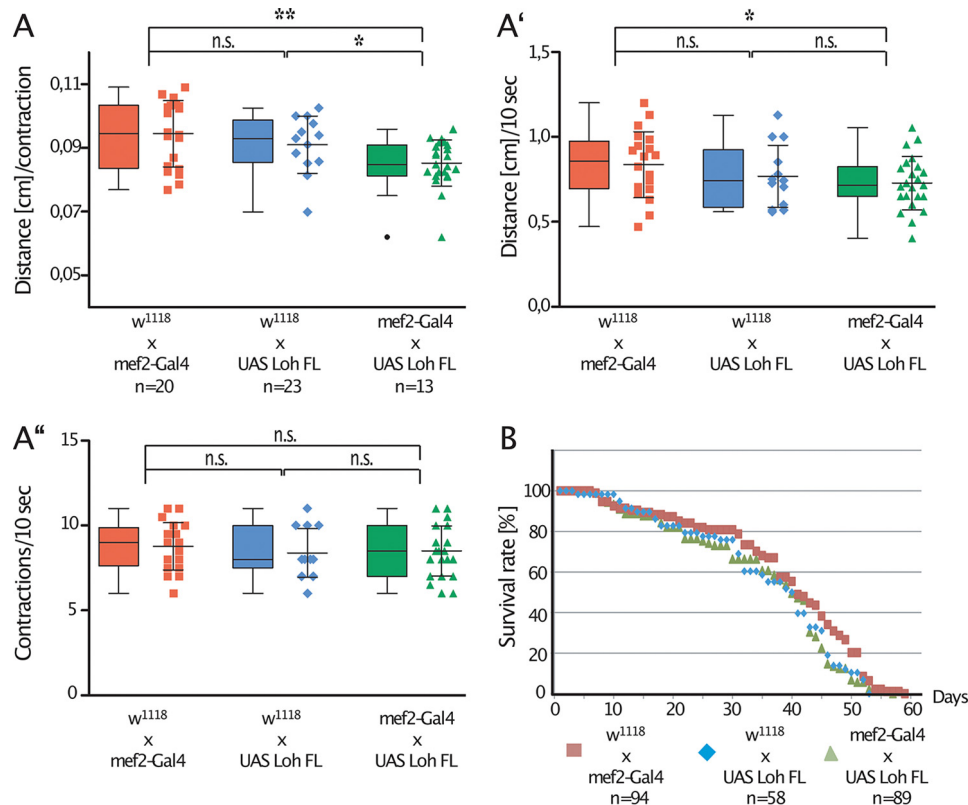


**Figure 8. Artificial recruitment of Pericardin affects muscle function.** A, ectopic expression of full-length Loh in muscles (*mef2-Gal4* × *UAS Loh FL*; green triangles) significantly impairs crawling performance. As controls, F1 animals from either a crossing of *mef2-Gal4* × *w<sup>1118</sup>* (red squares) or from *w<sup>1118</sup>* × *UAS-Loh FL* (blue diamonds) were used. Crawling performance was measured as crawling distance in cm/contraction (A) or crawling distance/10 s (A'). Crawling performance is significantly reduced if Pericardin is recruited to the muscle ECM (green triangles in A and A'). The contraction frequency is not significantly altered in corresponding animals (A''). Ectopic expression of full-length Loh (*mef2-Gal4* × *UAS Loh FL*; green triangles) has no effect on lifespan, compared with controls (*mef2-Gal4* × *w<sup>1118</sup>* (red squares) and *w<sup>1118</sup>* × *UAS Loh FL* (blue diamonds)) (B). Depicted are mean values ± S.D. (error bars). Corresponding significance levels are indicated (asterisks, Student's *t* test; \*,  $p < 0.05$ ; \*\*,  $p < 0.01$ ; n.s., not significant). Data are presented as box plots and scatter plots.

stress generated by the regular and repetitive contraction cycles of the heart. These unique biomechanical conditions require ECM adaptation, which is achieved predominantly by incorporating specific structural components into the respective matrices. In *Drosophila*, one of these components is the type IV collagen-like protein Pericardin, which is recruited specifically to cardiac tissue by its adaptor protein Lonely heart (13). However, until now, neither the recruitment process itself nor the relevance of Pericardin to the biomechanical properties of the cardiac ECM have been studied in detail. By conducting a recruitment assay based on systematically generated domain-specific Loh mutants, we found that presence of the first TSR1 domain is critical to localizing Loh to the ECM (Fig. 3D). Interestingly, mutating only the speculative GAG-binding site embedded within the first TSR1 domain is sufficient to abrogate Loh anchoring, indicating a high functional relevance of this distinct sequence motif (Fig. 3J). This result was confirmed by expressing the same constructs in Sf21 cells. Also in this system, deletion of the first TSR1 domain or mutation of the embedded putative GAG site resulted in considerably reduced surface localization of the respective Loh constructs (Fig. 2, D and I). Significantly, Western blot analysis detected the proteins in the culture medium (Fig. 2N), which indicates that production and secretion still occurred, whereas incorporation into the ECM was impaired. Thus, our data suggest that TSR1-1, with its embedded putative GAG-binding site, is cru-

cial for anchoring Loh to the ECM, which represents a prerequisite for the subsequent recruitment of Pericardin. On the other hand, the second speculative GAG binding site, embedded within the TSR1-4 domain, appears to be dispensable for localizing Loh (Figs. 2 (G, J, and N) and 3 (G and J)) but is required for efficient Pericardin recruitment (Fig. 4J). Of note, previous work identified the respective CXXTCXXG motif as a consensus site for *O*-fucosylation and showed that mutating this motif results in impaired protein secretion (24). Because the substitution in *UAS-Loh<sup>GAG2\*</sup>* covers this motif (Fig. 1A), slightly impaired secretion of this construct appears possible. However, its complete inability to recruit Pericardin (Fig. 4J) cannot be attributed to minor deficiencies in secretion. Thus, our findings indicate that both speculative GAG-binding sites are of high functional relevance, with the first site being essential to proper anchoring of Loh, whereas the second one appears to be required for Pericardin recruitment. Interestingly, also lack of the second TSR1 domain results in failure to recruit Pericardin (Fig. 4), whereas localization of Loh is not affected (Figs. 2 (E and N) and 3E). Thus, the TSR1-2 and TSR1-4 domains as well as the putative GAG2-binding site seem to be dispensable for localizing Loh but crucial to proper Pericardin interaction and recruitment. In this context, the distinct position of the respective domains within Loh is probably decisive. According to structural modeling, TSR1-2 and TSR1-4, the latter containing the predicted GAG2 site, exhibit

## Functional domains of Lonely heart

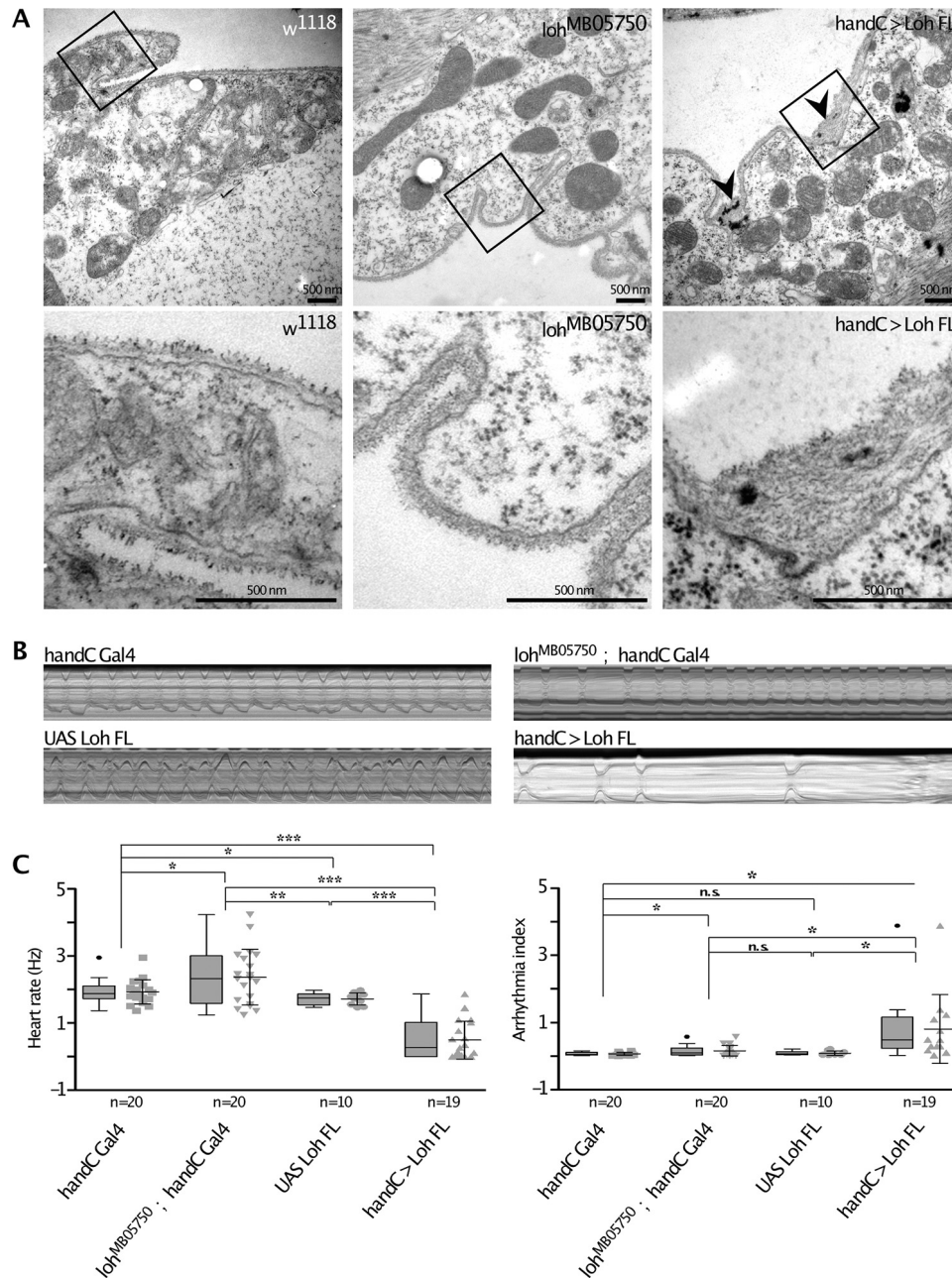


**Figure 9. Ultrastructural and physiological effects of modulated Loh levels in cardiac tissue.** *A*, transsections of the heart chamber of wandering third instar larvae analyzed by transmission EM. Images in the *top panels* represent overviews ( $\times 20,000$ ), whereas the *bottom panels* depicts *close-ups* of the marked areas. *Black arrowheads* indicate ECM accumulations that mainly occur at membrane invaginations of cardiomyocytes in *loh* overexpression animals (*handC > Loh FL*) but are absent in control animals (*w<sup>1118</sup>*) or *loh* null mutants (*loh<sup>MB05750</sup>*). *B*, representative M-modes (10-s videos) of third instar larvae of the depicted genotypes indicate heart rate over time and occurrence of arrhythmia. *C*, quantification of *B*. Both heart rate and rhythmicity (arrhythmia index) are significantly affected in *loh* knockout animals (*loh<sup>MB05750</sup>; handC-Gal4*) and *loh* overexpression larvae (*handC > Loh FL*), compared with controls (*handC-Gal4* and *UAS-Loh FL*). Depicted are mean values  $\pm$  S.D. (*error bars*). Corresponding significance levels are indicated (*asterisks*, Student's *t* test; \*,  $p < 0.05$ ; \*\*,  $p < 0.01$ ; \*\*\*,  $p < 0.001$ ; *n.s.*, not significant). Data are presented as box plots and scatter plots.

close spatial proximity (Fig. 1C). The fact that lack of either domain completely abolishes the capacity of Loh to recruit Pericardin (Fig. 4) indicates that these two domains constitute the interaction site between Loh and Prc, with the embedded speculative GAG binding site being of critical relevance. Subsequent to the initial binding, the nearby TSR1-3 and TSR1-5 domains may support interaction; however, their functional relevance is minor compared with TSR1-2 and TSR1-4 (Fig. 4). Taking these data into account, it appears likely that the N-terminal part of Loh, including the first TSR1 repeat and the

embedded predicted GAG binding site, is facing the plasma membrane and anchors the protein to the cell surface, probably via glycosaminoglycan binding. The C-terminal part of Loh would then be available for interaction with Pericardin, and possibly also with other ECM components, via the second and fourth TSR1 repeats. Of note, a function of the PLAC domain, which is present in several enzymes and ECM proteins, such as ADAMTS-2, -3, -10, and others, was not uncovered by our approach. Deleting the C-terminal PLAC domain in Loh has no distinct consequences, either for Loh secretion or for Pericar-

Pericardin N  C  
RGD motif

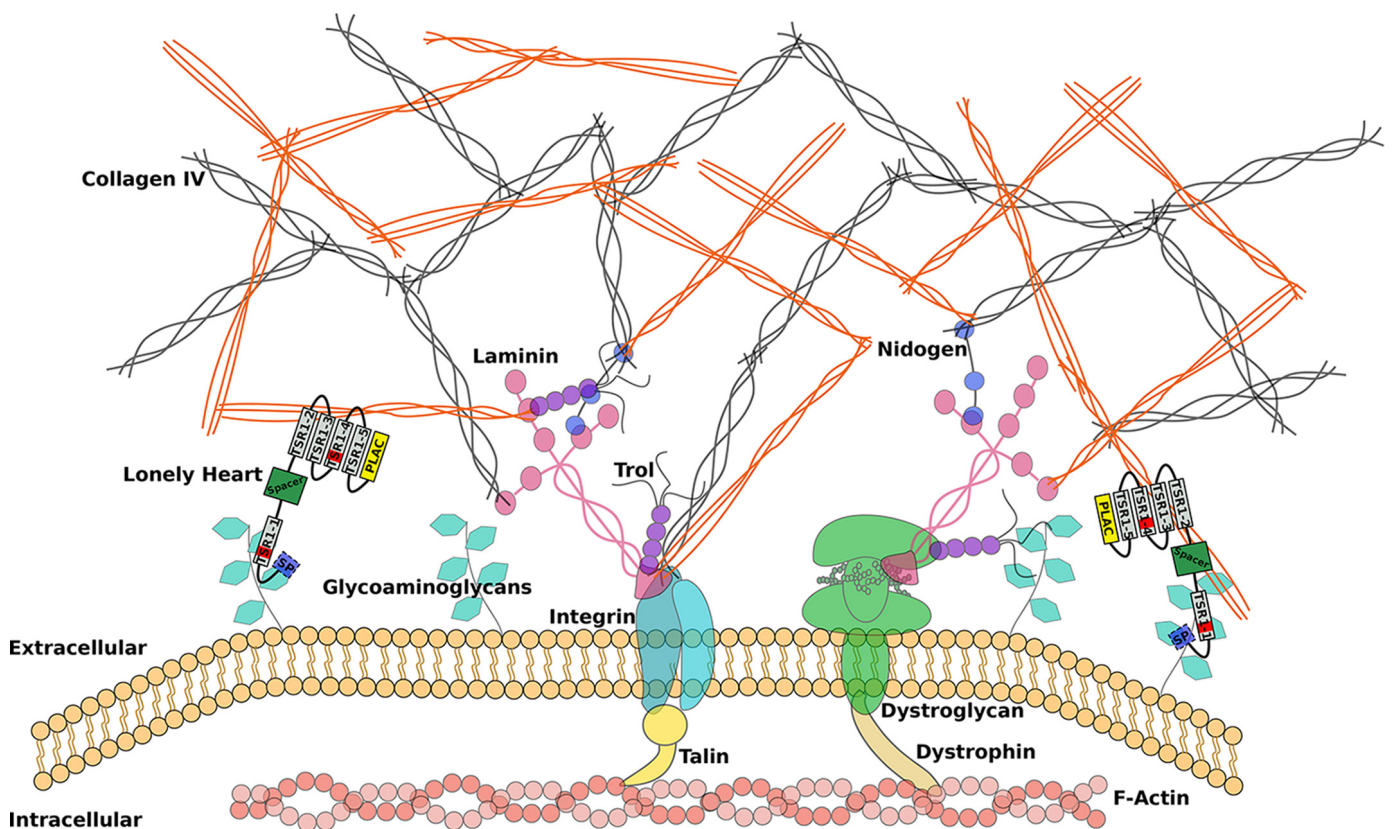


**Figure 10. Schematic representation of an extracellular matrix with incorporated Pericardin.** The ECM is coupled to the actin cytoskeleton via integrins or dystroglycans. Laminins form the connection between the large structural ECM constituents, including collagen IV, Pericardin, and integrin/dystroglycan. Based on our results, we postulate that Lonely heart binds to glycosaminoglycans of membrane-associated proteins via its first speculative GAG-binding site and to Pericardin (directly or indirectly) via its second and fourth thrombospondin type 1 repeat. Loh itself is shown as a protein domain scheme with a signal peptide indicated in *light blue*, the ADAMTS spacer in *green*, the PLAC domain in *yellow*, and the remaining thrombospondin type 1 repeats in *gray*, of which two harbor a predicted GAG binding site (*red bars*). The form of the scheme is based on the protein model shown in Fig. 1C. The depicted interaction between Pericardin and integrin is based solely on the presence of an RGD motif at the C terminus of Pericardin and is not experimentally proven.

din recruitment efficiency, as far as we can state in view of the sensitivity limitations of our test system. Results are summarized in Table S1.

Regarding the question of whether ECMs are generally capable of recruiting and incorporating Pericardin, we found that this is not the case. Whereas Loh-dependent recruitment was observed for fat body cells, somatic muscles, glial cells of the central nervous system, and wing discs, salivary gland cells did not incorporate Pericardin into the ECM, although Loh was present at the surface (Fig. 5). This result indicates that other, yet unknown ECM components are required, in addition to Loh, for proper recruitment of Pericardin and that at least one of these factors is not present in salivary gland cells. Identification of the respective constituents represents an important objective of future studies because it would complement the current understanding of the interconnections that form the cardiac extracellular matrix (Fig. 10). The alternative explanation, the presence of an inhibitory protein that prevents Pericardin incorporation into the ECM of salivary glands, appears unlikely, although we cannot rule out this possibility for sure.

When dissecting third instar larvae, Pericardin fibers randomly associated with various tissues are constantly observed (not shown). However, significant amounts of Pericardin, organized and incorporated into the meshwork of a matrix, are only present at the surface of the heart and chordotonal organs. This tissue specificity essentially depends on the presence of Loh (13), and this paper. The dispersed and random adhesion of Pericardin, synthesized and secreted by adipocytes, to other tissues presumably reflects an intrinsic property of the protein to interact, with low affinity, with matrix components other than Loh (*e.g.* with collagen IV or laminin) (Fig. 7). Thus, Pericardin is able to adhere to an existing matrix, yet efficient incorporation requires Loh presence. This hypothesis is also supported by the results of experiments expressing Loh at distinct surface areas of wing discs (Fig. 6). Therefore, we speculate that Loh is a primary anchor for Pericardin. Whether anchoring is mediated by direct or indirect interaction remains to be determined.

To understand the functional impact of Pericardin incorporation into extracellular matrices in more detail, we directed

## Functional domains of Lonely heart

the protein to the surface of somatic muscles by ectopically expressing Loh in this tissue. Because neither Loh nor Pericardin are present at the surface of WT somatic muscles, the setup allows distinct evaluation of the resulting biomechanical effects in corresponding transgenic animals. As depicted (Fig. 8), specimens with Pericardin incorporated into the muscle matrix exhibit a considerably reduced movement speed, which is caused by a reduction in the distance covered by a single contraction wave (Fig. 8A); the contraction rate is not altered in corresponding animals (Fig. 8A"). These effects are consistent with an increase in ECM stiffness as a result of Pericardin incorporation, which, in the case of body wall muscles, impairs flexibility and thus contraction efficiency. Of note, as has been shown in the aging mouse myocardium, an increase in cardiac stiffness correlates with the accumulation of collagen (25). Furthermore, fly hearts also exhibit reduced contraction efficiency with age, which manifests in decreased diastolic and systolic dimensions (26–28). The fact that Pericardin knockdown flies do not show this age-dependent decline (21) indicates that progressive Pericardin incorporation increases stiffness of the cardiac ECM in a similar way. Our data indicating that elevated Loh levels at the surface of cardiac cells result in increased matrix deposition and severely impaired heart function (Fig. 9) support this indication and emphasize the relevance of an adequate cardiac ECM composition to proper heart function. Aside from simply reflecting increased cardiac stiffness, the observed effects on heart rate and rhythmicity may also be indicative of altered chronotropy, caused by impaired activity of certain ion channels that in turn affects pacemaker function. This possibility is supported by recent data on *Drosophila* cardiac muscles, suggesting that basement membrane (BM) proteins are more than simple structural entities. Based on the fact that knockdown of Pericardin, laminin A, and viking increased cardiac contractility, whereas BM stiffness was apparently not altered, it was postulated that BM proteins are capable of regulating cardiac function by modulating interaction of the heart tube with adjacent muscle layers (21). By altering Loh abundance, and thus matrix composition, this interaction may be impaired, which could affect activity of corresponding mechanosensitive channels, eventually resulting in the observed phenotypes.

Whereas an in-depth understanding of Pericardin functionality clearly requires further studies, our current data suggest that the presence of the protein within the cardiac ECM is primarily required to ensure the structural integrity of the beating heart, rather than representing a means to increase flexibility of the tissue.

## Experimental procedures

### *Drosophila* stocks/fly lines

All UAS-Loh constructs were generated in this laboratory with the assistance of a commercial injection service (BestGene, Chino Hills, CA). *Drosophila* stocks labeled with BL numbers were obtained from the Bloomington stock center. For the WT, we used *w*<sup>1118</sup>. Gal4 driver lines used were *Cg*-Gal4 (29); *ci*-Gal4, *hh*-Gal4, *sd*-Gal4, *en*-Gal4 received from T. Klein (Düsseldorf, Germany); *dpp*-Gal4 received from H. Aberle

(Düsseldorf, Germany); *mef2*-Gal4 received from H. Nguyen (Erlangen, Germany); *pericardin*-Gal4 received from L. Perrin (Marseille, France); *repo*-Gal4 received from G. Technau (Mainz, Germany); and *sgs4-58*-Gal4 received from A. Hofmann (Berlin, Germany). Fly husbandry was carried out as described previously (30).

### Generation of Loh constructs

Loh constructs used to generate transgenic *Drosophila* were cloned into a yeast/*Escherichia coli*/*Saccharomyces cerevisiae* triple-shuttle vector (pJH1784) based on vectors described previously (31). The vector pJH1784 allows cloning via homologous recombination in yeast and site-specific integration into the *Drosophila* genome. All Loh constructs were introduced into the germ line by injections in the presence of the PhiC31 integrase (using line BL24749, Bloomington *Drosophila* Stock Center), which resulted in insertion into the 86F8 landing site on the 3R chromosome. Designs of the Loh constructs are depicted in Fig. 1B. All mutations were established by PCR and an appropriate primer design. Transgenic flies were generated using commercial services (BestGene). Complete sequences are available on request.

### Sf21 expression constructs and cell culture

Heterologous expression was performed in Sf21 cells (RRID: CVCL\_0518) using the Bac-to-Bac<sup>®</sup> baculovirus expression system (Life Technologies, Inc.). Full-length WT and mutated forms of Loh were cloned into an *E. coli*/*S. cerevisiae*/baculovirus triple-shuttle derivative of the pFastBac<sup>™</sup> Dual vector. The respective vector (pJH1460) was constructed similarly to the vectors described previously (31). Expression was induced as described previously (32). To track transfection efficiency, an *eGFP* reporter gene was inserted into the same vector under control of the p10 promoter. Transfected Sf21 cells were grown on coverslips in 6-well plates for 72 h. Subsequently, the coverslips were removed from the wells, and adherent cells were fixed in 3% paraformaldehyde in PBS for 30 min. After washing (3 × 5 min in PBS), cells were blocked and permeabilized in 2% BSA, 0.01% Triton X-100 (in PBS) for 20 min and incubated with primary antibodies (anti-Loh; 1:500) overnight (4 °C). Unbound antibodies were removed by washing (3 × 5 min in PBS), and cells were blocked again for 60 min (Roti Immunoblock, Carl Roth, Karlsruhe, Germany), followed by additional washing (3 × 5 min in PBS). Secondary antibodies (anti-guinea pig, Cy3 conjugate, Dianova) were diluted in PBS (1:200) and applied for 90 min at room temperature. Finally, cells were washed again (as described above) and mounted in Fluoromount-G (Southern Biotech, Birmingham, AL). Confocal images were captured with an LSM 5 Pascal confocal microscope (Zeiss, Jena, Germany).

### Immunoprecipitation

For each sample, 100 wandering third instar larvae were snap-frozen in liquid nitrogen and ground to powder. The powder was resuspended in 1 ml of lysis buffer (150 mM NaCl, 5% glycerol, 1% IGEPAL-CA-630, 1 mM MgCl<sub>2</sub>, 50 mM Tris, pH 7.5, 1× protease inhibitor mix from Sigma-Aldrich, Heidelberg, Germany) and incubated for 30 min at room temperature. Sub-

sequent to centrifugation (15 min,  $4000 \times g$ ), 800  $\mu\text{l}$  of the supernatant were mixed with paramagnetic beads precoupled to anti-GFP antibodies ( $\mu\text{MACS}$  GFP Isolation Kit, Miltenyi Biotec, Auburn, CA) and run over magnetic  $\mu$ -columns according to the manufacturer's instructions (Miltenyi Biotec). Elution fractions were subjected to SDS-PAGE and Western blotting as described previously (33). Primary antibodies were anti-GFP (made in goat, 1:2000; Abcam, Cambridge, UK), anti-Pericardin (made in mouse, 1:100; Developmental Studios Hybridoma Bank, Iowa City, IA), anti-nidogen (made in rabbit, 1:3000; gift from Stefan Baumgartner), and anti-KcLaminin (made in rabbit, 1:2000; gift from John Fessler). Secondary antibodies were anti-goat-AP (1:10,000; Sigma), anti-mouse-AP (1:10,000; Sigma), and anti-rabbit-AP (1:10,000; Sigma).

### Immunohistochemistry, Western blotting analyses, and confocal microscopy

Immunostainings were carried out as described previously (33). Antibodies used in this study were as follows: guinea pig anti-Loh (1:500; this laboratory), mouse anti-Pericardin/EC11 (1:5; Developmental Studios Hybridoma Bank), mouse anti- $\alpha$ -spectrin/3A9 (1:3; Developmental Studios Hybridoma Bank), rabbit anti-nidogen/entactin (1:1000; a gift from S. Baumgartner), rabbit anti-laminin (detects only secreted laminin trimers; a gift from J. Fessler), mouse anti- $\beta$ -Tubulin (1:5 to 1:200; Developmental Studios Hybridoma Bank), and rabbit anti-GFP (1:1000; Abcam). Secondary antibodies used were anti-mouse Cy2/Cy3 (1:100/1:200; Dianova), anti-rabbit-Cy2/Cy3 (1:100/1:200; Dianova), and anti-guinea pig Cy2/Cy3/Alexa633 (1:100/1:200/1:200; Thermo Fisher Scientific, Dianova, and Abcam). F-Actin was visualized by staining fixed tissues using TRITC coupled with phalloidin (Sigma) at a concentration of 0.4  $\mu\text{g}/\text{ml}$  (1:200) in  $1 \times$  PBS, for 2 h at room temperature. Confocal images were captured with a Zeiss LSM 5 Pascal cLSM. Z-stacks were acquired using standard settings and objectives. If not otherwise noted, Z-stacks are depicted as maximum projections. Image processing was done with ImageJ and Affinity Photo.

### Transmission EM

Larvae were processed as described previously with minor modifications (34). Briefly, abdomens of larvae were prepared and fixed for 4 h at room temperature in 2% glutaraldehyde (Sigma) in artificial hemolymph, subsequently washed in 0.5 M cacodylate buffer, pH 7.4, post-fixed for 2 h at room temperature in 1% osmium tetroxide in 0.5 M cacodylate buffer, pH 7.4 (Science Services, Munich, Germany), dehydrated stepwise in a graded ethanol series, and embedded in Epon 812. Ultrathin sections (70 nm) were assembled on an ultramicrotome (UC6 and UC7 Leica, Wetzlar, Germany) and mounted on copper slot grids. Sections were stained for 30 min in 2% uranyl acetate (Science Services) and for 20 min in 3% lead citrate (Carl Roth, Karlsruhe, Germany). TEM images were acquired with a Zeiss 902 or a Zeiss 120-kV transmission electron microscope. For all genotypes,  $n = 3$ .

### Recruitment assay and pixel intensity analysis

For the Pericardin recruitment assay, UAS-*loh* constructs (full-length WT or mutated forms of Loh) were expressed under the control of *mef2*-Gal4 (muscle cell lineage); *pericardin*-Gal4 (adipocytes and pericardial cells); *Cg*-Gal4 (adipocytes); *repo*-Gal4 (central nervous system); *sgs*-Gal4 (salivary glands); or *dpp*-Gal4, *ci*-Gal4, *hh*-Gal4, *sd*-Gal4, or *en*-Gal4 (imaginal disc). All crossings were set up, and offspring were allowed to grow up at 27 °C until the third instar wandering stage. Subsequently, animals were dissected, and tissues of interest were fixed for further processing (13, 35).

Confocal images of stained third instar larvae were obtained with an LSM5 Pascal confocal microscope (Zeiss). The Cy2 signal, depicting the distribution of Pericardin, was normalized to the TRITC signal of the phalloidin staining to adapt to variable parameters in the staining procedure, such as fixation or permeabilization efficiencies. Captured Z-stacks were further analyzed using ImageJ. After a reduction of the background, a maximum projection using the "sum slices" option was created. Subsequently, the pixel intensity within an ROI was measured (at least 10 animals/genotype). Further data analysis was conducted with GraphPad Prism (GraphPad Software, La Jolla, CA).

### Lifespan assay

Following an approved protocol (36), 2–10 male or female flies, collected within 1 day of eclosion, were transferred twice per week to fresh vials with standard food. A minimum of 55 flies were analyzed per genotype. Vials were kept at 27 °C for the duration of the lifespan assay. Surviving flies were counted after vial changes. All animals were maintained under constant 12-h/12-h, light/dark cycles. Data analysis was conducted with GraphPad Prism (GraphPad Software).

### Crawling assay and data analysis

Wandering third instar larvae were collected, and their locomotion activity was recorded with a standard digital camera under a Zeiss binocular (37). The larval linear forward crawling distance and the number of body wall contractions within a time frame of 10 s were assessed for each animal. Corresponding measurements were done for at least 13 animals per crossing. As negative controls, third instar offspring of *mef2*-Gal4  $\times$  *w*<sup>1118</sup>, as well as UAS-Loh FL  $\times$  *w*<sup>1118</sup> crossings, were analyzed. All distance measurements were performed using ImageJ, whereas further data analysis was conducted with GraphPad Prism (GraphPad Software).

### Animal preparation and video analysis

Wandering third instar larvae were pinned down with the dorsal side downward onto Sylgard 184 silicone elastomer plates, which were filled with artificial hemolymph. Artificial hemolymph contains 108 mM NaCl, 5 mM KCl, 2 mM CaCl<sub>2</sub>, 8 mM MgCl<sub>2</sub>, 1 mM NaH<sub>2</sub>PO<sub>4</sub>, 4 mM NaHCO<sub>3</sub>, and 5 mM HEPES, pH 7.1. Before use, the buffer was supplemented with sucrose (final concentration, 10 mM) and trehalose (final concentration, 10 mM) (38). After dissecting the animals, the specimens were allowed to rest for 10 min. To record heartbeat, a high-speed

## Functional domains of Lonely heart

video camera (Basler piA-640) was mounted on an upright microscope (Leica DMLB), equipped with a  $\times 10$  Leica Fluotar. Movies were captured with the software Firecapture® (freeware by Torsten Edelmann) and processed with ImageJ (39). Heart parameters were analyzed using SOHA (Semi-Automated Optical Heartbeat Analysis), a MATLAB application first introduced by Fink *et al.* (40, 41). Additional data analysis was done using Microsoft Excel and GraphPad Prism (GraphPad Software).

### Structural modeling

Yasara Structure 15.7.25 (42) was used to calculate a 3D homology model of Lonely heart. Templates for the homology modeling process were identified by performing a BLAST search of the *lonely heart* target sequence against ExpDB (43). 16 template structures were provided for building 56 homology models. Finally, one hybrid model of the 56 homology models was generated.

---

**Author contributions**—A. P. conceptualization; B. R., Y. P., M. R., K. L., A. B., H. M., and J. J. H. investigation; A. P. and H. M. writing-original draft; B. R., Y. P., H. M., and M. R. writing-review and editing; A. P. funding acquisition; B. R., H. M., and A. P. supervision.

---

**Acknowledgments**—We thank Mechthild Krabusch, Martina Biedermann, and Kerstin Etzold for excellent technical assistance and fly-keeping. We thank Markus Schneider for providing the Loh 3D model in Fig. 1C and Maik Drechsler, Ariane Wilmes, Philipp Merling, and Patrick Tiltmann for initial experiments. We thank Thomas Klein and Hermann Aberle for sharing fly stocks and reagents. We also thank the Bloomington *Drosophila* Stock Center for providing fly stocks and Flybase for providing genetic, genomic, and functional information.

---

### References

- Hynes, R. O. (1992) Integrins: versatility, modulation, and signaling in cell adhesion. *Cell* **69**, 11–25 [CrossRef Medline](#)
- Hynes, R. O., and Yamada, K. M. (2012) *Extracellular Matrix Biology*, Cold Spring Harbor Laboratory Press, Cold Spring Harbor, NY
- Timpl, R. (1996) Macromolecular organization of basement membranes. *Curr. Opin. Cell Biol.* **8**, 618–624 [CrossRef Medline](#)
- Kohfeldt, E., Sasaki, T., Göhring, W., and Timpl, R. (1998) Nidogen-2: a new basement membrane protein with diverse binding properties. *J. Mol. Biol.* **282**, 99–109 [CrossRef Medline](#)
- Pastor-Pareja, J. C., and Xu, T. (2011) Shaping cells and organs in *Drosophila* by opposing roles of fat body-secreted Collagen IV and Perlecan. *Dev. Cell* **21**, 245–256 [CrossRef Medline](#)
- Rotstein, B., and Paululat, A. (2016) On the morphology of the *Drosophila* heart. *J. Cardiovasc. Dev. Dis.* **3**, E15 [CrossRef Medline](#)
- Volk, T., Wang, S., Rotstein, B., and Paululat, A. (2014) Matricellular proteins in development: perspectives from the *Drosophila* heart. *Matrix Biol.* **37**, 162–166 [CrossRef Medline](#)
- Das, D., Aradhya, R., Ashoka, D., and Inamdar, M. (2008) Post-embryonic pericardial cells of *Drosophila* are required for overcoming toxic stress but not for cardiac function or adult development. *Cell Tissue Res.* **331**, 565–570 [CrossRef Medline](#)
- Ivy, J. R., Drechsler, M., Catterson, J. H., Bodmer, R., Ocorr, K., Paululat, A., and Hartley, P. S. (2015) Klf15 is critical for the development and differentiation of *Drosophila* nephrocytes. *PLoS One* **10**, e0134620 [CrossRef Medline](#)
- Tutor, A. S., Prieto-Sánchez, S., and Ruiz-Gómez, M. (2014) Src64B phosphorylates Dumbfounded and regulates slit diaphragm dynamics: *Drosophila* as a model to study nephropathies. *Development* **141**, 367–376 [CrossRef Medline](#)
- Tögel, M., Pass, G., and Paululat, A. (2008) The *Drosophila* wing hearts originate from pericardial cells and are essential for wing maturation. *Dev. Biol.* **318**, 29–37 [CrossRef Medline](#)
- Tögel, M., Pass, G., and Paululat, A. (2013) *In vivo* imaging of *Drosophila* wing heart development during pupal stages. *Int. J. Dev. Biol.* **57**, 13–24 [CrossRef Medline](#)
- Drechsler, M., Schmidt, A. C., Meyer, H., and Paululat, A. (2013) The conserved ADAMTS-like protein Lonely heart mediates matrix formation and cardiac tissue integrity. *PLoS Genet.* **9**, e1003616 [CrossRef Medline](#)
- Wilmes, A. C., Klinke, N., Rotstein, B., Meyer, H., and Paululat, A. (2018) Biosynthesis and assembly of the Collagen IV-like protein Pericardin in *Drosophila melanogaster*. *Biol. Open* **7**, bio030361 [CrossRef Medline](#)
- Kuno, K., and Matsushima, K. (1998) ADAMTS-1 protein anchors at the extracellular matrix through the thrombospondin type I motifs and its spacing region. *J. Biol. Chem.* **273**, 13912–13917 [CrossRef Medline](#)
- Apte, S. S. (2009) A disintegrin-like and metalloprotease (reprolysin-type) with thrombospondin type 1 motif (ADAMTS) superfamily: functions and mechanisms. *J. Biol. Chem.* **284**, 31493–31497 [CrossRef Medline](#)
- Tortorella, M. D., Malfait, F., Barve, R. A., Shieh, H. S., and Malfait, A. M. (2009) A review of the ADAMTS family, pharmaceutical targets of the future. *Curr. Pharm. Des.* **15**, 2359–2374 [CrossRef Medline](#)
- Adams, J. C., and Lawler, J. (2011) The thrombospondins. *Cold Spring Harb. Perspect. Biol.* **3**, a009712 [Medline](#)
- Tan, K., Duquette, M., Liu J.-H., Dong, Y., Zhang, R., Joachimiak, A., Lawler, J., and Wang, J.-H. (2002) Crystal structure of the TSP-1 type 1 repeats: A novel layered fold and its biological implication. *J. Cell Biol.* **159**, 373–382 [CrossRef Medline](#)
- Albrecht, S., Altenhein, B., and Paululat, A. (2011) The transmembrane receptor Uncoordinated5 (Unc5) is essential for heart lumen formation in *Drosophila melanogaster*. *Dev. Biol.* **350**, 89–100 [CrossRef Medline](#)
- Sessions, A. O., Kaushik, G., Parker, S., Raedschelders, K., Bodmer, R., Van Eyk, J. E., and Engler, A. J. (2017) Extracellular matrix downregulation in the *Drosophila* heart preserves contractile function and improves lifespan. *Matrix Biol.* **62**, 15–27 [CrossRef Medline](#)
- Sarov, M., Barz, C., Jambor, H., Hein, M. Y., Schmied, C., Suchold, D., Stender, B., Janosch, S., KJ, V. V., Krishnan, R. T., Krishnamoorthy, A., Ferreira, I. R., Ejsmont, R. K., Finkl, K., Hasse, S., *et al.* (2016) A genome-wide resource for the analysis of protein localisation in *Drosophila*. *eLife* **5**, e12068 [Medline](#)
- Gotwals, P. J., Paine-Saunders, S. E., Stark, K. A., and Hynes, R. O. (1994) *Drosophila* integrins and their ligands. *Curr. Opin. Cell Biol.* **6**, 734–739 [CrossRef Medline](#)
- Wang, L. W., Dlugosz, M., Somerville, R. P., Raed, M., Haltiwanger, R. S., and Apte, S. S. (2007) O-Fucosylation of thrombospondin type 1 repeats in ADAMTS-like-1/punctin-1 regulates secretion: implications for the ADAMTS superfamily. *J. Biol. Chem.* **282**, 17024–17031 [CrossRef Medline](#)
- Bradshaw, A. D., Baicu, C. F., Rentz, T. J., Van Laer, A. O., Bonnema, D. D., and Zile, M. R. (2010) Age-dependent alterations in fibrillar collagen content and myocardial diastolic function: role of SPARC in post-synthetic procollagen processing. *Am. J. Physiol. Heart Circ. Physiol.* **298**, H614–H622 [CrossRef Medline](#)
- Cammarato, A., Dambacher, C. M., Knowles, A. F., Kronert, W. A., Bodmer, R., Ocorr, K., and Bernstein, S. I. (2008) Myosin transducer mutations differentially affect motor function, myofibril structure, and the performance of skeletal and cardiac muscles. *Mol. Biol. Cell* **19**, 553–562 [Medline](#)
- Nishimura, M., Kumsta, C., Kaushik, G., Diop, S. B., Ding, Y., Bisharat-Kernizan, J., Catan, H., Cammarato, A., Ross, R. S., Engler, A. J., Bodmer, R., Hansen, M., and Ocorr, K. (2014) A dual role for integrin-linked kinase and  $\beta 1$ -integrin in modulating cardiac aging. *Aging Cell* **13**, 431–440 [CrossRef Medline](#)
- Kaushik, G., Spelnhauer, A., Sessions, A. O., Trujillo, A. S., Fuhrmann, A., Fu, Z., Venkatraman, V., Pohl, D., Tuler, J., Wang, M., Lakatta, E. G., Ocorr, K., Bodmer, R., Bernstein, S. I., Van Eyk, J. E., *et al.* (2015) Vinculin

- network-mediated cytoskeletal remodeling regulates contractile function in the aging heart. *Sci. Transl. Med.* **7**, 292ra99 [CrossRef Medline](#)
29. Asha, H., Nagy, I., Kovacs, G., Stetson, D., Ando, I., and Dearolf, C. R. (2003) Analysis of Ras-induced overproliferation in *Drosophila* hemocytes. *Genetics* **163**, 203–215 [Medline](#)
  30. Kölsch, V., and Paululat, A. (2002) The highly conserved cardiogenic bHLH factor Hand is specifically expressed in circular visceral muscle progenitor cells and in all cell types of the dorsal vessel during *Drosophila* embryogenesis. *Dev. Genes Evol.* **212**, 473–485 [CrossRef Medline](#)
  31. Paululat, A., and Heinisch, J. J. (2012) New yeast/*E. coli*/*Drosophila* triple shuttle vectors for efficient generation of *Drosophila* P element transformation constructs. *Gene* **511**, 300–305 [CrossRef Medline](#)
  32. Hallier, B., Schiemann, R., Cordes, E., Vitos-Faleato, J., Walter, S., Heinisch, J. J., Malmendal, A., Paululat, A., and Meyer, H. (2016) *Drosophila* neprilysins control insulin signaling and food intake via cleavage of regulatory peptides. *eLife* **5**, e19430 [Medline](#)
  33. Meyer, H., Panz, M., Zmojdzian, M., Jagla, K., and Paululat, A. (2009) Neprilysin 4, a novel endopeptidase from *Drosophila melanogaster*, displays distinct substrate specificities and exceptional solubility states. *J. Exp. Biol.* **212**, 3673–3683 [CrossRef Medline](#)
  34. Lehmacher, C., Abeln, B., and Paululat, A. (2012) The ultrastructure of *Drosophila* heart cells. *Arthropod. Struct. Dev.* **41**, 459–474 [CrossRef Medline](#)
  35. Lammers, K., Abeln, B., Hüsken, M., Lehmacher, C., Psathaki, O. E., Alcorta, E., Meyer, H., and Paululat, A. (2017) Formation and function of intracardiac valve cells in the *Drosophila* heart. *J. Exp. Biol.* **220**, 1852–1863 [CrossRef Medline](#)
  36. Linford, N. J., Bilgir, C., Ro, J., and Pletcher, S. D. (2013) Measurement of lifespan in *Drosophila melanogaster*. *J. Vis. Exp.* [CrossRef Medline](#)
  37. Nichols, C. D., Becnel, J., and Pandey, U. B. (2012) Methods to assay *Drosophila* behavior. *J. Vis. Exp.* [CrossRef Medline](#)
  38. Vogler, G., and Ocorr, K. (2009) Visualizing the beating heart in *Drosophila*. *J. Vis. Exp.* [CrossRef Medline](#)
  39. Rasband, W. S. (2016) *ImageJ*, National Institutes of Health, Bethesda, MD
  40. Fink, M., Callol-Massot, C., Chu, A., Ruiz-Lozano, P., Izipisua Belmonte, J. C., Giles, W., Bodmer, R., and Ocorr, K. (2009) A new method for detection and quantification of heartbeat parameters in *Drosophila*, zebrafish, and embryonic mouse hearts. *BioTechniques* **46**, 101–113 [CrossRef Medline](#)
  41. Ocorr, K., Vogler, G., and Bodmer, R. (2014) Methods to assess *Drosophila* heart development, function and aging. *Methods* **68**, 265–272 [CrossRef Medline](#)
  42. Krieger, E., and Vriend, G. (2014) View—molecular graphics for all devices—from smartphones to workstations. *Bioinformatics* **30**, 2981–2982 [CrossRef Medline](#)
  43. Schwede, T., Diemand, A., Guex, N., and Peitsch, M. C. (2000) Protein structure computing in the genomic era. *Res. Microbiol.* **151**, 107–112 [CrossRef Medline](#)
  44. Guo, N. H., Krutzsch, H. C., Nègre, E., Zabrenetzky, V. S., and Roberts, D. D. (1992) Heparin-binding peptides from the type I repeats of thrombospondin: structural requirements for heparin binding and promotion of melanoma cell adhesion and chemotaxis. *J. Biol. Chem.* **267**, 19349–19355 [Medline](#)
  45. Tuszynski, G. P., Rothman, V. L., Deutch, A. H., Hamilton, B. K., and Eyal, J. (1992) Biological activities of peptides and peptide analogues derived from common sequences present in thrombospondin, properdin, and malarial proteins. *J. Cell Biol.* **116**, 209–217 [CrossRef Medline](#)



## 5 Publication 3

### Identification and *In Vivo* Characterisation of Cardioactive Peptides in *Drosophila melanogaster*. (2018)

Ronja Schiemann, Kay Lammers, Maren Janz, Jana Lohmann, Achim Paululat and Heiko Meyer \*

Department of Zoology and Developmental Biology, University of Osnabrück, Barbaras-  
traße 11, 49076 Osnabrück

Neuropeptides and peptide hormones are evolutionarily conserved signalling molecules present from invertebrates to humans. *Drosophila* produces many neuropeptides and peptide hormones that play essential roles in regulating growth, development, reproduction, behaviour, physiology and other processes (Hewes and Taghert, 2001; Nässel and Zandawala, 2019). Previous studies have described the substrate specificity of the metallopeptidase Neprilysin 4 (Nep4), which localises to the heart surface (Meyer et al., 2009; Hallier et al., 2016). Multiple peptides are hydrolysed by Nep4, which hints at a heart modulatory function of these peptides. The study investigated a set of peptides for their ability to modulate cardiac function. Many peptides have been identified to significantly affect the heart function in semi-intact animals. My contribution to publication 3 was to determine the *in vivo* relevance of the specific peptides by using the HIRO software. Our results revealed physiological mechanisms that regulate heart rhythmicity in *Drosophila*. Due to the fact that heart parameters are evolutionarily conserved from *Drosophila* to humans (Sláma, 2012), these findings may be relevant for the understanding of cardiomodulatory factors in vertebrates.



Article

# Identification and In Vivo Characterisation of Cardioactive Peptides in *Drosophila melanogaster*

Ronja Schiemann, Kay Lammers, Maren Janz, Jana Lohmann, Achim Paululat and Heiko Meyer \*

Department of Zoology and Developmental Biology, University of Osnabrück, Barbarastrasse 11, 49076 Osnabrück, Germany; Ronja.Schiemann@biologie.uni-osnabrueck.de (R.S.);

kay.lammers@biologie.uni-osnabrueck.de (K.L.); Maren.Janz@biologie.uni-osnabrueck.de (M.J.); ja.lohmann@gmx.de (J.L.); achim.paululat@biologie.uni-osnabrueck.de (A.P.)

\* Correspondence: meyer@biologie.uni-osnabrueck.de

Received: 2 November 2018; Accepted: 22 November 2018; Published: 20 December 2018



**Abstract:** Neuropeptides and peptide hormones serve as critical regulators of numerous biological processes, including development, growth, reproduction, physiology, and behaviour. In mammals, peptidergic regulatory systems are complex and often involve multiple peptides that act at different levels and relay to different receptors. To improve the mechanistic understanding of such complex systems, invertebrate models in which evolutionarily conserved peptides and receptors regulate similar biological processes but in a less complex manner have emerged as highly valuable. *Drosophila melanogaster* represents a favoured model for the characterisation of novel peptidergic signalling events and for evaluating the relevance of those events *in vivo*. In the present study, we analysed a set of neuropeptides and peptide hormones for their ability to modulate cardiac function in semi-intact larval *Drosophila melanogaster*. We identified numerous peptides that significantly affected heart parameters such as heart rate, systolic and diastolic interval, rhythmicity, and contractility. Thus, peptidergic regulation of the *Drosophila* heart is not restricted to chronotropic adaptation but also includes inotropic modulation. By specifically interfering with the expression of corresponding peptides in transgenic animals, we assessed the *in vivo* relevance of the respective peptidergic regulation. Based on the functional conservation of certain peptides throughout the animal kingdom, the identified cardiomodulatory activities may be relevant not only to proper heart function in *Drosophila*, but also to corresponding processes in vertebrates, including humans.

**Keywords:** endocrine signalling; dorsal vessel; heart function; heart physiology; neuropeptides; peptide hormones; peptide signalling

## 1. Introduction

Peptide signalling represents an evolutionarily highly conserved mechanism for regulating numerous biological processes, including development, growth, reproduction, physiology, and behaviour [1–6]. Sessile animals with limited locomotory activities, such as Hydra, utilise distinct neuropeptides, e.g., for signal transmission between neurons and muscles [7–10]. More evolved animals, such as mammals, exhibit highly complex peptidergic signalling that is still far from being completely understood. The observations that most neuropeptides studied to date fulfil more than one function and that multiple neuropeptides must work in concert to coordinate certain physiological processes render the system extremely diverse [11]. Additionally, the recent and still ongoing identification of small open reading frames (sORFs/smORFs) present in RNAs, which were previously considered noncoding, has contributed to an increasingly complex picture, as many of these ORFs are translated into previously unknown peptides of crucial physiological functionality [12–15].

Nevertheless, in the last decades, considerable progress has been made toward understanding distinct peptidergic signalling systems [16–18]. In this context, invertebrate models have proven highly valuable for understanding the physiological bases of neuropeptide functionality in detail. Crustaceans and insects were commonly used to isolate biologically active peptide species and to measure their respective functionalities via specialised *in vitro* analyses [19–25]. More recently, the ability to specifically interfere with expression of peptide precursors or with the expression of the respective receptors has rendered *Drosophila melanogaster* a favoured organism for studying neuropeptide and peptide hormone function *in vivo* [26–30]. Corresponding analyses resulted in the identification of numerous mature neuropeptides that are released from individual neurohemal release sites of the *Drosophila* central nervous system [31–33]. In addition, a number of physiological and behavioural aspects were identified as being regulated, at least in part, by peptide signalling in *Drosophila*. These aspects include reproduction and growth [34–38], food intake [39–41], learning and memory [42–44], and circadian rhythmicity [45–49].

Despite its physiological significance, very little is known about the peptidergic regulation of the *Drosophila* heart. In former studies, we characterised the substrate specificity of Neprilysin 4 (Nep4), a heart surface bound metallopeptidase [40,50]. In the course of these investigations, we identified several peptides that were hydrolysed by Nep4 and considered cleavage by the heart bound peptidase initial indication for a putative heart modulatory function of the respective peptide. To assess the validity of this indication, in the present study, we analysed corresponding peptides for cardiomodulatory activity. Presence of the respective neuropeptides and peptide hormones in *Drosophila* has been experimentally confirmed previously [32,33,51–53]. As a result, we identified a number of peptides that significantly modulated heart function in semi-intact animals. Affected parameters included heart rate, systolic and diastolic interval, fractional shortening, and rhythmicity. By specifically interfering with the expression of the peptides' precursor genes, we further assessed the *in vivo* relevance of distinct peptides. Thus, our results contribute to an in-depth understanding of the physiological mechanisms that regulate heart function in *Drosophila*. Considering the functional conservation of certain peptides and receptors, the observed cardiomodulatory activities may also be relevant to corresponding processes in vertebrates, including humans.

## 2. Results

### 2.1. The Larval *Drosophila* Heart Is Highly Responsive to Peptide Application

In previous studies, peptides such as Angiotensin [54], CCAP [55,56], FMRFamide-related peptides [57,58], and Proctolin [59–61] were identified as efficient regulators of heart function in *Drosophila*. To identify additional cardiomodulatory peptides, we analysed a set of neuropeptides and peptide hormones for their ability to modulate distinct larval heart parameters. The presence of all respective peptides in *Drosophila*, as well as their corresponding molecular masses and sequences, was experimentally confirmed in previous studies [32,33,51–53]. In an initial screen, we individually applied each synthesised peptide species at a concentration of  $1 \times 10^{-7}$  M onto semi-intact larval heart preparations and measured the resulting effects on characteristic heart parameters such as heart rate, systolic and diastolic interval, fractional shortening, and rhythmicity via semi-automatic optical heartbeat analysis (SOHA [62]). The tested peptides were Adipokinetic hormone (AKH); Allatostatin A1, A2, A3, and A4 (AstA1–A4); Corazonin; Diuretic hormone 31 (DH31); Drosulfakinins 1 and 2 (DSK1, DSK2); Leucokinin; Proctolin; short Neuropeptide F (sNPF<sub>1–11</sub>, sNPF<sub>212–19</sub>); and Tachykinin 1 to 6 (Table 1).

As depicted in Figure 1, six peptides exhibited considerable cardioacceleratory activity. These were Corazonin (+28.1% heart rate increase), DH31 (+40.8% heart rate increase), Proctolin (+48.4% heart rate increase), Tachykinin 1 (+28.8% heart rate increase), Tachykinin 3 (+12.9% heart rate increase), and Tachykinin 5 (+32.6% heart rate increase). None of the tested peptides significantly reduced heart rate. Application of Allatostatin A4 resulted in a complete, yet reversible, heartbeat arrest.

**Table 1.** Peptides used in this study and corresponding effects on distinct heart parameters in semi-intact larvae.

| Peptide                | Sequence                    | Heart Rate | Diastolic Interval | Systolic Interval | Fractional Shortening | Arrhythmicity Index |
|------------------------|-----------------------------|------------|--------------------|-------------------|-----------------------|---------------------|
| AKH                    | QLTFSPDWa                   | /          | /                  | /                 | /                     | /                   |
| AstA1                  | VERYAFGLa                   | /          | /                  | /                 | +                     | /                   |
| AstA2                  | LPVYNFGLa                   | /          | -                  | +                 | /                     | /                   |
| AstA3                  | SRPYSFGLa                   | /          | /                  | /                 | /                     | /                   |
| AstA4                  | TTRPQPFNFGLa                | ⊖          | ⊖                  | ⊖                 | ⊖                     | ⊖                   |
| Corazonin              | QTFQYSRGWTNa                | ++         | -                  | +                 | /                     | /                   |
| DH31                   | TVDFGLARGYSGTQEAKHRMGLA     | +++        | -                  | -                 | /                     | /                   |
| DSK1                   | FDDYGHMRFa                  | /          | /                  | /                 | /                     | /                   |
| DSK2                   | GGDDQFDDYGHMRFa             | /          | /                  | /                 | /                     | /                   |
| Leucokinin             | NSVVLGKKQRFHSWGa            | /          | /                  | /                 | +                     | /                   |
| Proctolin              | RYLPT                       | +++        | —                  | /                 | /                     | +                   |
| sNPF1 <sub>1-11</sub>  | AQRSPSLRLRFa                | /          | /                  | /                 | /                     | /                   |
| sNPF1 <sub>4-11</sub>  | SPSLRLRFa                   | /          | /                  | /                 | /                     | /                   |
| sNPF2 <sub>12-19</sub> |                             | /          | /                  | /                 | /                     | /                   |
| Tachykinin 1           | APTSSFIGMRa                 | +++        | -                  | /                 | /                     | +                   |
| Tachykinin 2           | APLAFVGLRa                  | /          | /                  | /                 | /                     | /                   |
| Tachykinin 3           | APTGFTGMRa                  | +          | /                  | /                 | /                     | /                   |
| Tachykinin 4           | APVNSFVGMRa                 | /          | /                  | /                 | /                     | ++                  |
| Tachykinin 5           | APNGFLGMRa                  | +++        | -                  | /                 | /                     | /                   |
| Tachykinin 6           | AALSDSYDLRGKQRFADFNSKFVAVRa | /          | /                  | /                 | /                     | /                   |

Listed are all peptides applied in this study along with their respective sequence and the effects on individual heart parameters (at  $1 \times 10^{-7}$  M). Nomenclature indicates significance of the observed effects (+ = increase,  $p < 0.05$ ; ++ = increase,  $p < 0.01$ ; +++ = increase,  $p < 0.001$ ; - = decrease,  $p < 0.05$ ; -- = decrease,  $p < 0.01$ ; --- = decrease,  $p < 0.001$ ; / = no significant effect; paired sample Student's *t*-test). ⊖ indicates full arrest of heartbeat upon peptide application.

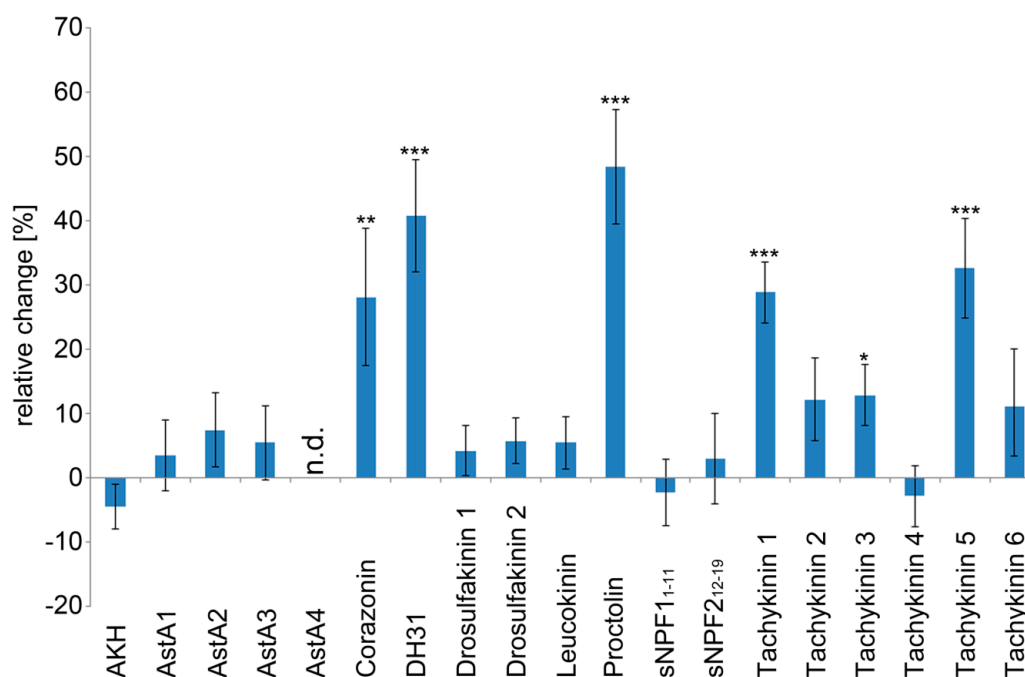


**Figure 1.** Heart rate is modulated by peptide signalling in semi-intact *Drosophila* larvae. Individual effects of the tested peptides ( $1 \times 10^{-7}$  M) on heart rate. Data are presented as mean values ( $\pm$  S.E.M.) of the relative changes in heart rate in relation to the individual control preparations (prior to peptide application). A minimum of ten animals per peptide were measured. Significance levels are indicated by asterisks (paired sample Student's *t*-test, \*  $p < 0.05$ ; \*\*  $p < 0.01$ ; \*\*\*  $p < 0.001$ ). Application of Allatostatin A4 resulted in a complete heartbeat arrest (heart rate not determined, n.d.).

To further specify these results, we performed dose–response experiments with the six identified cardioacceleratory peptides as well as with Allatostatin A4. Applied peptide concentrations were  $1 \times 10^{-11}$  M,  $1 \times 10^{-9}$  M,  $1 \times 10^{-7}$  M, and  $1 \times 10^{-5}$  M. As depicted (Figure 2), most peptides progressively

stimulated heart rate while their concentrations were increased from  $1 \times 10^{-11}$  M to  $1 \times 10^{-7}$  M. Only Proctolin and Tachykinin 5 required higher threshold concentrations to induce an effect ( $1 \times 10^{-7}$  M). Except for AstA4, all peptides tested exhibited the strongest cardioacceleratory effect at  $1 \times 10^{-7}$  M, with a further increase in concentration resulting in a diminished response. Interestingly, AstA4 induced heartbeat arrest at this particular concentration ( $1 \times 10^{-7}$  M), while  $1 \times 10^{-9}$  M and  $1 \times 10^{-5}$  M increased heart rate by 25.7% and 38.4%, respectively. In contrast to all other peptides, Tachykinin 3 decreased heart rate by 14% if applied at  $1 \times 10^{-11}$  M, while higher concentrations ( $1 \times 10^{-7}$  M) elicited a cardioacceleratory response (+12.9% increased heart rate).

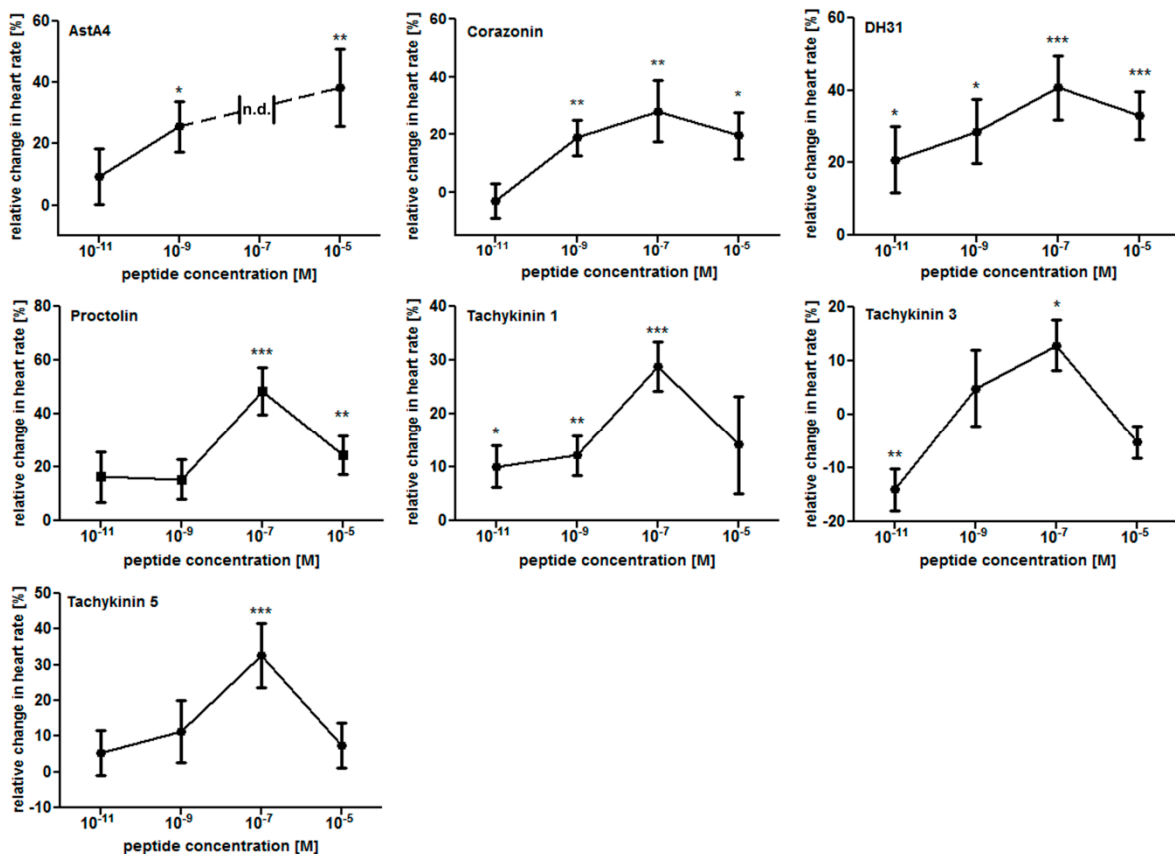


**Figure 2.** Dose–response curves for the effects of chronotropic peptides in semi-intact *Drosophila* larvae. Individual effects of the tested peptides at  $1 \times 10^{-11}$  M,  $1 \times 10^{-9}$  M,  $1 \times 10^{-7}$  M, and  $1 \times 10^{-5}$  M are shown. Data are presented as mean values ( $\pm$  S.E.M.) of the relative changes in heart rate in relation to the individual control preparations (prior to peptide application). A minimum of ten animals per peptide were measured. Significance levels are indicated by asterisks (paired sample Student’s *t*-test, \*  $p < 0.05$ ; \*\*  $p < 0.01$ ; \*\*\*  $p < 0.001$ ). n.d. indicates “not determined” (due to heartbeat arrest).

To assess whether the cardioacceleratory effects were caused by a decreased diastolic or systolic interval, we also measured these parameters individually. Due to the fact that for most peptides the strongest effects on heart rate were recorded at a concentration of  $1 \times 10^{-7}$  M (Figure 2), in this set of experiments, only this concentration was applied. Among the six cardioacceleratory peptides, five significantly reduced the diastolic interval: Corazonin (–21.6%), DH31 (–22.0%), Proctolin (–51.6%), Tachykinin 1 (–31.2%), and Tachykinin 5 (–26.2%) (Figure 3A). By contrast, the systolic interval was affected only by Corazonin (elongated by 13.3%) and DH31 (shortened by 16.4%) (Figure 3B). Thus, the increased heart rates are predominantly caused by decreased diastolic intervals. Interestingly, application of Allatostatin A2 resulted in a shortened diastolic interval (–16.5%), but an elongated systolic interval (+17.2%). In combination, these opposing effects cancelled each other, resulting in an unaltered heart rate (Figures 1 and 3A,B).

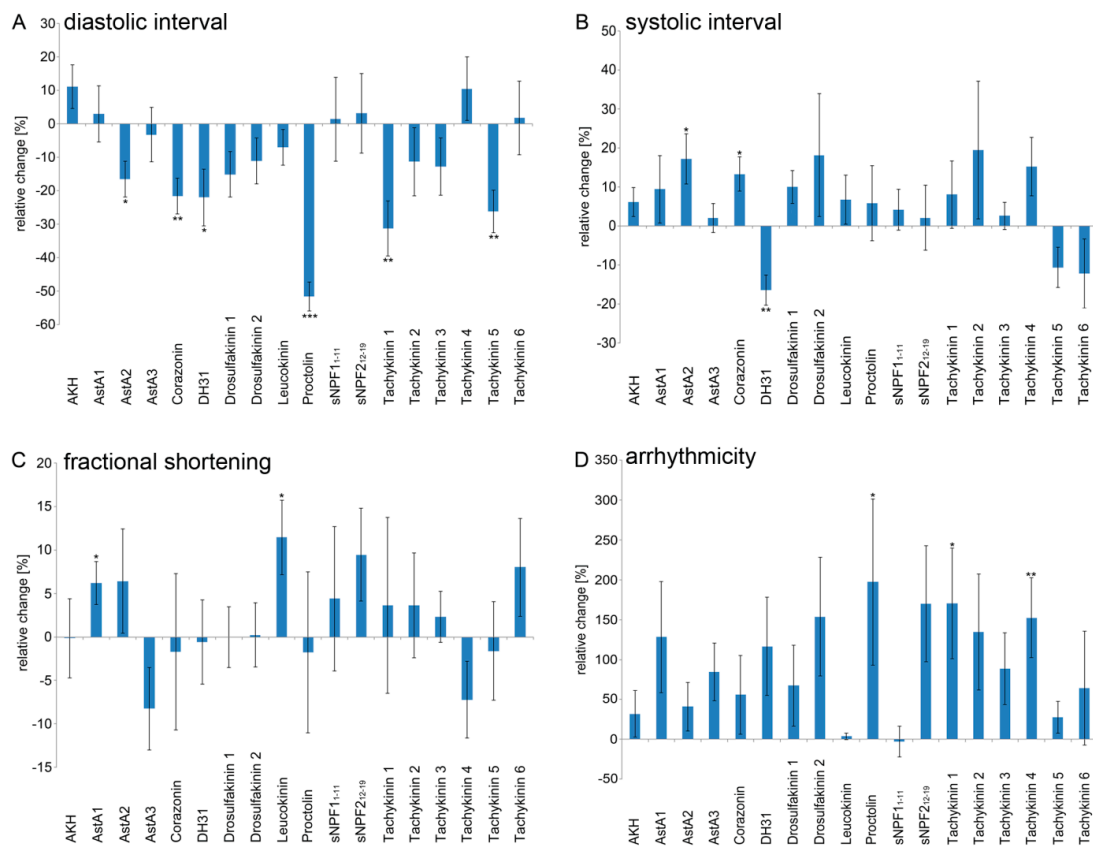


**Figure 3.** Diastolic and systolic intervals, fractional shortening and rhythmicity are modulated by peptide signalling in semi-intact *Drosophila* larvae. Individual effects of the tested peptides ( $1 \times 10^{-7}$  M) on: (A) diastolic interval; (B) systolic interval; (C) fractional shortening; and (D) rhythmicity. Data are presented as mean values ( $\pm$  S.E.M.) of the relative changes in the respective parameters in relation to the individual control preparations (prior to peptide application). A minimum of ten animals per peptide were measured. Significance levels are indicated by asterisks (paired sample Student's *t*-test, \*  $p < 0.05$ ; \*\*  $p < 0.01$ ; \*\*\*  $p < 0.001$ ).

To assess possible effects on cardiac muscle contraction, we measured peptide-induced changes in fractional shortening. As depicted in Figure 3C, Leucokinin increased contractility by 11.4 % and Allatostatin A1 increased it by 6.2%. As a final testing parameter, we measured possible peptidergic effects on heart rhythmicity. While application of Proctolin (+197.4%), Tachykinin 1 (+170.2%), and Tachykinin 4 (+152.5%) resulted in significantly increased arrhythmia, none of the remaining peptides affected this parameter in a statistically significant manner (Figure 3D).

The peptide-specific cardiomodulatory effects are summarised in Table 1. Corresponding raw data are presented in Table S1. Representative M-modes for the peptides that significantly affected heart rate are shown in Figure 4.

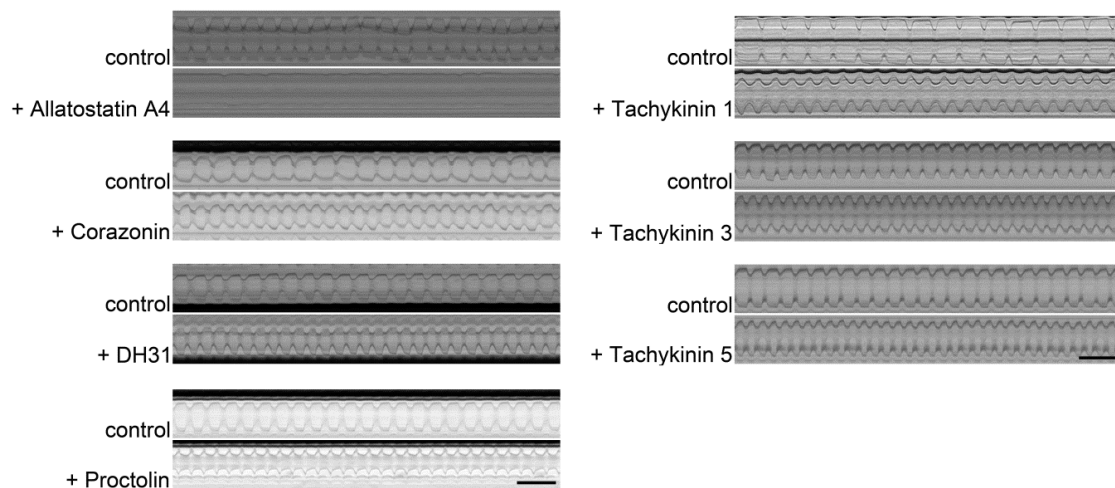


**Figure 4.** Representative M-modes of semi-intact larval *Drosophila* hearts incubated with distinct peptides ( $1 \times 10^{-7}$  M). The movement of the heart walls over time (10 s) is depicted. Application of Corazonin, DH31, Proctolin, or Tachykinins 1, 3, or 5 has a cardioacceleratory effect. Application of Allatostatin A4 results in cardiac arrest. Upper panels represent control hearts (prior to peptide application); lower panels depict the same hearts 1 min after peptide application. Scale bars indicate 1 s.

## 2.2. Peptidergic Signalling Affects Proper Heart Function In Vivo

As described above, 9 of the 19 peptides tested exhibited a significant modulation of chronotropic heart parameters in semi-intact animals (Allatostatin A2 and A4, Corazonin, DH31, Proctolin, and Tachykinin 1, 3, 4, and 5; Figures 1–4 and Table 1). To analyse the physiological relevance of these effects *in vivo*, we utilised an RNAi mediated knockdown approach, with the aim of reducing abundance of the respective peptide precursor proteins. Ubiquitous *daughterless*-Gal4 was used to drive RNAi expression in any tissue possibly producing and secreting the peptide of interest. To allow for discrete evaluation of the knockdown effects *in vivo*, we analysed intact 3rd instar larvae rather than using semi-intact preparations. Of note, due to technical restrictions regarding the reproducible measurement of the heart perimeter in intact animals, which requires a direct view of the tissue without refractive epidermal cells in the optical path, the *in vivo* analysis was limited to measuring heart rate and rhythmicity. To account for possible off-target effects or variable knockdown efficiencies, we analysed at least two independent RNAi lines per gene. All lines were pre-selected for the expression of individual hairpin sequences. Significant effects were considered valid only if they resulted from two transcript-specific hairpins. As depicted in Figure 5, ubiquitous knockdown of the selected precursor proteins caused discrete effects. Considering the validity criteria depicted above, reduced production of the Allatostatin A, Corazonin, Proctolin, and Tachykinin precursor proteins resulted in a significantly increased heart rate. By contrast, expression of one hairpin specific to the *DH31* precursor transcript reduced heart rate, while the second hairpin did not elicit any significant effects (Figure 5A). Regarding heart rhythmicity, knockdown of the Corazonin, DH31, and Tachykinin precursor proteins resulted in a tendency towards a more regular heartbeat. However, in all cases, only one of the analysed hairpins caused statistically significant effects, rendering the analysis of this parameter inconclusive (Figure 5B).

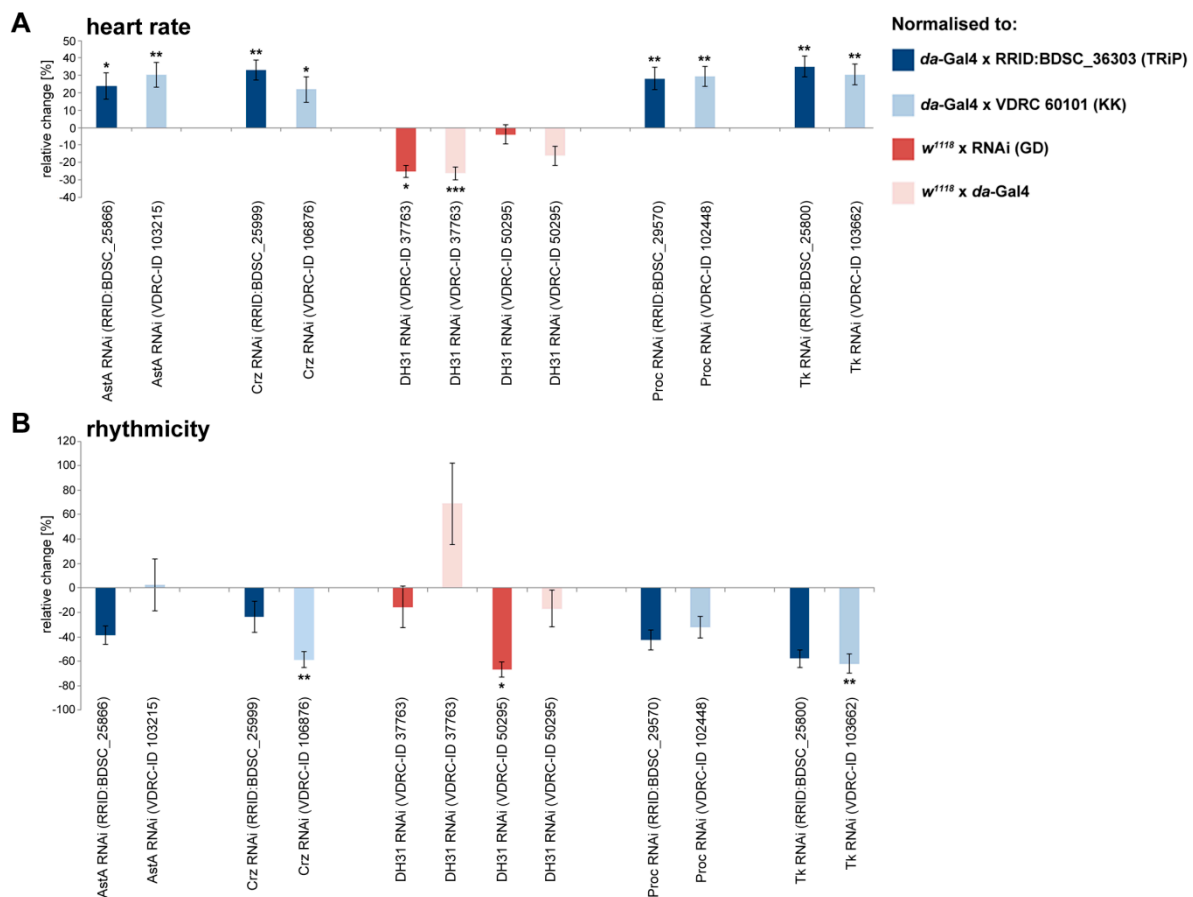


**Figure 5.** Knockdown of distinct peptide precursor proteins significantly affects heart function in intact *Drosophila* larvae. Depicted are the individual effects of peptide precursor protein knockdown on (A) heart rate and (B) rhythmicity. *daughterless-Gal4* (*da-Gal4*) was used as a ubiquitous driver. Data are presented as mean values ( $\pm$  S.E.M.) of the relative changes in the respective parameters in relation to the depicted controls. At least ten animals per genotype were measured. Significance levels are indicated by asterisks (Student's *t*-test, \*  $p < 0.05$ ; \*\*  $p < 0.01$ ; \*\*\*  $p < 0.001$ ).

To allow for a detailed evaluation of the knockdown effects, raw data for all lines tested are provided in Table S2.

### 3. Discussion

Peptidergic signalling represents an evolutionarily highly conserved means of regulating numerous fundamental biological processes. While peptidergic regulation of development, growth, reproduction, and behaviour has been investigated extensively, few studies to date have looked at peptide-based modulation of cardiac function. However, peptide-mediated effects on heart rate and heart contraction have repetitively been identified in *Drosophila* [54,57–61], with the corresponding peptides acting via distinct G protein-coupled receptors (GPCRs) that in turn activate specific cellular signal transduction pathways [63]. In addition, several studies report on peptide-mediated regulation of cardiac rhythmicity in humans: Endothelin-1 or Angiotensin II are well-known for their ability to modulate heart rhythmicity [64–69]. Furthermore, natriuretic peptides affect cardiac rhythmicity, most likely by regulating SERCA activity via cGMP and PKG mediated phosphorylation of Phospholamban. Impairments in this regulation result in cardiac arrhythmia [70,71]. In the present study, we screened a number of peptides evidentially produced in *Drosophila melanogaster* for their ability to modulate corresponding heart parameters in 3rd instar larvae. We selected this stage of animal development due to the myogenic nature of the larval heart [72]. Thus, all effects described herein should be



either intrinsic to heart or based on endocrine signalling, and do not involve any direct innervation component. Among the 19 peptides tested, 11 significantly modulated larval heart function in semi-intact preparations (Figures 1–3 and Table 1). While at first sight this ratio of cardioactive peptides appears to be rather high, it is likely consequential of the fact that we pre-selected the tested peptides and analysed only factors that have previously been identified as substrates of the heart surface bound peptidase Nep4 [40]. Since we consider cleavage by the peptidase indicative of a heart modulatory function, the high proportion of cardioactive peptides becomes more allegeable. In this respect, our results that, except for Tachykinin 3, all identified peptides acted exclusively as positive regulators of chronotropic (Figures 1 and 2) or inotropic heart parameters (Figure 3C) may suggest that the peptidergic regulation of larval heart physiology is largely restricted to augmenting respective parameters, while reduced heart rate/heart contractility is predominantly achieved through the removal of corresponding peptides from the haemolymph. The latter likely involves hydrolysis by certain peptidases present at the surface of muscle or heart cells, such as Nep4 [40,50]. Of note, some of the identified peptides affected multiple cardiac parameters, while others exhibited more functional specificity. For example, Proctolin and Tachykinin 1 modified heart rate and rhythmicity, while Corazonin, DH31, and Tachykinin 5 specifically increased heart rate. By contrast, Tachykinin 4 affected only heart rhythmicity (Figures 1–3 and Table 1). Interestingly, the only two peptides that altered fractional shortening, Allatostatin A1 and Leucokinin (Figure 3C), also exclusively modulated this parameter. Considering the fact that vice versa none of the chronotropic peptides affected fractional shortening (Table 1), these observations suggest that activity of cardiomodulatory peptides in general is either specific to chronotropic or to inotropic modulation. In addition, these results indicate a complex peptidergic regulation of the larval *Drosophila* heart that involves chronotropic and inotropic adaptation and requires simultaneous signalling from several specific factors. With regard to inotropic modulation, we identified Allatostatin A1 and Leucokinin as regulatory peptides. Interestingly, leucokinins have already been associated with muscle contractility and a stimulatory effect of the peptides on hindgut contraction in *Leucophaea maderae* has been reported [73,74]. The maximum response for each leucokinin species was recorded at  $2.1 \times 10^{-7}$  M; however, the heart did not respond to any of the peptides. By contrast, our data clearly show that Leucokinin increases the contractility of the larval *Drosophila* heart at comparable concentrations ( $1 \times 10^{-7}$  M, Figure 3C). Thus, while the general effect on muscle tissue seems to be conserved, leucokinins apparently exhibit species-dependent tissue specificities, probably based on the presence or absence of a corresponding receptor at the surface of a given tissue.

Regarding *Drosophila* tachykinins (DTKs), two receptors have been identified: NKD (neurokinin receptor from *Drosophila*), and DTKR (*Drosophila* tachykinin receptor). With respect to NKD, it has been shown that it can be activated only by DTK-6 [75]. Since we found that DTK-6 application did not affect cardiac activity (Figures 1 and 3), participation of NKD in the peptidergic regulation of the *Drosophila* heart appears unlikely. By contrast, DTKR has been reported to be responsive to all six *Drosophila* tachykinins, with DTK-1 inducing the strongest response ( $EC_{50} = 3.9 \times 10^{-9}$  M) and DTKs -2 to -6 being about one order of magnitude less active [76]. This broader specificity along with our results that numerous *Drosophila* tachykinins affected heart function (DTK-1, -3, -4, and -5; Figures 1–3) indicates that cardiac-specific tachykinin signalling is mainly relayed via DTKR. Interestingly, DTK-2 and DTK-6 did not elicit any significant effect, although they have been reported to activate DTKR expressed in HEK-293 cells [76]. This result indicates that DTK-2 and -6 may have additional functions in *Drosophila* larvae, probably mediated by binding to a receptor different from NKD or DTKR, which attenuate the effects of DTKR activation in cardiac tissue. Concentration dependent activation of distinct receptors may also be causal to our observation that DTK-3 reduces heart rate at  $1 \times 10^{-11}$  M, but increases the same parameter at  $1 \times 10^{-7}$  M (Figure 2). With respect to allatostatins, a similar situation may be present. Also for these peptides, two receptor proteins have been identified in *Drosophila* (DAR-1 and DAR-2). According to  $Ca^{2+}$  mobilisation assays in transfected CHO cells, both receptors exhibit  $EC_{50}$  values in the range of 20–100 nM for all allatostatins tested (AstA1–AstA4 [77]). Thus, similar cardiomodulatory effects would be expected for these peptides if DAR-1 and DAR-2

were the only responsive receptors in *Drosophila*. Interestingly, we observed a significant effect on heart function only in response to AstA2 and AstA4 application, while AstA1 and AstA3 did not affect any chronotropic heart parameter (Figures 1 and 3). This lack of activity observed for two of the four tested allatostatins indicates that neither DAR-1 nor DAR-2 is involved in regulating larval *Drosophila* heartbeat. Consequently, the distinct effects of AstA2 and AstA4 application are presumably mediated by activation of yet unknown receptors. As confirmed by dose–response experiments, AstA4 mediated activation of such a putative receptor resulted in an increased heart rate at ligand concentrations of  $1 \times 10^{-9}$  M and  $1 \times 10^{-5}$  M (Figure 2). Interestingly, at  $1 \times 10^{-7}$  M a complete, yet reversible heartbeat arrest occurred, indicating an unphysiologically strong response at this particular AstA4 concentration that may result in stress-induced heart failure.

To assess the *in vivo* relevance of these data in more detail, we analysed the physiological effects of all chronotropic peptides identified in our screen (Allatostatin A2 and A4, Corazonin, DH31, Proctolin, and Tachykinin 1, 3, 4, and 5) in intact transgenic larvae. In this respect, we used ubiquitous RNAi (*daughterless*-Gal4) to knockdown expression of the respective precursor proteins in any tissue possibly producing and secreting the peptide of interest. As shown in Figure 5, knockdown of all peptide precursors affected heart rate, which substantiates a cardiomodulatory activity of the mature peptides. Interestingly, only DH31 precursor knockdown resulted in a tendency to decrease this parameter, while reduced levels of the Allatostatin, Corazonin, Proctolin, and Tachykinin precursor increased heart rate (Figure 5A). These results are surprising, since our data from semi-intact heart preparations indicate a cardioacceleratory activity of all respective peptides (Figures 1 and 2). Thus, vice versa, knockdown of the respective precursor proteins should result in decreased heart rate. However, given the fact that neuropeptides typically have different roles during development and adulthood, the observed knockdown effects may reflect a combination of physiological and developmental impairments. In addition, knockdown of a precursor protein usually affects numerous mature peptides. This simultaneous loss of peptide signalling, probably interfering with multiple peptidergic systems, may cause considerable physiological stress that is sensed by the heart and results in an increased heart rate. On the other hand, the type of assay may also influence the effects on heart rate. In *Cancer magister*, it has been shown that different experimental setups can affect the results, as Proctolin application in intact animals decreased heart rate, while semi-isolated hearts exhibited a cardioacceleratory response [78]. At least with respect to Proctolin, this discrepancy is observed also in *Drosophila*: while Proctolin injection into 3rd instar larvae is reported to decrease heart rate [61], our results using semi-intact animals clearly show a cardioacceleratory activity of the peptide (Figures 1 and 2). Thus, a combination of methodical setups appears to be required to adequately characterise cardioactive peptides in *Drosophila*. However, considering the reduced complexity and the resulting gain in interpretability, we regard direct application analyses using semi-intact heart preparations as favourable techniques for initial peptide identification.

By combining semi-intact heart preparations with *in vivo* analyses, we have identified a number of cardioactive peptides in *Drosophila melanogaster*. While in-depth analyses of the distinct physiological functions of these peptides require further efforts, our data represent a valuable resource for designing corresponding studies in the future.

## 4. Materials and Methods

### 4.1. Fly Strains

*daughterless*-Gal4 (*da*-Gal4, RRID:BDSC\_55850) was used as a ubiquitous driver. RNAi lines (Table 2) were obtained from either the Vienna *Drosophila* Resource Center (VDRC) or the Bloomington *Drosophila* Stock Center (BDSC). The KK collection specific host strain VDRC-ID 60101 was used as a control for the KK RNAi lines, and the strain BDSC\_36303 served as a control for the TRiP RNAi lines (each of them crossed to *da*-Gal4). Both control lines share identical genetic backgrounds with the lines of the respective collection (KK or TRiP). The genetically distinct lines of the GD collection

(Table 2) were controlled by crossing both, the respective UAS-RNAi lines as well as the applied driver line (*da-Gal4*) to *w<sup>1118</sup>* (RRID:BDSC\_5905).

**Table 2.** RNAi lines used in this study.

| Provided by | Collection | Identifier      | Target Gene                  |
|-------------|------------|-----------------|------------------------------|
| VDRC        | KK         | VDRC-ID 103215  | CG13633; Allatostatin A      |
| VDRC        | GD         | VDRC-ID 50295   | CG13094; Diuretic hormone 31 |
| VDRC        | GD         | VDRC-ID 37763   | CG13094; Diuretic hormone 31 |
| VDRC        | KK         | VDRC-ID 106876  | CG3302; Corazonin            |
| VDRC        | KK         | VDRC-ID 102488  | CG7105; Proctolin            |
| VDRC        | KK         | VDRC-ID 103662  | CG14734; Tachykinin          |
| BDSC        | TRiP       | RRID:BDSC_25800 | CG14734; Tachykinin          |
| BDSC        | TRiP       | RRID:BDSC_25866 | CG13633; Allatostatin A      |
| BDSC        | TRiP       | RRID:BDSC_25999 | CG3302; Corazonin            |
| BDSC        | TRiP       | RRID:BDSC_29570 | CG7105; Proctolin            |

#### 4.2. Peptide Application Assay and Dose–Response Analysis

Prior to peptide application, wandering male 3rd instar larvae were dissected in artificial haemolymph (5 mM KCl, 8 mM MgCl<sub>2</sub>, 2 mM CaCl<sub>2</sub>, 108 mM NaCl, 1 mM NaH<sub>2</sub>PO<sub>4</sub>, 5 mM HEPES and 4 mM NaHCO<sub>3</sub>, pH 7.1). Prior to use, the buffer was supplemented with trehalose (final concentration: 5 mM) and sucrose (final concentration: 10 mM) [79]. Specimens were pinned down with the ventral side upwards onto Sylgard 184 silicone elastomer plates. All internal organs except for the heart and associated tissue (e.g. alary muscles, pericardial cells) were removed. After a resting period of 10 min, a 60 s video of the heartbeat was recorded and used as a control. Afterwards, the artificial haemolymph was removed and replaced with artificial haemolymph containing a candidate peptide (Table 1). After 1 min, the heartbeat was again recorded for 60 s and analysed for peptide-specific alterations in comparison to the respective control measurement. For an initial screen, only one peptide concentration was tested ( $1 \times 10^{-7}$  M). To further assess the dose–responsive relationship of positive candidates, three additional concentrations ( $1 \times 10^{-11}$  M,  $1 \times 10^{-9}$  M and  $1 \times 10^{-5}$  M) of the respective peptides were applied. All peptides were synthesised by JPT Peptide Technologies (Berlin, Germany) and were of >90 % purity. The proper sequence and mass of each peptide was confirmed using an ESI-ion trap (Amazon ETD Speed with a captive spray ionisation unit, Bruker Corporation, Billerica, MA, USA) by measuring the masses of the intact molecules as well as the masses of the fragments, which were generated by collision-induced dissociation (CID) of the corresponding parent ion.

#### 4.3. In Vivo Measurement of Heart Parameters

To measure the heart function of animals with ubiquitous knockdown of the peptide precursors or cardiac-specific knockdown of their receptors *in vivo*, wandering male 3rd instar larvae were anaesthetised for 8 min using ether. The anaesthetised animals were transferred with the dorsal side upwards to a moistened microscope slide and a 60 s video of the beating heart was captured through the cuticle. For optimal detection of the heartbeat, the camera was focused on a region in which the heart tube was in close proximity to trachea (dorsal trunks) or fat body tissue, allowing the simultaneous detection of the heartbeat and related movements of the surrounding tissues with high contrast.

#### 4.4. Video Analysis and Calculation of Cardiac Parameters

For heartbeat recording, a high-speed video camera (Basler piA-640) was mounted onto an upright microscope (Leica DMLB) equipped with a 10× Leica Fluotar. Movies were captured with the software Firecapture ®(freeware by Torsten Edelmann) and processed with ImageJ [80].

For the peptide screen, heart parameters were analysed using SOHA (semi-automated optical heartbeat analysis), a MATLAB application introduced by Fink et al. [62] and further developed by Ocorr et al. [81]. The SOHA software utilises two computer algorithms to combine overall darkness changes of a video (Frame Brightness Algorithm) with pixel-by-pixel intensity changes (Changing Pixel Intensity Algorithm), thereby allowing calculation of different heart beat parameters. Besides the heart rate [Hz] and systolic/diastolic intervals (duration of contraction and relaxation phases [ms]), also contractility ([%] of fractional shortening) as well as heart beat arrhythmia can be determined. To measure fractional shortening, the SOHA software allows manually annotating the edges of the heart tube at its maximally dilated and maximally contracted state. Based on these diameters, percentages of fractional shortening can be calculated:

$$\%FS = \frac{\text{Diastolic diameter} - \text{Systolic diameter}}{\text{Diastolic diameter}} \times 100 \quad (1)$$

As described in [62], the arrhythmicity index was calculated via dividing the standard deviation of the heart period by the median of the heart period:

$$AI = \frac{\text{Standard deviation (HP)}}{\text{Median (HP)}} \quad (2)$$

Additionally, the SOHA software also generates kymographs (M-modes) of heart wall movements (X-axis) over time (Y-axis). M-modes are horizontally aligned pixel slices from each frame of a respective heart beat video. In this way, an M-mode allows visualising distinct differences in heart performance (e.g. heart rate). Additional data analysis was done using Microsoft Excel and GraphPad Prism 5 (GraphPad Software, La Jolla, CA, USA).

Analysis of in vivo heart parameters was done by measuring the changes in light intensity that occur during a single heartbeat. For automated evaluation of the parameter values, a self-compiled Java script with OpenCV (Open Source Computer Vision, [82]) was employed. The resulting plots (Figure S1) were verified for proper heartbeat detection. Additional data analysis was done using Microsoft Excel.

#### 4.5. Statistics

Statistical analysis was performed using Microsoft Excel. For the peptide screen, a minimum of 10 animals per peptide were measured. Paired sample t-tests were performed to determine the statistical significance of peptide-specific effects. For statistical analysis of in vivo effects, an independent samples t-test was used. At least 10 animals per genotype were analysed.

**Supplementary Materials:** The following are available online at <http://www.mdpi.com/1422-0067/20/1/2/s1>, Figure S1: Representative plots of heartbeat detection in intact animals: (A) *da-Gal4* × BDSC\_60101 (control, KK); and (B) *da-Gal4* × BDSC\_103215 (KK). Detected heartbeats (black dots) are labelled by consecutive numbers. In contrast to control animals (A), knockdown of the Allatostatin precursor protein results in increased heart rate (B); Table S1: Raw data of peptide-specific cardiomodulatory effects in semi-intact animals; Table S2: Raw data of knockdown-specific cardiomodulatory effects in intact animals.

**Author Contributions:** H.M., R.S. and A.P. conceived and designed the experiments. R.S., M.J., K.L. and J.L. performed the experiments. H.M., R.S., M.J., K.L., J.L. and A.P. analysed the data. H.M. and A.P. wrote the paper.

**Funding:** This research was funded by the German Research Foundation (SFB 944: Physiology and Dynamics of Cellular Microcompartments) (A.P.), by a young investigator initiative of the SFB 944 (H.M.), by a stipend from the Hans Mühlenhoff Foundation (R.S.), and by the State of Lower-Saxony, Hannover, Germany, Grant 11-76251-99-15/12 (ZN2832) (A.P.). We also acknowledge the support of the Open Access Publishing Fund of Osnabrück University.

**Acknowledgments:** We thank Martina Biedermann, Mechthild Krabusch and Eva Cordes for excellent technical assistance. We also thank Christian Wegener for providing peptides. We further acknowledge the Vienna *Drosophila* Resource Center (VDRC) and the Bloomington *Drosophila* Stock Center (BDSC, NIH P40OD018537) for providing fly stocks.

**Conflicts of Interest:** The authors declare no conflict of interest.

## References

1. Bouwman, J.; Spijker, S.; Schut, D.; Wachtler, B.; Ylstra, B.; Smit, A.B.; Verhage, M. Reduced expression of neuropeptide genes in a genome-wide screen of a secretion-deficient mouse. *J. Neurochem.* **2006**, *99*, 84–96. [[CrossRef](#)]
2. Hewes, R.S.; Taghert, P.H. Neuropeptides and neuropeptide receptors in the *Drosophila melanogaster* genome. *Genome Res.* **2001**, *11*, 1126–1142. [[CrossRef](#)] [[PubMed](#)]
3. Hokfelt, T. Neuropeptides in perspective: the last ten years. *Neuron* **1991**, *7*, 867–879. [[CrossRef](#)]
4. Husson, S.J.; Landuyt, B.; Nys, T.; Baggerman, G.; Boonen, K.; Clynen, E.; Lindemans, M.; Janssen, T.; Schoofs, L. Comparative peptidomics of *Caenorhabditis elegans* versus *C. briggsae* by LC-MALDI-TOF MS. *Peptides* **2009**, *30*, 449–457. [[CrossRef](#)]
5. Li, B.; Predel, R.; Neupert, S.; Hauser, F.; Tanaka, Y.; Cazzamali, G.; Williamson, M.; Arakane, Y.; Verleyen, P.; Schoofs, L.; et al. Genomics, transcriptomics, and peptidomics of neuropeptides and protein hormones in the red flour beetle *Tribolium castaneum*. *Genome Res.* **2008**, *18*, 113–122. [[CrossRef](#)] [[PubMed](#)]
6. Nässel, D.R.; Winther, A.M. *Drosophila* neuropeptides in regulation of physiology and behaviour. *Prog. Neurobiol.* **2010**, *92*, 42–104. [[CrossRef](#)]
7. Anctil, M. Chemical transmission in the sea anemone *Nematostella vectensis*: A genomic perspective. *Comp. Biochem. Physiol. Part D Genom. Proteom.* **2009**, *4*, 268–289. [[CrossRef](#)]
8. Grimmelikhuijzen, C.J.; Leviev, I.; Carstensen, K. Peptides in the nervous systems of cnidarians: Structure, function, and biosynthesis. *Int. Rev. Cytol.* **1996**, *167*, 37–89. [[PubMed](#)]
9. Hansen, G.N.; Williamson, M.; Grimmelikhuijzen, C.J. A new case of neuropeptide coexpression (RGamide and LWamides) in *Hydra*, found by whole-mount, two-color double-labeling in situ hybridization. *Cell Tissue Res.* **2002**, *308*, 157–165. [[CrossRef](#)]
10. Takahashi, T.; Hayakawa, E.; Koizumi, O.; Fujisawa, T. Neuropeptides and their functions in *Hydra*. *Acta Biol. Hung.* **2008**, *59*, 227–235. [[CrossRef](#)]
11. Schoofs, L.; De Loof, A.; Van Hiel, M.B. Neuropeptides as regulators of behaviour in insects. *Annu. Rev. Entomol.* **2017**, *62*, 35–52. [[CrossRef](#)] [[PubMed](#)]
12. Anderson, D.M.; Anderson, K.M.; Chang, C.L.; Makarewich, C.A.; Nelson, B.R.; McAnally, J.R.; Kasaragod, P.; Shelton, J.M.; Liou, J.; Bassel-Duby, R.; et al. A micropeptide encoded by a putative long noncoding RNA regulates muscle performance. *Cell* **2015**, *160*, 595–606. [[CrossRef](#)] [[PubMed](#)]
13. Anderson, D.M.; Makarewich, C.A.; Anderson, K.M.; Shelton, J.M.; Bezprozvannaya, S.; Bassel-Duby, R.; Olson, E.N. Widespread control of calcium signalling by a family of SERCA-inhibiting micropeptides. *Sci. Signal.* **2016**, *9*, ra119. [[CrossRef](#)] [[PubMed](#)]
14. Nelson, B.R.; Makarewich, C.A.; Anderson, D.M.; Winders, B.R.; Troupes, C.D.; Wu, F.; Reese, A.L.; McAnally, J.R.; Chen, X.; Kavalali, E.T.; et al. A peptide encoded by a transcript annotated as long noncoding RNA enhances SERCA activity in muscle. *Science* **2016**, *351*, 271–275. [[CrossRef](#)] [[PubMed](#)]
15. Zanet, J.; Chanut-Delalande, H.; Plaza, S.; Payre, F. Small peptides as newcomers in the control of *Drosophila* development. *Curr. Top. Dev. Biol.* **2016**, *117*, 199–219. [[PubMed](#)]
16. Baraban, S.C.; Tallent, M.K. Interneuron Diversity series: Interneuronal neuropeptides—Endogenous regulators of neuronal excitability. *Trends Neurosci.* **2004**, *27*, 135–142. [[CrossRef](#)] [[PubMed](#)]
17. Hokfelt, T.; Broberger, C.; Xu, Z.Q.; Sergeev, V.; Ubink, R.; Diez, M. Neuropeptides—An overview. *Neuropharmacology* **2000**, *39*, 1337–1356. [[CrossRef](#)]
18. Zupanc, G.K. Peptidergic transmission: From morphological correlates to functional implications. *Micron* **1996**, *27*, 35–91. [[CrossRef](#)]
19. Keller, R. Crustacean neuropeptides: Structures, functions and comparative aspects. *Experientia* **1992**, *48*, 439–448. [[CrossRef](#)]
20. Moroz, L.L.; Edwards, J.R.; Puthanveettil, S.V.; Kohn, A.B.; Ha, T.; Heyland, A.; Knudsen, B.; Sahni, A.; Yu, F.; Liu, L.; et al. Neuronal transcriptome of *Aplysia*: Neuronal compartments and circuitry. *Cell* **2006**, *127*, 1453–1467. [[CrossRef](#)]
21. Nusbaum, M.P.; Blitz, D.M.; Swensen, A.M.; Wood, D.; Marder, E. The roles of co-transmission in neural network modulation. *Trends Neurosci.* **2001**, *24*, 146–154. [[CrossRef](#)]

22. O'Shea, M.; Schaffer, M. Neuropeptide function: The invertebrate contribution. *Annu. Rev. Neurosci.* **1985**, *8*, 171–198. [[CrossRef](#)] [[PubMed](#)]
23. Predel, R.; Nachman, R.J.; Gäde, G. Myostimulatory neuropeptides in cockroaches: Structures, distribution, pharmacological activities, and mimetic analogs. *J. Insect Physiol.* **2001**, *47*, 311–324. [[CrossRef](#)]
24. Predel, R.; Neupert, S.; Garczynski, S.F.; Crim, J.W.; Brown, M.R.; Russell, W.K.; Kahnt, J.; Russell, D.H.; Nachman, R.J. Neuropeptidomics of the mosquito *Aedes aegypti*. *J. Proteome Res.* **2010**, *9*, 2006–2015. [[CrossRef](#)] [[PubMed](#)]
25. Schoofs, L.; Vanden Broeck, J.; De Loof, A. The myotropic peptides of *Locusta migratoria*: Structures, distribution, functions and receptors. *Insect Biochem. Mol. Biol.* **1993**, *23*, 859–881. [[CrossRef](#)]
26. Dietzl, G.; Chen, D.; Schnorrer, F.; Su, K.C.; Barinova, Y.; Fellner, M.; Gasser, B.; Kinsey, K.; Oettel, S.; Scheiblauer, S.; et al. A genome-wide transgenic RNAi library for conditional gene inactivation in *Drosophila*. *Nature* **2007**, *448*, 151–156. [[CrossRef](#)]
27. Jones, W.D. The expanding reach of the GAL4/UAS system into the behavioural neurobiology of *Drosophila*. *BMB Rep.* **2009**, *42*, 705–712. [[CrossRef](#)]
28. Luo, L.; Callaway, E.M.; Svoboda, K. Genetic dissection of neural circuits. *Neuron* **2008**, *57*, 634–660. [[CrossRef](#)]
29. McNabb, S.L.; Baker, J.D.; Agapite, J.; Steller, H.; Riddiford, L.M.; Truman, J.W. Disruption of a behavioural sequence by targeted death of peptidergic neurons in *Drosophila*. *Neuron* **1997**, *19*, 813–823. [[CrossRef](#)]
30. Pfeiffer, B.D.; Jenett, A.; Hammonds, A.S.; Ngo, T.T.; Misra, S.; Murphy, C.; Scully, A.; Carlson, J.W.; Wan, K.H.; Lavery, T.R.; et al. Tools for neuroanatomy and neurogenetics in *Drosophila*. *Proc. Natl. Acad. Sci. (PNAS)* **2008**, *105*, 9715–9720. [[CrossRef](#)]
31. Predel, R.; Eckert, M.; Pollak, E.; Molnar, L.; Scheibner, O.; Neupert, S. Peptidomics of identified neurons demonstrates a highly differentiated expression pattern of FXPRLamides in the neuroendocrine system of an insect. *J. Comp. Neurol.* **2007**, *500*, 498–512. [[CrossRef](#)]
32. Predel, R.; Wegener, C.; Russell, W.K.; Tichy, S.E.; Russell, D.H.; Nachman, R.J. Peptidomics of CNS-associated neurohemal systems of adult *Drosophila melanogaster*: A mass spectrometric survey of peptides from individual flies. *J. Comp. Neurol.* **2004**, *474*, 379–392. [[CrossRef](#)] [[PubMed](#)]
33. Wegener, C.; Reinl, T.; Jänsch, L.; Predel, R. Direct mass spectrometric peptide profiling and fragmentation of larval peptide hormone release sites in *Drosophila melanogaster* reveals tagma-specific peptide expression and differential processing. *J. Neurochem.* **2006**, *96*, 1362–1374. [[CrossRef](#)] [[PubMed](#)]
34. Brogiolo, W.; Stocker, H.; Ikeya, T.; Rintelen, F.; Fernandez, R.; Hafen, E. An evolutionarily conserved function of the *Drosophila* insulin receptor and insulin-like peptides in growth control. *Curr. Biol. CB* **2001**, *11*, 213–221. [[CrossRef](#)]
35. Liu, H.; Kubli, E. Sex-peptide is the molecular basis of the sperm effect in *Drosophila melanogaster*. *Proc. Natl. Acad. Sci. (PNAS)* **2003**, *100*, 9929–9933. [[CrossRef](#)] [[PubMed](#)]
36. Rulifson, E.J.; Kim, S.K.; Nusse, R. Ablation of insulin-producing neurons in flies: Growth and diabetic phenotypes. *Science* **2002**, *296*, 1118–1120. [[CrossRef](#)] [[PubMed](#)]
37. Wigby, S.; Chapman, T. Sex peptide causes mating costs in female *Drosophila melanogaster*. *Curr. Biol. CB* **2005**, *15*, 316–321. [[CrossRef](#)]
38. Yapici, N.; Kim, Y.J.; Ribeiro, C.; Dickson, B.J. A receptor that mediates the post-mating switch in *Drosophila* reproductive behaviour. *Nature* **2008**, *451*, 33–37. [[CrossRef](#)]
39. Chen, J.; Reiher, W.; Hermann-Luibl, C.; Sellami, A.; Cognigni, P.; Kondo, S.; Helfrich-Forster, C.; Veenstra, J.A.; Wegener, C. Allatostatin A signalling in *Drosophila* regulates feeding and sleep and is modulated by PDF. *PLoS Genet.* **2016**, *12*, e1006346.
40. Hallier, B.; Schiemann, R.; Cordes, E.; Vitos-Faleato, J.; Walter, S.; Heinisch, J.J.; Malmendal, A.; Paululat, A.; Meyer, H. *Drosophila* neprilysins control insulin signalling and food intake via cleavage of regulatory peptides. *eLife* **2016**, *5*, e19430. [[CrossRef](#)]
41. Wang, Y.; Pu, Y.; Shen, P. Neuropeptide-gated perception of appetitive olfactory inputs in *Drosophila* larvae. *Cell Rep.* **2013**, *3*, 820–830. [[CrossRef](#)] [[PubMed](#)]
42. DeZazzo, J.; Xia, S.; Christensen, J.; Velinzon, K.; Tully, T. Developmental expression of an *amn(+)* transgene rescues the mutant memory defect of *amnesiac* adults. *J. Neurosci.* **1999**, *19*, 8740–8746. [[CrossRef](#)] [[PubMed](#)]
43. Feany, M.B.; Quinn, W.G. A neuropeptide gene defined by the *Drosophila* memory mutant *amnesiac*. *Science* **1995**, *268*, 869–873. [[CrossRef](#)] [[PubMed](#)]

44. Waddell, S.; Armstrong, J.D.; Kitamoto, T.; Kaiser, K.; Quinn, W.G. The amnesiac gene product is expressed in two neurons in the *Drosophila* brain that are critical for memory. *Cell* **2000**, *103*, 805–813. [[CrossRef](#)]
45. Cavey, M.; Collins, B.; Bertet, C.; Blau, J. Circadian rhythms in neuronal activity propagate through output circuits. *Nat. Neurosci.* **2016**, *19*, 587–595. [[CrossRef](#)] [[PubMed](#)]
46. Dubowy, C.M.; Cavanaugh, D.J. Sleep: A neuropeptidergic wake-up call for flies. *Curr. Biol. CB* **2014**, *24*, R1092–4. [[CrossRef](#)] [[PubMed](#)]
47. Hermann-Luibl, C.; Yoshii, T.; Senthilan, P.R.; Dirksen, H.; Helfrich-Forster, C. The ion transport peptide is a new functional clock neuropeptide in the fruit fly *Drosophila melanogaster*. *J. Neurosci.* **2014**, *34*, 9522–9536. [[CrossRef](#)] [[PubMed](#)]
48. Isaac, R.E.; Johnson, E.C.; Audsley, N.; Shirras, A.D. Metabolic inactivation of the circadian transmitter, pigment dispersing factor (PDF), by neprilysin-like peptidases in *Drosophila*. *J. Exp. Biol.* **2007**, *210 Pt 24*, 4465–4470. [[CrossRef](#)]
49. Shang, Y.; Donelson, N.C.; Vecsey, C.G.; Guo, F.; Rosbash, M.; Griffith, L.C. Short neuropeptide F is a sleep-promoting inhibitory modulator. *Neuron* **2013**, *80*, 171–183. [[CrossRef](#)] [[PubMed](#)]
50. Meyer, H.; Panz, M.; Zmojdzian, M.; Jagla, K.; Paululat, A. Neprilysin 4, a novel endopeptidase from *Drosophila melanogaster*, displays distinct substrate specificities and exceptional solubility states. *J. Exp. Biol.* **2009**, *212 Pt 22*, 3673–3683. [[CrossRef](#)]
51. Baggerman, G.; Boonen, K.; Verleyen, P.; De Loof, A.; Schoofs, L. Peptidomic analysis of the larval *Drosophila melanogaster* central nervous system by two-dimensional capillary liquid chromatography quadrupole time-of-flight mass spectrometry. *J. Mass Spectrom.* **2005**, *40*, 250–260. [[CrossRef](#)]
52. Yew, J.Y.; Wang, Y.; Barteneva, N.; Dikler, S.; Kutz-Naber, K.K.; Li, L.; Kravitz, E.A. Analysis of neuropeptide expression and localisation in adult *Drosophila melanogaster* central nervous system by affinity cell-capture mass spectrometry. *J. Proteome Res.* **2009**, *8*, 1271–1284. [[CrossRef](#)] [[PubMed](#)]
53. Anderson, M.S.; Halpern, M.E.; Keshishian, H. Identification of the neuropeptide transmitter proctolin in *Drosophila* larvae: Characterisation of muscle fiber-specific neuromuscular endings. *J. Neurosci.* **1988**, *8*, 242–255. [[CrossRef](#)] [[PubMed](#)]
54. Liao, F.T.; Chang, C.Y.; Su, M.T.; Kuo, W.C. Necessity of angiotensin-converting enzyme-related gene for cardiac functions and longevity of *Drosophila melanogaster* assessed by optical coherence tomography. *J. Biomed. Opt.* **2014**, *19*, 011014. [[CrossRef](#)] [[PubMed](#)]
55. Dulcis, D.; Levine, R.B.; Ewer, J. Role of the neuropeptide CCAP in *Drosophila* cardiac function. *J. Neurobiol.* **2005**, *64*, 259–274. [[CrossRef](#)]
56. Nichols, R.; Kaminski, S.; Walling, E.; Zornik, E. Regulating the activity of a cardioacceleratory peptide. *Peptides* **1999**, *20*, 1153–1158. [[CrossRef](#)]
57. Johnson, E.; Ringo, J.; Dowse, H. Native and heterologous neuropeptides are cardioactive in *Drosophila melanogaster*. *J. Insect Physiol.* **2000**, *46*, 1229–1236. [[CrossRef](#)]
58. Nichols, R.; McCormick, J.; Cohen, M.; Howe, E.; Jean, C.; Paisley, K.; Rosario, C. Differential processing of neuropeptides influences *Drosophila* heart rate. *J. Neurogenet.* **1999**, *13*, 89–104. [[CrossRef](#)]
59. Ormerod, K.G.; LePine, O.K.; Bhutta, M.S.; Jung, J.; Tattersall, G.J.; Mercier, A.J. Characterizing the physiological and behavioural roles of proctolin in *Drosophila melanogaster*. *J. Neurophysiol.* **2016**, *115*, 568–580. [[CrossRef](#)]
60. Taylor, C.A.; Winther, A.M.; Siviter, R.J.; Shirras, A.D.; Isaac, R.E.; Nässel, D.R. Identification of a proctolin preprohormone gene (Proct) of *Drosophila melanogaster*: Expression and predicted prohormone processing. *J. Neurobiol.* **2004**, *58*, 379–391. [[CrossRef](#)]
61. Zornik, E.; Paisley, K.; Nichols, R. Neural transmitters and a peptide modulate *Drosophila* heart rate. *Peptides* **1999**, *20*, 45–51. [[CrossRef](#)]
62. Fink, M.; Callol-Massot, C.; Chu, A.; Ruiz-Lozano, P.; Izpisua Belmonte, J.C.; Giles, W.; Bodmer, R.; Ocorr, K. A new method for detection and quantification of heartbeat parameters in *Drosophila*, zebrafish, and embryonic mouse hearts. *BioTechniques* **2009**, *46*, 101–113. [[CrossRef](#)] [[PubMed](#)]
63. Capote, L.A.; Mendez Perez, R.; Lymperopoulos, A. GPCR signaling and cardiac function. *Eur. J. Pharmacol.* **2015**, *763*, 143–148. [[CrossRef](#)] [[PubMed](#)]
64. Becker, R.; Merkely, B.; Bauer, A.; Geller, L.; Fazekas, L.; Freigang, K.D.; Voss, F.; Senges, J.C.; Kuebler, W.; Schoels, W. Ventricular arrhythmias induced by endothelin-1 or by acute ischemia: A comparative analysis using three-dimensional mapping. *Cardiovasc. Res.* **2000**, *45*, 310–320. [[CrossRef](#)]

65. Garg, S.; Narula, J.; Marelli, C.; Cesario, D. Role of angiotensin receptor blockers in the prevention and treatment of arrhythmias. *Am. J. Cardiol.* **2006**, *97*, 921–925. [[CrossRef](#)] [[PubMed](#)]
66. Gondo, N.; Kumagai, K.; Nakashima, H.; Saku, K. Angiotensin II provokes cesium-induced ventricular tachyarrhythmias. *Cardiovasc. Res.* **2001**, *49*, 381–390. [[CrossRef](#)]
67. Reid, A.C.; Brazin, J.A.; Morrey, C.; Silver, R.B.; Levi, R. Targeting cardiac mast cells: Pharmacological modulation of the local renin-angiotensin system. *Curr. Pharm. Des.* **2011**, *17*, 3744–3752. [[CrossRef](#)] [[PubMed](#)]
68. Von Lewinski, D.; Kockskämper, J.; Rübertus, S.U.; Zhu, D.; Schmitto, J.D.; Schöndube, F.A.; Hasenfuss, G.; Pieske, B. Direct pro-arrhythmogenic effects of angiotensin II can be suppressed by AT1 receptor blockade in human atrial myocardium. *Eur. J. Heart Fail.* **2008**, *10*, 1172–1176. [[CrossRef](#)]
69. Yahiro, E.; Ideishi, M.; Wang, L.X.; Urata, H.; Kumagai, K.; Arakawa, K.; Saku, K. Reperfusion-induced arrhythmias are suppressed by inhibition of the angiotensin II type 1 receptor. *Cardiology* **2003**, *99*, 61–67. [[CrossRef](#)]
70. Takata, Y.; Hirayama, Y.; Kiyomi, S.; Ogawa, T.; Iga, K.; Ishii, T.; Nagai, Y.; Ibukiyama, C. The beneficial effects of atrial natriuretic peptide on arrhythmias and myocardial high-energy phosphates after reperfusion. *Cardiovasc. Res.* **1996**, *32*, 286–293. [[CrossRef](#)]
71. Zois, N.E.; Bartels, E.D.; Hunter, I.; Kousholt, B.S.; Olsen, L.H.; Goetze, J.P. Natriuretic peptides in cardiometabolic regulation and disease. *Nat. Rev. Cardiol.* **2014**, *11*, 403–412. [[CrossRef](#)] [[PubMed](#)]
72. Dulcis, D.; Levine, R.B. Innervation of the heart of the adult fruit fly, *Drosophila melanogaster*. *J. Comp. Neurol.* **2003**, *465*, 560–578. [[CrossRef](#)]
73. Cook, B.J.; Holman, G.M.; Wagner, R.M.; Nachman, R.J. Pharmacological actions of a new class of neuropeptides, the Leucokinins-I-IV, on the visceral muscles of *Leucophaea maderae*. *Comp. Biochem. Physiol. C* **1989**, *93*, 257–262. [[CrossRef](#)]
74. Cook, B.J.; Holman, G.M.; Wagner, R.M.; Nachman, R.J. Comparative pharmacological actions of Leucokinins-V-VIII on the visceral muscles of *Leucophaea maderae*. *Comp. Biochem. Physiol. C* **1990**, *95*, 19–24. [[CrossRef](#)]
75. Poels, J.; Birse, R.T.; Nachman, R.J.; Fichna, J.; Janecka, A.; Vanden Broeck, J.; Nässel, D.R. Characterization and distribution of NKD, a receptor for *Drosophila* tachykinin-related peptide 6. *Peptides* **2009**, *30*, 545–556. [[CrossRef](#)] [[PubMed](#)]
76. Birse, R.T.; Johnson, E.C.; Taghert, P.H.; Nässel, D.R. Widely distributed *Drosophila* G-protein-coupled receptor (CG7887) is activated by endogenous tachykinin-related peptides. *J. Neurobiol.* **2006**, *66*, 33–46. [[CrossRef](#)] [[PubMed](#)]
77. Larsen, M.J.; Burton, K.J.; Zantello, M.R.; Smith, V.G.; Lowery, D.L.; Kubiak, T.M. Type A allatostatins from *Drosophila melanogaster* and *Diptera punctata* activate two *Drosophila* allatostatin receptors, DAR-1 and DAR-2, expressed in CHO cells. *Biochem. Biophys. Res. Commun.* **2001**, *286*, 895–901. [[CrossRef](#)]
78. McGaw, I.J.; Wilkens, J.L.; McMahon, B.R.; Airriess, C.N. Crustacean cardioexcitatory peptides may inhibit the heart in vivo. *J. Exp. Biol.* **1995**, *198 Pt 12*, 2547–2550.
79. Vogler, G.; Ocorr, K. Visualizing the beating heart in *Drosophila*. *J. Vis. Exp.* **2009**. [[CrossRef](#)]
80. Schneider, C.A.; Rasband, W.S.; Eliceiri, K.W. NIH Image to ImageJ: 25 years of image analysis. *Nat. Methods* **2012**, *9*, 671–675. [[CrossRef](#)]
81. Ocorr, K.; Vogler, G.; Bodmer, R. Methods to assess *Drosophila* heart development, function and aging. *Methods* **2014**, *68*, 265–272. [[CrossRef](#)] [[PubMed](#)]
82. Bradski, G. The OpenCV library. *Dr. Dobbs J.* **2000**, *120*, 122–125.





## 6 Unpublished Data

### 6.1 Introduction

*Drosophila* is an excellent model system for examining heart development and investigating cardiovascular diseases. Methods are available to measure the *Drosophila* heart rate; these include semiautomatic optical heart rate analysis (SOHA) (Ocorr et al., 2009), optical coherence tomography (OCT) (Choma et al., 2006) and the FTIR-based imaging method (Berh et al., 2018). However, none of the currently available software is an open-source, standalone, cross-platform solution that can analyse the heart rate of intact animals with minimal effort and maximum output. The heart analysis software Heart Image Recorder Osnabrück (HIRO) makes this feasible without dissection, which can affect the heart performance. In the present study, I demonstrated how HIRO works and showed the influence of the RNAi-mediated downregulation of critical ECM proteins in *Drosophila melanogaster*. At least two different RNAi lines were used for each protein. These were either from the Vienna Drosophila Resource Center (VDRC)-KK RNAi, VDRC-GD RNAi or VDRC-shRNAi construct collection (Table 3). It is recommended that RNAi crossings from the VDRC-KK collection use the VDRC-60101 as a control line (Vissers et al., 2016). Other lines were compared with the *handC*-Gal4; *handC*-GFP >  $w^{1118}$  or the *handC*-GFP; *prc*-Gal4 >  $w^{1118}$  control lines.

## 6.2 Materials and methods

### 6.2.1 Recording the *Drosophila* heart rate

All video recordings were done on an upright microscope (Leica DMLB). The heart rate was recorded for 60 seconds with a high-speed video camera (Basler piA-640) and the software Firecapture (v1.3). For this purpose, it was essential to focus the microscope on the heart tube location. Figure 5 shows a close-up of the region of interest (ROI), where the heartbeat can be derived from the movement of the neighbouring trachea. The heart tube was not visible using the tissue glue or diethyl ether method, but the trachea movement syncs with the heartbeat and can therefore be used for heart rate measurement. The files were saved as uncompressed audio video interleave (avi) files.

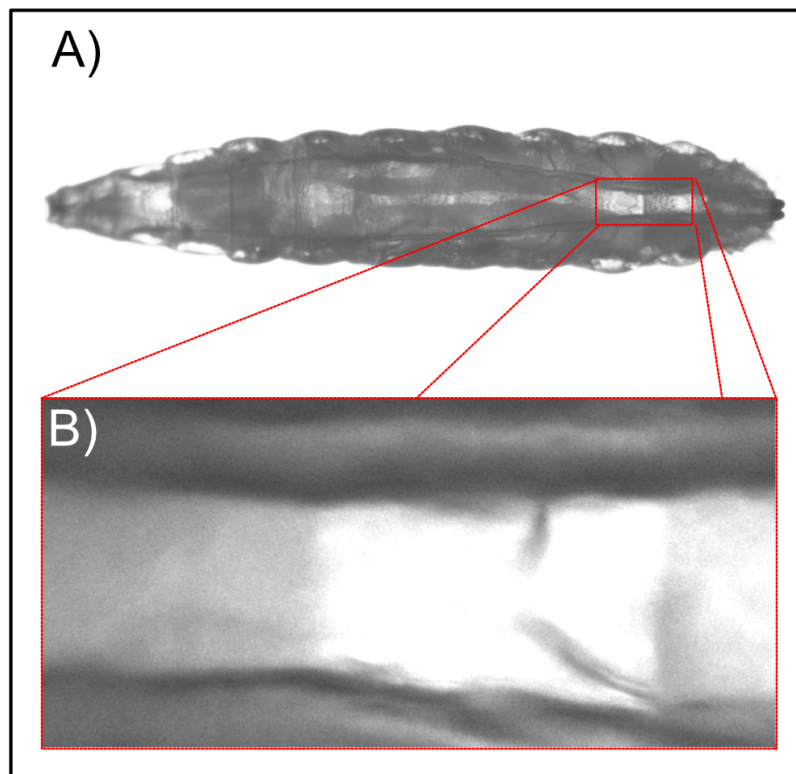


**Figure 5: Region of interest (ROI) selection for heartbeat recording.** The figure shows a close-up of the ROI, where the heartbeat can be derived from the movement of the neighbouring trachea. A) A *Drosophila* 3<sup>rd</sup> instar wandering larva under the microscope. It was anaesthetised with diethyl ether for 10 Minutes. The red rectangle represents the measured area within a frame. B) The upper and lower tubes are the trachea, which move synchronously with the beating heart (not visible itself).

### 6.2.2 Preparation of Sylgard®184 silicone elastomer plates

The Sylgard 184 Silicone Elastomer Base (DOW, Midland USA) was mixed with the Sylgard 184 Silicone Elastomer Curing Agent (DOW, Midland USA) with a ratio of 10:1. Following this, glass plates were filled with a 1mm thick layer of the elastomer.

### 6.2.3 Dissection method

After collection, the wandering third instar larvae were pinned onto Sylgard®184 silicone elastomer plates filled with tempered artificial haemolymph and dissected from the ventral side. Once the viscera were removed, the animals were allowed to recover for 10 minutes. Following this, they were placed dorsal side up on a cover slide on the focusing stage of the microscope.

### 6.2.4 Tissue glue fixation method

Wandering third instar larvae were collected and placed dorsal side up on a cover slide. Following this, they were covered with Histoacryl®(Braun, Rubi Spain). After glue hardening, the slide was dorsal side up placed on the focusing stage of the microscope.

### 6.2.5 Diethylether anaesthesia method

Once the wandering third instar larvae were collected, they were transferred into a glass tubule with an air-permeable bottom (Fig. 6). The tubule gets inserted into a conical flask that contains wool saturated with 1 ml Diethylether (Roth, Karlsruhe Deutschland). After 10 minutes, they were placed dorsal side up on a cover slide on the focusing stage of the microscope.

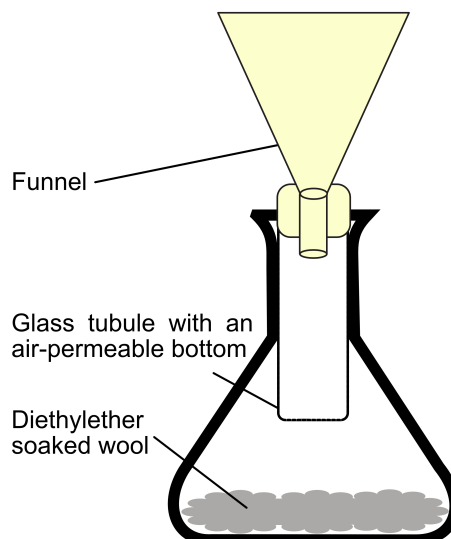


**Figure 6: Diethylether method.** Wandering third instar larvae were collected and transferred into a glass tubule with an air-permeable bottom. The tubule with the *Drosophila* larvae is placed into a conical flask that contains wool wetted with 1 ml Diethylether (Roth, Karlsruhe Deutschland). After 10 minutes, the larvae are anaesthetised and can be used for investigations.

### 6.2.6 HIRO software

HIRO is written in Java and uses the Swing graphical user interface. Its principal function is to recognise and evaluate *Drosophila* heartbeats within previously recorded video files. Various video capture software save those files with different video codecs. To handle this, the FFmpeg library has been implemented in HIRO so that it can work with both uncompressed and compressed video files. HIRO can be used with connected cameras and allows to record videos. The user can work with different colour models to be able to respond to different setup conditions. HIRO offers two algorithms to remove the background. The first algorithm works with thresholding (Otsu, 1979); the second is the Canny edge detector algorithm (Canny, 1986). The video tool offers a real-time preview and a real-time histogram.

#### Calculating the mean grey values

HIRO can calculate the heart rate by measuring the mean pixel intensity in each frame and compares them. It uses the OpenCV library to calculate each frame's brightness within one video. OpenCV is an open-source library for image and video analyses. Every video frame is converted into a specific OpenCV-Mat-Class, which is a matrix containing all pixel values of the frame. The beating heart waveform can be thought of as a collection of grey value data points (Fig. 7). Each frame's mean pixel intensity is then stored within a HIRO file next to the video file.

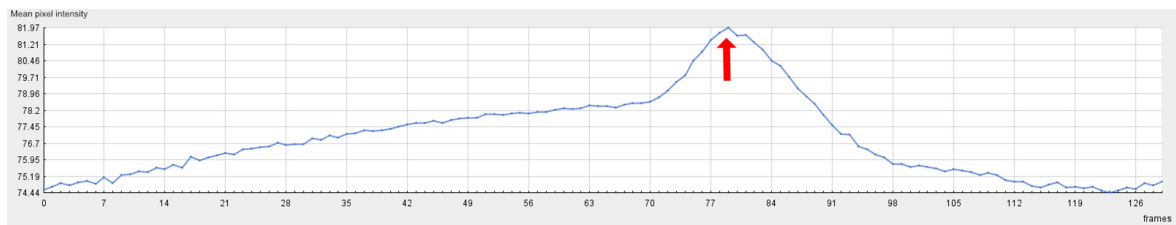


**Figure 7: Mean grey value of one heartbeat.** The figure shows the mean grey values of one heartbeat while working under a transmitted-light microscope. During a contraction, less light can pass through the heart tube. The maximum contraction point, represented by the highest grey value, is marked with a red arrow.

#### Smoothing noisy video signals

Measuring through cuticula may cause blurry signals. To handle this, HIRO employs the moving average algorithm to smooth the signal (Hansun, 2013). All values are saved within the HIRO data files. The algorithm calculates the average grey value over a period. It adds two or more data points, divides their sum by the total amount of data points that were added, and replaces the first data point in the file with the average grey value. The algorithm repeats this process with the second, third, etc. data point until the end of the file is reached. The result is a smoothed dataset with less noise (Fig. 8).

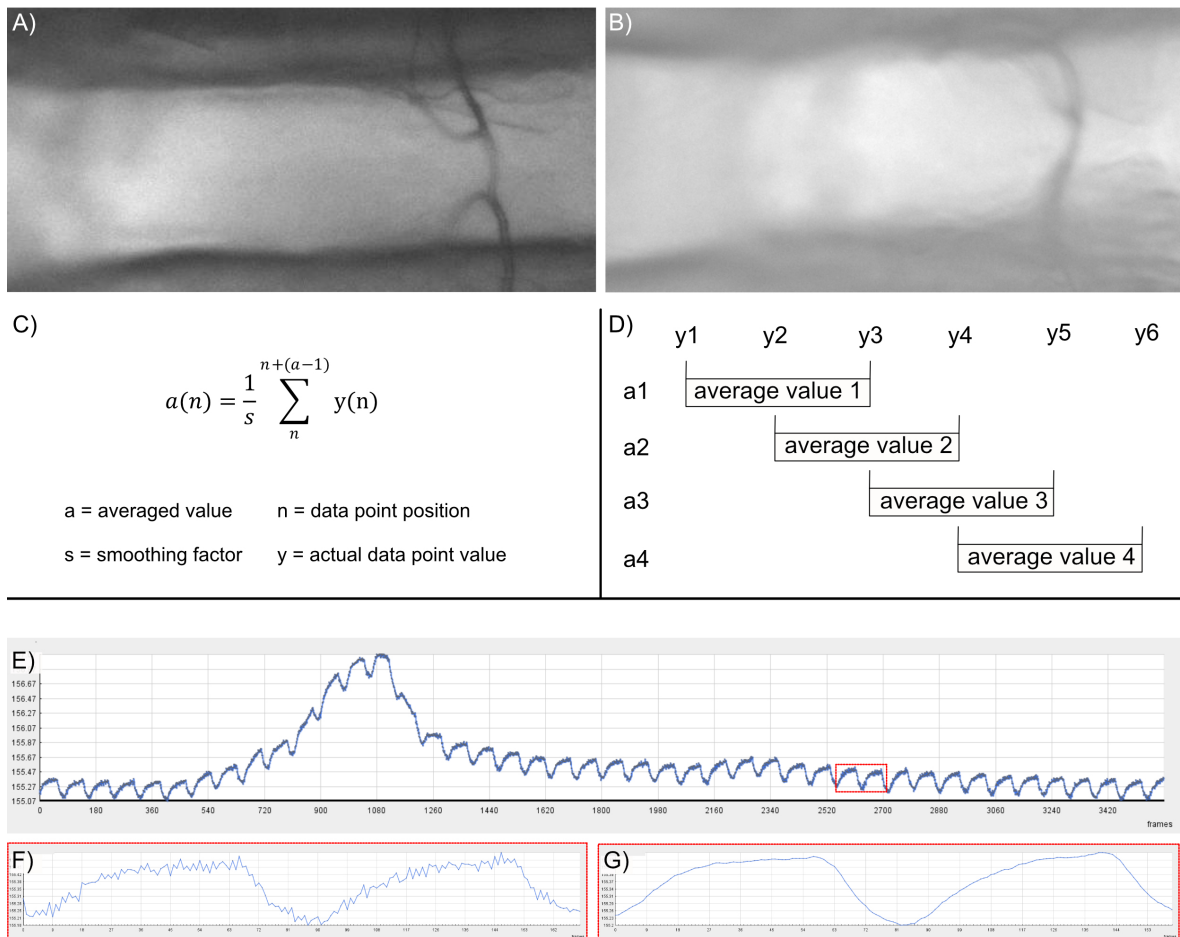


**Figure 8: The moving average algorithm.** A) Example frame of a clear view of the heart area. B) Example frame of a blurry view. C) The mathematical formula of the algorithm. D) The mean value  $a_n$  is calculated as the sum of ( $y_n, y_{n+1}, y_{n+2}$ ) divided by the smoothing factor (here 3). E) All data points from one heartbeat in a blurry diagram. F) A close-up of the data within the red rectangle in the noisy signal. G) Smooth amplitudes after applying the moving average algorithm.

### Automated heartbeat detection via HIRO

The main goal of the software is to automatically detect the heartbeat. A heart contracts and relaxes in one cycle. The contraction is called the systolic interval, and the relaxation phase is called the diastolic interval. To detect a heartbeat, the software tracks the peaks within the grey values (Fig. 9). One common way to do this is to utilise thresholds. Once the grey values reach the threshold value, a heartbeat is recognised. This process does not work with the ether preparation method, in which the values were increasing and decreasing, so it was impossible to use a threshold (Fig. 9). For heart rate searching, the graph is divided into parts and the algorithm searches for peaks (maximum intensity value (Fig. 10)). HIRO detects the recording speed of a movie file and calculates the elapsed time between frames. The heart rate frequency (in Hz) is the time between two detected systolic peaks, which represents the darkest frames.

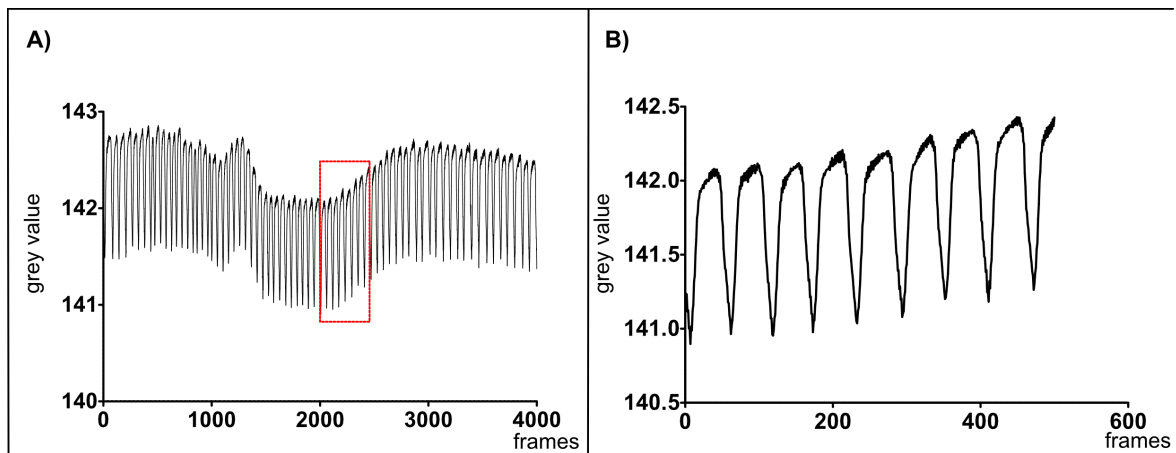


**Figure 9: Thresholds are not suitable for intact heartbeat detection.** Wild-type heartbeats did not show a constant level of grey values. A) Stunned larvae can stir, which leads to increasing and decreasing grey value levels while the heart is beating. B) Magnification of the red rectangle shows the increasing values while the heart was beating.

### HIRO detects systolic and diastolic intervals

The software can distinguish between systolic and diastolic intervals (Fig. 11). To detect the diastolic peaks, the graph is inverted and the algorithm searches again for peaks. The peaks represent the brightest frames within the video file and indicate the end of a diastolic interval. The start of a systolic interval is the darkest frame, and it ends with the next brightest frame. That frame determines the start of the diastolic interval, and that interval ends with the next darkest frame.

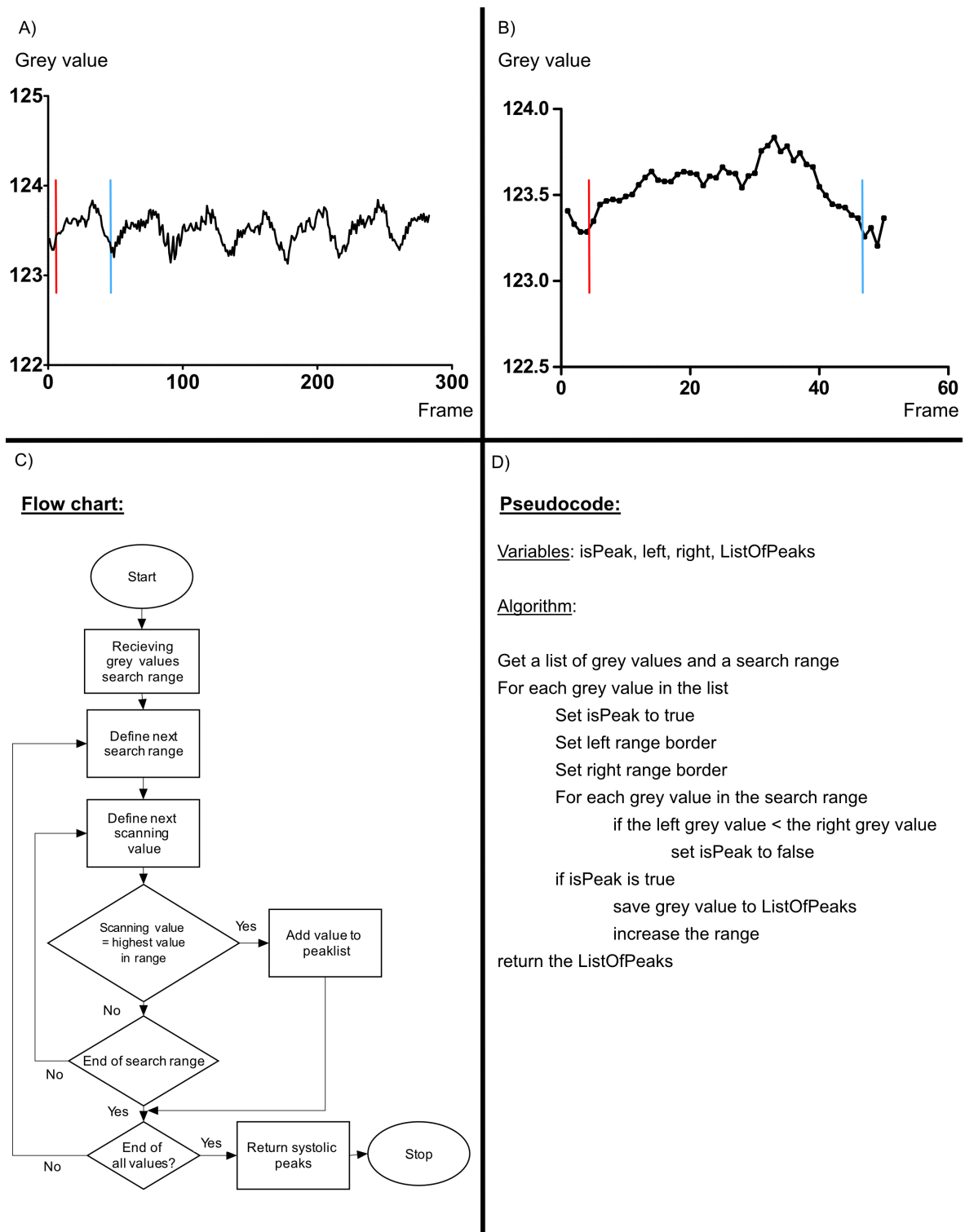


**Figure 10: The algorithm for heartbeat detection.** The maximum contraction of one heartbeat is the highest grey value in a series of frames. The algorithm aims to detect the peaks within the curves. A) The grey values of six wild-type *Drosophila* heartbeats. The red line marks the start, and the blue line marks the end of a search range. B) Magnification of the first heartbeat shown in A). C) Flowchart of the algorithm. D) Pseudocode of the algorithm.

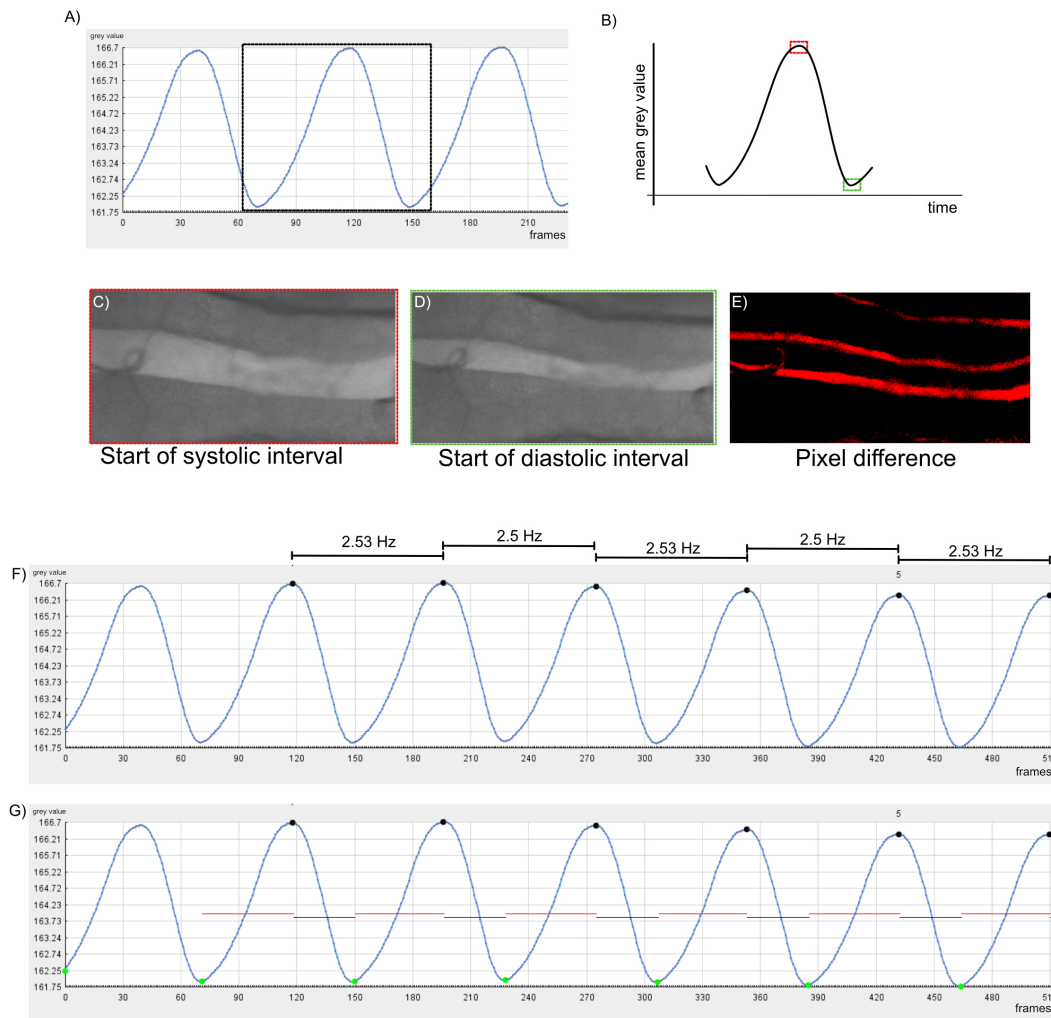


**Figure 11: The detection of systolic and diastolic intervals.** A) The grey values of three heartbeat intervals. B) Magnification of the black rectangle in A). The red box represents the start of the systolic interval, and the green box marks the start of the diastolic interval. C) and D) Real-time images of the systolic and diastolic intervals, respectively. E) The pixel differences from C) and D) during one heartbeat. F) The heart rate, which was calculated by measuring from one peak to another peak. G) A systolic interval starts with a green point and ends with a black point, and is *vice versa* in the diastolic interval. A systolic interval is depicted as a red line, and a diastolic interval is illustrated as a black line.



### 6.2.7 Fly lines

*handC-Gal4*<sup>4,2</sup>; *handC-GFP*<sup>3,1</sup> and *handC-GFP*<sup>2,3</sup>; *prc-Gal4* was used as driver and crossed with the UAS-RNAi lines. *Drosophila* GD and KK RNAi collection lines were obtained from the Vienna *Drosophila* Resource Center (VDRC, (Dietzl et al., 2007)), and NIG-FLY stocks were obtained from the National Institute of Genetics (NIG) in Japan (Table 3). The KK collection-specific VDRC-ID 60101 was used as a control for the KK RNAi lines. The GD RNAi lines were controlled by crossing the applied driver line to *w*<sup>1118</sup> (RRID : BDSC\_5905).

**Table 3: RNAi fly lines used in this thesis.**

| Protein               | Symbol | Annotation symbol | P-Element RNAi Library (GD) | phiC31 RNAi Library (KK) | NIG-RNAi Strains |
|-----------------------|--------|-------------------|-----------------------------|--------------------------|------------------|
| Integrin $\alpha$ PS2 | If     | CG9623            | v44885                      | v100770                  | -                |
| Integrin $\beta$ PS   | Mys    | CG1560            | v29620                      | v103704                  | -                |
| Laminin A             | LanA   | CG10236           | v18873                      | v330178                  | -                |
| Laminin B2            | LanB2  | CG3322            | v42559                      | v104013                  | -                |
| Lonely heart          | Loh    | CG6232            | v31020                      | -                        | 6232R-1          |
| Nidogen               | Ndg    | CG12908           | v13280                      | v109625                  | -                |
| Pericardin            | Prc    | CG5700            | v41320                      | v100357                  | -                |
| Trol                  | Trol   | CG33950           | v24549                      | v110494                  | -                |
| Viking                | Vkg    | CG16858           | v16986                      | v106812                  | -                |

**Table 4: Control and driver lines used in this thesis.**

| Control lines   |   |
|---|---|
| KK Control line (v60101)<br><i>w</i> <sup>1118</sup>  | (Vissers et al., 2016)<br>BL3605 Bloomington <i>Drosophila</i> Stock Center |
| Driver lines  |   |
| <i>handC-Gal4</i> <sup>4,2</sup> ; <i>handC-GFP</i> <sup>3,1</sup><br><i>handC-GFP</i> <sup>2,3</sup> ; <i>prc-Gal4</i> |   |

### 6.2.8 Software

**Table 5: Software used in this thesis.**

| Software                | Source /Company              | Purpose of application |
|-------------------------|------------------------------|------------------------|
| Affinity designer       | Serif                        | Create graphics        |
| Eclipse                 | Eclipse Foundation           | Java programming       |
| FireCapture Version 1.3 | Thorsten Edelmann ©2009-2017 | Recording videos       |
| GraphPad Prism 4        | GraphPad                     | Statistics             |
| HIRO                    | this work                    | Video processing       |

### 6.3 Results

The main function of HIRO is to detect the cardiac rhythm in living specimens at highest possible precision. Comparisons between heart measurements can only be made between animals of the same age and developmental stage.

#### 6.3.1 Identifying the optimal preparation stage

Three developmental stages (larval, pupal and adult) of *Drosophila* were used to test the functionality of HIRO (Fig. 12). The heartbeat was accurately detected for animals of all three developmental stages. The best results were obtained from larvae. Therefore, larvae were used for further investigations based on the consistent heart rhythm and straightforward handling.

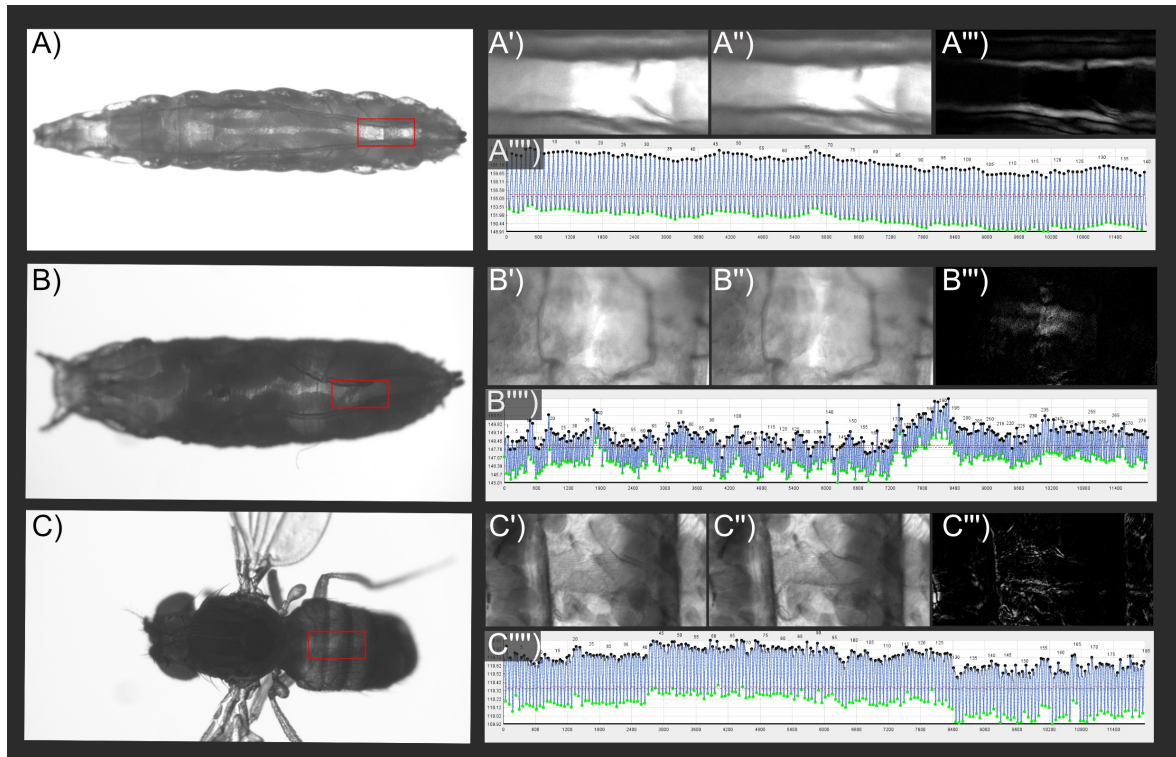


**Figure 12: Heatbeat detection in three developmental stages over 60 seconds.** The larval stage (A), the pupal stage (B) and the adult stage (C). The red rectangles represent the measured area within a frame. A'), B') and C') show the diastole. A''), B'') and C'') show the systole. A'''), B''') and C''') show the pixel subtraction from the diastolic and systolic images. A''''), B''''') and C''''') show HIRO detecting the heart rate while measuring the grey values (X-axis) over time (Y-axis). The blue lines represent the grey value of the measured area; the black dots represent the start of the systolic interval; and the green dots represent its end.

### 6.3.2 Determination of the optimal preparation method

The animals need to be fixed and anaesthetised without affecting the cardiac rhythm; therefore, various methods were tested. At least 11  $w^{1118}$  animals were used for every preparation. Dissecting the animal leads to a significantly decreased heart rate in comparison to the glue or ether method (Fig. 13 A). No significantly altered heart rate between the glue and ether method was detected (Fig. 13 A). Furthermore, ether-anaesthetised animals showed a significantly reduced arrhythmicity index compared with the other preparation methods (Fig. 13 B). Analysing the systolic and diastolic interval showed that immobilisation of glue and ether leads to a significantly decreased systolic and diastolic interval compared to dissected larvae (Fig. 13 C, D).

### 6.3.3 Confirming the heart rhythm of control lines

Follow-up experiments were conducted in larvae, which were anaesthetised with ether. Control lines were analysed to further confirm the proper functionality of HIRO. Various transgenic backgrounds might influence the cardiac rhythm. Different control lines were used depending on the experiment (Table 4). In the subsequent text, the *handC*-GFP; *prc*-Gal4 is abbreviated as *prc*-Gal4, and the *handC*-Gal4; *handC*-GFP driver is abbreviated as *handC*-Gal4.

The crossing of  $w^{1118}$  to *handC*-Gal4 or *prc*-Gal4 already reduces the heart rate significantly compared to  $w^{1118}$  alone (Fig. 14 A). Compared to  $w^{1118}$ , animals from the PhiC31 RNAi Library (KK) Line crossed with *handC*-Gal4 or *prc*-Gal4 show a significantly reduced heart rate (Fig. 14 A). No significantly altered heart rate between the *handC*-Gal4 >  $w^{1118}$  or the *prc*-Gal4 >  $w^{1118}$  line was detected (Fig. 14 A). Additionally, *prc*-Gal4 > KK<sup>v60101</sup> control line showed a significantly decreased heart rate compared to *prc*-Gal4 >  $w^{1118}$  (Fig. 14 A). *prc*-Gal4 >  $w^{1118}$  showed an increased arrhythmicity index (AI) in comparison to the  $w^{1118}$  and *prc*-Gal4 > KK control lines (Fig. 14 B).

### 6.3.4 Analysing the influence of RNAi-mediated downregulation of critical cardiac ECM proteins

In the following experiments, the influence of various heart ECM proteins on cardiac activity was tested. The RNAi lines were driven with either the *handC*-GFP; *prc*-Gal4 driver line or the *handC*-Gal4; *handC*-GFP driver line. *handC*-GFP; *prc*-Gal4 is abbreviated as *prc*-Gal4, and the *handC*-Gal4; *handC*-GFP driver is abbreviated as *handC*-Gal4.

#### Integrins

Integrins are heterodimers with associated  $\alpha$  and  $\beta$  subunits. They are receptors that link extracellular matrix molecules to cytoskeletal components.

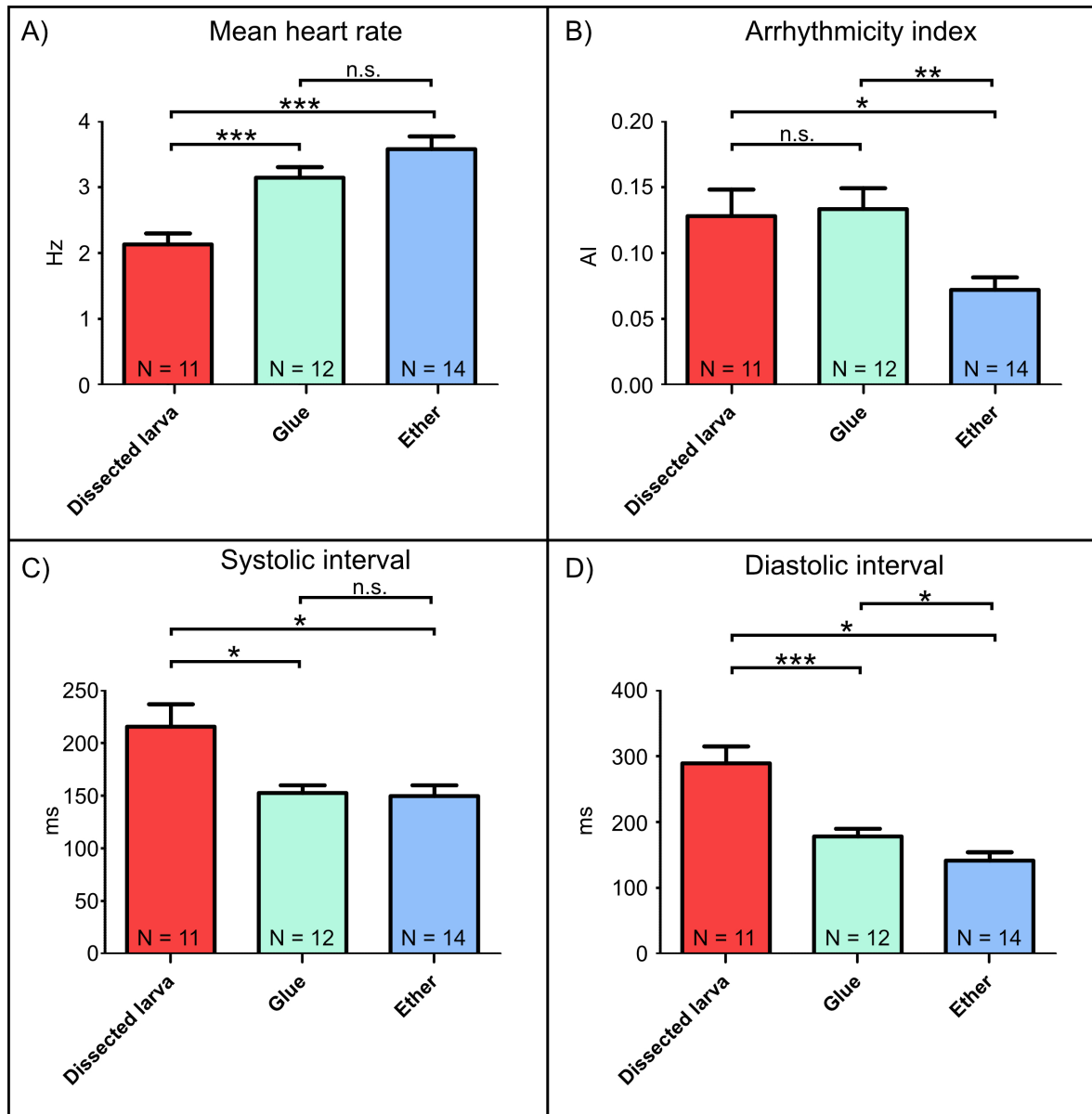


**Figure 13: Comparison of the preparation methods.** Red bars represent data from dissected larva, green bars represent data from animals fixed with glue, and blue bars represent data from animals anaesthetised with ether. Data are presented as mean values ( $\pm$  SEM). Significance levels are indicated by asterisks (paired sample Student's t-test, \*  $p < 0.05$ ; \*\*  $p < 0.005$ ; \*\*\*  $p < 0.0005$ ; n.s., not significant).

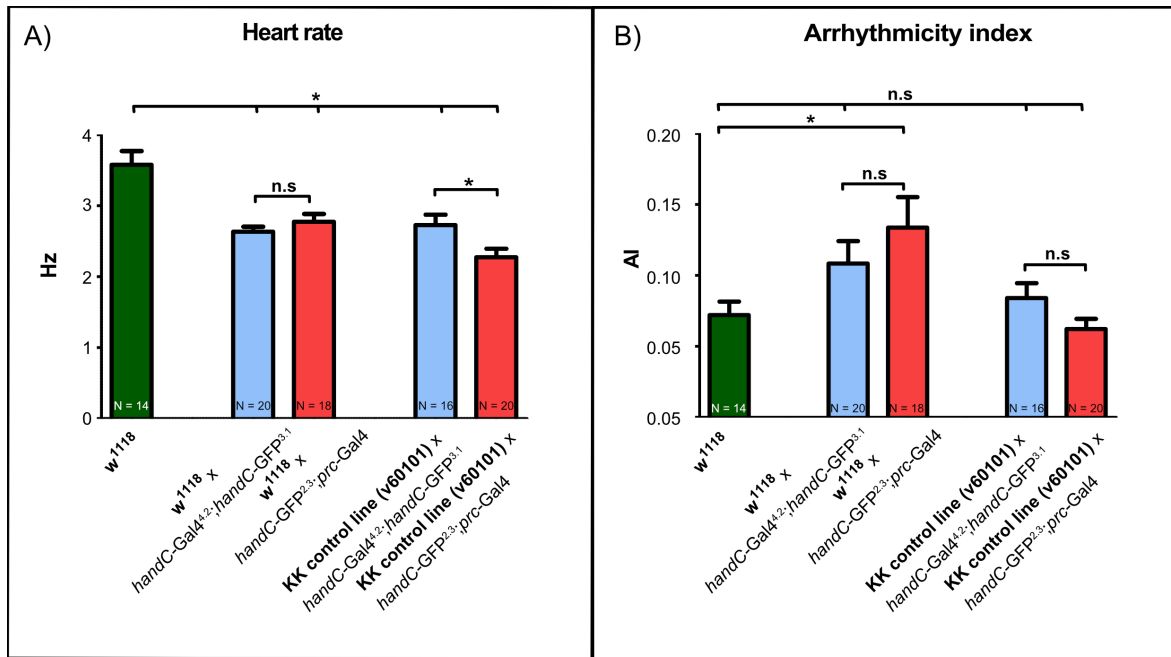


**Figure 14: Heart measurements of control animals.** Heart rate (A) and arrhythmicity index (B) of control lines. Data are presented as mean values ( $\pm$ SEM). Significance levels are indicated by asterisks (paired sample Student's t-test, \*  $p < 0.05$ ; \*\*  $p < 0.005$ ; \*\*\*  $p < 0.0005$ ; n.s., not significant).

### $\alpha$ PS2 Integrin - (If)

The *inflated* (If) gene encodes one of five Integrin  $\alpha$  subunits. Together with an Integrin  $\beta$  subunit, it forms a receptor for extracellular matrix proteins. The analysed If RNAi lines showed no significant difference independent of the driver line used (Fig. 15 A, A'; Fig. 16 A, A'). Only the *handC-Gal4* > If<sup>v110770</sup> RNAi showed a significant increase for the AI (Fig. 16 A).

### $\beta$ PS Integrin - (Mys)

The *mysospheroid* (Mys) gene encodes a  $\beta$  subunit of the integrin dimer. Only *handC-Gal4* > Mys<sup>v103704</sup> RNAi showed a significantly increased arrhythmicity index (Fig. 16 B). In contrast, *prc-Gal4* > Mys RNAi mediated knockdown has a significant decrease in heart rate, whereas the AI is significantly increased compared to the control. (Fig. 15 B, B'; Fig. 16 B, B'). The Mys<sup>v29620</sup> RNAi line had a significantly reduced heart rate and an increased AI. *prc-Gal4* > Mys<sup>v103704</sup> RNAi led to nonviable offspring; thus, it was not evaluated (Fig. 15 B', Fig. 16 B').

### Laminins

Laminins are heterotrimeric molecules found in all basement membranes. Laminin is composed of three polypeptides ( $\alpha$ ,  $\beta$  and  $\gamma$ ) (Beck et al., 1993; Miner and Yurchenco, 2004). The  $\alpha$  chain permits the interaction with Integrins, Dystroglycan and Perlecan, while the

$\beta$  and  $\gamma$  chains are responsible for the self-assembly of Laminin. RNAi lines that encode Laminin A ( $\alpha$ ) and Laminin B2 ( $\gamma$ ) were used in the following experiments.

### **Laminin A - (LanA)**

The *handC*-Gal4 driver crossed with both LanA RNAi lines showed no influence on the arrhythmicity index (Fig. 16 C). Only the *handC*-Gal4 > LanA<sup>v18873</sup> RNAi showed a significantly increased heart rate (Fig. 15 C). However, *prc*-Gal4 > LanA<sup>v18873</sup> RNAi and *prc*-Gal4 > LanA<sup>v330178</sup> RNAi showed a significantly altered heart rate (Fig. 15 C'). Remarkable, *prc*-Gal4 > LanA<sup>v18873</sup> had an increased heart rate and *prc*-Gal4 > LanA<sup>v330178</sup> RNAi had a strongly decreased HR (Fig. 15 C'). Additionally, *prc*-Gal4 > LanA<sup>v330178</sup> RNAi showed an increased arrhythmicity index (Fig. 16 C').

### **Laminin B2 - (LanB2)**

LanB2<sup>v42559</sup> RNAi crossed with both driver lines showed a significantly increased heart rate (Fig. 15 D, D'). The second line had no altered heart rate. Both LanB2 RNAi lines showed no significantly modified arrhythmicity index (Fig. 16 D, D').

### **Lonely heart - (Loh)**

Lonely heart recruits Pericardin into the cardiac matrix and is essential for heart development. Because only one GD RNAi line is available in the Vienna Stock Center, the second RNAi (6232R-1) was obtained from the NIG fly stock (Japan). *prc*-Gal4 > Loh<sup>v31020</sup> RNAi and *prc*-Gal4 > Loh<sup>6232R-1</sup> RNAi did not show any significantly altered heart rate or AI (Fig. 15 E', Fig. 16 E'). However, *handC*-Gal4 > Loh<sup>v31020</sup> RNAi and *handC*-Gal4 > Loh<sup>6232R-1</sup> RNAi had a significant effect on the heart rate and AI (Fig. 15 E, Fig. 16 E). Both lines exhibited an increased AI, but they showed contradictory results regarding HR. *handC*-Gal4 > Loh<sup>v31020</sup> RNAi had a significantly decreased heart rate, while *handC*-Gal4 > Loh<sup>6232R-1</sup> RNAi had an increased heart rate (Fig. 15 E).

### **Nidogen - (Ndg)**

BMs are mainly composed of mesh-like networks formed by CollagenIV and Laminin, linked by Nidogen (NDG). *handC*-Gal4 > Ndg<sup>v13280</sup> RNAi and *handC*-Gal4 > Ndg<sup>v109625</sup> RNAi showed no significantly altered heart rate or AI (Fig. 15 F; Fig. 16 F). Although the difference was not significant, the AI from *prc*-Gal4 > Ndg<sup>v13280</sup> was increased compared to the control (Fig. 16 F'). Additionally, *prc*-Gal4 > Ndg<sup>v109625</sup> RNAi led to a significantly increased AI (Fig. 16 F'). However, only *prc*-Gal4 > Ndg<sup>v13280</sup> RNAi had a significantly reduced heart rate (Fig. 15 F').

### **Pericardin - (Prc)**

Pericardin is a type IV Collagen-like protein. It is secreted into the haemolymph by nephrocytes and adipocytes. The anchor protein Lonely heart recruits it to the cardiac matrix

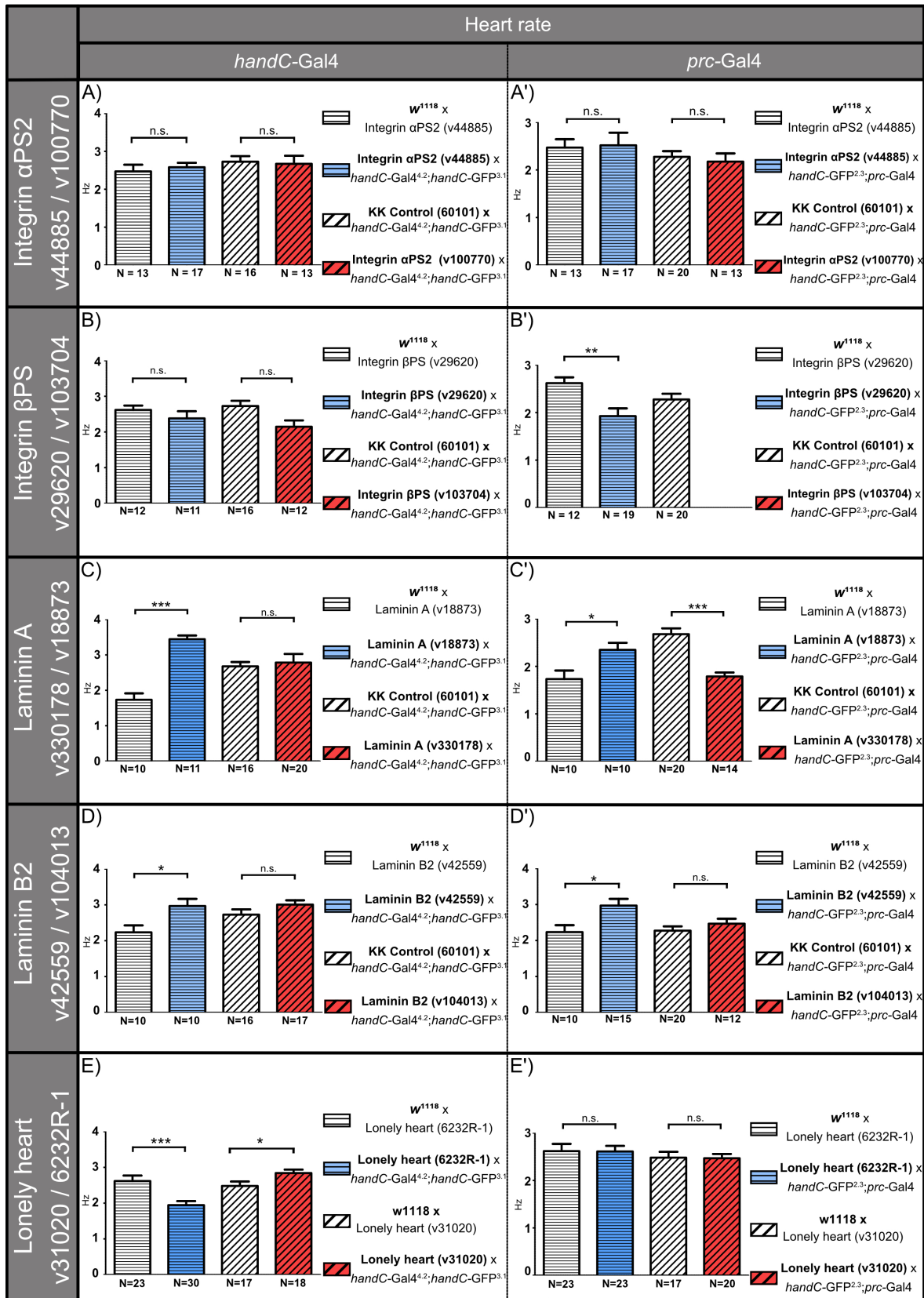
and forms a stable network. *handC*-Gal4 > Prc<sup>v31320</sup> RNAi and *handC*-Gal4 > Prc<sup>v100357</sup> RNAi showed no significantly altered heart rate or AI (Fig. 15 G; Fig. 16 G). Notably, a drastic influence on the heart rate was observed when the Prc RNAi lines were crossed with *prc*-Gal4. Interestingly, a non-beating heart was formed once *prc* was downregulated in adipocytes.

### **Trol - (Trol)**

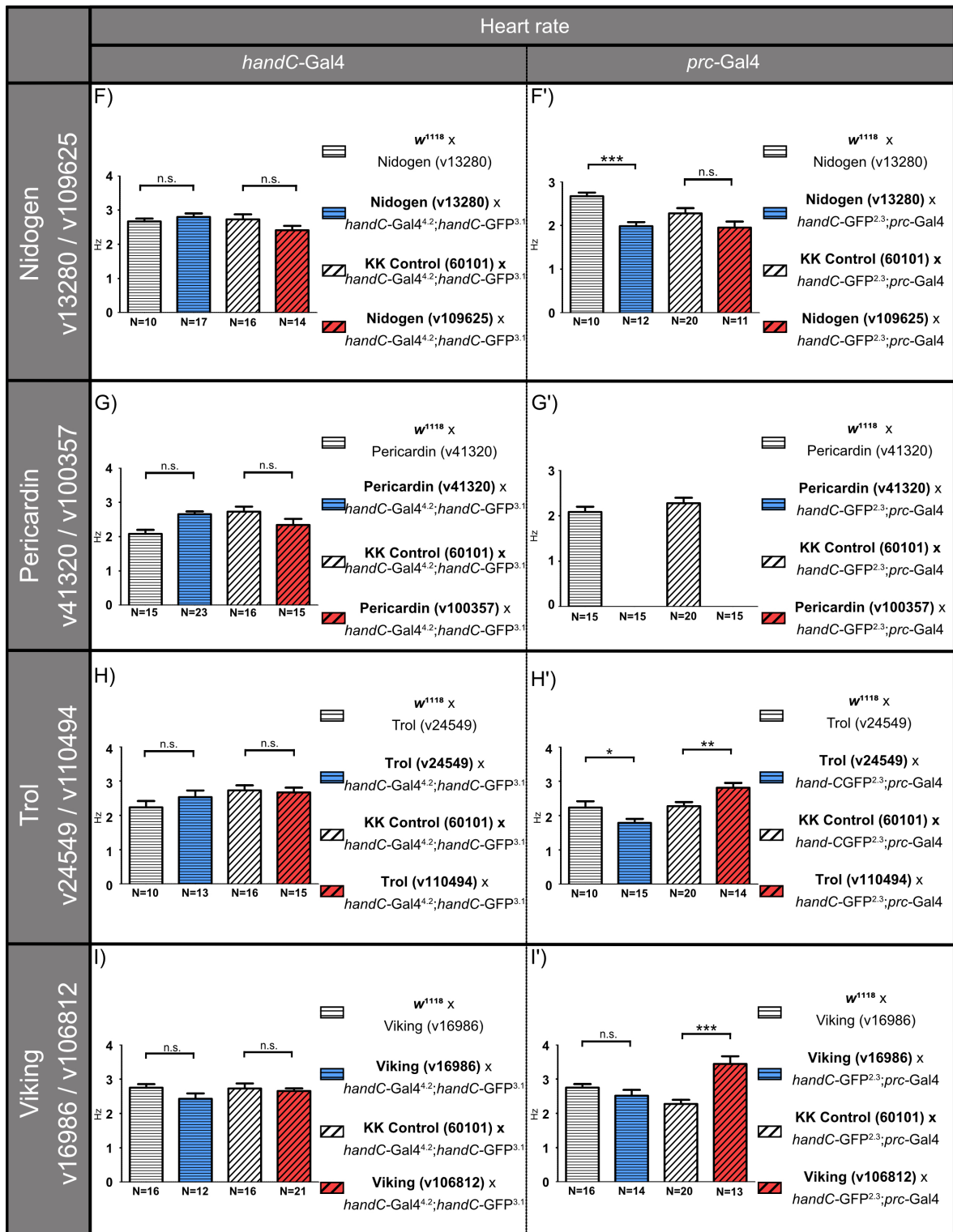
Basement membranes consist of Laminin, Nidogen, and the heparan sulfate proteoglycan Perlecan. *terribly reduced optic lobes* (*trol*) encodes the extracellular matrix component Perlecan. *handC*-Gal4 crossed with both RNAi lines showed no significantly altered heart rate (Fig. 15 H). *prc*-Gal4 > Trol<sup>v24549</sup> RNAi and *prc*-Gal4 > Trol<sup>v110494</sup> RNAi exhibited a significantly altered heart rate (Fig. 15 H'). Notably, *prc*-Gal4 > Trol<sup>v24549</sup> RNAi showed a decreased heart rate while *prc*-Gal4 > Trol<sup>v110494</sup> RNAi had an increased HR (Fig. 15 H'). Additionally, the *handC*-Gal4 > Trol<sup>v110494</sup> RNAi had a significantly increased AI (Fig. 16 H). Furthermore, *prc*-Gal4 > Trol<sup>v110494</sup> RNAi led to an increased AI (Fig. 16 H').

### **Viking - (Vkg)**

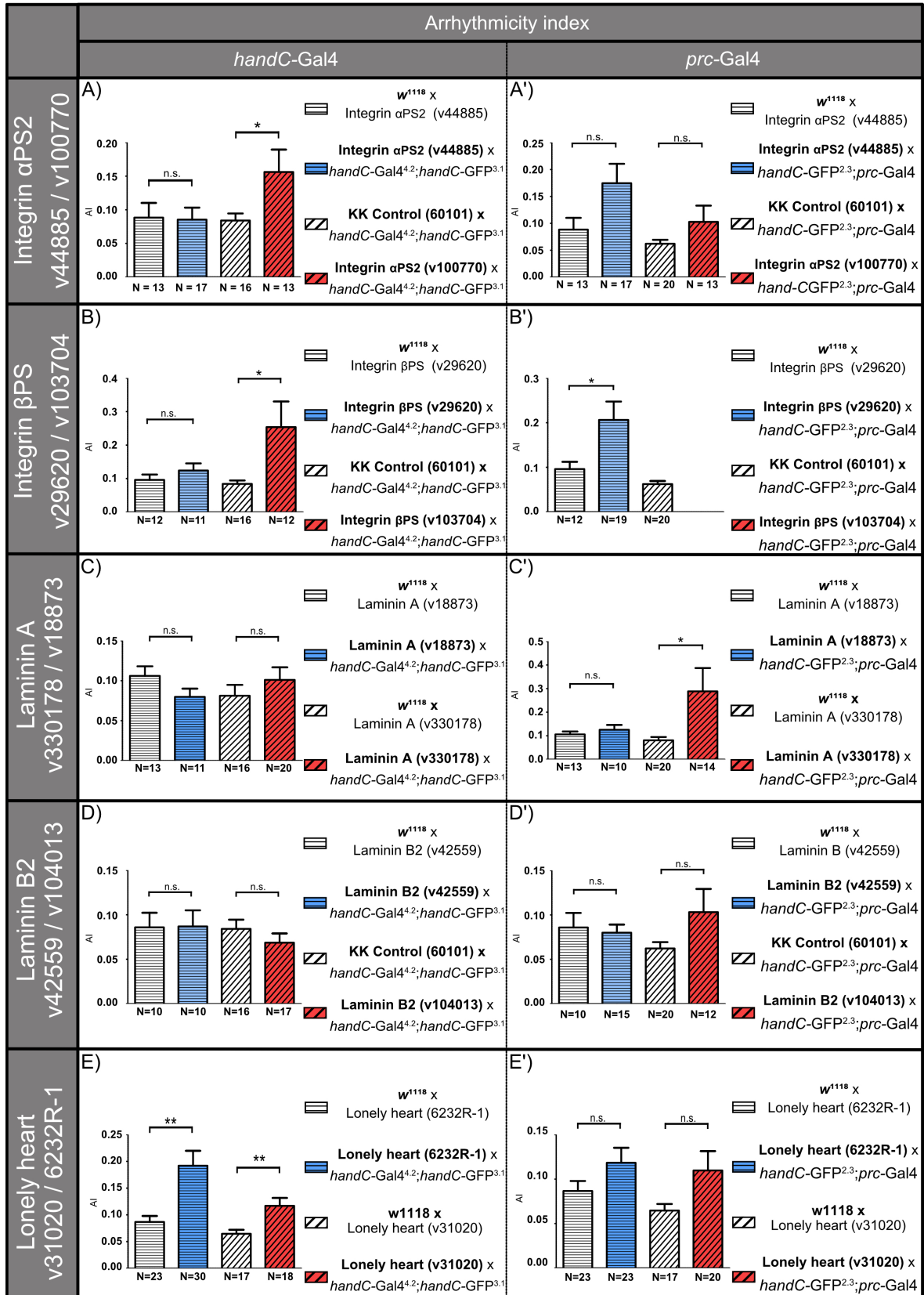
The *viking* gene encodes a subunit of Collagen IV and is an essential part of basement membranes. Both, the *handC*-Gal4 > Vkg<sup>v16986</sup> RNAi and *handC*-Gal4 > Vkg<sup>106812</sup> RNAi did not affect the heart rate or the AI (Fig. 15 I; Fig. 16 I). This was also observed for *prc*-Gal4 > Vkg<sup>v16986</sup> RNAi (Fig. 15 I'; Fig. 16 I'). Only *prc*-Gal4 > Vkg<sup>v106812</sup> RNAi showed a significantly increased heart rate (Fig. 15 I'). Although the difference was not significant, the AI from *prc*-Gal4 > Vkg<sup>v16986</sup> RNAi was increased compared to the control (Fig. 16 I').







**Figure 15: Heart rate effects of RNAi-mediated downregulation of crucial ECM proteins in third instar larvae.** RNAi lines were driven with either the *handC-Gal4*; *handC-GFP* driver line (left column) or with the *handC-GFP*; *prc-Gal4* driver line (right column). Data are presented as mean values ( $\pm$ SEM). Significance levels are indicated by asterisks (paired sample Student's t-test, \*  $p < 0.05$ ; \*\*  $p < 0.005$ ; \*\*\*  $p < 0.0005$ ; n.s., not significant).



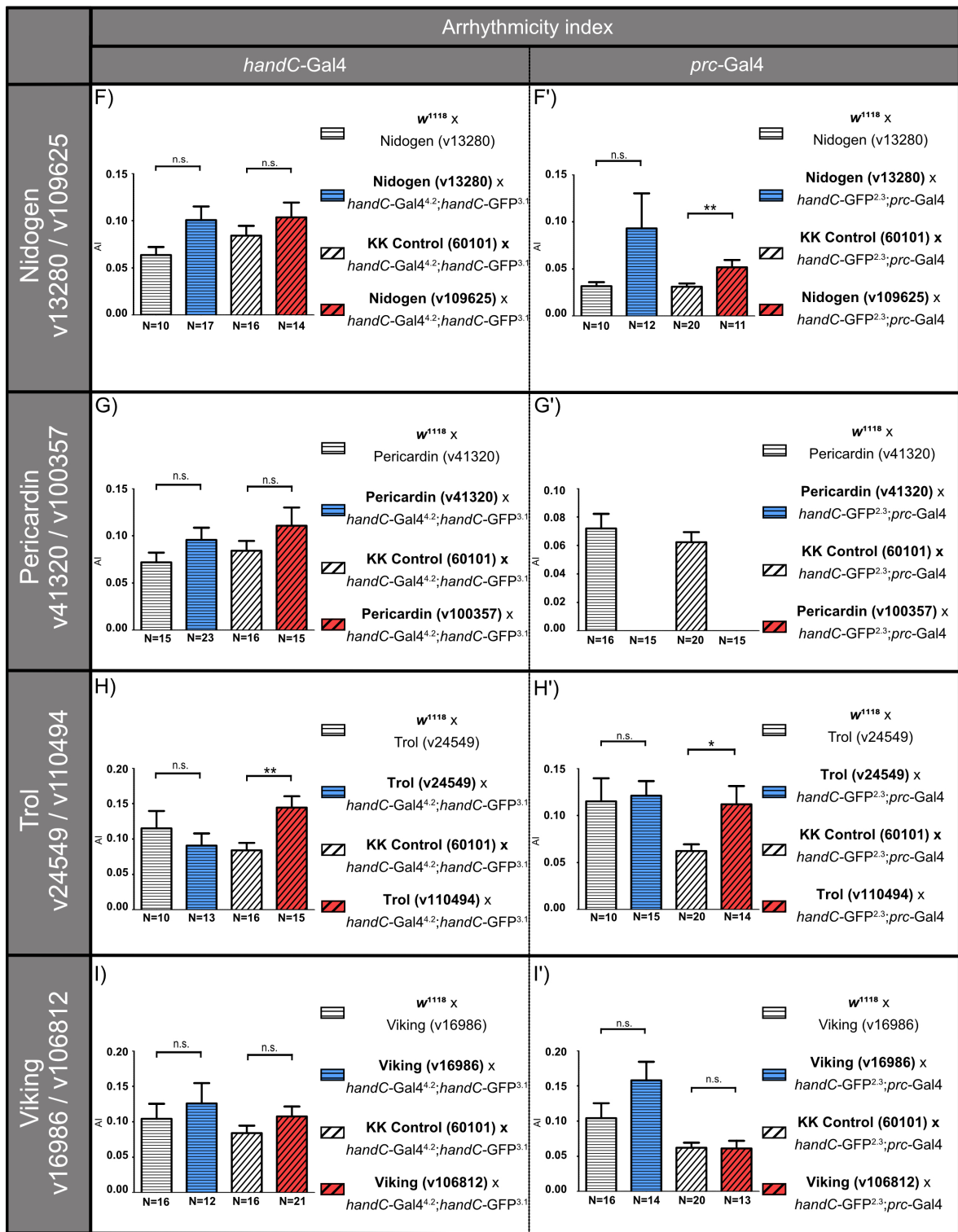


**Figure 16: Heart rhythmicity effects of RNAi-mediated downregulation of crucial ECM protein in third instar larvae.** RNAi lines were driven with either the *handC-Gal4*; *handC-GFP* driver line (left column) or with the *handC-GFP*; *prc-Gal4* driver line (right column). Data are presented as mean values ( $\pm$ SEM). Significance levels are indicated by asterisks (paired sample Student's t-test, \*  $p < 0.05$ ; \*\*  $p < 0.005$ ; \*\*\*  $p < 0.0005$ ; n.s., not significant).

## 6.4 Discussion

### 6.4.1 Intact anaesthetised *Drosophila* larvae are the most reliable for heartbeat recordings

*Drosophila* has several developmental stages including the embryo, three larval stages, 15 pupal stages, and the final adult fly, which can live up to 50 days (Linford et al., 2013). It has been shown that ageing causes cardiac dysfunction (Cannon et al., 2017); thus, it is crucial to analyse animals that have the same age. The functionality of HIRO was tested using the larval stage, the white prepupa stage, and the adult fly of *Drosophila* (Fig. 12).

Wandering, late third instar larvae were used because they have the same age, have a transparent cuticula, and have simple handling requirements (Fig. 12 A). The pupal cuticle becomes darker with increasing stage. The dark cuticle hinders the detection of heart parameters and during metamorphosis muscle movement within the body can affect the heart performance (Fig. 12 B'''). A more accessible approach to detect heart parameters is to select white prepupa (Fig. 12 B). One week old flies were sedated and fixed with their wings spread (Fig. 12 C). In general, the experiments showed that HIRO functions properly with all three animal stages. Wandering, late third instar larvae were used for the high-throughput assay because of the simple handling requirements.

In this work, the immobilisation techniques dissection, glue and ether for late third instar larvae were tested (Section 6.2.3, 6.2.4, 6.2.5). Dissection was also used for the SOHA method (Ocorr et al., 2009). Comparing the heart rate after glue or ether immobilisation showed that the dissection method has a significant effect. After dissection, the heart rate decreases, while the systolic and diastolic interval significantly increase compared to the glue and ether (Fig. 13 A, C, D). Furthermore, dissection showed a similar arrhythmicity index compared to the glue method but an increased arrhythmicity index compared to the ether method (Fig. 13 B). Dissection has an increased risk of damaging the alary muscles. A recent study showed that the internal architecture of larvae is constrained by alary muscles (Bataillé et al., 2020); thus, dissection might influence the heart parameters.

Fixing third instar larvae with glue was the second immobilisation approach (Section 6.2.4). The heart rate and systolic interval were not significantly different between the glue and ether immobilisation (Fig. 13 A, C). However, the diastolic interval and AI showed significantly increased values (Fig. 13 B, D). These results are in contrast with a previous study that showed that FlyNap is less detrimental for cardiac function than ether or CO<sub>2</sub> (Paternostro et al., 2001). FlyNap is a triethylamine-based cocktail used to anaesthetise *Drosophila*. The previous study used adult flies, whereas the current study used larvae. Another previous study used epoxy, CO<sub>2</sub> and FlyNap, and the authors found that the heart rate became irregular and the heart function was significantly decreased in adult flies (Tsai et al., 2011). Furthermore, FlyNap was shown to increase the heart rate of *Anopheles gambiae* (Chen and Hillyer, 2013). Based on the obtained results and those of previous studies, heartbeat

recordings of ether-anesthetised unprepared non-dissected third instar larvae were chosen for subsequent experiments.

Different control lines were used depending on the type of experiment (Table 4). The various transgenic backgrounds might influence cardiac rhythm. Indeed, *handC-Gal4 > w<sup>1118</sup>* and *prc-Gal4 > w<sup>1118</sup>* showed a significantly lower heart rate than the *w<sup>1118</sup>* line (Fig. 14 A). This observation was surprising and led to the assumption that the *white* locus may influence the cardiac function. A few studies have analysed the heart rate of third instar larvae (Table 6). These studies have used either optical coherence microscopy (Men et al., 2016), visual counting (Gu and Singh, 1995; Zhu et al., 2016), or the MetaMorph software from Universal Imaging (Lalevée et al., 2006; Sénatore et al., 2010). The genetic backgrounds and methods are different, but the detected heart rate ranges are similar to our results (Fig. 14). This indicated that the selected lines can be used, and the heart rate detection method works.

**Table 6: Recent publications with heartbeat measurements of intact *Drosophila* third instar larvae.**

| Publication             | Genotype                            | Heart rate           | Preparation                 |
|-------------------------|-------------------------------------|----------------------|-----------------------------|
| (Gu and Singh, 1995)    | <i>Canton-S</i>                     | 2.58 Hz <sup>*</sup> | anterior and posterior pins |
| (Lalevée et al., 2006)  | <i>y,w;Canton-S</i>                 | 2.61 Hz              | mounted on tape             |
| (Sénatore et al., 2010) | <i>1029-Gal4 &gt; y,w; Canton-S</i> | 2.73 Hz              | mounted on tape             |
| (Men et al., 2016)      | <i>24B-GAL4/+</i>                   | 4,6 Hz <sup>*</sup>  | mounted on tape             |
| (Zhu et al., 2016)      | <i>Canton-S</i>                     | 3 Hz <sup>*</sup>    | The ant farm                |

The asterisks represent values obtained from figures

#### 6.4.2 Reduced expression of different heart ECM proteins significantly affects heart performance

Our research group is specialised in studying the process of heart formation and heart function in *Drosophila*. Therefore, the first approach to test the HIRO software was to investigate RNAi-mediated downregulation of important heart ECM proteins. Heart integrity is lost without a functional ECM, resulting in heart failure and heart collapse (Drechsler et al., 2013; Wilmes et al., 2018). The ECM is a network of proteins that spans the space between cells and organs. It consists of three component groups: structural components, secreted adaptor proteins and transmembrane receptors.

#### Myospheroid is essential for proper heart function

Integrins are heterodimeric transmembrane receptors. They enable intercellular signalling by bridging the ECM and the intracellular actin cytoskeleton (Campbell and Humphries, 2011). A previous study found that unregulated Integrin activation leads to contractile

dysfunction and arrhythmias in mice (Valencik et al., 2006). *Drosophila* has a small Integrin family with only two  $\beta$  and five  $\alpha$  subunits (Bloor and Brown, 1998; Brown et al., 2000). The *inflated* gene ( $\alpha$ PS2 Integrin) encodes one of these subunits and was used in this thesis. Only the *handC*-Gal4 > If<sup>v110770</sup> RNAi showed a significantly increased AI (Fig. 16 A). There is a high functional redundancy between the five  $\alpha$  subunits, which might have led to the observed results.

The *mysospheroid* ( $\beta$ PS Integrin) gene encodes one of the two  $\beta$ PS subunits. Only *handC*-Gal4 > Mys<sup>v103704</sup> RNAi showed an increased AI, while *handC*-Gal4 > Mys<sup>v29620</sup> RNAi line showed no significantly different cardiac function compared with the control line (Fig. 15 B, Fig. 16 B). By contrast, there was a strong effect when Mys<sup>v103704</sup> RNAi was crossed with the *prc*-Gal4 driver (Fig. 15 B', Fig. 16 B'). *prc*-Gal4 > Mys<sup>v29620</sup> RNAi showed a significantly reduced heart rate and an increased AI. *prc*-Gal4 > Mys<sup>v103704</sup> RNAi led to nonviable offspring, so it was not evaluated. This could have been caused by the strong effect of the RNAi-mediated downregulation of Myospheroid. Previous studies showed that the  $\beta$ PS subunit is the most abundant subunit, and its absence causes lethality at an earlier stage than the lack of any  $\alpha$  subunit does (Gotwals et al., 1994; Roote and Zusman, 1996). The Mys<sup>v103704</sup> RNAi line might be more effective than the Mys<sup>v29620</sup> RNAi line. One option would be to validate the relative gene expression by quantitative real-time PCR (RT-qPCR).

### **RNAi-mediated downregulation of Laminin A has an impact on heart rate**

The shape of tissue is primarily dictated by the basement membrane (BM), a particular type of ECM that forms a meshed network of protein polymers that surrounds organs, providing them with structural support and flexibility (Yurchenco, 2011). Laminins are essential for BM assembly because they can bind to cells, to themselves and to other BM components (Li et al., 2002; Pozzi et al., 2017). In *Drosophila*, four genes encode two Laminin  $\alpha$ , one Laminin  $\beta$  and one Laminin  $\gamma$  subunit, which form the only two Laminin heterotrimers in the fly (Henchcliffe et al., 1993). Only *prc*-Gal4 > LanA<sup>v330178</sup> RNAi had a significantly increased AI (Fig. 15 C'). Either *handC*-Gal4 or *prc*-Gal4 driven LanA<sup>v18873</sup> RNAi showed a significantly increased heart rate (Fig. 15 D, D'); in contrast, *prc*-Gal4 > LanA<sup>v330178</sup> RNAi showed a decreased heart rate compared to its KK control line (Fig. 15 C'). Recent studies showed that a lack of Laminin A prevents tube formation (Haag et al., 1999; Urbano et al., 2009), and null mutations in the *lanA* gene result in embryonic lethality with defects in the heart tube (Henchcliffe et al., 1993; Yarnitzky and Volk, 1995). RNAi-mediated downregulation of LanA might lead to a less massive effect on the heart, resulting in tachycardia. It is surprising that both RNAi lines driven with *prc*-Gal4 showed a contrary heartbeat influence. One option to confirm these results is to repeat future measurements with different RNAi lines (Kyoto: 207443, BDSC:28071).

LanB<sup>v42559</sup> RNAi crossed with both driver lines showed a significantly increased heart rate, while the other RNAi line did not have a significantly altered heart rate (Fig. 15 D, D'). RNAi downregulation showed no influence on the AI. The contrasting results from the LanA

RNAi approach indicate that the newly developed HIRO software is more suitable to detect stronger phenotypes and weaker in detecting only marginal effects. At first, the efficiency of the RNAi lines should be validated. Examining the RNAi efficiency due to RT-qPCR might be an option to prove this assumption. Furthermore, other studies have observed an abnormal accumulation of Collagen IV and Perlecan in LanB null mutant tissues (Urbano et al., 2009).

### **Lonely heart is essential for proper cardiac function**

The lack of Lonely heart (Loh) causes heart failure (Drechsler et al., 2013). The second publication described in this thesis demonstrated that the overexpression of Lonely heart in cardiac cells leads to a reduced heart rate and arrhythmia (Rotstein et al., 2018). In the RNAi approach described in this thesis, neither of the Lonely heart RNAi lines crossed with the *prc*-Gal4 driver showed significant alterations in cardiac performance (Fig. 15 E', Fig. 16 E'). In contrast, *handC*-Gal4 > Loh<sup>v31020</sup> RNAi and *handC*-Gal4 > Loh<sup>6232R-1</sup> RNAi showed a significantly altered heart rate and an increased AI. Surprisingly, *handC*-Gal4 > Loh<sup>v31020</sup> RNAi had an increased heart rate while *handC*-Gal4 > Loh<sup>6232R-1</sup> RNAi had a decreased heart rate (Fig. 15 E). To further analyse this contrast, the RNAi lines should be investigated in more detail, and to further verify the measured effect, follow-up experiments such as immunostaining should be conducted. These experiments would rule out any morphological heart defects. Additionally, measuring the ECM stiffness via atomic force microscopy would help to understand the cardiac phenotypes better (Kular et al., 2014).

### **Nidogen plays a role in maintaining a regular heart rhythm, and Trol influences the heart rate**

Another adaptor protein is Nidogen (Ndg). It plays a crucial role in BM assembly by providing a link between the Laminin and Col IV networks by integrating other ECM proteins, such as Perlecan (Fox et al., 1991; Reinhardt et al., 1993). Ndg has been found in the BMs surrounding most larval tissues, including the heart (Dai et al., 2018). In the RNAi approach used in this thesis, *prc*-Gal4 > Ndg<sup>v13280</sup> RNAi displayed an increased AI. The difference was not significant, yet the AI from *prc*-Gal4 > Ndg<sup>v13280</sup> RNAi was also increased compared to the control (Fig. 16 F'). A previous study showed that Nidogen double-null mice survive to birth but die within 24 h, possibly due to either pulmonary or cardiovascular failure (Bader et al., 2005).

The final adaptor protein investigated is Perlecan. This protein provides anchoring points for additional proteins and acts as a stabiliser (LeBleu et al., 2007; Bix and Iozzo, 2008). Perlecan is encoded by the *trol* (terribly reduced optic lobes) gene and is one component of the extracellular matrix (Friedrich et al., 2000; Voigt et al., 2002). Both of the Trol RNAi lines crossed with *prc*-Gal4 showed a significantly altered heart rate (Fig. 15 H). Similar to the Loh RNAi approach, one line showed a reduced heart rate, and one line showed an

increased heart rate. All in all, these data indicate that HIRO is considered to be used as a good indicator for alterations in heart parameters on a high throughput level. Nevertheless, HIRO should be applied as an indicator for follow up experiments.

### **RNAi-mediated downregulation of Collagen IV may not affect the heart parameters**

Collagen IV forms a mesh-like network stabilising the structure of BMs. Two genes encode for type IV collagens (*col4a1* and *viking*) (Le Parco et al., 1986; Rodriguez et al., 1996). Viking accumulates in all regions of ageing adult hearts (Vaughan et al., 2018). In this thesis, only *prc-Gal4 > Vkg<sup>v106812</sup>* RNAi showed a significantly increased heart rate (Fig. 15 I). A previous study found that Viking knockdown increased the contractility of adult hearts during ageing (Sessions et al., 2017). The fact that only one Viking RNAi line showed a significant effect leads to the conclusion that either Viking has no effect on the heart parameters of *Drosophila* or that the RNAi approach is not sensitive enough to detect small alterations in the heart parameters. Another option is that the RNAi did not work properly or resulted in a marginal effect. RT-qPCR could verify this assumption.



## 6.5 Summary

The following table summarises the results from the RNAi high throughput screening (Table 7).

**Table 7: Summary of the high throughput RNAi screen.** The arrows represent increased or decreased heart parameter. The hyphen represents a not significant result. Significance levels are indicated by asterisks (paired sample Student's t-test, \*  $p < 0.05$ ; \*\*  $p < 0.005$ ; \*\*\*  $p < 0.0005$ ). HR, heart rate; AI, arrhythmicity index; n.v. not viable; n.e. not evaluable

| Gen         | Line ID | <i>handC</i> -Gal4 |      | <i>prc</i> -Gal4 |      |
|-------------|---------|--------------------|------|------------------|------|
|             |         | HR                 | AI   | HR               | AI   |
| <i>if</i>   | v44885  | -                  | -    | -                | -    |
|             | v100770 | -                  | ↑ *  | -                | -    |
| <i>mys</i>  | v29620  | -                  | -    | ↓ **             | ↑ *  |
|             | v103704 | -                  | ↑ *  | n.v.             | n.v. |
| <i>lanA</i> | v18873  | ↑ ***              | -    | ↑ *              | -    |
|             | v330178 | -                  | -    | ↓ ***            | ↑ *  |
| <i>lanB</i> | v42559  | ↑ *                | -    | ↑ *              | -    |
|             | v104013 | -                  | -    | -                | -    |
| <i>prc</i>  | v41320  | -                  | -    | n.e.             | n.e. |
|             | v100357 | -                  | -    | n.e.             | n.e. |
| <i>loh</i>  | 6232R-1 | ↓ ***              | ↑ ** | -                | -    |
|             | v31020  | ↑ *                | ↑ ** | -                | -    |
| <i>ndg</i>  | v13280  | -                  | -    | ↓ ***            | -    |
|             | v109625 | -                  | -    | -                | ↑ ** |
| <i>vkg</i>  | v16986  | -                  | -    | -                | -    |
|             | v106812 | -                  | -    | ↑ ***            | -    |
| <i>trol</i> | v24549  | -                  | -    | ↓ *              | -    |
|             | v110494 | -                  | ↑ ** | ↑ **             | ↑ *  |

### HIRO can calculate systolic and diastolic intervals

HIRO can detect the systolic and diastolic interval (Fig. 13); however, the software might incorrectly detect the heartbeat signal within noisy data in some cases. The user can discard the video or delete that specific peak. The user should also keep in mind that systolic and diastolic intervals are calculated from one heartbeat to the next (Fig. 11). Hence, the missing point will not affect the heart rate or AI, but it will affect the systolic and diastolic intervals. Future HIRO versions should overcome this problem.

### HIRO can be used for high-throughput heart parameters screening

The RNAi screen conducted in this thesis revealed Myospheroid and Laminin A as promising candidates for further investigation (Fig. 15 B'; Fig. 16 B', C'). The adaptor proteins Lonely heart and Perlecan showed contrasting results (Fig.15 E, H'). One option to reconcile these results is to validate the relative gene expression by RT-qPCR. RNAi is a potent technique, but its potential off-target effects might influence the heart function. Additional

RNAi lines ( BDSC: 14237, BDSC 14730) should be tested to minimise the off-target risk. HIRO can be used as a high-throughput screening software option that has a simple setup. This novel software makes it possible to efficiently identify promising candidates that can be confirmed and analysed in further experiments.

## 6.6 Outlook

### **Automatic detection of usable videos**

Over time, computers have become increasingly efficient. Machine learning provides new approaches in several disciplines, including medicine and biology. One way to increase the efficiency of HIRO is to apply autodetection of blurry videos. A neural network may help to detect unusable videos from several recorded videos. A recent study investigated the use of neural networks in carrying out data selection (Wang et al., 2019).

### **Real-time quantitative PCR**

RNAi is a gene silencing method which is initiated by short double-stranded RNA (siRNA) molecules. siRNAs vary in efficiency, and the absence of competent siRNA results in an ineffective knockdown. Real-time quantitative PCR (RT-qPCR) is one method to quantitatively measure RNAi efficiency (Milstein et al., 2013). After total RNA extraction from tissues, cDNA synthesis is performed. A common method is to use the SYBR green, which is a dye that emits fluorescence when it binds to double-stranded DNA. The detection of the fluorescence signal allows determining the amount of DNA with each amplification cycle (Milstein et al., 2013).

### **Hardware for the real-time detection of heart rhythm under a microscope**

Raspberry Pi is a single-board computer for low-cost embedded systems and can be used for signal processing, image processing and robotic applications. The computer provides an interface for connecting a camera and other external devices, such as an OLED display for visualising data (Fig. 17). Another option is to connect a USB camera to the system. Raspberry Pi's operation system, called Raspbian, can run programs that are written in either Java or Python. This setup allows real-time measurement at the microscope and would further accelerate the high throughput screening.

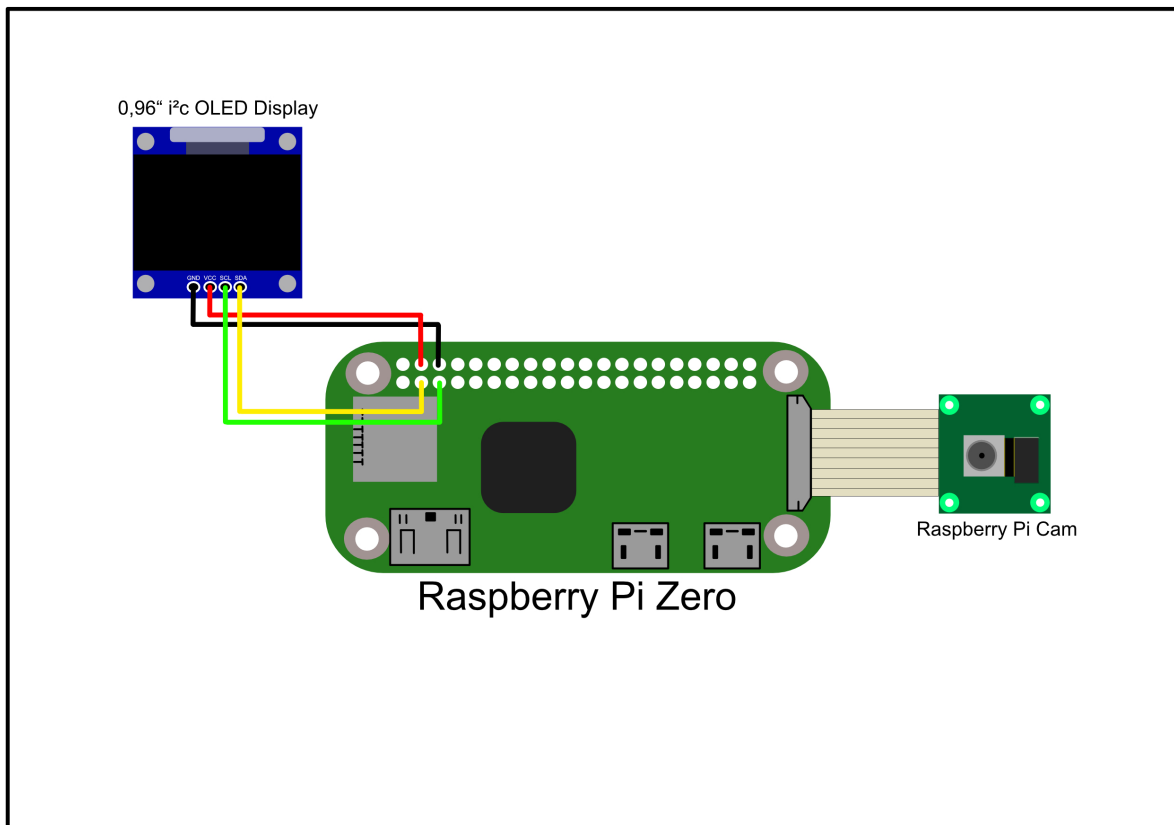


**Figure 17: A possible hardware setup for real-time heartbeat measurements.** The camera should be mounted on the ocular, while the OLED display shows the values.

## References

- Abraham, D. M. and Wolf, M. J. (2013). Disruption of Sarcoendoplasmic Reticulum Calcium ATPase Function in *Drosophila* Leads to Cardiac Dysfunction. *PLOS ONE*, 8(10):1–9.
- Alex, A., Li, A., Tanzi, R. E., and Zhou, C. (2015). Optogenetics: Optogenetic pacing in *Drosophila melanogaster*. *Science Advances*, 1(9).
- Artero, R., Selma-Soriano, E., Chakraborty, M., Llamusi, B., and Artero, R. (2018). Ex-vivo characterization of *Drosophila* heart functional parameters. *Protocol Exchange, Preprint*, viewed 13 July 2021, pages 1–21.
- Aumann, S., Donner, S., and Fischer, J. (2019). *High Resolution Imaging in Microscopy and Ophthalmology*. Springer, Cham.
- Bader, B. L., Smyth, N., Nedbal, S., Miosge, N., Baranowsky, A., Mokkaapati, S., Murshed, M., and Nischt, R. (2005). Compound Genetic Ablation of Nidogen 1 and 2 Causes Basement Membrane Defects and Perinatal Lethality in Mice. *Molecular and Cellular Biology*, 25(15):6846–6856.
- Bataillé, L., Colombié, N., Pelletier, A., Paululat, A., Lebreton, G., Carrier, Y., Frendo, J. L., and Vincent, A. (2020). Alary muscles and thoracic alary-related muscles are atypical striated muscles involved in maintaining the position of internal organs. *Development*, 147(8).
- Beck, K., Dixon, T. W., Engel, J., and Parry, D. A. (1993). Ionic Interactions in the Coiled-coil Domain of Laminin Determine the Specificity of Chain Assembly. *Journal of Molecular Biology*, 231(2):311–323.
- Berh, D., Scherzinger, A., Otto, N., Jiang, X., Klämbt, C., and Risse, B. (2018). Automatic non-invasive heartbeat quantification of *Drosophila* pupae. *Computers in Biology and Medicine*, 93(1):189–199.
- Bix, G. and Iozzo, R. (2008). Novel Interactions of Perlecan: Unraveling Perlecan’s Role in Angiogenesis. *Microscopy Research and Technique*, 71(5):339–348.
- Bloor, J. W. and Brown, N. H. (1998). Genetic analysis of the *Drosophila*  $\alpha$ (PS2) integrin subunit reveals discrete adhesive, morphogenetic and sarcomeric functions. *Genetics*, 148(3):1127–1142.
- Bodmer, R. (1993). The gene tinman is required for specification of the heart and visceral muscles in *Drosophila*. *Development*, 118(3):719–729.
- Brown, N. H., Gregory, S. L., and Martin-Bermudo, M. D. (2000). Integrins as mediators of morphogenesis in *Drosophila*. *Developmental Biology*, 223(1):1–16.

- Bunney, P. E., Zink, A. N., Holm, A. A., Billington, C. J., and Kotz, C. M. (2017). Orexin activation counteracts decreases in nonexercise activity thermogenesis (NEAT) caused by high-fat diet. *Physiology and Behavior*, 176(1):139–148.
- Burch, M. (1971). The electrocardiogram of the *Drosophila*. *American Heart Journal*, 82(4):574–575.
- Calpena, E., Del Amo, V. L., Chakraborty, M., Llamusi, B., Artero, R., Espinós, C., and Galindo, M. I. (2018). The *Drosophila* junctophilin gene is functionally equivalent to its four mammalian counterparts and is a modifier of a Huntingtin poly-Q expansion and the Notch pathway. *Disease Models and Mechanisms*, 11(1).
- Cammarato, A., Ocorr, S., and Ocorr, K. (2015). Enhanced assessment of contractile dynamics in *Drosophila* hearts. *BioTechniques*, 58(2):77–80.
- Campbell, I. D. and Humphries, M. J. (2011). Integrin structure, activation, and interactions. *Cold Spring Harbor Perspectives in Biology*, 3(3):1–14.
- Cannon, L., Zambon, A. C., Cammarato, A., Zhang, Z., Vogler, G., Munoz, M., Taylor, E., Cartry, J., Bernstein, S. I., Melov, S., and Bodmer, R. (2017). Expression patterns of cardiac aging in *Drosophila*. *Aging Cell*, 16(1):82–92.
- Canny, J. (1986). A Computational Approach to Edge Detection. *Institute of Electrical and Electronics Engineers*, 8(6):641–644.
- Chakraborty, M., Sellier, C., Ney, M., Pascal, V., Charlet-Berguerand, N., Artero, R., and Llamusi, B. (2018). Daunorubicin reduces MBNL1 sequestration caused by CUG-repeat expansion and rescues cardiac dysfunctions in a *Drosophila* model of myotonic dystrophy. *Disease Models and Mechanisms*, 11(4).
- Chang, K., Kang, P., Liu, Y., Huang, K., Miao, T., Sagona, A. P., Nezis, I. P., Bodmer, R., Ocorr, K., and Bai, H. (2020). TGFB-INHB/activin signaling regulates age-dependent autophagy and cardiac health through inhibition of MTORC2. *Autophagy*, 16(10):1807–1822.
- Chartier, A., Zaffran, S., Astier, M., Sémériva, M., and Gratecos, D. (2002). Pericardin, a *Drosophila* type IV collagen-like protein is involved in the morphogenesis and maintenance of the heart epithelium during dorsal ectoderm closure. *Development*, 129(13):3241–3253.
- Chen, W. and Hillyer, J. F. (2013). FlyNap (Triethylamine) Increases the Heart Rate of Mosquitoes and Eliminates the Cardioacceleratory Effect of the Neuropeptide CCAP. *PLoS ONE*, 8(7):1–12.
- Choma, M. A., Izatt, S. D., Wessells, R. J., Bodmer, R., and Izatt, J. A. (2006). In vivo imaging of the adult *Drosophila melanogaster* heart with real-time optical coherence tomography. *Circulation*, 114(2):35–36.

- Choma, M. A., Suter, M. J., Vakoc, B. J., Bouma, B. E., and Tearney, G. J. (2010). Heart wall velocimetry and exogenous contrast-based cardiac flow imaging in *Drosophila melanogaster* using Doppler optical coherence tomography. *Journal of Biomedical Optics*, 15(5):056020.
- Choma, M. A., Suter, M. J., Vakoc, B. J., Bouma, B. E., and Tearney, G. J. (2011). Physiological homology between *Drosophila melanogaster* and vertebrate cardiovascular systems. *Disease Models and Mechanisms*, 4(3):411–420.
- Dai, J., Estrada, B., Jacobs, S., Sánchez-Sánchez, B. J., Tang, J., Ma, M., Magadán-Corpas, P., Pastor-Pareja, J. C., and Martín-Bermudo, M. D. (2018). Dissection of Nidogen function in *Drosophila* reveals tissue-specific mechanisms of basement membrane assembly. *Plos Genetics*, 14(9):1–31.
- Dietzl, G., Chen, D., Schnorrer, F., Su, K. C., Barinova, Y., Fellner, M., Gasser, B., Kinsey, K., Oppel, S., Scheiblaue, S., Couto, A., Marra, V., Keleman, K., and Dickson, B. J. (2007). A genome-wide transgenic RNAi library for conditional gene inactivation in *Drosophila*. *Nature*, 448(7150):151–156.
- Dorn, G. W., Clark, C. F., Eschenbacher, W. H., Kang, M. Y., Engelhard, J. T., Warner, S. J., Matkovich, S. J., and Jowdy, C. C. (2011). MARF and Opa1 control mitochondrial and cardiac function in *Drosophila*. *Circulation Research*, 108(1):12–17.
- Drechsler, M., Schmidt, A. C., Meyer, H., and Paululat, A. (2013). The Conserved ADAMTS-like Protein Lonely heart Mediates Matrix Formation and Cardiac Tissue Integrity. *PLoS Genetics*, 9(7):16–18.
- Fox, J., Mayer, U., Nischt, R., Aumailley, M., Reinhardt, D., Wiedemann, H., Mann, K., Timpl, R., Krieg, T., and Engel, J. (1991). Recombinant nidogen consists of three globular domains and mediates binding of laminin to collagen type IV. *The EMBO Journal*, 10(11):3137–3146.
- Friedrich, M. V., Göhring, W., Mörgelin, M., Brancaccio, A., David, G., and Timpl, R. (1999). Structural basis of glycosaminoglycan modification and of heterotypic interactions of perlecan domain V. *Journal of Molecular Biology*, 294(1):259–270.
- Friedrich, M. V. K., Schneider, M., Timpl, R., and Baumgartner, S. (2000). Perlecan domain V of *Drosophila melanogaster*. *European Journal of Biochemistry*, 267(11):3149–3159.
- Gotwals, P. J., Paine-Saunders, S. E., Stark, K. A., and Hynes, R. O. (1994). *Drosophila* integrins and their ligands. *Current Opinion in Cell Biology*, 6(5):734–739.
- Gu, G. G. and Singh, S. (1995). Pharmacological analysis of heartbeat in *Drosophila*. *Journal of Neurobiology*, 28(3):269–280.

- Guo, S.-Y., Liao, F.-T., Su, M.-T., Chang, C.-Y., Su, H.-R., Huang, J.-C., and Kuo, W.-C. (2013). Semiautomatic and rapid quantification of heartbeat parameters in *Drosophila* using optical coherence tomography imaging. *Journal of Biomedical Optics*, 18(2):026004.
- Haag, T. A., Haag, N. P., Lekven, A. C., and Hartenstein, V. (1999). The Role of Cell Adhesion Molecules in *Drosophila* Heart Morphogenesis: Faint Sausage, Shotgun/DECadherin, and Laminin A Are Required for Discrete Stages in Heart Development. *Developmental Biology*, 69:1–14.
- Hallier, B., Schiemann, R., Cordes, E., Vitos-Faleato, J., Walter, S., Heinisch, J. J., Malmendal, A., Paululat, A., and Meyer, H. (2016). *Drosophila* neprilysins control insulin signaling and food intake via cleavage of regulatory peptides. *eLife*, 5:1–22.
- Hansun, S. (2013). A new approach of moving average method in time series analysis. *Institute of Electrical and Electronics Engineers - Explore*.
- Hardy, C. M., Birse, R. T., Wolf, M. J., Yu, L., Bodmer, R., and Gibbs, A. G. (2015). Obesity-associated cardiac dysfunction in starvation-selected *Drosophila melanogaster*. *American Journal of Physiology - Regulatory Integrative and Comparative Physiology*, 309(6):R658–R667.
- Henchcliffe, C., Garcia-Alonso, L., Tang, J., and Goodman, C. S. (1993). Genetic analysis of laminin A reveals diverse functions during morphogenesis in *Drosophila*. *Development*, 118(2):325–337.
- Hewes, R. S. and Taghert, P. H. (2001). Neuropeptides and neuropeptide receptors in the *Drosophila melanogaster* genome. *Genome Research*, 11(6):1126–1142.
- Hopf, M., Göhring, W., Mann, K., and Timpl, R. (2001). Mapping of binding sites for nidogens, fibulin-2, fibronectin and heparin to different IG modules of perlecan. *Journal of Molecular Biology*, 311(3):529–541.
- Hynes, R. O. (1987). Integrins: a family of cell adhesion receptors. *Cell*, 48:549–554.
- Ivy, J. R., Drechsler, M., Catterson, J. H., Bodmer, R., Ocorr, K., Paululat, A., and Hartley, P. S. (2015). Klf15 is critical for the development and differentiation of *Drosophila* nephrocytes. *PLoS ONE*, 10(8):1–17.
- Kaptoge, S., Pennells, L., De Bacquer, D., Cooney, M. T., Kavousi, M., Stevens, G., Riley, L. M., Savin, S., Khan, T., Altay, S., Amouyel, P., Assmann, G., Bell, S., Ben-Shlomo, Y., Berkman, L., Beulens, J. W., Björkelund, C., Blaha, M., Blazer, D. G., Bolton, T., Bonita Beaglehole, R., Brenner, H., Brunner, E. J., Casiglia, E., Chamnan, P., Choi, Y. H., Chowdry, R., Coady, S., Crespo, C. J., Cushman, M., Dagenais, G. R., D’Agostino, R. B., Daimon, M., Davidson, K. W., Engström, G., Ford, I., Gallacher, J., Gansevoort, R. T., Gaziano,



- T. A., Giampaoli, S., Grandits, G., Grimsgaard, S., Grobbee, D. E., Gudnason, V., Guo, Q., Tolonen, H., Humphries, S., Iso, H., Jukema, J. W., Kauhanen, J., Kengne, A. P., Khalili, D., Koenig, W., Kromhout, D., Krumholz, H., Lam, T. H., Laughlin, G., Marín Ibañez, A., Meade, T. W., Moons, K. G., Nietert, P. J., Ninomiya, T., Nordestgaard, B. G., O'Donnell, C., Palmieri, L., Patel, A., Perel, P., Price, J. F., Providencia, R., Ridker, P. M., Rodriguez, B., Rosengren, A., Rousset, R., Sakurai, M., Salomaa, V., Sato, S., Schöttker, B., Shara, N., Shaw, J. E., Shin, H. C., Simons, L. A., Sofianopoulou, E., Sundström, J., Völzke, H., Wallace, R. B., Wareham, N. J., Willeit, P., Wood, D., Wood, A., Zhao, D., Woodward, M., Danaei, G., Roth, G., Mendis, S., Onuma, O., Varghese, C., Ezzati, M., Graham, I., Jackson, R., Danesh, J., and Di Angelantonio, E. (2019). World Health Organization cardiovascular disease risk charts: revised models to estimate risk in 21 global regions. *The Lancet Global Health*, 7(10):e1332–e1345.
- Kronert, W. A., Bell, K. M., Viswanathan, M. C., Melkani, G. C., Trujillo, A. S., Huang, A., Melkani, A., Cammarato, A., Swank, D. M., and Bernstein, S. I. (2018). Prolonged cross-bridge binding triggers muscle dysfunction in a *Drosophila* model of myosin-based hypertrophic cardiomyopathy. *eLife*, 7:1–27.
- Kular, J. K., Basu, S., and Sharma, R. I. (2014). The extracellular matrix: Structure, composition, age-related differences, tools for analysis and applications for tissue engineering. *Journal of Tissue Engineering*, 5(1).
- Lalévée, N., Monier, B., Sénatore, S., Perrin, L., and Sémériva, M. (2006). Control of Cardiac Rhythm by ORK1, a *Drosophila* Two-Pore Domain Potassium Channel. *Current Biology*, 16(15):1502–1508.
- Lam, A., Karekar, P., Shah, K., Hariharan, G., Fleyshman, M., Kaur, H., Singh, H., and Gururaja Rao, S. (2018). *Drosophila* Voltage-Gated Calcium Channel  $\alpha 1$ -Subunits Regulate Cardiac Function in the Aging Heart. *Scientific Reports*, 8(1):1–13.
- Lammers, K., Abeln, B., Hüsken, M., Lehmacher, C., Psathaki, O. E., Alcorta, E., Meyer, H., and Paululat, A. (2017). Formation and function of intracardiac valve cells in the *Drosophila* heart. *Journal of Experimental Biology*, 220(10):1852–1863.
- Le Parco, Y., Knibiehler, B., Cecchini, J. P., and Mirre, C. (1986). Stage and tissue-specific expression of a collagen gene during *Drosophila melanogaster* development. *Experimental Cell Research*, 163(2):405–412.
- LeBleu, V. S., MacDonald, B., and Kalluri, R. (2007). Structure and function of basement membranes. *Experimental Biology and Medicine*, 232(9):1121–1129.
- Lee, C. Y., Wang, H. J., Jhang, J. D., and Cho, I. C. (2019). Automated *Drosophila* heartbeat counting based on image segmentation technique on optical coherence tomography. *Scientific Reports*, 9(1):1–9.

- Lehmacher, C., Abeln, B., and Paululat, A. (2012). The ultrastructure of *Drosophila* heart cells. *Arthropod Structure and Development*, 41(5):459–474.
- Li, A., Zhou, C., Moore, J., Zhang, P., Tsai, T.-H., Lee, H.-C., Romano, D., McKee, M., Schoenfeld, D., Serra, M., Raygor, M., Cantiello, H., Fujimoto, J., and Tanzi, R. (2015). Changes in the Expression of the Alzheimer's Disease- Associated Presenilin Gene in *Drosophila* Heart Leads to Cardiac Dysfunction. *Journal of Investigative Dermatology*, 135(2):612–615.
- Li, S., Harrison, D., Carbonetto, S., Fässler, R., Smyth, N., Edgar, D., and Yurchenco, P. D. (2002). Matrix assembly, regulation, and survival functions of laminin and its receptors in embryonic stem cell differentiation. *Journal of Cell Biology*, 157(7):1279–1290.
- Liao, F.-T., Chang, C.-Y., Su, M.-T., and Kuo, W.-C. (2013). Necessity of angiotensin-converting enzyme-related gene for cardiac functions and longevity of *Drosophila melanogaster* assessed by optical coherence tomography. *Journal of Biomedical Optics*, 19(1):011014.
- Lim, H., Wang, W., Chen, J., Ocorr, K., and Bodmer, R. (2014). ROS Regulate Cardiac Function via a Distinct Paracrine Mechanism. *Cell Reports*, 7(1):35–44.
- Linford, N. J., Bilgir, C., Ro, J., and Pletcher, S. D. (2013). Measurement of lifespan in *Drosophila melanogaster*. *Journal of Visualized Experiments*, (71):1–9.
- Lo, P. C. and Frasch, M. (2001). A role for the COUP-TF-related gene seven-up in the diversification of cardioblast identities in the dorsal vessel of *Drosophila*. *Mechanisms of Development*, 104(1-2):49–60.
- Lockwood, W. K. and Bodmer, R. (2002). The patterns of wingless, decapentaplegic, and tinman position the *Drosophila* heart. *Mechanisms of Development*, 114(1-2):13–26.
- Mann, K., Deutzmann, R., Ausmailley, M., Timpl, R., Raimondi, L., Yamada, Y., Pan, T. C., Conway, D., and Chu, M. L. (1989). Amino acid sequence of mouse nidogen, a multidomain basement membrane protein with binding activity for laminin, collagen IV and cells. *The EMBO Journal*, 8(1):65–72.
- Manso, A. M., Elsherif, L., Kang, S. M., and Ross, R. S. (2006). Integrins, membrane-type matrix metalloproteinases and ADAMs: Potential implications for cardiac remodeling. *Cardiovascular Research*, 69(3):574–584.
- Martínez-Morentin, L., Martínez, L., Piloto, S., Yang, H., Schon, E. A., Garesse, R., Bodmer, R., Ocorr, K., Cervera, M., and Arredondo, J. J. (2015). Cardiac deficiency of single cytochrome oxidase assembly factor scox induces p53-dependent apoptosis in a *Drosophila* cardiomyopathy model. *Human Molecular Genetics*, 24(13):3608–3622.

- Men, J., Jerwick, J., Wu, P., Chen, M., Alex, A., Ma, Y., Tanzi, R. E., Li, A., and Zhou, C. (2016). *Drosophila* preparation and longitudinal imaging of heart function in vivo using optical coherence microscopy (OCM). *Journal of Visualized Experiments*, (118):1–11.
- Meyer, H., Panz, M., Zmojdzian, M., Jagla, K., and Paululat, A. (2009). Neprilysin 4, a novel endopeptidase from *Drosophila melanogaster*, displays distinct substrate specificities and exceptional solubility states. *Journal of Experimental Biology*, 212(22):3673–3683.
- Millburn, G. H., Crosby, M. A., Gramates, L. S., Tweedie, S., Gelbart, W., Perrimon, N., Extavour, C., Broll, K., Dos Santos, G., Emmert, D., Falls, K., Matthews, B., Gelbart, S. R., Schroeder, A., Tabone, C., Zhou, P., Zytkevich, M., Brown, N., Antonazzo, G., Attrill, H., Costa, M., Marygold, S., Ponting, L., Rey, A., Staudt, N., Stefancsik, R., Urbano, J. M., Kaufman, T., Goodman, J., Grumblin, G., Strelets, V., Thurmond, J., Cripps, R., Werner-Washburne, M., and Baker, P. (2016). Fly Base portals to human disease research using *Drosophila* Models. *Disease Models and Mechanisms*, 9(3):245–252.
- Miller, T. A. (1997). Control of circulation in insects. *General Pharmacology*, 29(1):23–38.
- Milstein, S., Nguyen, M., Meyers, R., and De Fougères, A. (2013). Measuring RNAi knock-down using qPCR. *Methods in Enzymology*, 533:57–77.
- Miner, J. H. and Yurchenco, P. D. (2004). Laminin Functions in Tissue Morphogenesis. *Annual Review of Cell and Developmental Biology*, 20(1):255–284.
- Molina, M. R. and Cripps, R. M. (2001). Ostia, the inflow tracts of the *Drosophila* heart, develop from a genetically distinct subset of cardiac cells. *Mechanisms of Development*, 109:51–59.
- Monck, H., Toppe, D., Michael, E., Sigrist, S., Richter, V., Hilpert, D., Raccuglia, D., Efetova, M., and Schwärzel, M. (2017). A new method to characterize function of the *Drosophila* heart by means of optical flow. *Journal of Experimental Biology*, 220(24):4644–4653.
- Nässel, D. R. and Zandawala, M. (2019). Recent advances in neuropeptide signaling in *Drosophila*, from genes to physiology and behavior. *Progress in Neurobiology*, 179:101607.
- Natzle, J. E., Monson, J. M., and McCarthy, B. J. (1982). Cytogenetic location and expression of collagen-like genes in *Drosophila*. *Nature*, 296(5855):368–371.
- Ocorr, K., Fink, M., Cammarato, A., Bernstein, S. I., and Bodmer, R. (2009). Semi-automated optical Heartbeat Analysis of small hearts. *Journal of Visualized Experiments*, (31):3–6.
- Otsu, N. (1979). A Threshold Selection Method from Gray-Level Histograms. *IEEE Transactions on Systems, Man and Cybernetics*, 20(1):62–66.

- Paternostro, G., Vignola, C., Bartsch, D.-u., Omens, J. H., Mcculloch, A. D., and Reed, J. C. (2001). Age-associated cardiac dysfunction in *Drosophila melanogaster*. *Circulation Research*, 88(10):1053–1058.
- Piazza, N. and Wessells, R. J. (2011). *Drosophila* models of cardiac disease. *Progress in Molecular Biology and Translational Science*, 100:155–210.
- Pozzi, A., Yurchenco, P. D., and Iozzo, R. V. (2017). The nature and biology of basement membranes. *Matrix Biology*, 57-58:1–11.
- Reinhardt, D., Mann, K., Nischt, R., Fox, J. W., Chu, M. L., Krieg, T., and Timpl, R. (1993). Mapping of nidogen binding sites for collagen type IV, heparan sulfate proteoglycan, and zinc. *Journal of Biological Chemistry*, 268(15):10881–10887.
- Rodriguez, A., Zhou, Z., Tang, M. L., Meller, S., Chen, J., Bellen, H., and Kimbrell, D. A. (1996). Identification of immune system and response genes, and novel mutations causing melanotic tumor formation in *Drosophila melanogaster*. *Genetics*, 143(2):929–940.
- Roote, C. E. and Zusman, S. (1996). Alternatively spliced forms of the *Drosophila*  $\alpha$ ps 2 subunit of integrin are sufficient for viability and can replace the function of the  $\alpha$ ps1 subunit of integrin in the retina. *Development*, 122(6):1985–1994.
- Rotstein, B. and Paululat, A. (2016). On the Morphology of the *Drosophila* Heart. *Journal of Cardiovascular Development and Disease*, 3(2):15.
- Rotstein, B., Post, Y., Reinhardt, M., Lammers, K., Buhr, A., Heinisch, J. J., Meyer, H., and Paululat, A. (2018). Distinct domains in the matricellular protein Lonely heart are crucial for cardiac extracellular matrix formation and heart function in *Drosophila*. *Journal of Biological Chemistry*, 293(20):7864–7879.
- Rugendorff, A., Younossi-Hartenstein, A., and Hartenstein, V. (1994). Embryonic origin and differentiation of the *Drosophila* heart. *Roux's Archives of Developmental Biology*, 203(5):266–280.
- Ruoslahti, E. P. M. (1987). New Perspectives in Cell Adhesion. *Science*, 238(4826):1286.
- Sellin, J., Albrecht, S., Kölsch, V., and Paululat, A. (2006). Dynamics of heart differentiation, visualized utilizing heart enhancer elements of the *Drosophila melanogaster* bHLH transcription factor Hand. *Gene Expression Patterns*, 6(4):360–375.
- Sénatore, S., Reddy, V. R., Sémériva, M., Perrin, L., and Lalevée, N. (2010). Response to mechanical stress is mediated by the TRPA channel painless in the *Drosophila* heart. *PLoS Genetics*, 7(2).

- Sessions, A. O., Kaushik, G., Parker, S., Raedschelders, K., Bodmer, R., Van Eyk, J. E., and Engler, A. J. (2017). Extracellular Matrix Downregulation in the *Drosophila* Heart Preserves Contractile Function and Improves Lifespan. *Matrix Biology*, 176(62):15–27.
- Sláma, K. (2012). A new look at the comparative physiology of insect and human hearts. *Journal of Insect Physiology*, 58(8):1072–1081.
- Talts, J. F., Andac, Z., Göhring, W., Brancaccio, A., and Timpl, R. (1999). Binding of the G domains of laminin  $\alpha 1$  and  $\alpha 2$  chains and perlecan to heparin, sulfatides,  $\alpha$ -dystroglycan and several extracellular matrix proteins. *The EMBO Journal*, 18(4):863–870.
- Tao, Y. and Schulz, R. A. (2007). Heart development in *Drosophila*. *Seminars in Cell and Developmental Biology*, 18(1):3–15.
- Timpl, R. and Rohde, H. (1979). Laminin-A Glycoprotein from Basement Membranes. *Journal of Biological Chemistry*, 254(19):9933–9937.
- Töpfer, U. and Holz, A. (2020). Analysis of extracellular matrix composition in the visceral muscles of Nidogen mutant larvae in *Drosophila*. *microPublication biology*, 2020.
- Tsai, M. T., Chang, F. Y., Lee, C. K., Chi, T. T., Yang, K. M., Lin, L. Y., Wu, J. T., and Yang, C. C. (2011). Observations of cardiac beating behaviors of wild-type and mutant *Drosophilae* with optical coherence tomography. *Journal of Biophotonics*, 4(9):610–618.
- Urbano, J. M., Torgler, C. N., Molnar, C., Tepass, U., López-Varea, A., Brown, N. H., de Celis, J. F., and Martín-Bermudo, M. D. (2009). *Drosophila* laminins act as key regulators of basement membrane assembly and morphogenesis. *Development*, 136(24):4165–4176.
- Valencik, M. L., Zhang, D., Punske, B., Hu, P., McDonald, J. A., and Litwin, S. E. (2006). Integrin activation in the heart: A link between electrical and contractile dysfunction? *Circulation Research*, 99(12):1403–1410.
- Vaughan, L., Marley, R., Miellet, S., and Hartley, P. S. (2018). The impact of SPARC on age-related cardiac dysfunction and fibrosis in *Drosophila*. *Experimental Gerontology*, 109:59–66.
- Vissers, J. H., Manning, S. A., Kulkarni, A., and Harvey, K. F. (2016). A *Drosophila* RNAi library modulates Hippo pathway-dependent tissue growth. *Nature Communications*, 7:1–6.
- Voigt, A., Pflanz, R., Schäfer, U., and Jäckle, H. (2002). Perlecan participates in proliferation activation of quiescent *Drosophila* neuroblasts. *Developmental Dynamics*, 224(4):403–412.
- Wang, X., Zhang, S., Liang, X., Zhou, H., Zheng, J., and Sun, M. (2019). Accurate and Fast Blur Detection Using a Pyramid M-Shaped Deep Neural Network. *IEEE Access*, 7:86611–86624.

- White, L. A., Ringo, J. M., and Dowse, H. B. (1989). Effects of deuterium oxide and temperature on heart rate in *Drosophila melanogaster*. *Journal of Comparative Physiology*, 287(3):343–366.
- Wilmes, A. C., Klinke, N., Rotstein, B., Meyer, H., and Paululat, A. (2018). Biosynthesis and assembly of the Collagen IV-like protein Pericardin in *Drosophila melanogaster*. *Biology Open*, 7(4):1–14.
- Wolf, M. J., Amrein, H., Izatt, J. A., Choma, M. A., Reedy, M. C., and Rockman, H. A. (2006). *Drosophila* as a model for the identification of genes causing adult human heart disease. *Proceedings of the National Academy of Sciences of the United States of America*, 103(5):1394–1399.
- Wolfstetter, G., Dahlitz, I., Pfeifer, K., Töpfer, U., Alt, J. A., Pfeifer, D. C., Lakes-Harlan, R., Baumgartner, S., Palmer, R. H., and Holz, A. (2019). Characterization of *Drosophila* Nidogen/entactin reveals roles in basement membrane stability, barrier function and nervous system patterning. *Development*, 146(2):1–12.
- Yarnitzky, T. and Volk, T. (1995). Laminin is required for heart, somatic muscles, and gut development in the *Drosophila* embryo. 169(2):609–618.
- Yu, L., Lee, T., Lin, N., and Wolf, M. J. (2010). Affecting Rhomboid-3 function causes a dilated heart in adult *Drosophila*. *PLoS Genetics*, 6(5):4.
- Yurchenco, P. D. (2011). Basement membranes: Cell scaffoldings and signaling platforms. *Cold Spring Harbor Perspectives in Biology*, 3(2):1–27.
- Zaffran, S. and Frasch, M. (2002). Early signals in cardiac development. *Circulation Research*, 91(6):457–469.
- Zhou, C., Alex, A., Rasakanthan, J., and Ma, Y. (2013). Space-division multiplexing optical coherence tomography. *Optics Express*, 21(16):19219–19227.
- Zhu, Y. C., Yocom, E., Sifers, J., Uradu, H., and Cooper, R. L. (2016). Modulatory effects on *Drosophila* larva hearts: room temperature, acute and chronic cold stress. *Journal of Comparative Physiology*, 186(7):829–841.

## 7 Appendix

### 7.1 Abbreviations

| <b>Abbreviation</b> | <b>Complete meaning</b>  |
|---------------------|--|
| AI                  | Arrhythmicity index  |
| ADAMTS              | A Distintegrin and Metalloprotease with Thrombospondin Type 1 Motifs |
| BM                  | Basement membrane  |
| BPM                 | Beats per minute   |
| Cg25c               | Collagen at 25C  |
| Dpp                 | Decapentaplegic  |
| ECM                 | Extracellular matrix   |
| GAG                 | Glycosaminoglycan  |
| HIRO                | Heart Image Recorder Osnabrück                                       |
| HR                  | Heart rate   |
| HZ                  | Hertz  |
| If                  | Inflated   |
| LanA                | Laminin A  |
| LanB2               | Laminin B2   |
| Loh                 | Lonely heart   |
| Mys                 | Myospheroid  |
| Ndg                 | Nidogen  |
| OCT                 | Optical coherence tomography   |
| PLAC                | Protease and Lacunin   |
| Prc                 | Pericardin   |
| RT-qPCR             | Quantitative real-time PCR   |
| ROI                 | Region of interest   |
| SOHA                | Semi-automatic Optical Heartbeat Analysis                            |
| Svp                 | Seven up   |
| Tin                 | Tinman   |
| Trol                | Terribly reduced optic lobes   |
| TSR                 | Thrombospondin type repeat   |
| UAS                 | Upstream Activating Sequence   |
| VDRC                | Vienna Drosophila Resource Center                                    |
| Vkg                 | Viking   |
| W                   | White  |
| WG                  | Wingless   |

## 7.2 Java Code

### 7.2.1 Java UML diagrams

| <b>MathMethods</b>  |
|---|
| mittelwert ( ArrayList < double > ) : double                        |
| stabw ( ArrayList < double > ) : double                             |
| median ( ArrayList < double > ) : double                            |
| ttest_check ( ArrayList < double >, ArrayList < double > ) : double |
| onesample_ttest_check( double, ArrayList < double > ) : double      |

**Figure 1:** The MathMethods class. It provides methods for statistical analysis.

| <b>PeakHandler</b>  |
|---|
| PeakHandler ( )   |
| nPeaks ( ArrayList < double >, int ) : ArrayList < String >                                   |
| removeGaps ( ArrayList < double >, int ) : ArrayList < String >                               |
| getAverage ( ArrayList < double >, int ) : ArrayList < double >                               |
| DetectPeaks ( String, File, int, int, int, int, int ) : void                                  |
| draw ( ArrayList < double >, ArrayList < double >, ArrayList < double >, String, int ) : void |

**Figure 2:** The PeakHandler class. The methods DetectPeaks and nPeaks recognize the peaks within a signal. PeakHandler contains the methods draw, which call the class Graph-Panel.



| <b>HeartbeatDrawer</b>  |
|---|
| padding : int<br>labelPadding : int<br>lineColor: Color<br>pointColor : Color<br>gridColor : Color<br>Graph_Stroke : Stroke<br>pointWidth : int<br>numberYDivisions : int<br>scores : List< double ><br>peaks : List< double ><br>real_systole : List< double ><br>serialVersionUID : long  |
| GraphPanel ( List< double >, List< double >, List< double > )<br>paintComponent ( Graphics ) : void<br>getMinScore ( ) : double<br>getMaxScore ( ) : double<br>ControlImage ( ArrayList<double> ) : double<br>SetScores ( List< double > ) : void<br>GetScores ( List< double > ) : List< double ><br>saveImage ( String, String ) : void |

**Figure 3:** The HeartbeatDrawer class. It generates the grey-value overview pictures.

| <b>GreyAnalyser</b>   |
|---|
| data : JList <String><br>selectedlx : int []<br>filename : String<br>researcher : String<br>temperature : String<br>path : File |
| VideoAnalyser ( String, String, int [], File, JList <String> )<br>run ( ) : void  |

**Figure 4:** GreyAnalyser. This class calculates the grey values from all frames of selected videos.

| <b>RecorderFrame</b>  |
|---|
| videobox: JFrame<br>histo : JPanel<br>contentPane : JPanel<br>toolbox : JFrame<br>infos : JPanel<br>scalare : ArrayList < Integer ><br>nextLoop : boolean<br>fps : JLabel<br>recordtime : JLabel<br>record : JButton<br>stop : JButton<br>Storage : ArrayList < Mat ><br>go : boolean<br>aufnahme gestartet : boolean |
| RecorderFrame ( int, File, int, int, int, int, int, String, String, int, int )<br>RecorderFrame ( Graphics ) : void<br>write ( ) : void<br>img2Mat ( BufferedImage ) : Mat  |

**Figure 5:** The RecorderFrame class. It provides the Graphic User Interface for video recording and draws the real-time histogram.

| <b>Recorder</b>   |
|---|
| cap: VideoCapture<br>filter : int<br>threshold1 : int<br>threshold2 : int<br>aperature : int<br>maxValue : int<br>adaptiveMethod : String<br>Threshold : String<br>blockSize : int<br>constant : int<br>VideoFile : File<br>useCam : int  |
| Recorder ( int, File, int, int, int, int, int, String, String, int, int )<br>getOneFrame ( ) : BufferedImage<br>getFPS ( ) : double<br>setFPS ( double ) : void<br>getWidth ( ) : double<br>getHeight ( ) : double<br>getGain ( ) : double<br>getBrightness ( ) : double<br>setBrightness ( double ) : void<br>getExposure ( ) : double<br>Mat2BufferedImage(Mat) : BufferedImage |

**Figure 6:** The Recorder class. It records one frame from the camera.

## 7.2.2 Important Java methods

```
int counter =0;
for (int i = 0; i < selectedIx.length; i++) {
    String file = path.getAbsolutePath()+"\\"+data.getModel().getElementAt(
        selectedIx[i]);
    Mat frame = new Mat();
    VideoCapture cap = new VideoCapture(file);
    String savefile = file;
    if (savefile.indexOf(".") > 0)
        savefile = savefile.substring(0, savefile.lastIndexOf("."));
    try {
        PrintWriter pWriter = new PrintWriter(new BufferedWriter(new FileWriter(
            savefile+".hir", false)));
        pWriter.println((int)cap.get(5));
        pWriter.println(researcher);
        pWriter.println(temperature);
        while(true){
            if (cap.read(frame)){
                Scalar value = Core.mean(frame);
                pWriter.println(value.val[0]);
            }else {
                break;
            }
        }
        pWriter.flush();
        pWriter.close();
    } catch (IOException e) {
        JOptionPane.showMessageDialog(null, "Something went wrong in
            VideoAnalyser. Files integrity may be corrupted.");
    }
    counter++;
}
JOptionPane.showMessageDialog(null, "Done. "+counter+" movies were analyzed.");
```

**Listing 1:** The GreyAnalyser calculates the grey values from a video file.

```
public ArrayList<String> nPeaks(ArrayList<Double> array, int range) {

    ArrayList<String> resultarray = new ArrayList<String>();
    int l, r, tmpj;
    tmpj=0;
    String tmpstr="";
    for (int i = 0; i < array.size(); i++) {
        boolean isPeak = true;
        // Check from left to right
        l = Math.max(0, i - range);
        r = Math.min(array.size() - 1, i + range);
        for (int j = l; j <= r; j++) {
            // Skip if we are on current
            if (i == j) {
                continue;
            }
            if (array.get(i) < array.get(j)) {
                isPeak = false;
                tmpj=j;
                break;
            }
        }
        if (isPeak) {
            tmpstr=Double.toString(array.get(tmpj));
            if (!(resultarray.contains(tmpstr))) {
                resultarray.add(tmpstr);
            }
            i += range;
        }
    }
    return resultarray;
}
```

**Listing 2:** The nPeaks method detects the peaks within the grey values.

```

Mat tmp = new Mat();
BufferedImage bi = videoCap.getOneFrame();
BufferedImage coordinates = new BufferedImage(620, 620, BufferedImage.
    TYPE_BYTE_GRAY);
tmp = img2Mat(bi);
g = contentPane.getGraphics();
g.drawImage(videoCap.getOneFrame(), 0, 0, this);
g = histo.getGraphics();

Scalar value = Core.mean(tmp);
if(Scalarcounter<255) {
    if(!nextLoop){
        scalare.add(Scalarcounter, (int)value.val[0]);
    } else {
        scalare.set(Scalarcounter, (int)value.val[0]);
    }
} else {
    Scalarcounter=0;
    nextLoop=true;
}
Graphics2D histogramm = coordinates.createGraphics();
histogramm.setFont(new Font("TimesRoman", Font.BOLD, 15));
histogramm.setRenderingHint(RenderingHints.KEY_TEXT_ANTIALIASING,
    RenderingHints.VALUE_TEXT_ANTIALIAS_ON);
histogramm.setStroke(new BasicStroke(2f));
histogramm.fillRect(0, 0, 620, 620);
histogramm.setColor(Color.black);
histogramm.drawLine(30, 570, 570, 570);
histogramm.drawLine(30, 570, 30, 30);
histogramm.drawString("Time", 550, 585);
histogramm.drawString("Grey Value", 10, 10);
histogramm.drawLine(20,30,30,30);
histogramm.drawString("255", 5, 25);
histogramm.drawLine(20,570,30,570);
histogramm.drawString("0", 5, 570);
histogramm.drawLine(20,320,30,320);
histogramm.drawString("130", 5, 320);
histogramm.drawString("Gray Value", 10, 10);

histogramm.setColor(Color.cyan);
histogramm.setStroke(new BasicStroke(3f));
for(int i=0; i<scalare.size(); i++) {
    if(scalare.get(i)!=null && i>0)
        histogramm.drawLine((i-1+30)*2, ((285-scalare.get(i-1))*2), (i
            +30)*2, ((285-scalare.get(i))*2));
}
histogramm.dispose();
g.drawImage(coordinates, 0, 0, this);

```

```
Scalarcounter++;  
if(aufnahme gestartet) {  
    Storage.add(img2Mat(bi));  
}
```

**Listing 3:** The drawHistogram method generates live histograms while recording.

```

String video = new String();
String line = new String();
String[] data = new String[5];
MathMethods calculator = new MathMethods();

ArrayList<Double> FileSystole = new ArrayList<>();
ArrayList<Double> ConcludeSystole = new ArrayList<>();
ArrayList<Double> FileDiastole = new ArrayList<>();
ArrayList<Double> ConcludeDiastole = new ArrayList<>();
ArrayList<Double> FileHeartperiod = new ArrayList<>();
ArrayList<Double> ConcludeHeartperiod = new ArrayList<>();
ArrayList<Double> FileHz = new ArrayList<>();
ArrayList<Double> ConcludeHz = new ArrayList<>();
ArrayList<Double> FileAI = new ArrayList<>();
ArrayList<Double> ConcludeAI = new ArrayList<>();

File path = new File(defaultdata.getAbsolutePath());
PrintWriter pWriter = new PrintWriter(new BufferedWriter(new FileWriter(
    path+"\\conclude.csv", false)));
pWriter.println("Filename;Systolic intervall;Diastolic intervall;
    Heartbeat duration;Median Hz;Mean Hz; Arhythmicity index");
for(int i=0; i<filenames.size(); i++ ) {
    FileReader fr = new FileReader(filenames.get(i));
    BufferedReader br = new BufferedReader(fr);
    int counter=0;
    FileSystole.clear();
    FileDiastole.clear();
    FileHeartperiod.clear();
    FileHz.clear();
    FileAI.clear();
    while((line = br.readLine())!=null) {
        data=line.split(";");
        if(counter==1) {
            video=data[0];
        }
        if((counter>2)) {
            FileSystole.add(Double.parseDouble(data[2]));
            FileDiastole.add(Double.parseDouble(data[3]));
            FileHeartperiod.add(Double.parseDouble(data[4]));
            FileHz.add(Double.parseDouble(data[5]));
        }
        counter++;
    }

    ConcludeSystole.add(calculator.mittelwert(FileSystole));
    ConcludeDiastole.add(calculator.mittelwert(FileDiastole));
    ConcludeHeartperiod.add(calculator.mittelwert(FileHeartperiod));
    ConcludeHz.add(calculator.mittelwert(FileHz));
    ConcludeAI.add((calculator.stabw(FileHz)/calculator.median(FileHz)));

```



```
        pWriter.println(video+" "+calculator.mittelwert(FileSystole)+" "+
            calculator.mittelwert(FileDiastole)+" "+calculator.mittelwert(
                FileHeartperiod)+" "+calculator.median(FileHz) + " "+calculator.
                mittelwert(FileHz)+" "+(calculator.stabw(FileHz)/calculator.
                    median(FileHz)));
        counter=0;
        br.close();
        fr.close();
    }

    pWriter.println();
    pWriter.println("Mean "+calculator.mittelwert(ConcludeSystole)+" "+
        calculator.mittelwert(ConcludeDiastole)+" "+calculator.mittelwert(
            ConcludeHeartperiod)+" "+calculator.median(ConcludeHz)+" "+calculator
                .mittelwert(ConcludeHz)+" "+calculator.mittelwert(ConcludeAI));
    pWriter.flush();
    pWriter.close();
```

**Listing 4:** The Conclude method calculates the mean values of .csv files.

```

static String create_MMode (String hir_file, int slider) {
    String filename = hir_file.replaceAll("hir", "avi");
    String finalfile = "";
    VideoCapture cap = new VideoCapture(filename);
    ArrayList<Mat> rows = new ArrayList<Mat>();
    Mat output=new Mat();
    Mat frame = new Mat();
    int counter=0;
    try {
    while(true){
        if (cap.read(frame)){
            Mat row= new Mat();
            frame.col((slider*frame.width()/100)).copyTo(row);
            if(counter>0) {
                org.opencv.core.Core.reduce(frame,row, 1 , 1);
                rows.add(row);
            }
            counter++;
        } else {
            break;
        }
    }
    cap.release();
    org.opencv.core.Core.hconcat(rows, output);
    BufferedImage image = new BufferedImage(output.width(),output.height(),
        BufferedImage.TYPE_INT_RGB);
    image=Mat2BufferedImage(output);
    String savepath = filename.substring(0,filename.lastIndexOf("\\")+1+
        "Data\\");
    String savefile = filename.substring( filename.lastIndexOf( "\\\" ) + 1,
        filename.lastIndexOf( "." ) );
    finalfile = savepath+savefile+"_mmode.png";
    ImageIO.write(image, "PNG", new File(finalfile));
    } catch (Exception f) { JOptionPane.showMessageDialog(null, "Something went
        wrong. Files integrity may be corrupted.");    }
    return finalfile;
}

```

**Listing 5:** The MMode method generates a kymograph.

### 7.3 Index of figures, tables, UML Diagrams and crucial code listings

#### List of Figures

|    |  |    |
|----|--|----|
| 1  | The larval heart of <i>Drosophila</i> . . . . .  | 4  |
| 2  | The <i>Drosophila</i> heart in all developmental stages . . . . .  | 5  |
| 3  | The cardiac ECM of <i>Drosophila</i> . . . . .   | 9  |
| 4  | OCT and SOHA methods for heart measurements . . . . .  | 11 |
| 5  | Video recording overview . . . . .   | 61 |
| 6  | Ether preparation . . . . .  | 62 |
| 7  | Mean grey value of one heartbeat . . . . .   | 63 |
| 8  | The moving average algorithm . . . . .   | 64 |
| 9  | Intact heartbeat detection . . . . .   | 65 |
| 10 | Heartbeat detection algorithm . . . . .  | 66 |
| 11 | The detection of systolic and diastolic intervals . . . . .  | 67 |
| 12 | Heartbeat detection in three different developmental stages . . . . .  | 69 |
| 13 | Comparison of the preparation methods . . . . .  | 71 |
| 14 | Heart rate control animals . . . . .   | 72 |
| 15 | Heart rate effects of RNAi-mediated downregulation of crucial ECM proteins in third instar larvae. . . . .       | 76 |
| 16 | Heart rhythmicity effects of RNAi-mediated downregulation of crucial ECM protein in third instar larvae. . . . . | 78 |
| 17 | Wiring Raspberry Pi with camera and OLED display . . . . .   | 87 |

## List of Tables

|   |  |    |
|---|--|----|
| 1 | Recent publications with OCT measurements . . . . .  | 12 |
| 2 | Recent publications with SOHA measurements. . . . .  | 13 |
| 3 | RNAi fly lines used in this thesis. . . . .  | 68 |
| 4 | Control and driver lines used in this thesis. . . . .  | 68 |
| 5 | Software used in this thesis. . . . .  | 68 |
| 6 | Recent publications with heartbeat measurements of intact <i>Drosophila</i> third instar larvae. . . . . | 80 |
| 7 | Summary of the high throughput RNAi screen . . . . .   | 84 |

## List of Java UML diagrams

|   |                           |     |
|---|---------------------------|-----|
| 1 | MathMethods . . . . .     | 99  |
| 2 | PeakHandler . . . . .     | 99  |
| 3 | HeartbeatDrawer . . . . . | 100 |
| 4 | GreyAnalyser . . . . .    | 100 |
| 5 | RecorderFrame . . . . .   | 101 |
| 6 | Recorder . . . . .        | 102 |

## Listings

|   |   |     |
|---|---|-----|
| 1 | The GreyAnalyser calculates the grey values from a video file. . . . .  | 103 |
| 2 | The nPeaks method detects the peaks within the grey values. . . . .     | 104 |
| 3 | The drawHistogram method generates live histograms while recording. . . | 105 |
| 4 | The Conclude method calculates the mean values of .csv files. . . . .   | 107 |
| 5 | The MMode method generates a kymograph. . . . .                         | 109 |

## 8 Curriculum vitae

---

Name: Kay Lammers

Day of Birth: 04.11.1983

Place of Birth: Vechta

---

### Academic education:

**10/2008 - 03/2013:** Bachelor of Science (B.Sc.) - Berufliche Bildung - Berufliche Fachrichtung Informatik, Münster University of Applied Sciences

**10/2011 - 01/2015:** Bachelor of Science (B.Sc.) - 2-Fächer Bachelor (Informatik-Biologie), , University of Osnabrück

**10/2014 - 10/2015:** Master of Science (M.Sc.) - Biology (General Biology), University of Osnabrück

**11/2015 - 12/2018:** PhD student as part of the SFB 944 under the supervision of Prof. Dr. Achim Paululat.

---

### School education:

**09/2004 - 06/2007:** Vocational baccalaureate diploma - Pictorius Berufskolleg Coesfeld

**09/2004 - 06/2007:** Apprenticeship - IT specialist for system integration, Gemeinsamen Kommunalen Datenzentrale (GKD) Recklinghausen

---

### Work Experience:

**06/2007 - 06/2008:** IT specialist, Gemeinsamen Kommunalen Datenzentrale (GKD) Recklinghausen

**since 05/2019:** Teacher at "Gymnasium der Mariannahiller Missionare", Maria Veen

## 9 Erklärung über die Eigenständigkeit der wissenschaftlich erbrachten Leistungen

Ich erkläre hiermit, dass die vorliegende Arbeit ohne unzulässige Hilfe Dritter und ohne Benutzung anderer als der angegebenen Hilfsmittel angefertigt habe. Die aus anderen Quellen direkt oder indirekt übernommenen Daten und Konzepte sind unter Angabe der Quelle gekennzeichnet. Bei der Auswahl und Auswertung folgenden Materials haben mir die nachstehend aufgeführten Personen in der jeweils beschriebenen Weise unentgeltlich geholfen.

- Hannah Schulte - im Rahmen ihrer Bachelorarbeit bei der Erhebung der Daten zur Untersuchung potentieller RNAi - Kandidaten mit veränderter Herz Morphologie
- Ronja Schiemann - in Rahmen von Publikation 3 bei der Kreuzungsvorbereitung für die in vivo Messungen intakter Larven

Weitere Personen waren an der inhaltlichen materiellen Erstellung der vorliegenden Arbeit nicht beteiligt. Insbesondere habe ich hierfür nicht die entgeltliche Hilfe von Vermittlungs- bzw. Beratungsdiensten (Promotionsberater oder andere Personen) in Anspruch genommen. Niemand hat von mir unmittelbar oder mittelbar geldwerte Leistungen für Arbeiten erhalten, die im Zusammenhang mit dem Inhalt der vorgelegten Dissertation stehen. Die Arbeit wurde bisher weder im In- noch im Ausland in gleicher oder ähnlicher Form einer anderen Prüfungsbehörde vorgelegt.

---

Ort, Datum

---

Unterschrift



## **10 Erklärung über etwaige frühere Promotionsversuche**

gem. §8 Abs. 2 Buchstabe g der Promotionsordnung der Fachbereiche Physik, Biologie/-Chemie und Mathematik/Informatik der Universität Osnabrück.

Hiermit bestätige ich, dass die vorzulegende Dissertation bisher weder im In- noch im Ausland in gleicher oder ähnlicher Form einer anderen Prüfungsbehörde vorgelegt wurde.

---

Ort, Datum

---

Unterschrift

## 11 Danksagung

Mein Dank gilt meinem Doktorvater Herrn Prof. Dr. Achim Paululat für die Ermöglichung der Dissertation und für die Bereitstellung des interessanten Themas. Danke für die Gespräche, die Unterstützung, das Verständnis und die Geduld. Dem SFB 944 inklusive dem IRTG danke ich für die finanzielle Unterstützung und die Möglichkeit sich weiterzubilden.

Herrn Prof. Dr. Jürgen Heinisch danke ich für die freundliche Übernahme des Zweitgutachtens.

Ich danke Herrn Prof. Dr. Purschke für ihre Bereitschaft, meiner Prüfungskommission anzugehören.

Herrn Dr. Heiko Harten danke ich für die freundliche Teilnahme an meiner Prüfungskommission. Seine gute Laune und seine optimistische und geduldige Art hat so manches Problem schnell kleiner werden lassen.

Ein besonderer Dank gilt meinen Kollegen Lena Dehnen, Yanina Post, Benjamin Hallier, Ronja Schiemann und Marcel Reinhardt die mich all die Jahre in der Zoologie begleitet haben. Wir hatten viel Spaß zusammen und aus Arbeitskollegen sind Freunde geworden. Ich liebte die Doppelkopfrunden und finde es toll, dass wir immer noch Kontakt haben. Hoffentlich wird er noch lange erhalten bleiben.

Der gesamten Arbeitsgruppe Zoologie möchte ich für die freundliche Aufnahme und die sehr freundliche Arbeitsatmosphäre danken. Ich habe mich all die Jahre sehr wohl gefühlt. Das resultierte in einer Bachelor-, Master-, als auch Doktorarbeit. Ein besonderer Dank gilt Dr. Maik Drechsler, Ariane Schmidt und Mirko Huesken, die mich all die Jahre in der Zoologie begleitet haben. Weiterhin möchte ich Martina Biedermann, Mechthild Krabusch und Lydia Reckers für ihre große Hilfsbereitschaft danken.

Meinen Eltern möchte ich besonders für die jahrelange Unterstützung danken! Es bedeutet mir sehr viel, dass ihr mich immer motiviert und aufgemuntert habt. Es ist ein gutes Gefühl zu wissen, dass ihr immer für mich da seid.

Meiner Frau Sarah danke ich für das grenzenlose Verständnis und die unendliche Unterstützung in allen Lebenslagen! Auch meinem Sohn Hanno möchte ich für die Geduld danken, wenn Papa mal keine Zeit zum Spielen hatte.